

UC San Diego

UC San Diego Electronic Theses and Dissertations

Title

Advancing the use of radiocarbon in studies of global and regional carbon cycling with high precision measurements of ^{14}C in CO_2 from the Scripps CO_2 Program

Permalink

<https://escholarship.org/uc/item/1sd4g4dd>

Author

Graven, Heather Dawn

Publication Date

2008

Peer reviewed|Thesis/dissertation

UNIVERSITY OF CALIFORNIA, SAN DIEGO

Advancing the use of radiocarbon in studies of global and regional carbon cycling
with high precision measurements of ^{14}C in CO_2 from the Scripps CO_2 Program

A dissertation submitted in partial satisfaction of the
requirements for the degree Doctor of Philosophy
in
Earth Sciences

by

Heather Dawn Graven

Committee in charge:

Professor Ralph Keeling, Chair
Doctor Thomas Guilderson
Professor Devendra Lal
Professor Jeffrey Severinghaus
Professor Mark Thiemens
Professor Ray Weiss

2008

Copyright
Heather Dawn Graven, 2008
All rights reserved.

The dissertation of Heather Dawn Graven is approved,
and it is acceptable in quality and form for publication
on microfilm:

Chair

University of California, San Diego

2008

How do you go about doing science when you need decades of record?

Carl Wunsch, Massachusetts Institute of Technology, 2006

TABLE OF CONTENTS

Signature Page	iii
Epigraph	iv
Table of Contents	v
List of Abbreviations	ix
List of Figures	x
List of Tables	xii
Acknowledgments	xiii
Vita	xv
Abstract	xvii
Chapter 1: Introduction	1
1.1 Background	3
1.2 Atmospheric measurements	5
1.3 ^{14}C in carbon cycle studies	5
1.4 Continued interest in atmospheric measurements of $^{14}\text{CO}_2$	6
1.5 Achievements in measurement precision	7
1.6 Measurements from the Scripps CO_2 Program	9
1.7 Airborne measurements of ^{14}C	9
1.8 Contribution of the Scripps $\Delta^{14}\text{CO}_2$ dataset	10
Chapter 2: Methods for High Precision Analysis of $\Delta^{14}\text{C}$ in CO_2	11
Abstract	11
2.1 Introduction	12
2.2 Flask sampling	16
2.3 Analysis of CO_2 concentration	16
2.4 Extraction of CO_2 from flasks	16
2.5 Extraction of CO_2 from reference cylinders	18
2.6 Reference cylinders for ^{14}C	18
2.7 Graphitization and sample handling	19
2.8 Accelerator Mass Spectrometry	23
2.9 Data processing	27
2.10 Modifications implemented for high precision $^{14}\text{CO}_2$ analysis	31
2.11 Uncertainty analysis	34
2.12 Updated uncertainty analysis	40

2.13	Observed biases in $\Delta^{14}\text{C}$ of Cyl-1 and Cyl-2 measured on different wheels	41
2.14	Elimination of OXI artifacts	42
2.15	Normalization by Cyl-1 and Cyl-2	45
	2.15.1 Calculation of $\Delta^{14}\text{C}$ in Cyl-normalized ratios	46
	2.15.2 Total uncertainty in $\Delta^{14}\text{C}$ using Cyl-1 normalization	50
2.16	Adjustments to OXI normalization	51
	2.16.1 Group designation on early wheels	52
	2.16.2 Definition of wheel factors (α_w)	56
	2.16.3 Calculation of α_w using Cyl-1 and Cyl-2	56
	2.16.4 Calculation of α_w using replicate La Jolla samples	57
	2.16.5 Estimation of α_w for wheel analyzed on 2/15/04	59
	2.16.6 Application of α_w and calculation of total uncertainty	61
2.17	Fractionation caused by incomplete graphitization	62
2.18	Special handling of flasks from Palmer Station	66
	2.18.1 Comparison of $\Delta^{14}\text{C}$ of air in different flasks	67
	2.18.2 Experiments on $\delta^{13}\text{C}$ in second extraction	68
2.19	$^{14}\text{CO}_2$ Laboratory Intercomparison	76
2.20	Summary	78
2.21	Future measurements from the Scripps archive	80
	Acknowledgement	82
Chapter 3:	A 15-year record of variability in $\Delta^{14}\text{C}$ of CO_2 at La Jolla, California	83
	Abstract	83
3.1	Introduction	84
3.2	Sampling and analysis of clean air samples at La Jolla	85
3.3	The Scripps CO_2 archive	86
3.4	$\Delta^{14}\text{C}$ analysis	87
3.5	$\Delta^{14}\text{C}$ observations	88
	3.5.1 Comparison with $\Delta^{14}\text{C}$ at Jungfraujoch and Niwot Ridge	90
	3.5.2 $\Delta^{14}\text{C}$, CO_2 and $\delta^{13}\text{C}$	93
3.6	Secular trend of $\Delta^{14}\text{C}$	95
3.7	Interannual variability in $\Delta^{14}\text{C}$	99
	3.7.1 Interannual variability in air-sea gas exchange	101
	3.7.2 Interannual variability in land biosphere exchange	106
	3.7.3 Interannual variability in stratosphere-troposphere exchange	107
	3.7.4 Interannual variability in cosmic ray flux	110
	3.7.5 Interannual variability in fossil fuel emissions	111
	3.7.6 Conclusions about secular trend of $\Delta^{14}\text{C}$	111
3.8	Seasonal cycle	112
	3.8.1 Observation of seasonal cycle	112
	3.8.2 Variation in amplitude and phase of seasonal cycle	114

3.8.3	Discussion of seasonal cycle	118
3.8.4	Biospheric exchange	118
3.8.5	Fossil fuel emissions	120
3.8.6	Stratosphere-troposphere exchange	122
3.8.7	Vertical mixing in the troposphere	128
3.8.8	Conclusions about the seasonal cycle at La Jolla	129
3.9	Summary	130
3.10	Recommendations for future $\Delta^{14}\text{C}$ measurements at La Jolla . . .	131
	Acknowledgement	133
Chapter 4: Recent patterns of $\Delta^{14}\text{C}$ in CO_2 at 7 global sampling sites		134
	Abstract	134
4.1	Introduction	135
4.2	The Scripps CO_2 archive	136
4.3	Analysis of clean air samples	137
4.4	$\Delta^{14}\text{C}$ observations	139
4.4.1	$\Delta^{14}\text{C}$, CO_2 and $\delta^{13}\text{C}$	139
4.5	Trends of $\Delta^{14}\text{C}$ at each station	143
4.6	Seasonal cycles of $\Delta^{14}\text{C}$ at each station	152
4.7	Discussion of seasonal cycles of $\Delta^{14}\text{C}$	156
4.8	Latitudinal gradient of $\Delta^{14}\text{C}$	160
4.9	Changes in variability at Point Barrow and the South Pole since the 1980s	162
4.10	Evolution of the latitudinal profile of $\Delta^{14}\text{C}$	165
4.11	Summary	171
4.12	Recommendations for future $\Delta^{14}\text{C}$ measurements in the Scripps CO_2 Program	172
	Acknowledgement	174
Chapter 5: Vertical profiles of biogenic and fossil fuel-derived CO_2 from air- borne measurements of $\Delta^{14}\text{C}$ and CO_2 above Colorado		175
	Abstract	175
5.1	Introduction	176
5.2	Methods	178
5.3	CO_2 Source Partitioning	181
5.3.1	Calculating Sources	181
5.3.2	Rural and Urban Patterns	185
5.3.3	$\delta^{13}\text{C}$ source signatures	193
5.4	Correlation of C_{ff} with CO	194
5.5	Summary	199
	Acknowledgement	200
Chapter 6: Conclusions		201

Appendix A: MATLAB Scripts for Data Processing	203
A.1 Normalization	204
A.2 Calculation of $\Delta^{14}\text{C}$	209
Appendix B: $\Delta^{14}\text{CO}_2$ Data from 7 Scripps Stations	210
B.1 Observations of $\Delta^{14}\text{C}$	210
B.1.1 Measurements from La Jolla	211
B.1.2 Measurements from Point Barrow	219
B.1.3 Measurements from Kumukahi	221
B.1.4 Measurements from Mauna Loa	223
B.1.5 Measurements from Samoa	226
B.1.6 Measurements from Palmer Station	228
B.1.7 Measurements from the South Pole	229
B.2 Monthly values of $\Delta^{14}\text{C}$	232
B.2.1 Monthly values of $\Delta^{14}\text{C}$ at La Jolla	233
B.2.2 Monthly values of $\Delta^{14}\text{C}$ at Point Barrow	234
B.2.3 Monthly values of $\Delta^{14}\text{C}$ at Kumukahi	235
B.2.4 Monthly values of $\Delta^{14}\text{C}$ at Mauna Loa	236
B.2.5 Monthly values of $\Delta^{14}\text{C}$ at Samoa	237
B.2.6 Monthly values of $\Delta^{14}\text{C}$ at Palmer Station	238
B.2.7 Monthly values of $\Delta^{14}\text{C}$ at the South Pole	239
Appendix C: Airborne $\Delta^{14}\text{CO}_2$ Data	240
C.1 Airborne measurements, May 2004	241
C.2 Airborne measurements, July 2004	242
References	243

LIST OF ABBREVIATIONS

AGL	Altitude above ground level
AMS	Accelerator Mass Spectrometry or Spectrometer
ASL	Altitude above sea level
AORG	Atmospheric Oxygen Research Group
CAMS	Center for Accelerator Mass Spectrometry
CIO	Center for Isotope Research, University of Groningen
Cyl-1	CO ₂ extracted from the whole air reference cylinder 00326
Cyl-2	CO ₂ extracted from the whole air reference cylinder 55280
ENSO	El Niño/Southern Oscillation
INSTAAR	Institute of Arctic and Alpine Research, University of Colorado
IRGA	Infrared Gas Analysis or Analyzer
IRMS	Isotope Ratio Mass Spectrometry or Spectrometer
KUM	Kumukahi, Hawaii
LJO	La Jolla, California
LLNL	Lawrence Livermore National Laboratory
MLO	Mauna Loa, Hawaii
NCAR	National Center for Atmospheric Research
NOAA	National Oceanic and Atmospheric Administration
OXI	Oxalic Acid I
PDO	Pacific Decadal Oscillation
PSA	Palmer Station, Antarctica
PTB	Point Barrow, Alaska
QBO	Quasi-Biennial Oscillation
SAM	Cape Matatula, American Samoa
SIO	Scripps Institution of Oceanography
SPO	South Pole, Antarctica
STE	Stratosphere-troposphere exchange

LIST OF FIGURES

Figure 2.1:	Records of atmospheric $\Delta^{14}\text{C}$	13
Figure 2.2:	Schematic of the CO_2 extraction manifold	17
Figure 2.3:	Schematic of the CO_2 graphitization manifold	20
Figure 2.4:	Schematic of the accelerator mass spectrometer	24
Figure 2.5:	Measurements of $\Delta^{14}\text{C}$ in Cyl-1 and Cyl-2 during 2005 . .	32
Figure 2.6:	$\Delta^{14}\text{C}$ in OXI, prepared by different methods	39
Figure 2.7:	$\Delta^{14}\text{C}$ in all Cyl-1 and Cyl-2, normalized to OXI	43
Figure 2.8:	$\Delta^{14}\text{C}$ in all Cyl-2, normalized to OXI and Cyl-1	44
Figure 2.9:	Estimation of α_w for wheel analyzed 2/15/04	60
Figure 2.10:	Results of fractionation experiment	64
Figure 2.11:	$\delta^{13}\text{C}$ in second extraction	70
Figure 2.12:	$\delta^{13}\text{C}$ at Palmer Station	73
Figure 2.13:	$\delta^{13}\text{C}$ at Mauna Loa	75
Figure 2.14:	Adjusted $\Delta^{14}\text{C}$ at Samoa	79
Figure 3.1:	Status of the Scripps CO_2 archive from La Jolla	87
Figure 3.2:	$\Delta^{14}\text{C}$ observations from La Jolla	89
Figure 3.3:	Derivative of $\Delta^{14}\text{C}$ observations from La Jolla	90
Figure 3.4:	Comparison of $\Delta^{14}\text{C}$ measured at La Jolla, Jungfraujoch and Niwot Ridge	91
Figure 3.5:	Observations of $\Delta^{14}\text{C}$, CO_2 and $\delta^{13}\text{C}$ at La Jolla	94
Figure 3.6:	$\Delta^{14}\text{C}$ observations from La Jolla fit to linear and exponen- tial models	97
Figure 3.7:	$\Delta^{14}\text{C}$ observations from La Jolla fit to a polynomial model	98
Figure 3.8:	$\Delta^{14}\text{C}$ with annual cycles removed, and linear and exponen- tial trend removed	100
Figure 3.9:	Derivative of $\Delta^{14}\text{C}$ anomaly and MEI, PDO index and sunspot counts	103
Figure 3.10:	Power spectra of $\Delta^{14}\text{C}$ at La Jolla and Quasi-Biennial Os- cillation, and correlation	109
Figure 3.11:	Seasonal variation in detrended $\Delta^{14}\text{C}$ observations from all years	113
Figure 3.12:	$\Delta^{14}\text{C}$ observations from La Jolla fit with linear trend and one harmonic	114
Figure 3.13:	Average annual cycle of $\Delta^{14}\text{C}$ at La Jolla	115
Figure 3.14:	Timing of maximum annual $\Delta^{14}\text{C}$ in the Northern Hemi- sphere	116
Figure 3.15:	Amplitude of the $\Delta^{14}\text{C}$ seasonal cycle at La Jolla and deriva- tive of the $\Delta^{14}\text{C}$ anomaly, shifted by 2 years	117
Figure 3.16:	Seasonality of fossil fuel emissions and influence on the sea- sonal $\Delta^{14}\text{C}$ cycle in the Northern Hemisphere	121
Figure 3.17:	Tropospheric destinations of deep stratospheric intrusions	123

Figure 3.18:	Annual variation of the net downward mass transport across the extratropical tropopause	124
Figure 3.19:	Estimated seasonal influence of stratosphere-troposphere exchange on $\Delta^{14}\text{C}$ in the extratropical Northern Hemisphere . . .	126
Figure 3.20:	Seasonal cycle of N_2O and CFCs at Mace Head and Cape Grim	127
Figure 3.21:	Components of seasonal cycle at Fruholmen, Norway 1985-1990	130
Figure 4.1:	Map of clean air sampling stations in the Scripps CO_2 Program and AORG networks where samples were collected for $\Delta^{14}\text{C}$ analysis	137
Figure 4.2:	Status of the Scripps CO_2 archive from all stations	138
Figure 4.3:	Observations in the Northern Hemisphere at Point Barrow and La Jolla	140
Figure 4.4:	Observations in the Tropics at Kumukahi, Mauna Loa and Samoa	141
Figure 4.5:	Observations in the Southern Hemisphere at Palmer Station and the South Pole	142
Figure 4.6:	Observations of $\Delta^{14}\text{C}$, CO_2 and $\delta^{13}\text{C}$ at Point Barrow . .	144
Figure 4.7:	Observations of $\Delta^{14}\text{C}$, CO_2 and $\delta^{13}\text{C}$ at Kumukahi	145
Figure 4.8:	Observations of $\Delta^{14}\text{C}$, CO_2 and $\delta^{13}\text{C}$ at Mauna Loa	146
Figure 4.9:	Observations of $\Delta^{14}\text{C}$, CO_2 and $\delta^{13}\text{C}$ at Samoa	147
Figure 4.10:	Observations of $\Delta^{14}\text{C}$, CO_2 and $\delta^{13}\text{C}$ at Palmer Station .	148
Figure 4.11:	Observations of $\Delta^{14}\text{C}$, CO_2 and $\delta^{13}\text{C}$ at the South Pole .	149
Figure 4.12:	Linear trends at each station	151
Figure 4.13:	Detrended $\Delta^{14}\text{C}$ at each station, with individual years overlain	153
Figure 4.14:	$\Delta^{14}\text{C}$ observations fit with linear trend and one harmonic	155
Figure 4.15:	Annual means and annual cycles of $\Delta^{14}\text{C}$	159
Figure 4.16:	Smoothed $\Delta^{14}\text{C}$ at all stations	161
Figure 4.17:	Annual cycles at Point Barrow and South Pole, 1985-91 and 1999-2006	164
Figure 4.18:	Evolution of the $\Delta^{14}\text{C}$ gradient between the Northern and Southern Hemispheres	166
Figure 4.19:	Shift in latitudinal profile of $\Delta^{14}\text{C}$ since 1980s	168
Figure 5.1:	Schematic of the airborne flask sampling apparatus	180
Figure 5.2:	$\Delta^{14}\text{C}$ and CO_2 in background air	184
Figure 5.3:	Morning profiles sampled in the rural area	186
Figure 5.4:	Morning profiles sampled in the urban area	188
Figure 5.5:	Afternoon profiles sampled in the urban area in a shallow boundary layer	190
Figure 5.6:	Afternoon profiles sampled in the urban area in a deep boundary layer	192
Figure 5.7:	Regressions between C_{ff} and CO	196

LIST OF TABLES

Table 2.1:	Example of a wheel loaded for high precision $^{14}\text{CO}_2$ analysis.	26
Table 2.2:	The mean and standard deviation in $\Delta^{14}\text{C}$ of replicate Cyl-1 targets	35
Table 2.3:	Example of group assignments	53
Table 2.4:	α_g and number of OXI targets in each group	54
Table 2.5:	Number of Cyl-1 and Cyl-2 targets on early wheels	57
Table 2.6:	Number of CO_2 samples from La Jolla replicated from early wheels	58
Table 2.7:	α_w and $(\sigma_{BW})_w$ calculated for the first 15 wheels	61
Table 2.8:	Results of fractionation experiment	65
Table 2.9:	Comparison of $\Delta^{14}\text{C}$ in different flask types	68
Table 2.10:	$\delta^{13}\text{C}$ in second extraction	71
Table 4.1:	Clean air sampling stations for $\Delta^{14}\text{C}$ in the Scripps CO_2 Program	136
Table 4.2:	Observed trends at each station	152
Table 4.3:	Mean annual cycle and trend at all stations	156
Table 4.4:	Mean annual cycle and trend at Point Barrow and the South Pole for 1985-1991 and 1999-2006	163
Table 5.1:	Emission ratios from observations and inventories	197
Table B.1:	Measurements from La Jolla	211
Table B.2:	Measurements from Point Barrow	219
Table B.3:	Measurements from Kumukahi	221
Table B.4:	Measurements from Mauna Loa	223
Table B.5:	Measurements from Samoa	226
Table B.6:	Measurements from Palmer Station	228
Table B.7:	Measurements from the South Pole	229
Table B.8:	Monthly values of $\Delta^{14}\text{C}$ at La Jolla	233
Table B.9:	Monthly values of $\Delta^{14}\text{C}$ at Point Barrow	234
Table B.10:	Monthly values of $\Delta^{14}\text{C}$ at Kumukahi	235
Table B.11:	Monthly values of $\Delta^{14}\text{C}$ at Mauna Loa	236
Table B.12:	Monthly values of $\Delta^{14}\text{C}$ at Samoa	237
Table B.13:	Monthly values of $\Delta^{14}\text{C}$ at Palmer Station	238
Table B.14:	Monthly values of $\Delta^{14}\text{C}$ at the South Pole	239
Table C.1:	Airborne measurements, May 2004	241
Table C.2:	Airborne measurements, July 2004	242

ACKNOWLEDGMENTS

Chapter 2:, in part, contains some material as it appears in Radiocarbon 2007. Graven, Heather D.; Guilderson, Thomas P., Keeling, Ralph F., University of Arizona, 2007. The dissertation author was the primary investigator and author of this paper.

Chapter 2:, in part, is being prepared for publication. Graven, Heather D.; Guilderson, Thomas P.; Keeling, Ralph F. The dissertation author is the primary investigator and author of this paper.

Chapter 3:, in part, is being prepared for publication. Graven, Heather D.; Guilderson, Thomas P.; Keeling, Ralph F. The dissertation author is the primary investigator and author of this paper.

Chapter 4:, in part, is being prepared for publication. Graven, Heather D.; Guilderson, Thomas P.; Keeling, Ralph F. The dissertation author is the primary investigator and author of this paper.

Chapter 5:, in part, is being prepared for publication. Graven, Heather D.; Stephens, Britton B.; Guilderson, Thomas P.; Campos, Teresa L.; Schimel, David S.; Keeling, Ralph F. The dissertation author is the primary investigator and author of this paper.

I am grateful for the financial support I received through a NASA Earth and Space Science Fellowship (2005-2008) and a University of California Office of the President mini-grant (2004-2005).

The fieldwork reported in Chapter 5 as part of the Airborne Carbon in the Mountains Experiment was funded by the National Science Foundation and the National Center for Atmospheric Research. I am grateful for the generous contribution of time and expertise to this project by Britton Stephens, Teresa Campos, Elliott Campbell, and David Schimel. I thank Alane Bollenbacher for conducting CO₂ and stable isotope analyses on the samples, Guy Emanuel for teaching me to run CO₂ extractions in the Sealab. Design and construction of the

flask sampling apparatus was provided by the NCAR Research Aviation Facility crew, Dave Moss, Bill Paplawsky and Adam Cox.

Working in the Keeling labs gave me an opportunity to build friendships with terrific people who helped me immensely in my graduate work, especially Alane Bollenbacher, Cindy Uribe, Steve Piper, Adam Cox, Bill Paplawsky, Kim Bracchi and Tim Whorf. Many thanks to Alane for performing so many CO₂ and isotopic analyses for my samples and experiments. I am also grateful for all the help from and the good times with scientists at Livermore: Tom Brown, Chris Swanston, Paula Zermeño and Dot Kurdyla.

My family has given me so much love and support, thanks Mom, Dad, Suzanne, Jeff, Lee, Josh, Adrian and Sprocket. I was very fortunate to form many wonderful new friendships in San Diego and to keep up old friendships from high school and college. I want to thank especially Melissa and Travis, who have been there for everything.

My undergraduate research advisors at Caltech, Karena McKinney and Paul Wennberg, were wonderful mentors whose encouragement guided my path toward graduate studies and atmospheric research. I want to thank Britt Stephens for his constant friendship and guidance. I sincerely appreciate working with Tom Guilderson, who sacrificed so much time to running our samples on the accelerator and always believed in our project and in me. I want to thank my advisor, Ralph Keeling for providing me the opportunity to study in his lab and for teaching me how to ask the right questions. Finally, I would like to express my deep gratitude to Dr. Charles David Keeling for his tremendous contributions to our field and to society.

VITA

- 2001 B.S., Chemical Engineering
California Institute of Technology
- 2003 M.S., Earth Sciences
Scripps Institution of Oceanography,
University of California, San Diego
- 2008 Ph.D., Earth Sciences
Scripps Institution of Oceanography,
University of California, San Diego

PUBLICATIONS

Graven, H.D., T.P. Guilderson and R.F. Keeling, 2007: Methods for High-precision ^{14}C AMS Measurement of Atmospheric CO_2 at LLNL. *Radiocarbon*, **49(2)**, 349-356.

PRESENTATIONS

Graven, H.D., B.B. Stephens, J.B. Miller, R.F. Keeling, C. Gerbig, J. Lin and S.C. Wofsy, 2003: Airborne flask measurements of O_2/N_2 , Ar/N_2 , CO_2 , and other species during COBRA-NA 2003, *American Geophysical Union Fall Meeting*, San Francisco.

Graven, H.D., T.P. Guilderson, R.F. Keeling and C.D. Keeling, 2005: Developing precise measurements of background $^{14}\text{CO}_2$, *7th International Carbon Dioxide Conference*, Boulder.

Guilderson, T.P., H.D. Graven, K. Caldeira, R.F. Keeling and C.D. Keeling, 2005: $^{14}\text{CO}_2$ Measurements on the Scripps Flask Archive - A Unique Tool to Study the Carbon Cycle, *17th Annual Frontiers of Science Symposium of the National Academy of Sciences*, Irvine.

Graven, H.D., T.P. Guilderson and R.F. Keeling, 2006: High-precision AMS ^{14}C measurements on atmospheric CO_2 samples at CAMS, *19th International Radiocarbon Conference*, Oxford.

Graven, H.D., B.B. Stephens, R.F. Keeling, T.P. Guilderson, T.L. Campos and D.S. Schimel, 2006: Identifying CO_2 sources with vertical profiles of $^{14}\text{CO}_2$ above Colorado, *American Geophysical Union Fall Meeting*, San Francisco.

Graven, H.D., T.P. Guilderson and R.F. Keeling, 2007: Developing high-precision measurements of $^{14}\text{CO}_2$ for carbon cycle studies, *North American Carbon Program Investigators Meeting*, Colorado Springs.

Graven, H.D., T.P. Guilderson and R.F. Keeling, 2007: Measurements of $^{14}\text{CO}_2$ from the Scripps CO_2 Program, *14th WMO/IAEA Meeting of Experts on Carbon Dioxide, Other Greenhouse Gases, and Related Tracer Measurement Techniques*, Helsinki.

Graven, H.D., T.P. Guilderson and R.F. Keeling, 2007: New Observations of Regional Variability in Delta- ^{14}C of Background CO_2 from the Scripps CO_2 Program, *American Geophysical Union Fall Meeting*, San Francisco.

ABSTRACT OF THE DISSERTATION

Advancing the use of radiocarbon in studies of global and regional carbon cycling with high precision measurements of ^{14}C in CO_2 from the Scripps CO_2 Program

by

Heather Dawn Graven

Doctor of Philosophy in Earth Sciences

University of California, San Diego, 2008

Professor Ralph Keeling, Chair

Measurements of ^{14}C in atmospheric CO_2 have served as a powerful geochemical tracer since the first observation programs began over 50 years ago. As the nuclear weapons tests of the 1950s and 60s caused an enormous perturbation to natural atmospheric ^{14}C levels, tracking the response of ^{14}C in CO_2 provided a measure of exchange rates between different regions of the atmosphere and between the troposphere and the ocean surface and terrestrial biosphere. Early measurements of $^{14}\text{C}/^{12}\text{C}$, or $\Delta^{14}\text{C}$, in tree rings provided clear evidence that rising CO_2 concentrations were due to human activities by revealing the dilution of ^{14}C in the atmosphere by the combustion of million year old fossil carbon, a process termed the “Suess Effect”.

This thesis aimed to continue and expand the use of $\Delta^{14}\text{C}$ in atmospheric CO_2 for investigating carbon cycle dynamics. Since much of the excess ^{14}C derived from nuclear weapons testing has been redistributed into oceanic and biospheric reservoirs, trends and gradients in $\Delta^{14}\text{C}$ of CO_2 have diminished to levels that are nearly commensurate with measurement precision at most laboratories. Development of improved methods for $\Delta^{14}\text{C}$ analysis by accelerator mass spectrometry at Lawrence Livermore National Laboratory advanced measurement uncertainty to $\pm 1.7\text{‰}$.

Application of the improved analytical procedures to an archive of CO₂ samples from the Scripps CO₂ Program produced 2-15 year monthly time series of $\Delta^{14}\text{C}$ at seven global sampling stations. The high precision observations show variability in the secular trend of $\Delta^{14}\text{C}$ that could enable new insights to the climatic influences on CO₂ exchange. Measurement of a shift in the $\Delta^{14}\text{C}$ gradient between the Northern and Southern Hemispheres since the 1980s also places constraints on regional fluxes of carbon, with particular relevance to Southern Ocean dynamics. The measurements presented here contribute significantly to the amount and global coverage of recent $\Delta^{14}\text{C}$ observations available to the community.

The thesis also demonstrates the application of $\Delta^{14}\text{C}$ measurements for identifying fossil fuel-derived CO₂ in vertical profiles sampled by aircraft. Similar measurements could be used to distinguish regional sources of industrial or biospheric CO₂ or to investigate the mixing of surface CO₂ fluxes in the troposphere.

Chapter 1:

Introduction

Through his careful measurements of atmospheric composition, Charles David Keeling found that the concentration of carbon dioxide in air is increasing. Hans Suess demonstrated that the added CO₂ was derived from fossil fuels by examining records of atmospheric radiocarbon (¹⁴C) stored in tree rings. These two discoveries uncovered a “large-scale geophysical experiment,” in the words of Roger Revelle, which has formed the basis of an interdisciplinary field of research.

Investigation of the exchanges of carbon driving the observed concentrations of CO₂ in the atmosphere has been carried out by hundreds of scientists using various analytical techniques. We have learned that the amount of CO₂ accumulated in the atmosphere, the “airborne fraction”, is only about half of the estimated CO₂ emitted by the combustion of fossil fuels and by cement manufacture (Keeling et al., 1976; Denman et al., 2007). The relative uptake of anthropogenic carbon by the ocean and the terrestrial biota, and the specific regions where such processes occur, are not yet fully understood.

Several tools have contributed to our understanding of global carbon fluxes. Measurements of the ratios O₂/N₂ and ¹³C/¹²C in CO₂, which are influenced more by terrestrial than oceanic CO₂ exchanges, suggest that 50-75 % of the CO₂ removed from the atmosphere in the past 15-20 years has been taken up by the ocean while the remaining fraction was incorporated into terrestrial biota

(Ciais et al., 1995; Keeling et al., 1996; Battle et al., 2000; Manning and Keeling, 2006). Developments in atmospheric and oceanic transport modeling and data assimilation have additionally aided in constraining the land-ocean partitioning of CO₂ uptake and in investigating the regions serving as net sources or sinks of CO₂ (Fan et al., 1998; Bousquet et al., 2000; Gurney et al., 2002). However, uncertainties in the land-ocean partitioning of CO₂ sinks are roughly 25 % and regional flux estimates often have uncertainties of ± 100 % or more (Le Quéré et al., 2003; Stephens et al., 2007). Innovation of different techniques to investigate carbon cycling are urgently needed to improve our understanding and prediction of the global response to continued anthropogenic emissions of CO₂.

Radiocarbon, or ¹⁴C, in CO₂ is a unique tracer of carbon fluxes. ¹⁴CO₂ is sensitive to the turnover rates of oceanic and biospheric carbon reservoirs, which currently contribute key uncertainties to projections of future CO₂ concentrations (Sarmiento and Gruber, 2002; Friedlingstein et al., 2003). Radiocarbon measurements also have the potential to help constrain estimates of CO₂ emissions from fossil fuel combustion. Estimates of fossil fuel emissions are currently formulated using economic inventories (Marland et al., 2007), but it is likely such inventories will become less reliable as CO₂ emissions acquire value through government regulation (Nisbet, 2005).

Applications of ¹⁴CO₂ measurements to recent carbon cycle studies at global or continental scales have thus far been limited by a lack of sufficient measurement coverage and by small atmospheric gradients that are close to the measurement precision available at most laboratories. This thesis has aimed to advance the use of radiocarbon in studies of the carbon cycle through the achievement of these goals:

1. Development of high precision measurements of ¹⁴C/¹²C, or $\Delta^{14}\text{C}$, in CO₂ to enable detection of small atmospheric gradients
2. Analysis of an archive of CO₂ samples from the Scripps CO₂ program to describe global variability of $\Delta^{14}\text{C}$ at clean air stations

3. Identification of processes driving $\Delta^{14}\text{C}$ variability and changing patterns of $\Delta^{14}\text{C}$
4. Demonstration of the use of $\Delta^{14}\text{C}$ to identify fossil and biospheric additions of CO_2 in regional studies of carbon cycling

The following sections of the introduction provide background information on radiocarbon and radiocarbon measurements and summarize the main findings of the thesis chapters.

1.1 Background

Radiocarbon, or ^{14}C , is a rare isotope of carbon, having an abundance roughly 10^{-12} times that of ^{12}C (Libby, 1946; Libby et al., 1949). Cosmic radiation produces ^{14}C naturally in the atmosphere through a cascade of reactions forming neutrons that react with atmospheric nitrogen. The amount of cosmic radiation entering the atmosphere is modulated spatially by the Earth's magnetic field and temporally by the activity of the Sun, where a more active sun shields cosmic radiation and reduces natural ^{14}C production in the atmosphere (Lingenfelter, 1963). Cosmogenically produced ^{14}C atoms form $^{14}\text{CO}_2$, mostly by initial formation of ^{14}CO , which is oxidized to $^{14}\text{CO}_2$ in a matter of months, but also by a small amount of direct formation of $^{14}\text{CO}_2$ (MacKay et al., 1963).

Radiocarbon decays with a half-life of 5730 ± 40 years (Godwin, 1962). Measurements of the extent of radiocarbon decay have provided a powerful means of determining the age of carbon-containing material. The age of a carbon sample refers to amount of time elapsed since that material became isolated from CO_2 in the atmosphere.

Measurements of ^{14}C used for geochemical studies are usually reported in $\Delta^{14}\text{C}$ notation (Stuiver and Polach, 1977). $\Delta^{14}\text{C}$ is a measure of $^{14}\text{C}/^{12}\text{C}$ in part per thousand deviation from the Modern Standard, defined using the reference material "Oxalic Acid I". $\Delta^{14}\text{C}$ values incorporate two corrections. The first

correction accounts for the decay of a sample between the time of isolation from the atmosphere and the time of analysis. For the CO₂ measurements presented in this thesis, samples that had been archived for 15 years decayed by approximately 2 ‰. The second correction is applied to account for mass dependent fractionation using knowledge of the stable isotope ratio $\delta^{13}\text{C}$ in the sample, which may be measured in a contemporaneous sample. Samples are normalized to a $\delta^{13}\text{C}$ level of -25 ‰. $\Delta^{14}\text{C}$ is thus approximated by:

$$\Delta^{14}\text{C} = \left(\frac{R}{R_s} e^{-\lambda t} - 1 \right) (10^3 - 2(\delta^{13}\text{C} + 25)) - 2(\delta^{13}\text{C} + 25) \quad (1.1)$$

where R is the measured ratio $^{14}\text{C}/^{12}\text{C}$ and R_s is the ratio $^{14}\text{C}/^{12}\text{C}$ in the Modern Standard. t is the number of years elapsed between sampling and analysis and λ is the decay constant for radiocarbon: 8267 yr. Note that in this thesis geochemical samples with age correction are expressed as $\Delta^{14}\text{C}$, as in Equation 1.1, whereas Stuiver and Polach (1977) refer to geochemical samples with age correction as simply Δ .

By utilizing the $\Delta^{14}\text{C}$ notation, we can eliminate the influence of processes that fractionate carbon isotopes based on mass. This transforms ^{14}C into a unique tracer that responds differently than CO₂ concentration or $\delta^{13}\text{C}$ to fluxes of carbon. $\Delta^{14}\text{C}$ in atmospheric CO₂ is only influenced by exchanges of carbon carrying a $\Delta^{14}\text{C}$ signature that is different than the atmosphere. The $\Delta^{14}\text{C}$ of carbon will change by radioactive decay over the residence time of the carbon in the ocean or in terrestrial organic matter. Fossil fuels present the extreme case where radioactive decay has removed ^{14}C entirely. Conversely, cosmogenic production of radiocarbon creates ^{14}C atoms but has no effect on ^{12}C or ^{13}C .

$\Delta^{14}\text{C}$ in CO₂ changed substantially during the 20th century because of two different anthropogenic perturbations. The first, as mentioned above, is the dilution of ^{14}C in the atmosphere by fossil fuel-derived CO₂ containing only stable isotopes of carbon. The second anthropogenic perturbation came from the period of intensive testing of nuclear weapons during the 1950s and early 1960s, where the production of excess ^{14}C from numerous detonations nearly doubled the natural

inventory. Nuclear power generation also contributes a small, but ongoing anthropogenic source of ^{14}C to the atmosphere. ^{14}C currently produced by nuclear power sources is thought to be small, however, these point sources may be important in interpreting regional patterns of $\Delta^{14}\text{C}$ in the Northern Hemisphere (Levin et al., 2003, 2008).

1.2 Atmospheric measurements

The longest continuous record of $\Delta^{14}\text{C}$ in CO_2 began in 1954 at Wellington, New Zealand (Rafter and Fergusson, 1957; Manning et al., 1990). Several other measurement stations were instituted around that time, owing to the International Geophysical Year in 1957 and monitoring of fallout from nuclear weapons testing. The early measurements were conducted by counting decay rates of pure CO_2 samples which were collected by absorption in alkaline solutions. This method of sampling and analysis is still in practice by several laboratories (Levin and Kromer, 2004; Manning et al., 1990). Many other laboratories use accelerator mass spectrometry (AMS) to measure $\Delta^{14}\text{C}$. AMS measurement techniques are advantageous as they require much shorter analysis times and much smaller carbon samples.

1.3 ^{14}C in carbon cycle studies

Natural ^{14}C is a useful tracer of carbon in the earth system because it serves as a clock recording the residence time of carbon in different reservoirs. For instance, oceanic measurements of $\Delta^{14}\text{C}$ in dissolved inorganic carbon have helped to define large-scale oceanic circulation by demonstrating the age of water masses in different regions (Stuiver et al., 1983).

Excess ^{14}C from weapons testing has also served as a useful tracer. As most ^{14}C was initially deposited in the northern stratosphere, observing the rate at which the pulse of excess ^{14}C entered the troposphere provided a measure of the

stratosphere-troposphere exchange time (Lal and Rama, 1966). Similarly, inter-hemispheric exchange rates could be observed by comparing $\Delta^{14}\text{C}$ in tropospheric air from both hemispheres (Nydal and Lövseth, 1965; Lal and Rama, 1966). Studies have utilized atmospheric $\Delta^{14}\text{C}$ observations (Hesshaimer et al., 1994; Naegler et al., 2006), oceanic survey data (Broecker et al., 1985; Sweeney et al., 2007) or both (Lassey et al., 1996; Krakauer et al., 2006), to estimate the air-sea exchange time of CO_2 and the oceanic uptake of anthropogenic CO_2 . Bomb-derived ^{14}C has also been utilized in estimates of biospheric carbon residence time, for individual components (Trumbore, 2000) and for whole ecosystems (Goudriaan, 1992; Randerson et al., 2002).

1.4 Continued interest in atmospheric measurements of $^{14}\text{CO}_2$

Though atmospheric gradients in atmospheric $^{14}\text{CO}_2$ have greatly diminished since the conclusion of weapons testing, $\Delta^{14}\text{C}$ in atmospheric CO_2 is still influenced by exchanges of carbon that are not well understood (Levin and Hesshaimer, 2000; Guilderson et al., 2000). Continued measurement of $\Delta^{14}\text{C}$ in CO_2 therefore has potential to produce new insights on carbon cycling, particularly for fluxes that are important for predicting atmospheric CO_2 concentrations in the future.

The Suess Effect, whereby atmospheric ^{14}C is diluted by fossil fuel emissions, alters $\Delta^{14}\text{C}$ in atmospheric CO_2 on various scales. Observations of $\Delta^{14}\text{C}$ distinguish local additions of fossil fuel CO_2 , which may be used to estimate fossil fuel emissions within a catchment area (Levin et al., 2003). Observations of the secular trend in background $\Delta^{14}\text{C}$ also has the potential to constrain global fossil fuel emissions of CO_2 , providing an independent verification of economic inventories (Nisbet, 2005).

An important influence on atmospheric gradients of $\Delta^{14}\text{C}$ is the air-sea

exchange of old waters depleted in $\Delta^{14}\text{C}$ in the Southern Ocean (Levin and Hesshaimer, 2000). As the fluxes of CO_2 in the Southern Ocean comprise significant uncertainty in global carbon budgets and projections of CO_2 concentration (Friedlingstein et al., 2003), $\Delta^{14}\text{C}$ observations in the atmosphere could provide constraints on the dynamics of the Southern Ocean (Levin and Hesshaimer, 2000; Randerson et al., 2002). Air-sea exchange in other regions of deep upwelling (i.e. the Northwest Pacific) may also produce detectable influences on atmospheric $\Delta^{14}\text{C}$.

The turnover rate of the land biosphere is an important determinant of the potential for terrestrial biota to serve as a sink of anthropogenic CO_2 . As the excess ^{14}C absorbed by the terrestrial biosphere is released back into the atmosphere, the rate and magnitude of this release will influence $\Delta^{14}\text{C}$ in CO_2 and provide a measure of the average biospheric residence time of carbon (Caldeira et al., 1998; Randerson et al., 2002).

High precision measurements of $\Delta^{14}\text{C}$ in background CO_2 with global coverage continuing over long periods are an essential component to these applications of $\Delta^{14}\text{C}$ (Levin and Hesshaimer, 2000).

1.5 Achievements in measurement precision

Investigations of the carbon cycle using ^{14}C have been instrumental to our understanding of exchange rates and mixing of carbon through different reservoirs. Measurements of $\Delta^{14}\text{C}$ in CO_2 will continue to provide insights to carbon cycling as long as spatial and temporal gradients of interest can be detected by available analytical techniques.

Through extensive testing and development of analysis procedures, we have achieved routine measurement of CO_2 samples with 1.7 ‰ reproducibility at the Center for Accelerator Mass Spectrometry (CAMS) at Lawrence Livermore National Laboratory (LLNL). Early results of the method development were pre-

sented at the 19th International Radiocarbon Conference in Oxford, UK in April 2006 and published in *Radiocarbon* in 2007.

Advances were made by introducing new reference materials for $\Delta^{14}\text{CO}_2$ analysis and by conducting careful uncertainty analysis on repeated measurements. The new reference materials, “Cyl-1” and “Cyl-2,” are CO_2 extracted from two compressed air cylinders that were filled with clean air from the atmosphere. The usual reference materials used for $\Delta^{14}\text{C}$ are composed of oxalic acid, wood and sucrose. CO_2 from whole air cylinders is similar in composition and undergoes similar handling procedures as the CO_2 from whole air flask samples. We found that analysis of the primary oxalic acid standard, OXI, introduced significant uncertainty to the $\Delta^{14}\text{C}$ measurements. Using measurements of “Cyl-1,” we developed an alternative normalization method to eliminate uncertainty contributed by OXI. Other improvements to sample handling and analytical conditions additionally improved the reproducibility of $\Delta^{14}\text{C}$ in CO_2 .

The progress achieved in analytical and data processing techniques as part of this thesis enables the detection of smaller gradients in $\Delta^{14}\text{C}$, as required to apply contemporary measurements to carbon cycle studies. The measurement capability we developed at LLNL can continue to be applied to samples from the Scripps CO_2 Program as well as other programs, including, for example, the Ameriflux observational tower network. Our work can also assist other laboratories with their own development of high precision measurements of $\Delta^{14}\text{C}$ in CO_2 . We will be formulating Chapter 2 into a publication to provide guidelines for other AMS laboratories to incorporate whole air reference cylinders into their measurement and data processing routines.

1.6 Measurements from the Scripps CO₂ Program

The Scripps CO₂ Program provided a unique opportunity to produce long time series of $\Delta^{14}\text{C}$ in CO₂ by collecting and archiving pure CO₂ samples from a set of global sampling stations. This thesis presents measurements of $\Delta^{14}\text{C}$ in 674 clean air CO₂ samples from the Scripps CO₂ Program. Monthly observations from 7 sampling sites were achieved, comprising 15 years of data at La Jolla, California, 7 years at Point Barrow, Alaska and the South Pole, 6 years at Kumukahi and Mauna Loa, Hawaii and American Samoa, and 2 years at Palmer Station, Antarctica.

Measurements of $\Delta^{14}\text{C}$ in CO₂ from La Jolla since 1992 are presented in Chapter 3. The secular trend and seasonal cycle of $\Delta^{14}\text{C}$ is examined, and influences on variability over these timescales are discussed.

Measurements of $\Delta^{14}\text{C}$ in CO₂ from all stations in the Scripps network are presented in Chapter 4. Trends and seasonal cycles are compared between all of the stations. The latitudinal gradient in annual mean $\Delta^{14}\text{C}$ is presented and discussed in reference to prior measurements of latitudinal differences.

These measurements have been presented at several conferences, including the 14th WMO/IAEA Meeting of Experts on Carbon Dioxide, Other Greenhouse Gases, and Related Tracer Measurement Techniques in Helsinki, Finland and the North American Carbon Program Investigators Meeting in Colorado Springs in 2007. We are currently preparing manuscripts to publish these observations.

1.7 Airborne measurements of ^{14}C

Measurements of $\Delta^{14}\text{C}$ were also performed on CO₂ samples collected as part of an airborne field campaign over Colorado in 2004: the Airborne Carbon in the Mountains Experiment (ACME). These measurements, presented in Chapter 5, were included in an oral presentation at the American Geophysical Union Fall

Meeting in 2006 and in a seminar to the San Diego State University Ecology and Evolutionary Biology Department in October 2007. Chapter 5 is in preparation to be submitted for publication.

Airborne sampling allowed observations of $\Delta^{14}\text{C}$ in CO_2 at surface levels, through the boundary layer and up to the free troposphere in urban and rural locations in Colorado. These measurements resolved vertical gradients in $\Delta^{14}\text{C}$ created by surface fluxes of CO_2 and by diurnal mixing. By using $\Delta^{14}\text{C}$ to distinguish and quantify the amount of the fossil fuel CO_2 present at each vertical level, we were able to identify air that experienced net biospheric uptake or release of CO_2 . Building on the measurements conducted here, airborne sampling for $\Delta^{14}\text{C}$ measurements in future studies could be employed to estimate regional fluxes of biospheric and fossil fuel CO_2 , or to investigate vertical mixing of air and the “rectifier” effect.

1.8 Contribution of the Scripps $\Delta^{14}\text{CO}_2$ dataset

The achievement of new high precision time series of $\Delta^{14}\text{C}$ in atmospheric CO_2 with global coverage will serve as a substantial contribution to the carbon cycle community. This new dataset greatly expands the number of recent $\Delta^{14}\text{C}$ observations and provides the most extensive global coverage from a single laboratory. Interpretation of these data with atmospheric transport modeling, simple box diffusion models and by correlation with other carbon cycle tracers are likely to improve our understanding of gross carbon fluxes from fossil fuel combustion, Southern Ocean ventilation and the turnover of carbon in northern ecosystems.

Chapter 2:

Methods for High Precision

Analysis of $\Delta^{14}\text{C}$ in CO_2

ABSTRACT

Development of ^{14}C analysis with precision better than 2 ‰ has the potential to expand the utility of $^{14}\text{CO}_2$ measurements for carbon cycle investigations as atmospheric gradients currently approach the typical measurement precision of 2-5 ‰. The Accelerator Mass Spectrometer (AMS) at Lawrence Livermore National Laboratory (LLNL) produces high and stable beam currents that enable efficient acquisition times for large numbers of ^{14}C counts. One million ^{14}C atoms can be detected in approximately 25 minutes in modern samples, suggesting that near 1 ‰ counting precision is economically feasible at LLNL. Overall uncertainty in measured $\Delta^{14}\text{C}$ is larger than the counting uncertainty because of additional uncertainty from sample handling and analysis. Measurements of replicate samples of CO_2 extracted from a whole air cylinder (Cyl-1) revealed that the additional sources of uncertainty in the usual preparation and analysis procedures at LLNL were considerable. We made various changes to improve the sample handling and analysis procedures. A main source of uncertainty was found to be the poor reproducibility in Oxalic Acid I (OXI) standard samples, which are used in data normalization but prepared differently than CO_2 samples. To eliminate the uncer-

tainty contributed by OXI, we replaced OXI with Cyl-1 in the data normalization. We have additionally conducted experiments to test the extraction of CO₂ from whole air samples in slightly different flasks from the Atmospheric Oxygen Research Group to enable measurement of $\Delta^{14}\text{C}$ and $\delta^{13}\text{C}$ at Palmer Station. The improvements we have made at LLNL have successfully advanced the measurement reproducibility to 1.7 ‰ in $\Delta^{14}\text{C}$.

2.1 Introduction

The first measurements of $^{14}\text{CO}_2$ in the atmosphere began in 1954, even before atmospheric CO₂ concentration was accurately known (Rafter, 1955). These early measurements captured enormous changes in atmospheric $^{14}\text{CO}_2$ during the intense period of nuclear testing in the 1950s and 60s (Levin et al., 1985; Nydal and Lovseth, 1983; Manning et al., 1990; Levin and Kromer, 2004). The addition of bomb-derived excess ^{14}C approximately doubled the natural atmospheric inventory of ^{14}C .

Excess ^{14}C has since been distributed throughout the atmosphere and into the oceanic and terrestrial biospheric carbon reservoirs according to natural exchange processes. This redistribution has led to a steady decline in the spatial and temporal gradients of $^{14}\text{CO}_2$ in the atmosphere (Figure 2.1). The evolution of tropospheric $\Delta^{14}\text{C}$ has been measured throughout the past five decades and used in many applications, including studies of atmospheric mixing, air-sea gas exchange rates, oceanic uptake of anthropogenic CO₂, and carbon turnover rates in various ecosystems (e.g. Nydal 1968; Naegler et al. 2006; Trumbore 2000).

The main objective of this thesis work was to produce high precision time series of $\Delta^{14}\text{C}$ in atmospheric CO₂, continuing observations from other laboratories of the trend and variability in $^{14}\text{CO}_2$ resulting from recent carbon fluxes. We have measured $\Delta^{14}\text{C}$ in archived CO₂ that was sampled at a set of background air stations as part of the Scripps CO₂ Program, initiated by Charles D. Keeling.

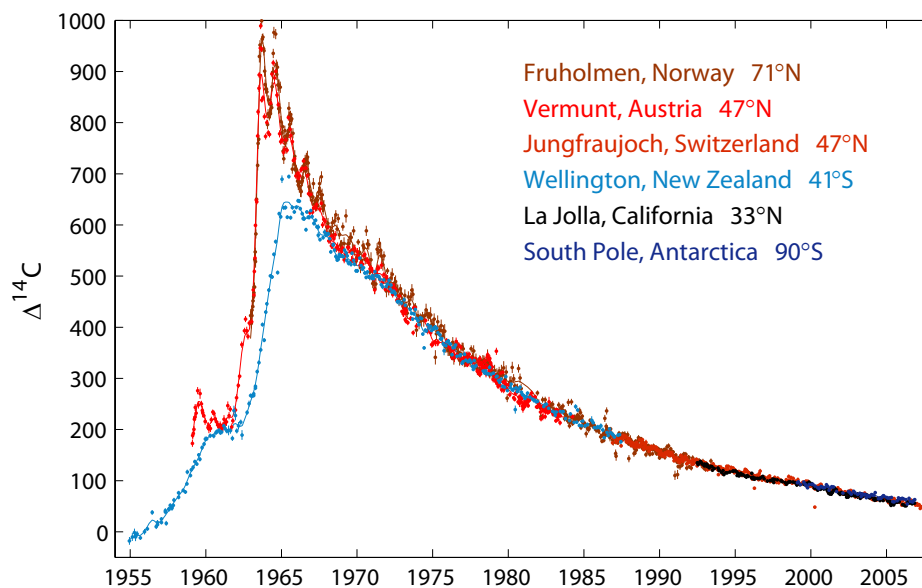


Figure 2.1: Records of atmospheric $\Delta^{14}\text{C}$. In red colors are measurements from Fruholmen, Norway (Nydal and Lovseth, 1983), Vermunt, Austria and Jungfrau-joch, Switzerland (Levin et al., 1985; Levin and Kromer, 2004). Measurements from Wellington, New Zealand (Manning et al., 1990) are shown in light blue. Also shown are measurements from this work at La Jolla, California and the South Pole, Antarctica.

Figure 2.1 shows measurements of $\Delta^{14}\text{C}$ in atmospheric CO_2 conducted by several laboratories, including measurements from La Jolla, California and the South Pole, Antarctica that will be presented in later chapters of this thesis.

In the 1960s, seasonal and spatial gradients of 100-400 ‰ were observed in the atmosphere (Figure 2.1). Over the past 5 to 15 years, when samples began to be collected for the Scripps CO_2 archive, spatial gradients and seasonal variations in background $\Delta^{14}\text{C}$ have become much smaller, less than 10 ‰ on an annual basis.

Though current gradients are small, variation in $^{14}\text{CO}_2$ still reflects carbon exchanges with the atmosphere as different sources of CO_2 have distinct ^{14}C signatures (Levin and Hesshaimer, 2000). The interest in $\Delta^{14}\text{C}$ of CO_2 for investigations of the carbon cycle today lies in the ability of ^{14}C to trace fossil fuel combustion sources of CO_2 to the atmosphere, distinguish average turnover rates

of carbon in terrestrial ecosystems, and quantify regional oceanic CO₂ exchanges.

Measurements of atmospheric $\Delta^{14}\text{C}$ may continue to be an important tool in global and regional carbon cycle studies; however, their utility is limited by measurement precision. Current precision in atmospheric $^{14}\text{CO}_2$ analysis for counting and AMS techniques at most laboratories is 2-5 ‰ (Levin and Kromer, 2004; Meijer et al., 2006; Turnbull et al., 2007), similar to the seasonal and spatial variability in some regions.

One of the goals of this dissertation work was to demonstrate improvement of the $\Delta^{14}\text{C}$ measurement reproducibility to a level that would enable better resolution of small atmospheric gradients (< 2 ‰). Enhanced precision could expand the use of ^{14}C for identifying and quantifying carbon fluxes.

Improvement in $\Delta^{14}\text{C}$ measurement precision first requires the detection of a larger number of ^{14}C atoms to reduce the Poisson counting uncertainty ($1/\sqrt{n}$). Acquiring enough ^{14}C counts for a counting uncertainty near 1 ‰ increases the AMS analysis time by a factor of four compared to a counting uncertainty of 2 ‰. Rapid ^{14}C count rates are necessary to reduce the cost of such high precision analyses. The High Voltage Electronics Corporation (HVEC) FN Tandem accelerator facility at the Center for Accelerator Mass Spectrometry, Lawrence Livermore National Laboratory (Davis, 1989; Davis et al., 1990), is capable of count rates between 500-1000 counts per second for modern samples of 25-80 $\mu\text{mol C}$ (0.3-1 mg C). This is accomplished through a high efficiency cesium sputter ion source ($\sim 35\%$ C⁻ production efficiency) and wide-open beam transport that essentially eliminates beam losses (Southon and Roberts, 2000; Fallon et al., 2007).

Counting uncertainty is not the only factor that limits the precision attainable in radiocarbon measurements. Additional uncertainty may be introduced during sampling, CO₂ extraction and graphitization. Machine instabilities and differences in the character and behavior of graphite targets during analysis will also contribute to the AMS measurement uncertainty. We have attempted to identify and remove some of these uncertainties by introducing several improvements to

the standard procedures at LLNL.

Much of the reduction in measurement uncertainty at LLNL was enabled by the implementation of new reference materials for ^{14}C in CO_2 . These are CO_2 extracted from two whole air cylinders, “Cyl-1” and “Cyl-2”. The new CO_2 reference materials are handled in exactly the same manner as similar reference materials for stable isotope analysis at Scripps and in nearly the same way as the CO_2 from flask samples in the Scripps Program. These new materials allowed uncertainties to be estimated by measuring replicate samples of reference CO_2 that undergo the same handling and analysis procedures as unknown CO_2 samples.

We have realized significant methodological improvements in this work. The major achievements have been:

1. The creation of new reference materials for $\Delta^{14}\text{C}$ in CO_2
2. The identification and minimization of several sources of uncertainty in sample handling, analysis and data processing
3. The establishment of a standard procedure for preparation and analysis of high-precision $\Delta^{14}\text{C}$ in CO_2 samples at LLNL, including a new method of data normalization

These advancements have enabled an overall measurement uncertainty of 1.7 ‰ in the Scripps CO_2 samples.

A journal article outlining the early results and uncertainty analysis of methodological improvements at LLNL was published in 2007 (Graven et al., 2007). This chapter includes and expands on the material presented in the 2007 paper and provides a more detailed description of the methodology developed specifically for high-precision measurements of $\Delta^{14}\text{C}$ in Scripps CO_2 samples at LLNL. A new method of data normalization is introduced, utilizing the Cyl-1 reference material. Special treatment of early measurements that could not be normalized with Cyl-1 is outlined. This chapter also includes the results of several experiments testing

different types of flasks for whole air sampling and investigating the potential for a single 5 liter air sample to provide 2 separate samples of pure CO₂.

2.2 Flask sampling

The Scripps CO₂ Program uses 5 liter glass flasks to sample whole air at background sampling stations. The flasks are evacuated in the Scripps laboratory and then shipped to the sampling site. To collect an air sample, the evacuated flask is exposed by opening the greased stopcock and waiting a few seconds for the flask to fill to the local atmospheric pressure. At La Jolla 6 flasks are sampled at once, at Mauna Loa, Samoa, and South Pole flasks are sampled in triplicate and at Kumukahi and Point Barrow flasks are sampled in duplicate. Flasks are stored in the shade to prevent photochemical degradation of the grease and may be stored for several months before their return to the Scripps laboratory and subsequent analysis.

2.3 Analysis of CO₂ concentration

Upon return to Scripps, all flasks are analyzed for CO₂ concentration with an Applied Physics Corporation infrared gas analyzer. The measurement uncertainty is 0.1 parts per million (ppm), where CO₂-in-air reference gases are calibrated by manometric measurements (Keeling et al., 2002). Replicate flasks must agree within 0.4 ppm and must fall within 3- σ of the value projected by a function combining an exponential trend, 4 harmonics, annual gain factor and smoothing spline (Keeling et al., 1989), otherwise the flask samples are rejected.

2.4 Extraction of CO₂ from flasks

Following analysis of CO₂ concentration, the remaining whole air inside a flask sample is used to produce a pure CO₂ sample. The CO₂ is extracted from

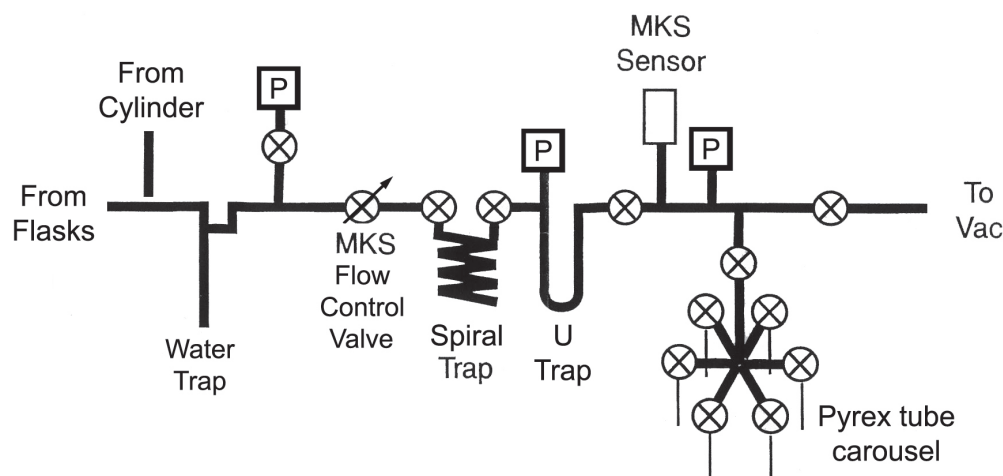


Figure 2.2: Schematic of the vacuum manifold used to perform CO₂ extractions from whole air flask samples and from whole air reference cylinders at Scripps.

whole air cryogenically in the laboratory at Scripps. The extraction procedure uses a glass vacuum manifold, depicted in Figure 2.2. The air is first dried with cold traps immersed in a mixture of dry ice and ethanol. Then the air is passed through a spiral trap immersed in liquid nitrogen at a flow rate of 0.2 L/min for 10 minutes, producing a CO₂ sample of 25-40 $\mu\text{mol C}$ (0.3-0.5 mg C) from approximately 2 L of air. An additional liquid nitrogen bath is placed around a U trap downstream of the spiral trap (Figure 2.2) during the extraction to ensure that all CO₂ is removed. The flow rate is maintained by a control valve upstream of the spiral trap using an MKS flow controller. After the 10-minute extraction is complete, the remaining air is evacuated from the manifold. Then, the liquid nitrogen bath is removed from the U trap and the spiral trap is heated to sublime the frozen CO₂ sample. The sample is transferred into one of six Pyrex® tubes by immersing the Pyrex® tube in liquid nitrogen. When the transfer is complete, the tube is sealed by heating with a custom Ruska fusing system. Tubes are labeled with the extraction number, sampling and extraction dates, fuser number and the user's initials. The CO₂ samples contained in the Pyrex® tubes are stored in a drawer anywhere from a few days to over 15 years.

2.5 Extraction of CO₂ from reference cylinders

CO₂ in whole air is stored in cylinders for continual use as a reference material for both stable isotope and ¹⁴C analysis. Air from these reference cylinders is extracted to produce pure CO₂ samples using the same equipment as for the flask samples. To adjust the vacuum line to receive air from a cylinder instead of a flask, a section of glass tubing is removed and the vacuum line is connected to the regulator of the reference cylinder using Synflex® and copper tubing as shown in Figure 2.2. The remaining steps of the extraction are executed in exactly the same manner as the flask extraction. CO₂ samples from reference cylinders are also stored in Pyrex® tubes for several weeks to years.

2.6 Reference cylinders for ¹⁴C

As part of this thesis work, two whole air cylinders were designated as reference cylinders for ¹⁴CO₂ analysis. These cylinders were filled with ambient air at the Scripps Pier in La Jolla in November 2004. The air in both cylinders had CO₂ concentration of 380.5 ± 0.1 ppm. One cylinder, number 55280, was adjusted by spiking with industrial ¹⁴C-dead CO₂ in order to reduce the $\Delta^{14}\text{C}$ of the air. The other cylinder, number 00326, was not adjusted from its initial composition. Stable isotope measurements conducted at SIO showed $\delta^{13}\text{C}$ of -8.55 ± 0.03 ‰ in cylinder 00326 and -9.85 ± 0.03 ‰ in cylinder 55280, after spiking.

The reference CO₂ extracted from these cylinders is referred to as Cyl-1 for 00326 and Cyl-2 for 55280. The best estimate of $\Delta^{14}\text{C}$ in Cyl-1 is 61.0 ± 2.4 ‰, from averaging repeated analyses of Cyl-1 in 121 samples. For Cyl-2, the best estimate of $\Delta^{14}\text{C}$ in Cyl-1 is 11.3 ± 2.4 ‰, from averaging repeated analyses of Cyl-2 in 93 samples. The standard deviation in replicate measurements of Cyl-1 and Cyl-2, 2.4 ‰, reflects the uncertainty in the absolute $\Delta^{14}\text{C}$ in the reference CO₂. This scatter is not an accurate measure of the reproducibility of high-precision CO₂ measurements however, as measurements of the oxalic acid (OXI) primary

reference material were found to have higher uncertainty than measurements of Cyl-1 and Cyl-2. Section 2.11 will describe the measurement uncertainty in more detail.

The ^{14}C reference cylinders were initially filled to 1900 psi in November 2004. As of February 2007, 191 individual extractions had been taken from cylinder 00326 (Cyl-1) and 138 from cylinder 55280 (Cyl-2) with cylinder pressure greater than 1500 psi remaining. 154 Cyl-1 samples and 111 Cyl-2 samples were analyzed by accelerator mass spectrometry; 7 Cyl-1 samples and 7 Cyl-2 samples were analyzed by stable isotope mass spectrometry. Presuming that 25 Cyl-1 and Cyl-2 samples will be analyzed annually, the air in these cylinders should last for more than 10 years, providing a long term reference for high precision $^{14}\text{CO}_2$ analysis of Scripps CO_2 .

2.7 Graphitization and sample handling

CO_2 samples are prepared for AMS analysis at CAMS. First, the CO_2 must be converted to graphite or “graphitized.” Graphitization is achieved by heating the CO_2 sample with H_2 gas and an iron catalyst at 570°C for several hours. The reaction takes place in Kimax® NMR tubes, which are first baked in a 400°C oven for one hour. The tubes are then filled with 5.5 ± 0.3 mg iron powder, which is weighed manually. The iron powder catalyst used for the majority of our work was obtained from Alfa Aesar®.

The vacuum manifold used at CAMS to transfer CO_2 samples into graphitization reactors is depicted in Figure 2.3. The manifold contains 12 individual reactors (labeled d. in Figure 2.3), allowing 12 CO_2 samples to be graphitized concurrently. The reactor tubes with iron powder inside are placed on the vacuum line and evacuated. The reactor tubes are then heated to 400°C with 1 atm of H_2 gas for 1 hour. This “preconditioning” step releases water and CO_2 that may be adsorbed on the iron powder and reduces any CO_2 that is present into CO and

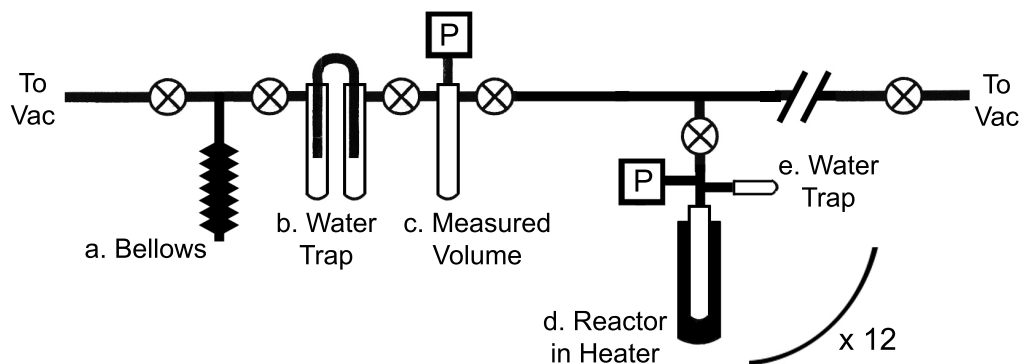


Figure 2.3: Schematic of the vacuum manifold used to transfer CO_2 samples into individual reactors for graphitization at CAMS. The vacuum manifold contains 12 reactors which are configured in the same manner as the reactor pictured here.

CH_4 . The reactor is then evacuated, eliminating potential contaminants.

To transfer a CO_2 sample from a Pyrex® tube into a reactor for graphitization, liquid nitrogen baths are used to freeze the CO_2 sample into consecutive components of the evacuated manifold shown in Figure 2.3. First, the Pyrex® tube containing the CO_2 sample is placed in the bellows (labeled a. in Figure 2.3) and the entire vacuum manifold is evacuated. Once vacuum is achieved, the Pyrex® tube is broken, and the CO_2 sample is expanded over a isopropanol-dry ice cold trap (b. in Figure 2.3) to freeze any water that may be present. Since the air samples are dried during the CO_2 extraction at Scripps, there is normally very little water to remove in this step. Then, the sample is frozen into a glass tube with a known volume (c. in Figure 2.3). 2 minutes are allowed to ensure the CO_2 is completely frozen and the manifold is evacuated once again to remove any non-condensable gases that may be present and that could interfere with the completion of the graphitization reaction. There are usually no measurable non-condensable gases in the Scripps samples. When a couple of samples did exhibit the presence of non-condensable gases, it indicated that the Pyrex® tubes had been compromised and the CO_2 samples contaminated. After evacuation, the sample is allowed to sublime within the known volume and the pressure is noted, allowing a measure of the size of the CO_2 sample. Usually, the Scripps samples are about $40 \mu\text{mol C}$

or 0.45 mg C, with slightly smaller samples from the high altitude sites at Mauna Loa and South Pole. The CO₂ is then transferred into a reactor (d. in Figure 2.3) by freezing into a liquid nitrogen bath. Once all the reactors are filled with CO₂ samples, H₂ gas is added to each reactor in an amount adjusted to each reactor to achieve a stoichiometric ratio of 2.1 mol H₂/mol C. The graphitization reaction proceeds by heating the reactors to 570°C for at least 1.5 hours to as long as 7 hours. The graphitization time depends on the time of day the reaction is started and how many samples are waiting to be graphitized. Each reactor is attached to a small Kimax® NMR tube (e. in Figure 2.3) filled with magnesium perchlorate to trap the water that evolves as the CO₂ is reduced to graphite.

Reference CO₂ from cylinder air, Cyl-1 and Cyl-2, is graphitized in exactly the same manner as the CO₂ from flask samples at CAMS. Each Cyl-1 or Cyl-2 CO₂ sample is transferred into a single reactor, producing one graphite sample.

Additional ¹⁴C reference materials are prepared at CAMS using slightly different procedures. Oxalic acid materials OXI and OXII are commonly used standards in most radiocarbon laboratories. For a short time barley mash materials VIRI A and C were also used as reference material. Both oxalic acid and barley mash materials must be combusted to form CO₂. Before combustion, the barley mash first undergoes an acid-base-acid pretreatment. Combustion proceeds by heating a batch of the material in a 900 °C oven in the presence of copper oxide. Each combustion batch produces 300-500 μmol C (4-6 mg C) in CO₂ gas. After introducing the CO₂ gas into the bellows of the vacuum manifold in Figure 2.3 the CO₂ is split by expanding the gas into a larger volume (not shown in Figure 2.3), allowing 2 minutes to isotopically equilibrate, then transferring an aliquot from the larger volume into a reactor. Reactors are filled to approximately 40 μmol C (0.5 mg C) by transferring 1-3 aliquots of CO₂. Each combustion batch is split into 5-12 individual graphite samples.

Aluminum target holders are used to hold the resulting graphite samples, which are a mixture of graphite and iron powder. The target holders are aluminum

cylinders approximately 1 cm in diameter and 3 cm in length with a 0.052" diameter hole drilled 0.120" into the conically recessed top. The graphite-iron sample is put into the target holder by carefully tapping the glass reactor to drop the graphite-iron sample onto the top of the target holder and using a drill stem to pack the graphite-iron sample into the hole of the target holder. The drill stem is cleaned using sandpaper before transferring each sample. The graphite-iron samples are then pressed into the aluminum target holders using a sample press to ensure consistency in the compaction of the graphite-iron samples. The sample press has a digital pressure gauge. The relationship between the pressure at the head of the drill stem and the gauge pressure has not been determined, restricting the specification of a compaction pressure though still enabling consistency in sample compaction. The gauge generally reads between 9 and 20 at atmospheric pressure. The samples are pressed until the gauge reads 300-400, where the particular value is determined by the user at the beginning of the pressing session. Usually, at least 20 samples are pressed in one session. The user inspects the pressed graphite-iron sample under a microscope to ensure consistency has been achieved and that the sample is pressed firmly enough. A firmly pressed graphite-iron sample has a silver sheen when viewed under a microscope. A graphite-iron sample that is not pressed firmly enough appears black and might have a slight silver sheen; a graphite-iron sample that is pressed too firmly appears silver but grainy. The graphite-iron sample, inside the aluminum sample holder, is referred to as a "target."

During the initial stages of this work, graphite-iron samples were manually pressed into the aluminum target holders using a drill stem and a hammer. The change to a sample press occurred in the spring of 2006 as one of several changes intended to reduce uncertainty and improve consistency in the processing of CO₂ samples (described in Section 2.10).

After pressing, the targets are wrapped in aluminum foil. The foil-wrapped targets are usually analyzed within 5 days of pressing; however, some targets were stored for approximately 2 weeks. Previous experience of T. Guilder-

son at CAMS has demonstrated that a few weeks of storage time does not affect the measured $\Delta^{14}\text{C}$ in the graphite.

2.8 Accelerator Mass Spectrometry

Analysis of $\Delta^{14}\text{C}$ was conducted using the HVEC FN Tandem accelerator facility at CAMS (Davis, 1989; Davis et al., 1990). A schematic of the accelerator configured for ^{14}C detection is pictured in Figure 2.4. The analysis proceeds by thermal ionization of the graphite sample with a cesium sputter source. The iron powder that served as a catalyst during graphitization now serves as a heat conductor and a source of electrons for ionization. The cesium source at CAMS has particularly high production efficiency of approximately 35% (Fallon et al., 2007), which refers to the number of $^{14}\text{C}^-$ ions output from the source divided by the total number of ^{14}C atoms in the sample. The $^{14}\text{C}^-$ and $^{13}\text{C}^-$ atoms generated in the source are injected by the low energy mass spectrometer into the tandem accelerator in sequential pulses. The center of the accelerator is held at +6.5 MV where the negative ions are impacted onto a carbon foil. This impact breaks up any molecular isobars of $^{14}\text{C}^-$ and $^{13}\text{C}^-$ and strips electrons from $^{14}\text{C}^-$ and $^{13}\text{C}^-$ ions. Positive ions are accelerated out of the tandem and $^{14}\text{C}^{4+}$ and $^{13}\text{C}^{4+}$ are selected by the high energy mass spectrometer. The $^{13}\text{C}^{4+}$ ions are directed into an off-axis faraday cup. The $^{14}\text{C}^{4+}$ ions proceed down the beamline, where they are further selected for specific charge, mass and velocity by a rigidity filter and a velocity filter. $^{14}\text{C}^{4+}$ ions are detected by the ionization of an argon-methane gas mixture. The relationship between the rate of energy loss and total energy of the incoming ion characterizes the ionization caused by $^{14}\text{C}^{4+}$. A small amount of $^{14}\text{N}^{4+}$ and $^7\text{Li}^{2+}$ ions may also enter the ionization chamber (Lloyd et al., 1991), however these ions can be identified by the expression of a different relationship between the rate of energy loss and total energy.

The large facility at CAMS enables wide-open beam transport that es-

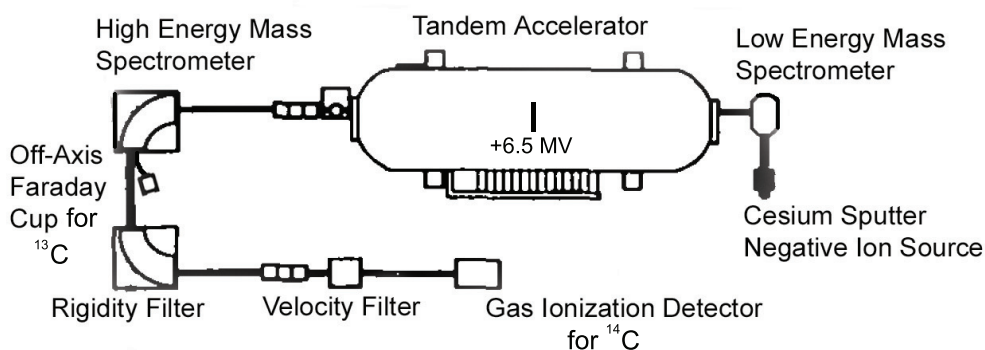


Figure 2.4: Schematic of the accelerator mass spectrometer at CAMS used for ^{14}C analysis (modified from Davis et al. 1990).

essentially eliminates beam losses (Southon and Roberts, 2000; Fallon et al., 2007). This efficiency in beam transport together with the highly efficient cesium source enables count rates between 500-1000 counts per second for modern samples of 25-80 $\mu\text{mol C}$ (0.3-1 mg C).

To perform the AMS analysis, targets are placed in a sample “wheel.” Each wheel constitutes an individual batch of samples that are analyzed together. An example of a wheel of samples is given in Table 2.1. Table 2.1 shows the position of the target, the name of the sample, the minimum and maximum number of counts to be acquired in one sputtering period (Min. Cts. and Max. Cts.), as well as the maximum amount of time for a sputtering period (Max. Time). The information listed in Table 2.1 is the input to the software that controls sample changing during the AMS run. Measurements of $^{14}\text{C}^{4+}/^{13}\text{C}^{4+}$ ratios are acquired by counting $^{14}\text{C}^{4+}$ atoms in the detector and by measuring charge collected in the faraday cup from incident $^{13}\text{C}^{4+}$ atoms. The graphite samples, or targets, are sputtered in periods of ~ 50 -90 seconds, where a period lasts until 50,000 ^{14}C counts are recorded in the detector (Max. Cts., Table 2.1). The targets are sputtered sequentially and the wheel is cycled at least 20 times to perform 20 sputtering periods and acquire one million counts on each target (Min. Reps., Table 2.1). The integrated $^{14}\text{C}/^{13}\text{C}$ ratio is recorded for each sputtering period.

The Warm-up is the number of seconds to wait after beginning sputtering before starting to record data. The Precision gives a minimum in the standard deviation of the raw $^{14}\text{C}/^{13}\text{C}$ ratios between sputtering periods. Up to 4 additional periods (Max. Reprs., Table 2.1) may be performed on a target if the standard deviation in the target's $^{14}\text{C}/^{13}\text{C}$ ratios over the 20 periods exceeds 0.7% (Precision, Table 2.1). This is usually only necessary for one or two targets in each wheel due to an outlier or a low ratio in the first one or two sputtering periods as the target is warming up. A standard deviation of 0.7% in the $^{14}\text{C}/^{13}\text{C}$ ratios of a CO_2 sample translates to a standard error of 1.0-1.5 ‰ in $\Delta^{14}\text{C}$ after averaging over 20 cycles and normalizing to OXI. A target is specified as Kind "S" for the OXI standard and "U" for all other targets. The "S" designation regulates that OXI targets will continue to be analyzed as long as any other target requires more sputtering periods. This is to ensure that there are enough OXI measurements as necessary for the normalization procedure.

The first position on the wheel contains a used target that will be sputtered as the AMS is warming up and anytime the AMS is on but sputtering of an actual sample is not desired. The 5-8 positions after the first target are filled with reference materials that are used to tune the AMS. These reference targets will be sputtered 4-6 times and their ratios will be checked against known values before starting the analysis of actual samples. They will also be used to check the tuning periodically and to re-tune if changes to the electrostatic lens settings need to be made or if the carbon foil inside the accelerator needs to be changed. The rest of the wheel contains at least 6 OXI targets and at least 3 OXII, 3 Cyl-1 and 3 Cyl-2 targets scattered regularly around the wheel. Approximately 15 unknown CO_2 samples are placed on each wheel, interspersed with the reference targets.

The first 15 wheels analyzed as part of this work were filled with close to 64 targets, utilizing all the slots on the wheel. As part of a set of methodological changes that were implemented in the spring of 2006, the number of targets on each wheel was reduced to approximately 30. Decreasing the number of targets

Table 2.1: Example of a wheel loaded for high precision $^{14}\text{CO}_2$ analysis.

Position	Sample Name	Min. Cts.	Max. Cts.	Max. Time	Min. Reps.	Max. Reps.	Warm-up	Precision (%)	Kind
1	Junk	100	15000	200	3	4	20	5	U
2	OXI	100	30000	200	3	4	10	0.8	U
3	OXI	100	30000	200	3	4	10	0.8	U
4	OXII	100	30000	200	3	4	10	0.8	U
5	ANU	100	30000	200	3	4	10	0.8	U
6	TIRI Wood	100	30000	200	3	4	10	0.8	U
7	OXI	100	30000	200	3	4	10	0.8	U
8	OXI	100	30000	200	3	4	10	0.8	U
9	OXI	100	50000	200	20	24	15	0.7	S
10	OXII	100	50000	200	20	24	15	0.7	U
11	Cyl-2	100	50000	200	20	24	15	0.7	U
12	Cyl-1	100	50000	200	20	24	15	0.7	U
13	Sample	100	50000	200	20	24	15	0.7	U
14	OXI	100	50000	200	20	24	15	0.7	S
15	Sample	100	50000	200	20	24	15	0.7	U
16	OXII	100	50000	200	20	24	15	0.7	U
17	Sample	100	50000	200	20	24	15	0.7	U
18	Sample	100	50000	200	20	24	15	0.7	U
19	OXI	100	50000	200	20	24	15	0.7	S
20	Sample	100	50000	200	20	24	15	0.7	U
21	Cyl-1	100	50000	200	20	24	15	0.7	U
22	Sample	100	50000	200	20	24	15	0.7	U
23	Sample	100	50000	200	20	24	15	0.7	U
24	OXI	100	50000	200	20	24	15	0.7	S
25	Sample	100	50000	200	20	24	15	0.7	U
26	Cyl-2	100	50000	200	20	24	15	0.7	U
27	OXII	100	50000	200	20	24	15	0.7	U
28	Sample	100	50000	200	20	24	15	0.7	U
29	Sample	100	50000	200	20	24	15	0.7	U
30	OXI	100	50000	200	20	24	15	0.7	S
31	Sample	100	50000	200	20	24	15	0.7	U
32	Cyl-2	100	50000	200	20	24	15	0.7	U
33	Sample	100	50000	200	20	24	15	0.7	U
34	Sample	100	50000	200	20	24	15	0.7	U
35	OXI	100	50000	200	20	24	15	0.7	S
36	Sample	100	50000	200	20	24	15	0.7	U
37	Cyl-1	100	50000	200	20	24	15	0.7	U
38	Sample	100	50000	200	20	24	15	0.7	U
39	Sample	100	50000	200	20	24	15	0.7	U
40	Spare OXI	100	50000	200	20	24	15	0.7	S

was intended to reduce uncertainty by cutting the length of time of analysis to reduce the instrument drift encountered on each wheel and to reduce the amount of time between sputtering periods for each target (see Section 2.10).

2.9 Data processing

The data acquired during AMS analysis is processed using custom software at LLNL. The data processing normalizes the raw data using measurements of the OXI standard targets. It then calculates a weighted mean over all the sputtering periods of each target. Uncertainty in the normalized mean ratio is calculated from both the counting uncertainty and the variance across sputtering periods, incorporating a propagation of error from the OXI measurements. These normalized ratios and uncertainties are used to calculate $\Delta^{14}\text{C}$. The equations in this algorithm were developed by John Vogel at LLNL.

Much of the data reduction is performed at CAMS using the custom software “Fudger.” The Fudger software calculates normalized ratios and uncertainties and allows the user to view the measured ratios graphically. The user can mark particular sputtering periods that appear to be outliers by a simple mouse click. The sputtering periods that are marked out by the user are then omitted from the calculation of the final normalized ratio, \bar{R} , and in the case of OXI sputtering periods, not used in normalization.

First, the operator visually inspects the raw $^{14}\text{C}/^{13}\text{C}$ ratios (r) in all sputtering periods of each target to identify any gross outliers. The operator also visually inspects the normalized ratios (R) according to:

$$R = \frac{r}{\bar{r}_{std}} \quad (2.1)$$

where \bar{r}_{std} is the mean of r in the OXI targets used to normalize each sputtering period. Usually the 6 bracketing OXI targets are used in normalization, which are the 3 OXI targets run most immediately before and after. The normalization to bracketing OXI targets largely cancels a small amount of drift in r in all samples

during analysis. Usually $< 1\%$ drift in r is observed over the ~ 14 hour course of measurements. R tends not to drift unless there is a problem with a particular target.

Frequently, the first 1-3 sputtering periods in a particular target will appear to have low values of r and R . This indicates that the target has not yet sufficiently heated up. These sputtering periods marked out in the data reduction and additional sputtering periods may be performed. Occasionally, a sputtering period that occurs later in the analysis will appear to have r and R that is very high or very low which may be identified as an outlier. These outliers may occur when the optimal tuning parameters in the AMS lenses have shifted during the course of the run or when there is a problem with the graphite target. Outliers may also occur randomly.

The uncertainty in the measured raw $^{14}\text{C}/^{13}\text{C}$ ratio (r) for an individual sputtering period (σ) is given by the Poisson uncertainty:

$$\sigma = \frac{r}{\sqrt{c}} \quad (2.2)$$

where c represents the number of ^{14}C counts recorded during the sputtering period and is usually a little over 50,000.

To calculate the uncertainty in the normalized ratio (R) for an individual sputtering period, σ_{norm} , the uncertainty in $\overline{r_{std}}$ must be accounted for. The uncertainty in $\overline{r_{std}}$, $\sigma_{\overline{r_{std}}}$, is given by the larger of either the deviation in the $\overline{r_{std}}$:

$$\sigma_{\overline{r_{std}}} = \sqrt{\frac{\sum_{i=1}^n ((r_{std})_i - \overline{r_{std}})^2}{n(n-1)}} \quad (2.3)$$

or the total standard error:

$$\sigma_{\overline{r_{std}}} = \frac{\sqrt{\sum_{i=1}^n (\sigma_{std})_i^2}}{n} \quad (2.4)$$

where $(\sigma_{std})_i$ is the uncertainty in the i^{th} OXI sputtering period calculated by (2.2) and n is the number of OXI sputtering periods used for normalization, usually 6.

The larger of either (2.3) or (2.4) is then used to calculate the uncertainty in R :

$$\sigma_{norm} = R \sqrt{\left(\frac{\sigma}{r}\right)^2 + \left(\frac{\sigma_{std}}{r_{std}}\right)^2} \quad (2.5)$$

To produce the mean normalized ratio for an individual target, \bar{R} , the results from all sputtering periods are incorporated via a weighted mean:

$$\bar{R} = \frac{\sum_{i=1}^n \frac{R_i}{(\sigma_{norm})_i^2}}{\sum_{i=1}^n \frac{1}{(\sigma_{norm})_i^2}} \quad (2.6)$$

Here, the sum is performed over the n sputtering periods of the target.

The uncertainty in \bar{R} is calculated as both a counting uncertainty, σ_{Cnt} , incorporating uncertainty due to the Poisson counting uncertainty and OXI normalization, and as a standard error, σ_{StdErr} , which quantifies the scatter between R measured in all sputtering periods. σ_{Cnt} is given by:

$$\sigma_{Cnt} = \sqrt{\frac{1}{\sum_{i=1}^n \frac{1}{(\sigma_{norm})_i^2}}} \quad (2.7)$$

and σ_{StdErr} is given by:

$$\sigma_{StdErr} = \sqrt{\frac{\sum_{i=1}^n (R_i - \bar{R})^2}{n(n-1)}} \quad (2.8)$$

The \bar{R} , σ_{Cnt} and σ_{StdErr} are the values that are used in the calculation of $\Delta^{14}\text{C}$ and the measurement uncertainty of $\Delta^{14}\text{C}$ for each target.

The preceding steps are generally carried out using the Fudger software. The Fudger software can produce several datafiles including a “clean” file, which includes a table of all of the raw data that were not marked as outliers by the user, and a “norm” file which includes only the \bar{R} , σ_{Cnt} and σ_{StdErr} for each target. For the processing of high precision CO_2 data, the “clean” file produced by Fudger was imported into Matlab and processed with a script incorporating the equations above to calculate \bar{R} , σ_{Cnt} and σ_{StdErr} (See Appendix A.1).

The next step is to calculate $\Delta^{14}\text{C}$ and the internal uncertainty in $\Delta^{14}\text{C}$ for each target from \bar{R} , σ_{Cnt} and σ_{StdErr} . The $\Delta^{14}\text{C}$ notation accounts for decay that has occurred while the sample has been stored and corrects for mass-dependent fractionation to a reference level of -25 ‰ in $\delta^{13}\text{C}$ (Stuiver and Polach, 1977). The “Modern” standard is defined as 95% of the activity of OXI in 1950, corrected to -19 ‰ (Stuiver and Polach, 1977).

To convert the \bar{R} for each sample into $\Delta^{14}\text{C}$, the “Fraction Modern” (FM) is first calculated as:

$$FM = 1.0200 \frac{\bar{R} - b}{(1 + \delta^{13}\text{C}/10^3)(1 - b)} \quad (2.9)$$

The coefficient 1.0200 accounts for the assignment of the “Modern” standard as 95% of OXI in 1950, for the $\delta^{13}\text{C}$ value of -19 ‰ in OXI and for the normalization of the sample to -25 ‰, as will be demonstrated in Section 2.15.1 (Stuiver and Polach, 1977; Southon, 1989). The subtraction of the parameter b accounts for the background level of ^{14}C (Brown and Southon, 1997); b is 0.0015 for modern CO_2 measured at LLNL. For the Scripps CO_2 samples, $\delta^{13}\text{C}$ was measured at Scripps on CO_2 from concurrently sampled air samples.

$\Delta^{14}\text{C}$ is then calculated from FM using the date of sampling (y_s) and date of analysis (y_a) to correct for decay:

$$\Delta^{14}\text{C} = 10^3 \left(FM \exp \left(\frac{(1950 - y_a) - (y_s - y_a)}{8267} \right) - 1 \right) \quad (2.10)$$

The internal uncertainty in $\Delta^{14}\text{C}$, σ_{Int} , is calculated using the greater of the counting (σ_{Cnt}) or standard error (σ_{StdErr}) calculated above. The background ^{14}C level is also incorporated into the uncertainty:

$$\sigma_{Int} = 10^3 FM \sqrt{\left(\frac{\max(\sigma_{Cnt}, \sigma_{StdErr})}{\bar{R}} \right)^2 + \left(\frac{0.0005(\bar{R} - 1)}{(\bar{R} - b)(1 - b)} \right)^2} \quad (2.11)$$

Usually the standard error of the normalized ratios is slightly higher than the counting uncertainty. The calculation of FM , $\Delta^{14}\text{C}$ and σ_{Int} is also conducted in Matlab (see Matlab script in Appendix A.2).

σ_{Int} is largely determined by the total number of ^{14}C atoms detected during analysis and the variability of the normalized $^{14}\text{C}/^{13}\text{C}$ ratios in different sputtering periods, characteristics that only incorporate the analytical precision within a single wheel of samples. σ_{Int} therefore does not indicate the amount of total measurement uncertainty in $\Delta^{14}\text{C}$ for a particular target because it does not include the uncertainty added when targets are analyzed on several wheels. As the following sections show, the between-wheel uncertainty at CAMS was found to be substantial and required additional analytical improvements and changes to the data reduction procedures.

2.10 Modifications implemented for high precision $^{14}\text{CO}_2$ analysis

The aim of this Ph.D. work to initiate and conduct $\Delta^{14}\text{C}$ analysis of Scripps CO_2 samples with precision of better than 2 ‰ required us to extend the usual analytical protocol and push the limits of the AMS measurement capabilities at CAMS. Regular sample processing at CAMS involves many types of sample materials which are analyzed at 3-5 ‰ precision. To attain higher precision with the Scripps CO_2 samples, we began by analyzing samples using standard practices at CAMS and simply increasing the analysis time in order to attain more ^{14}C counts and thereby reduce the counting uncertainty.

Counting uncertainty is not the only factor that limits the precision attainable in radiocarbon measurements. Additional uncertainty may be introduced during sampling, CO_2 extraction and graphitization. Machine instabilities and differences in the character and behavior of graphite targets during analysis will also contribute to the AMS measurement uncertainty.

A preliminary study at CAMS in 2003 collected near 1 million ^{14}C counts on samples of oceanic dissolved inorganic carbon. The samples were split into 2 targets for analysis and generally showed better than 1 ‰ agreement. 33 pairs of

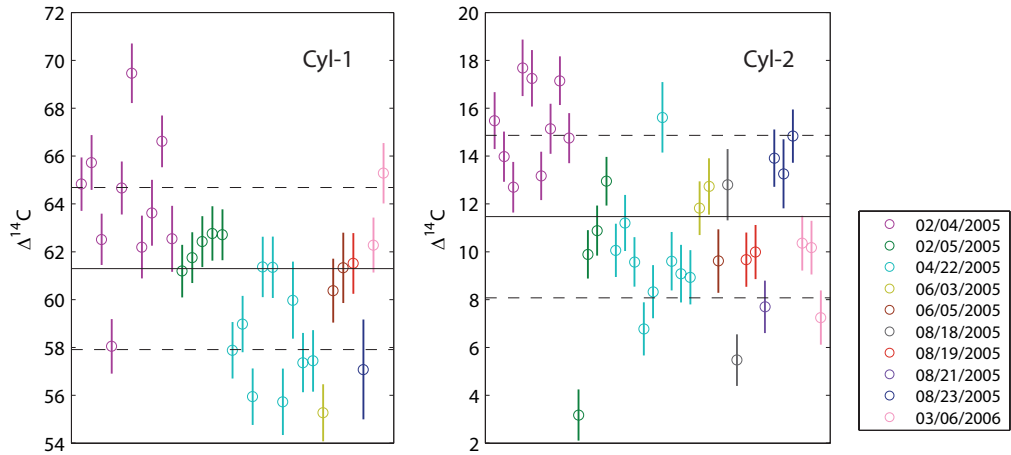


Figure 2.5: Measured $\Delta^{14}\text{C}$ in Cyl-1 and Cyl-2 during analyses conducted over 9 wheels in 2005 and one wheel in 2006. Error bars show σ_{Int} , as calculated by 2.11. The solid line shows mean $\Delta^{14}\text{C}$ and the dashed lines show 1-sigma deviation from the mean, 61.3 ± 3.4 ‰ for Cyl-1 and 11.5 ± 3.4 ‰ for Cyl-2.

targets were analyzed, ranging in value from ~ 0 ‰ to -240 ‰ (Guilderson et al., 2006). This preliminary work showed promise for high-precision measurements at CAMS, suggesting that additional sources of uncertainty other than counting uncertainty were small.

However, measurements of Cyl-1 and Cyl-2 targets conducted in 2005 and early 2006 revealed that the reproducibility of $\Delta^{14}\text{C}$ of Cyl-1 and Cyl-2 at CAMS was worse than expected from the reduction in counting uncertainty achieved by acquiring more ^{14}C counts. Over 10 wheels, the standard deviation in Cyl-1 was 3.4 ‰ and the standard deviation in Cyl-2 was also 3.4 ‰. Figure 2.5 shows all measurements of Cyl-1 and Cyl-2 in 2005 and one wheel in March 2006, separated by wheel. The average σ_{Int} for these analyses was 1.2 ‰. These analyses clearly demonstrated that a substantial amount of uncertainty was added to the internal uncertainty during handling and analysis of CO_2 samples.

Noting the poor reproducibility of the cylinder CO_2 reference materials in 2005, we adjusted several aspects of the sampling handling and analysis procedures

at CAMS to eliminate potential sources of uncertainty. The specific changes we have made to the standard procedures at LLNL for high precision sample preparation and analysis are:

- Selecting a batch of iron catalyst from Alfa Aesar® that produces finer, looser graphite. The use of finer graphite reduces the possibility of spatial inhomogeneities in the isotopic concentration of the graphite and homogenizes the graphite-iron distribution in the target, producing more regular heating of the target in the ion source.
- Weighing the iron catalyst to 5.5 ± 0.3 mg to provide a more consistent ratio of graphite to iron than is possible from approximating the amount of iron with a measuring spoon.
- Replacing dry ice-isopropanol cold traps with magnesium perchlorate in the graphitization reactors. The magnesium perchlorate provides lower water vapor pressure in the reactor. In addition, the risk of contamination is reduced because less dry ice is exposed to the laboratory air, decreasing the ambient CO₂ concentration and increasing its $\Delta^{14}\text{C}$.
- Compacting graphite samples to a constant pressure using a sample press to eliminate the differences in consistency of manually pounded graphite.
- Reducing the number of targets in each wheel from 55 or more to 30 to decrease the total analysis time for each wheel and, thereby, reduce the amount of instrument drift experienced over the measurement of a wheel.
- Eliminating the designation of groups in analysis. Analysis of targets on a single wheel is then more comparable because the OXI targets used to normalize are the same and because all targets experience the same instrument drift.
- Splitting the individual samples of OXI into approximately 0.5 mg C samples instead of 1 mg C so that they are more similar in size to the CO₂ samples.

Because of the high cost and demand of analysis time, we were unable to carry out sufficient characterization of the significance of each of these changes; however the use of these procedures resulted in a precision of better than 2 ‰ in replicate measurements of Cyl-1 targets.

The difficulties faced in sample handling are smaller for modern CO₂ samples compared to carbon from other materials because the samples are already conveniently in the form of CO₂, the starting material for graphitization. This reduces the risk of errors introduced during sample pre-treatment and contamination from laboratory or instrument backgrounds (Ramsey et al., 2004).

2.11 Uncertainty analysis

After implementing the methodological changes to the sample preparation and analysis for CO₂ samples, we examined the improvement in reproducibility of Cyl-1. Measuring replicate samples of reference materials that undergo the same handling and analysis procedures as unknown samples allowed us to estimate additional contributions of uncertainty. These results were presented at the 19th International Radiocarbon Conference in Oxford, UK in April 2006 and published in *Radiocarbon* in 2007 (Graven et al., 2007).

Over the month of May 2006, we measured 36 Cyl-1 targets in 10 wheels, with 2-5 Cyl-1 targets on each wheel. The average σ_{Int} in the 36 Cyl-1 targets was 1.2 ‰. The number of Cyl-1 targets and the mean and standard deviation of $\Delta^{14}C$ in Cyl-1 targets from each wheel and in all Cyl-1 targets are shown in Table 2.2.

We regard the standard deviation in $\Delta^{14}C$ over all 36 Cyl-1 targets to be the total measurement uncertainty in high-precision CO₂ analysis at CAMS: 1.7 ‰. Assuming the total uncertainty, σ_{Tot} , is a quadrature sum of independent contributions (Ellison et al., 2000), we can estimate the within-wheel contribution of uncertainty, σ_{IW} , and the additional between-wheel contribution of uncertainty,

Table 2.2: Results from 10 wheels analyzed at LLNL using high-precision methods. The mean and standard deviation in $\Delta^{14}\text{C}$ of N number of replicate Cyl-1 targets is shown for each wheel. The standard deviation in $\Delta^{14}\text{C}$ of replicate OXI targets is also shown for each wheel. The bottom row shows the mean and standard deviation in $\Delta^{14}\text{C}$ of all 36 Cyl-1 targets and all 62 OXI targets analyzed.

Wheel	N Cyl-1	Mean Cyl-1 $\Delta^{14}\text{C}$ (‰)	Standard Deviation in Cyl-1 $\Delta^{14}\text{C}$ (‰)	Standard Deviation in OXI $\Delta^{14}\text{C}$ (‰)
1	5	61.4	1.6	1.5
2	3	60.7	0.9	3.0
3	4	62.0	1.4	2.7
4	2	59.9	1.9	2.0
5	4	62.4	1.6	3.6
6	4	62.2	1.8	1.5
7	4	59.8	0.7	1.9
8	3	60.9	0.5	1.8
9	4	62.0	1.4	1.8
10	3	57.9	0.6	2.3
Total	36	61.3	1.7	2.4

σ_{IW} , in measurements of $\Delta^{14}\text{C}$ in Cyl-1 according to:

$$\sigma_{Tot}^2 = \sigma_{Int}^2 + \sigma_{IW}^2 + \sigma_{BW}^2 \quad (2.12)$$

We assume that fractionation or contamination during CO_2 extraction at Scripps is negligible based on the established reliability of these procedures for $\delta^{13}\text{C}$ analysis in similar samples. The same air sample and cylinder extraction techniques are employed for stable isotope analysis of CO_2 at Scripps. These techniques have been calibrated to 0.03 ‰ precision and accuracy in $\delta^{13}\text{C}$ by long term reference materials and interlaboratory comparisons (Guenther et al., 2001).

The scatter in $\Delta^{14}\text{C}$ of several Cyl-1 targets within one wheel incorporates the uncertainty due to graphitization and the differences in behavior of individual targets during analysis. Scatter observed between wheels may additionally reflect wheel-to-wheel differences in individual target behavior or detection efficiency, and differences in the relative $^{14}\text{C}/^{13}\text{C}$ ratios between different wheels' ensembles of OXI and Cyl-1 targets. Since the values of the OXI and Cyl-1 reference materials differ

by only 30 ‰ in $\Delta^{14}\text{C}$ and 11 ‰ in $\delta^{13}\text{C}$, we don't expect nonlinearities in analysis to be significant.

First, we estimate σ_{IW} by assessing the within-wheel repeatability of $\Delta^{14}\text{C}$ in the Cyl-1 targets. The standard deviation of $\Delta^{14}\text{C}$ in Cyl-1 targets on a single wheel ranged from 0.5 to 1.9 ‰ (Table 2.2). To combine the results from all wheels, we calculated the pooled standard deviation (s_p) of $\Delta^{14}\text{C}$ in Cyl-1 over the ten wheels, given by:

$$\sigma_p = \sqrt{\frac{\sum_{i=1}^k (N_i - 1) \sigma_i^2}{(N - k)}} \quad (2.13)$$

The pooled standard deviation is the square root of a weighted average of group variances. In this case, each wheel of Cyl-1 targets constitutes a group. In Equation 2.13, σ_i^2 is the variance of the i^{th} group, N_i is the sample size of the i^{th} group, N is the total sample size (the sum of N_i), and k is the number of groups.

The pooled standard deviation of Cyl-1 is 1.3 ‰, representing the total within-wheel uncertainty observed in this study. If we consider Equation 2.12 for Cyl-1 samples within the same wheel, then $\sigma_{Tot} = 1.3$ ‰, $\sigma_{Int} = 1.2$ ‰ and $\sigma_{BW} = 0$ ‰. Using these values to calculate σ_{IW} by Equation 2.12 reveals that σ_{IW} must be very small (≤ 0.5 ‰) because σ_{Tot} and σ_{Int} are essentially the same. This analysis suggests that the within-wheel repeatability is the same as the internal uncertainty, and that graphitization or individual target behavior do not substantially contribute any additional uncertainty to $\Delta^{14}\text{C}$ in Cyl-1 targets measured on the same wheel, i.e. $\sigma_{IW} = 0$ ‰.

Next, we determine σ_{BW} by considering the between-wheel reproducibility of $\Delta^{14}\text{C}$ in the Cyl-1 targets. The standard deviation of $\Delta^{14}\text{C}$ measured in all 36 Cyl-1 targets is 1.7 ‰. This represents the total uncertainty characterized in this study: $\sigma_{Tot} = 1.7$ ‰. By substituting $\sigma_{Tot} = 1.7$ ‰, $\sigma_{Int} = 1.2$ ‰ and $\sigma_{IW} = 0$ ‰ in Equation 2.12, we calculate $\sigma_{BW} = 1.2$ ‰. This indicates that the uncertainty introduced when targets are analyzed on several wheels, σ_{BW} , is substantial and comparable in magnitude to the internal uncertainty, σ_{Int} .

Part of σ_{BW} comes from the variability of the $^{14}\text{C}/^{13}\text{C}$ ratios in OXI targets. The reproducibility of OXI targets affects the reproducibility of Cyl-1 $\Delta^{14}\text{C}$ because measurements of $^{14}\text{C}/^{13}\text{C}$ ratios in OXI are used in the data normalization procedure. To examine the scatter of $\Delta^{14}\text{C}$ in OXI targets within a wheel, we reverse the normalization procedure from Section 2.9 and use Cyl-1 as the primary standard to calculate $\Delta^{14}\text{C}$ in OXI targets; this procedure is explained in Section 2.15. We thus calculate the standard deviation in $\Delta^{14}\text{C}$ in the OXI targets on each wheel, shown in Table 2.2, and again combine the results from all wheels into a pooled standard deviation. The pooled standard deviation of $\Delta^{14}\text{C}$ in OXI targets is 2.3 ‰, considerably larger than the pooled standard deviation in Cyl-1 of 1.3 ‰. The $\Delta^{14}\text{C}$ in OXI targets also have an average internal uncertainty ($\sigma_{IW,OXI}$) of 1.2 ‰, so for OXI targets $\sigma_{IW,OXI} = 2.0$ ‰, showing that a substantial amount of uncertainty is added to OXI targets analyzed on a single wheel.

We believe the poorer within-wheel repeatability of the OXI targets compared to the Cyl-1 targets must be due to differences in sample preparation. Since the CO_2 gas from each combustion batch of OXI is split into several different samples, we would expect all the samples to be homogeneous, but perhaps the splitting procedure itself affects the samples. The Oxalic Acid II and VIRI A barley mash targets, which undergo similar preparation by combustion and splitting, showed standard deviations of 2.0 and 2.3 ‰, respectively, in $\Delta^{14}\text{C}$ of all targets over the 10 wheels. This scatter is larger than the overall standard deviation in Cyl-1 targets but similar to the pooled standard deviation of OXI targets. Though there were only 2 targets of OXII and VIRI A on each wheel, the large overall scatter supports the idea that targets prepared by splitting large combustions are statistically different from each other.

Variability in OXI does not have a large effect on the within-wheel repeatability of Cyl-1 $\Delta^{14}\text{C}$ because a running mean which typically includes all OXI targets on the wheel is used in normalization (Equation 2.1). The running mean will not be biased toward any particular OXI target and will vary only randomly

and with instrument drift, thus it tends not to introduce differences in the $\Delta^{14}\text{C}$ calculated for Cyl-1 targets on an individual wheel.

On the other hand, significant wheel-to-wheel variability in the difference between the mean Cyl-1 $^{14}\text{C}/^{13}\text{C}$ ratio and the mean OXI $^{14}\text{C}/^{13}\text{C}$ ratio will increase the overall scatter in Cyl-1 $\Delta^{14}\text{C}$. Mean $\Delta^{14}\text{C}$ values for the Cyl-1 targets in each wheel ranged from 57.9-62.4 ‰ (Table 2.2), demonstrating that the relative $^{14}\text{C}/^{13}\text{C}$ ratios between the Cyl-1 targets and the OXI targets do vary between wheels. An error in the mean OXI $^{14}\text{C}/^{13}\text{C}$ ratio on a particular wheel will result in a systematic error in the $\Delta^{14}\text{C}$ of Cyl-1 targets on that wheel. Uncertainty in the mean OXI $^{14}\text{C}/^{13}\text{C}$ ratio can be estimated by dividing the pooled standard deviation in OXI, 2.3 ‰, by the square root of the number of OXI targets on each wheel, 6. The standard error in OXI is 0.9 ‰, suggesting that errors in the mean OXI $\Delta^{14}\text{C}$ account for a large portion of σ_{BW} ($\sigma_{BW} = 1.2$ ‰). Improvements in the reproducibility of OXI therefore might have the potential to improve the overall precision of CO_2 measurements at LLNL.

We have conducted preliminary work to examine the effect of changing the sample preparation of OXI targets. In March 2007, we prepared several batches of OXI targets in a different manner than the aliquot-by-aliquot splitting procedure described in Section 2.7. The new preparation technique simply expanded the OXI CO_2 gas into the vacuum manifold and 6 reactors simultaneously. The gas was allowed to reside within that volume for 15 minutes, whereupon the reactors were closed.

Measured $\Delta^{14}\text{C}$, normalized by Cyl-1 and Cyl-2, for the OXI targets prepared in the new manner is shown in Figure 2.6. $\Delta^{14}\text{C}$ in OXI targets analyzed on previous wheels is also shown for comparison. Mean $\Delta^{14}\text{C}$ and standard deviation in 6-11 targets analyzed on each wheel are represented by the different colored symbols and error bars.

The results from March 2007 suggest that the new OXI preparation method has reduced or eliminated the additional uncertainty from splitting OXI

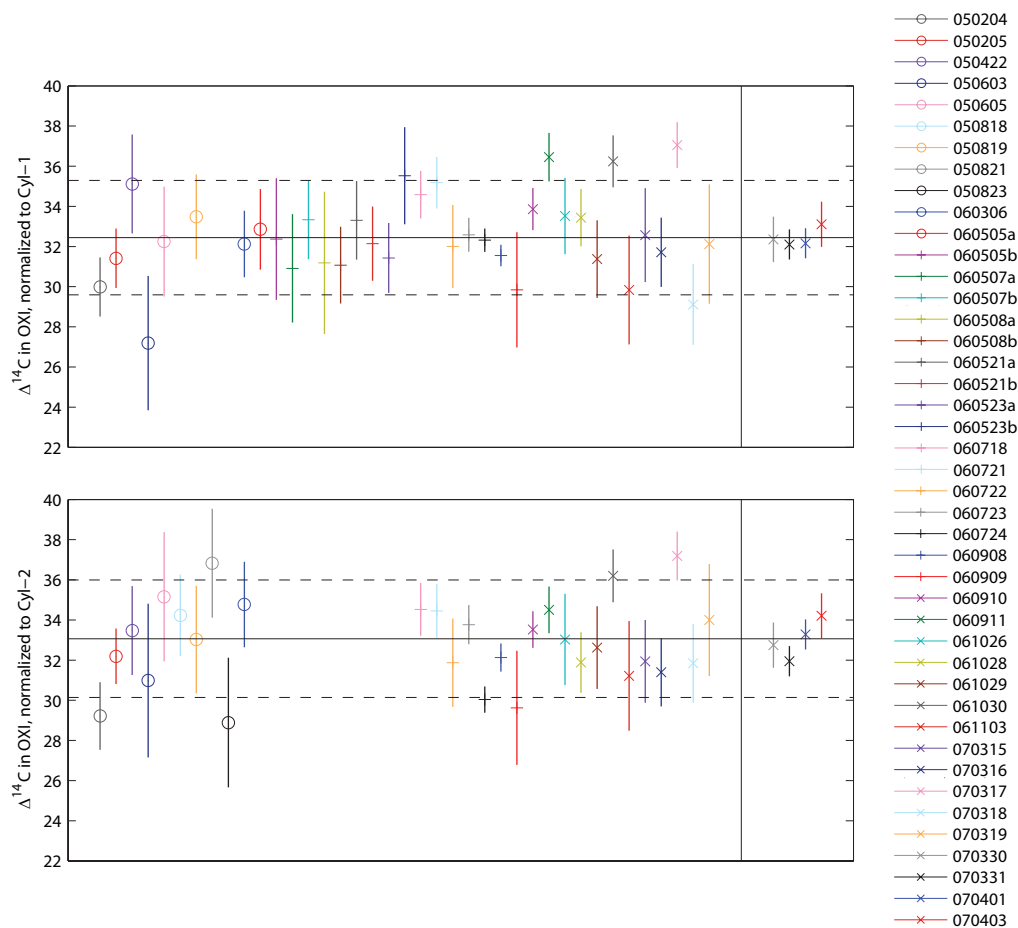


Figure 2.6: Mean and standard deviation in $\Delta^{14}\text{C}$ of 6-11 OXI targets analyzed on each wheel. OXI targets were prepared by splitting CO_2 with aliquots as described in Section 2.7 (plotted to the left of the vertical line), or by expanding OXI CO_2 into several reactors at once (plotted to the right of the vertical line). The upper panel shows $\Delta^{14}\text{C}$ in OXI calculated by normalization to Cyl-1; the lower panel shows $\Delta^{14}\text{C}$ in OXI calculated by normalization to Cyl-2. Solid horizontal lines show overall mean $\Delta^{14}\text{C}$ and dashed lines show overall standard deviation in $\Delta^{14}\text{C}$: 32.4 ± 2.8 ‰ for Cyl-1 normalization and 33.1 ± 2.9 ‰ for Cyl-2 normalization.

CO₂. This work is not conclusive, however. More testing is necessary to prove that this type of OXI preparation does reduce uncertainty. If this technique is not shown to be sufficient in reducing uncertainty, other changes in OXI preparation could be investigated. Improvements to the new OXI preparation method could be achieved by increasing the residence time to longer than 15 min and thermally insulating the manifold. Alternative techniques could incorporate individual 0.5 mg C sized combustions or the combustion of a very large amount of OXI that could be stored in a cylinder and used for single 0.5 mg C sized aliquots of OXI CO₂ gas.

Though we have focused on the uncertainty added in the OXI preparation, we cannot rule out other contributions to the wheel-to-wheel uncertainty. Additional uncertainty may arise from daily variability in several components of the AMS, including the stability of power supplies, variations in room temperature, the level of vacuum achieved, carbon foil thickness, cesium beam intensity, etc. There may also be differences in the character of the graphite-iron mixture in targets on different wheels. These sources of variation could cause small differences in the ionization, stripping, or detection efficiency of ¹⁴C compared to ¹³C that may not be accounted for by the OXI normalization procedure. Such contributions to uncertainty are difficult to diagnose other than by observing the long-term reproducibility of measurements of $\Delta^{14}\text{C}$ on replicate samples, but our quadrature sum indicates they may be as large as 0.8 ‰ for measurements of Cyl-1.

2.12 Updated uncertainty analysis

The previous section discussed the uncertainty of $\Delta^{14}\text{C}$ in Cyl-1 on 10 wheels analyzed in May 2006. As we continued to measure ~ 3 Cyl-1 targets and ~ 3 Cyl-2 targets on each wheel since then, we can update the uncertainty analysis using 23 more wheels of data.

The overall standard deviation in Cyl-1 analyzed on 33 wheels since May

5, 2006 was 2.0 ‰. For Cyl-2, the overall standard deviation was also 2.0 ‰. The pooled standard deviation over this period was 1.6 ‰ for Cyl-1 and 1.4 ‰ for Cyl-2. Average σ_{Int} over these 33 wheels was 1.2 ‰ for both Cyl-1 and Cyl-2.

Repeating the previous calculation for σ_{IW} using the quadrature sum of 2.12, we find again that σ_{IW} must be small as the pooled standard deviation is not much larger than the average σ_{Int} for Cyl-1 and Cyl-2. The analysis from the 33 wheels analyzed after May 2006 does suggest that σ_{IW} may be larger than indicated in May 2006. According to the quadrature sum of uncertainties, σ_{IW} could be as large as 1.0 ‰ for Cyl-1 or 0.7 ‰ for Cyl-2.

Calculating σ_{BW} according to the quadrature sum of 2.12, we find again that σ_{BW} is 1.2 ‰ for Cyl-1. Cyl-2 measurements indicate that σ_{BW} is slightly larger, 1.4 ‰.

The analyses conducted since May 2006 support the conclusion that the “between-wheel” uncertainty contributed when samples are analyzed on several wheels is the largest source of uncertainty for measurements of $\Delta^{14}\text{C}$ in CO_2 at LLNL. However, it appears that the performance of the Cyl-1 targets over the 10 wheels analyzed in May 2006 was slightly better than the overall scatter in Cyl-1 when measured over a longer period. The reproducibility of Cyl-1 and Cyl-2 targets since May 2006 suggest that CO_2 samples analyzed according to the procedures described in the previous sections and processed with OXI normalization have a measurement uncertainty of only 2.0 ‰.

2.13 Observed biases in $\Delta^{14}\text{C}$ of Cyl-1 and Cyl-2 measured on different wheels

Whether sample preparation or internal conditions of the AMS cause variability in the mean $^{14}\text{C}/^{13}\text{C}$ of OXI target, it is evident that wheel-to-wheel differences in $\Delta^{14}\text{C}$ of Cyl-1 and Cyl-2 result from the use of OXI in normalization. Figure 2.7 shows measurements of Cyl-1 and Cyl-2, normalized to OXI. Several

wheels exhibit consistently low (e.g. 9/11/06, 10/30/06 and 3/17/07) or consistently high (e.g. 9/9/06, 10/29/06 and 3/18/07) values in $\Delta^{14}\text{C}$ of all Cyl-1 and Cyl-2 targets measured in that wheel.

It is apparent that the wheel-to-wheel biases are mostly a result of normalizing with OXI targets because normalizing Cyl-2 with Cyl-1 instead of OXI eliminates a large portion of the between-wheel variability. Figure 2.8 shows all measurements of Cyl-2, normalized with Cyl-1 targets. The overall standard deviation in Cyl-2 is reduced to 1.9 ‰ when normalized with Cyl-1, compared with a standard deviation of 2.4 ‰ when normalized with OXI.

2.14 Elimination of OXI artifacts

As the OXI targets have been shown to introduce additional error through the normalization procedure, we have taken steps to remove the influence of OXI targets in the calculation of $\Delta^{14}\text{C}$ in CO_2 . The simplest way of removing OXI is to use a different reference material for normalization. In place of OXI, we now use Cyl-1 as the primary reference material for normalization. Yet for 15 early wheels which were analyzed before the Cyl-1 reference cylinder was created or before Cyl-1 targets were fully implemented into the analysis protocols, other procedures had to be adopted. For one other wheel, analyzed on 10/28/06, there was only 1 unflagged Cyl-1 target available so we instead used Cyl-2 as the reference material for normalization for that wheel.

In the following two sections, we outline the specific procedure used to implement Cyl-1 (and Cyl-2) normalization and describe the special treatment of $^{14}\text{C}/^{13}\text{C}$ ratios measured on early wheels.

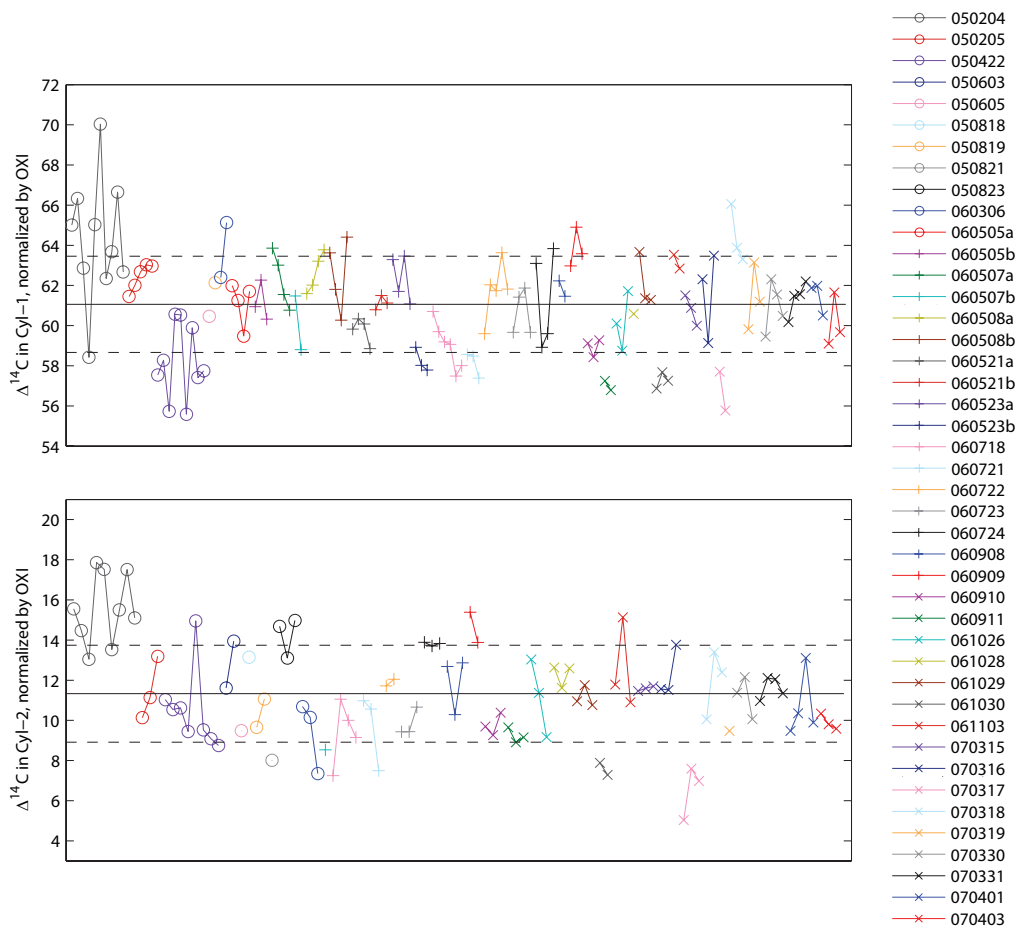


Figure 2.7: Measured $\Delta^{14}\text{C}$ in Cyl-1 and Cyl-2, as normalized by OXI. Targets from different wheels are shown as different symbols; targets from each wheel are connected by straight lines. The solid line shows the mean values and the dashed lines show the overall standard deviation, $61.0 \pm 2.4 \text{ ‰}$ for Cyl-1 and $11.3 \pm 2.4 \text{ ‰}$ for Cyl-2.

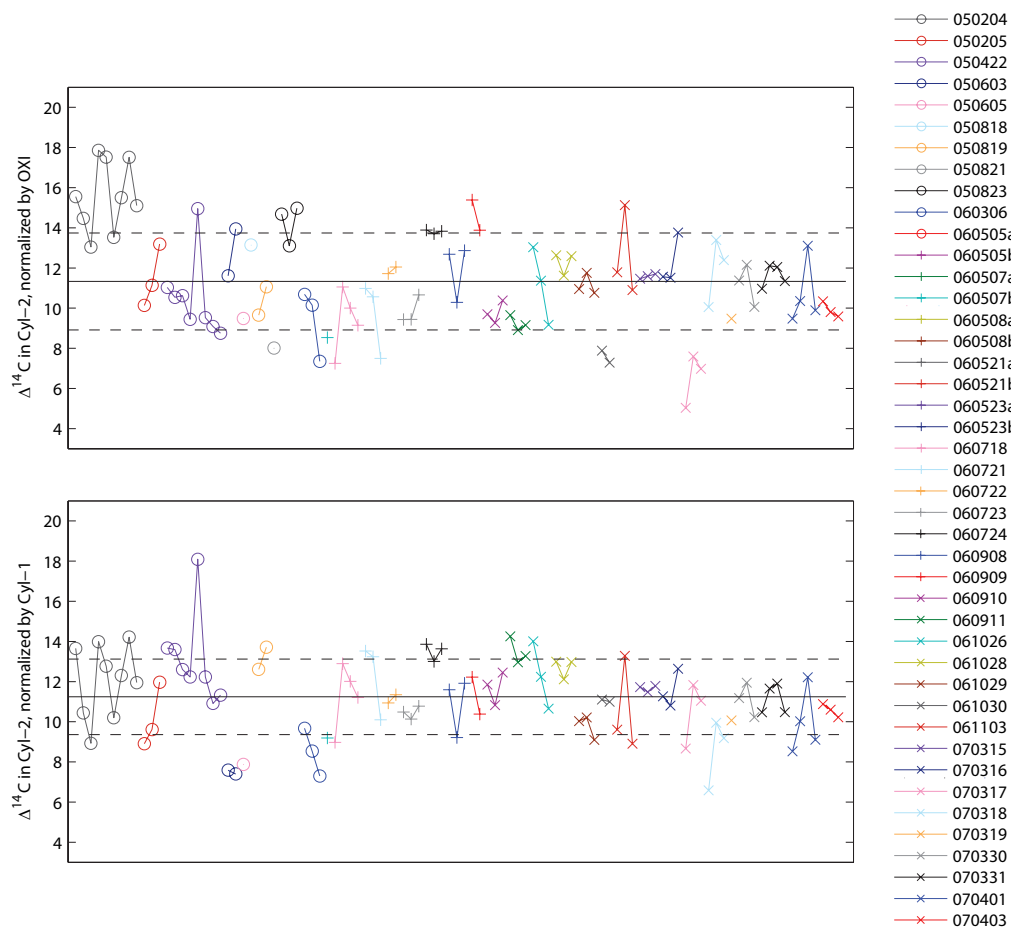


Figure 2.8: Measured $\Delta^{14}\text{C}$ in Cyl-2, as normalized by OXI (top panel) and Cyl-1 (bottom panel). The top panel is repeated from Figure 2.7. For Cyl-2 normalized by Cyl-1, the overall mean and standard deviation are 11.2 ± 1.9 ‰ (solid and dashed lines).

2.15 Normalization by Cyl-1 and Cyl-2

To eliminate the uncertainty contributed by the OXI normalization procedure, we began normalizing measured $^{14}\text{C}/^{13}\text{C}$ ratios using Cyl-1 targets instead of OXI targets. As the Cyl-1 targets are more similar to the CO_2 samples in $\Delta^{14}\text{C}$ and $\delta^{13}\text{C}$ and are prepared more similarly to the CO_2 samples, Cyl-1 provides a better reference material to use in normalization. As shown in Figure 2.8, normalization by Cyl-1 resulted in significantly less scatter in the measured $\Delta^{14}\text{C}$ of Cyl-2 samples.

For 32 wheels analyzed after 3/6/2006, CO_2 samples were normalized by Cyl-1. The wheel analyzed on 10/28/2006 included only one unflagged Cyl-1 target on that wheel. Therefore, we used Cyl-2 in normalizing the targets analyzed on 10/28/2006.

To normalize with Cyl-1, we replace r_{std} in Equation 2.1 with the mean of the bracketing N Cyl-1 targets, where N is equal to the number of Cyl-1 targets on the wheel. Equations 2.3, 2.3 and 2.5 also then refer to the bracketing Cyl-1 targets rather than the bracketing OXI targets. Normalization with Cyl-2 uses the bracketing Cyl-2 targets in these equations.

After calculating \bar{R} , σ_{Cnt} and σ_{StdErr} in the Cyl-1 or Cyl-2 normalization, $\Delta^{14}\text{C}$ is calculated according to:

$$FM_{Cyl-1} = 1.0589 \frac{\bar{R}_{Cyl-1} - b}{(1 + \delta^{13}\text{C}/10^3)(1 - b)} \quad (2.14)$$

$$\Delta^{14}\text{C} = 10^3 \left(FM_{Cyl-1} \exp \left(\frac{(1950 - y_a) - (y_s - y_a)}{8267} \right) - 1 \right) \quad (2.15)$$

$$\sigma_{Int} = 10^3 FM_{Cyl-1} \sqrt{\left(\frac{\max(\sigma_{Cnt, Cyl-1}, \sigma_{StdErr, Cyl-1})}{\bar{R}_{Cyl-1}} \right)^2 + \left(\frac{0.0005 (\bar{R}_{Cyl-1} - 1)}{(\bar{R}_{Cyl-1} - b)(1 - b)} \right)^2} \quad (2.16)$$

for Cyl-1, and:

$$FM_{Cyl-2} = 1.0080 \frac{\bar{R}_{Cyl-2} - b}{(1 + \delta^{13}C/10^3)(1 - b)} \quad (2.17)$$

$$\Delta^{14}C = 10^3 \left(FM_{Cyl-2} \exp \left(\frac{(1950 - y_a) - (y_s - y_a)}{8267} \right) - 1 \right) \quad (2.18)$$

$$\sigma_{Int} = 10^3 FM_{Cyl-2} \sqrt{\left(\frac{\max(\sigma_{Cnt,Cyl-2}, \sigma_{StdErr,Cyl-2})}{\bar{R}_{Cyl-2}} \right)^2 + \left(\frac{0.0005 (\bar{R}_{Cyl-2} - 1)}{(\bar{R}_{Cyl-2} - b)(1 - b)} \right)^2} \quad (2.19)$$

for Cyl-2. These equations are very similar to those used in the OXI normalization, except a different coefficient is used in the calculation of FM . The following section explains how the coefficients of 1.0589 and 1.0080 were determined for Cyl-1 and Cyl-2.

2.15.1 Calculation of $\Delta^{14}C$ in Cyl-normalized ratios

To calculate $\Delta^{14}C$ in ratios that have been normalized by either Cyl-1 or Cyl-2, we must account for the difference in $^{14}C/^{12}C$ of Cyl-1 or Cyl-2 compared to the ‘‘Modern’’ Standard. The following algorithms are modeled after an unpublished article by John Southon, ‘‘The calculation of ^{14}C ages from AMS $^{14}C/^{13}C$ ratio measurements’’ (Southon, 1989) and are similar to those presented in Donahue et al. (1990).

First, we go through the derivation of the equation used to calculate FM from OXI-normalized ratios \bar{R} . Then, we apply the same derivation to Cyl-1 and Cyl-2 normalized ratios \bar{R}_{Cyl-1} and \bar{R}_{Cyl-2} .

The Modern Standard A_{ON} is defined as having a specific activity of 0.95 times the specific activity of Oxalic Acid I, normalized to $\delta^{13}C = -19\text{‰}$ and measured simultaneously with the sample:

$$A_{ON} = 0.95 A_{OXI[-19]} \quad (2.20)$$

To correct for mass dependent fractionation in the sample, the measured activity of the sample is normalized to -25 ‰ in $\delta^{13}\text{C}$. The normalization for mass dependent fractionation proceeds according to:

$$A_{SN} = A_{S[-25]} = A_S \frac{(1 - 25/10^3)^2}{(1 + \delta_S/10^3)^2} = A_S \frac{(0.975)^2}{(1 + \delta_S/10^3)^2} \quad (2.21)$$

Then, the Fraction Modern (FM) is defined by:

$$FM = \frac{A_S}{0.95 A_{OXI[-19]}} \frac{(0.975)^2}{(1 + \delta_S/10^3)^2} \quad (2.22)$$

The specific activity of ^{14}C in a sample, A_S is proportional to the ratio $^{14}\text{C}/\text{C}$. The ratio of $^{14}\text{C}/\text{C}$ in the sample divided by the $^{14}\text{C}/\text{C}$ in the Modern Standard can be closely approximated by using $^{14}\text{C}/^{12}\text{C}$ ratios instead of $^{14}\text{C}/\text{C}$. As the quantity measured at LLNL is $^{14}\text{C}/^{13}\text{C}$, we must convert $^{14}\text{C}/^{13}\text{C}$ into $^{14}\text{C}/^{12}\text{C}$.

The $^{14}\text{C}/^{12}\text{C}$ ratio in a sample, $(^{14}\text{C}/^{12}\text{C})_S$, can be calculated using measured $\delta^{13}\text{C}$ in the sample:

$$\begin{aligned} (^{14}\text{C}/^{12}\text{C})_S &= (^{14}\text{C}/^{13}\text{C})_S (^{13}\text{C}/^{12}\text{C})_S \\ &= (^{14}\text{C}/^{13}\text{C})_S (^{13}\text{C}/^{12}\text{C})_{PDB} (1 + \delta_S/10^3) \end{aligned} \quad (2.23)$$

A similar calculation can be performed to obtain the $^{14}\text{C}/^{12}\text{C}$ ratio in the OXI standard:

$$\begin{aligned} (^{14}\text{C}/^{12}\text{C})_{OXI[-19]} &= (^{14}\text{C}/^{13}\text{C})_{OXI} (^{13}\text{C}/^{12}\text{C})_{PDB} (1 - 19/10^3) \\ &= 0.981 (^{14}\text{C}/^{13}\text{C})_{OXI} (^{13}\text{C}/^{12}\text{C})_{PDB} \end{aligned} \quad (2.24)$$

The $^{13}\text{C}/^{12}\text{C}$ ratio in the PDB reference of $\delta^{13}\text{C}$ ($(^{13}\text{C}/^{12}\text{C})_{PDB}$) is known to be 0.01124 (Craig, 1957).

Substituting the previous formulations of $(^{14}\text{C}/^{12}\text{C})_S$ and $(^{14}\text{C}/^{12}\text{C})_{OXI}$ into the equation for Fraction Modern (2.22), provides the following, in terms of $^{13}\text{C}/^{12}\text{C}$:

$$FM = \frac{(^{14}\text{C}/^{13}\text{C})_S (1 + \delta_S/10^3)}{0.95 \cdot 0.981 (^{14}\text{C}/^{13}\text{C})_{OXI}} \frac{(0.975)^2}{(1 + \delta_S/10^3)^2}$$

$$FM = \frac{1.0200}{(1 + \delta_S/10^3)} \frac{(^{14}C/^{13}C)_S}{(^{14}C/^{13}C)_{OXI}} \quad (2.25)$$

or,

$$FM = \frac{1.0200\bar{R}}{(1 + \delta_S/10^3)} \quad (2.26)$$

This equation is the same as Equation 2.9, though the background correction terms are not taken into account here.

Now we calculate an equivalent equation to use when Cyl-1 is used as the normalizing standard, with a different coefficient than 1.0200. The overall mean values in $\Delta^{14}C$ and $\delta^{13}C$ for Cyl-1 are:

$$\Delta^{14}C_{Cyl-1} = 61.0 \text{ ‰} \text{ and } \delta^{13}C_{Cyl-1} = -8.55 \text{ ‰}$$

Expressed in FM and in activity, corrected for mass dependent fractionation:

$$FM_{Cyl-1} = 1.0610, \text{ or } A_{Cyl-1[-25]} = 1.0610 \text{ times Modern}$$

Now, expressed in terms of $^{14}C/^{12}C$ ratios, this is equivalent to:

$$0.95(^{14}C/^{12}C)_{OXI[-19]} = (1/1.0610)(^{14}C/^{12}C)_{Cyl-1[-25]} \exp(-\lambda(2004 - 1950)) \quad (2.27)$$

The last term above accounts for the decay in the OXI standard that has occurred between 1950 and the creation of the Cyl-1 reference material in 2004. λ is the decay constant for radiocarbon, $1/8267 \text{ yr}^{-1}$.

From (2.21), the $^{14}C/^{12}C$ ratio for Cyl-1, normalized to $\delta^{13}C = -25 \text{ ‰}$, is related to the measured $(^{14}C/^{12}C)_{Cyl-1}$ (corresponding to the actual $\delta^{13}C_{Cyl-1}$ of -8.55 ‰) by:

$$\begin{aligned} (^{14}C/^{12}C)_{Cyl-1[-25]} &= (^{14}C/^{12}C)_{Cyl-1} \frac{(0.975)^2}{(1 - 8.55/10^3)^2} \\ &= (^{14}C/^{12}C)_{Cyl-1} \frac{(0.975)^2}{(0.9915)^2} \end{aligned} \quad (2.28)$$

Therefore, the Modern Standard relates to Cyl-1 via:

$$0.95(^{14}C/^{12}C)_{OXI} = (1/1.0610)(^{14}C/^{12}C)_{Cyl-1} \frac{(0.975)^2}{(0.9915)^2(1.0066)}$$

$$\begin{aligned}
&= 0.9425(^{14}\text{C}/^{13}\text{C})_{\text{Cyl-1}}(^{13}\text{C}/^{12}\text{C})_{\text{Cyl-1}} \frac{(0.975)^2}{(0.9915)^2(1.0066)} \\
&= 0.9425(^{14}\text{C}/^{13}\text{C})_{\text{Cyl-1}}(^{13}\text{C}/^{12}\text{C})_{\text{PDB}} \frac{(0.975)^2}{0.9916 \cdot 1.0066}
\end{aligned} \tag{2.29}$$

Substituting equations 2.29 and 2.23 in 2.22 gives:

$$FM = \frac{(^{14}\text{C}/^{13}\text{C})_S}{0.9425(^{14}\text{C}/^{13}\text{C})_{\text{Cyl-1}}} \frac{(0.975)^2}{(1 + \delta_S/10^3)} \frac{(0.9915)(1.0066)}{(0.975)^2} \tag{2.30}$$

which reduces to:

$$FM = \frac{1.0589}{(1 + \delta_S/10^3)} \frac{(^{14}\text{C}/^{13}\text{C})_S}{(^{14}\text{C}/^{13}\text{C})_{\text{Cyl-1}}} \tag{2.31}$$

or,

$$FM = \frac{1.0589\bar{R}_{\text{Cyl-1}}}{(1 + \delta_S/10^3)} \tag{2.32}$$

The coefficient 1.0589 is substituted for 1.0200 in Equation 2.9 when Cyl-1 is used for normalization.

Following the same procedure for Cyl-2 provides the corresponding equation for samples normalized with Cyl-2. The overall mean values in $\Delta^{14}\text{C}$ and $\delta^{13}\text{C}$ for Cyl-2 are:

$$\Delta^{14}\text{C}_{\text{Cyl-2}} = 11.3 \text{ ‰} \text{ and } \delta^{13}\text{C}_{\text{Cyl-2}} = -9.85 \text{ ‰}$$

That is,

$$FM_{\text{Cyl-2}} = 1.0113, \text{ or } A_{\text{Cyl-2}[-25]} = 1.0113 \text{ times Modern}$$

This is equivalent to:

$$0.95(^{14}\text{C}/^{12}\text{C})_{\text{OXI}[-19]} = (1/1.0113)(^{14}\text{C}/^{12}\text{C})_{\text{Cyl-2}[-25]} \exp(-\lambda(2004 - 1950)) \tag{2.33}$$

From (2.21), the $^{14}\text{C}/^{12}\text{C}$ ratio for Cyl-2, normalized to $\delta^{13}\text{C} = -25 \text{ ‰}$, is related to the measured $(^{14}\text{C}/^{12}\text{C})_{\text{Cyl-2}}$ (corresponding to the actual $\delta^{13}\text{C}_{\text{Cyl-2}}$ of -9.85 ‰) by:

$$\begin{aligned}
(^{14}\text{C}/^{12}\text{C})_{\text{Cyl-2}[-25]} &= (^{14}\text{C}/^{12}\text{C})_{\text{Cyl-2}} \frac{(0.975)^2}{(1 - 9.85/10^3)^2} \\
&= (^{14}\text{C}/^{12}\text{C})_{\text{Cyl-2}} \frac{(0.975)^2}{(0.9902)^2}
\end{aligned} \tag{2.34}$$

Therefore, the Modern Standard relates to Cyl-2 via:

$$\begin{aligned}
0.95(^{14}\text{C}/^{12}\text{C})_{OXI} &= (1/1.0113)(^{14}\text{C}/^{12}\text{C})_{\text{Cyl-2}} \frac{(0.975)^2}{(0.9902)^2(1.0066)} \\
&= 0.9888(^{14}\text{C}/^{13}\text{C})_{\text{Cyl-2}}(^{13}\text{C}/^{12}\text{C})_{\text{Cyl-2}} \frac{(0.975)^2}{(0.9902)^2(1.0066)} \\
&= 0.9888(^{14}\text{C}/^{13}\text{C})_{\text{Cyl-2}}(^{13}\text{C}/^{12}\text{C})_{\text{PDB}} \frac{(0.975)^2}{0.9902 \cdot 1.0066}
\end{aligned} \tag{2.35}$$

Substituting Equations 2.35 and 2.23 in 2.22 then leads to:

$$FM = \frac{(^{14}\text{C}/^{13}\text{C})_S}{0.9888(^{14}\text{C}/^{13}\text{C})_{\text{Cyl-2}}} \frac{(0.975)^2}{(1 + \delta_S/10^3)} \frac{(0.9902)(1.0066)}{(0.975)^2} \tag{2.36}$$

which reduces to:

$$FM = \frac{1.0080}{(1 + \delta_S/10^3)} \frac{(^{14}\text{C}/^{13}\text{C})_S}{(^{14}\text{C}/^{13}\text{C})_{\text{Cyl-2}}} \tag{2.37}$$

or,

$$FM = \frac{1.0080 \bar{R}_{\text{Cyl-2}}}{(1 + \delta_S/10^3)} \tag{2.38}$$

The coefficient 1.0080 is substituted for 1.0200 in Equation 2.9 when Cyl-2 is used for normalization.

2.15.2 Total uncertainty in $\Delta^{14}\text{C}$ using Cyl-1 normalization

The total uncertainty in measurements of $\Delta^{14}\text{C}$ in CO_2 using Cyl-1 normalization is determined by the reproducibility of $\Delta^{14}\text{C}$ in Cyl-2, when normalized by Cyl-1. The standard deviation in Cyl-2, normalized by Cyl-1, was 1.5 ‰ in 63 targets measured over 22 wheels since May 2006.

Another measure of the reproducibility of CO_2 samples processed with Cyl-1 normalization is the pooled standard deviation of replicate CO_2 samples from La Jolla, when normalized by Cyl-1. For 21 pairs of replicate samples measured between May 2006 and April 2007, the pooled standard deviation was 1.8 ‰. This estimate of pooled standard deviation was calculated by omitting one outlier pair which had a standard deviation of 4.8 ‰.

Averaging both measures of uncertainty (overall Cyl-2 scatter in 2006-07 of 1.5 ‰ and pooled standard deviation in La Jolla replicates in 2006-07 of 1.8 ‰), I estimate the total measurement uncertainty for samples measured in 2006-07, σ_{Tot} , to be 1.7 ‰. This estimate of σ_{Tot} represents the current reproducibility of $\Delta^{14}\text{C}$ in CO_2 samples analyzed at LLNL, utilizing all improvements in sample handling and analysis and processing measured $^{14}\text{C}/^{13}\text{C}$ ratios by normalization with Cyl-1 targets.

2.16 Adjustments to OXI normalization

For wheels that were analyzed before the Cyl-1 and Cyl-2 reference cylinders were created or before Cyl-1 and Cyl-2 targets were fully implemented into the analysis protocols, other procedures had to be adopted. This section describes the method by which CO_2 targets analyzed in the first 15 wheels were normalized and adjusted to correct for the additional uncertainty contributed by OXI during normalization.

The “Adjusted” OXI normalization generally proceeds following the description in Section 2.9. Before the normalized R values are converted to \bar{R} and \bar{R} to $\Delta^{14}\text{C}$, two corrections are applied. First, the assignment of “groups” of targets on each wheel resulted in different sets of OXI targets used to normalize CO_2 targets within one wheel. The differences in mean $^{14}\text{C}/^{13}\text{C}$ between groups of OXIs is accounted for so that all sample targets run on a single wheel were comparable. The difference between groups of OXI targets is corrected by multiplying all measurements of R in each group by a “group factor,” α_g . Then, for each wheel, a bias in \bar{R} of the CO_2 samples is diagnosed using either Cyl-1 and Cyl-2 targets, replicate samples from La Jolla, or surrounding samples from Mauna Loa and Samoa. The resulting “wheel factor,” α_w , is applied to \bar{R} in each target on that wheel before calculating $\Delta^{14}\text{C}$.

2.16.1 Group designation on early wheels

Prior to the instatement of methodological improvements specific to the CO₂ samples in the spring of 2006, we used similar analysis procedures as were regularly used for other sample materials at CAMS. As part of these procedures, the targets within a wheel were assigned to “groups”. Depending on the total number of targets on that wheel, a wheel of targets would be divided into 3-5 overlapping groups. Each target was assigned to at least 2 groups. The groups were analyzed individually and in sequence, where a minimum number of sputtering periods or tolerance in raw ratios was achieved in each target of the group before the analysis of the group was complete. The analysis then proceeded to the next group. An example of group assignments is shown in Table 2.3 for the wheel analyzed on August 18, 2005.

As demonstrated in Table 2.3, different OXI targets were included in different groups. Targets in different groups were thus normalized with different sets of OXI targets. Therefore, error could be introduced within a wheel because of differences in the mean raw ¹⁴C/¹³C ratio of a group’s particular ensemble of OXI targets. The previous section demonstrated that differences in the ensemble mean of r_{OXI} contributed a significant amount of uncertainty to the reproducibility of Cyl-1.

To correct for the group-to-group differences that could contribute additional error, we applied a correction to the normalized ratios of each sputtering period of all targets. This correction, α_g , was characterized by comparing the normalized ratios of the OXI targets in a particular group to the entire set of OXI targets analyzed in that wheel. α_g was calculated as the mean \bar{R} in the OXI targets included in a particular group, divided by the mean \bar{R} in all OXI targets in that wheel:

$$\alpha_g = \frac{\frac{1}{N_g} \sum_{i=1}^{N_g} \overline{R_{OXIi}}}{\frac{1}{N_w} \sum_{i=1}^{N_w} \overline{R_{OXIi}}} \quad (2.39)$$

Table 2.3: Group assignments for the wheel analyzed on August 18, 2005.

Position	Name	Groups	Position	Name	Groups
5	OXI	1, 2	30	55280.048 (Cyl-2)	2, 3
6	OXII	1, 2, 3, 4	31	M01-412	2, 3
7	VIRI A	1, 2, 3, 4	32	VIRI C	2, 3
8	VIRI C	1, 2, 3, 4	33	OXI	2, 3
9	OXI	1, 3	34	M01-296	3, 4
10	M01-259	1, 2	35	M01-326	3, 4
11	M01-317	1, 2	36	55280.013 (Cyl-2)	3, 4
12	M01-231	1, 2	37	M01-314	3, 4
13	M01-273	1, 2	38	OXI	1, 3
14	M01-269	1, 2	39	M01-359	2, 3
15	OXI	1, 4	40	M01-311	2, 3
16	M01-368	1, 3	41	M01-293	2, 3
17	M01-256	1, 3	42	M01-418	2, 3
18	M01-244	1, 3	43	VIRI A	2, 3
19	M01-288	1, 3	44	OXI	2, 3, 4
20	VIRI A	1, 3	45	M01-210	1, 4
21	OXI	1, 2	46	M01-348	1, 4
22	M01-345	2, 4	47	M01-267	1, 4
23	M01-351	2, 4	48	VIRI C	1, 4
24	M01-214	2, 4	49	OXI	1, 4
25	M01-307	2, 4	50	M01-242	1, 4
26	OXII	2, 4	51	M01-321	1, 4
27	OXI	2, 4	52	OXII	1, 4
28	M01-216	2, 3	53	OXI	1, 4
29	M01-206	2, 3	54	OXI	2, 3

Here, N_g is the number of OXI targets in the group and N_w is the total number of OXI targets on the wheel. A different α_g is calculated for all groups in each wheel.

Of course, as the OXI targets are the reference material used in normalization, the denominator of Equation 2.39 is very close to 1. α_g was found to range between 0.9981 and 1.0008. A value of α_g that is greater than 1 indicates that R_{OXI} was higher in that group than in the rest of the wheel, and that R in the CO₂ sample targets of that group is correspondingly low. Conversely, a value of α_g that is less than 1 indicates that R_{OXI} was lower in that group than in the rest of the wheel, and that R in the CO₂ sample targets of that group is correspondingly high. Table 2.4 shows α_g for each group of the first 15 wheels analyzed between 11/17/2003 and 3/6/2006.

We also ensured that the number of OXI targets in a group was the same as the number of OXI targets used in normalization. For a group that contained 7 OXI targets, 7 bracketing OXI targets were used in normalization. Using a number of targets other than 7 would bias $\overline{r_{std}}$ toward certain OXI targets. Then, the average R_{OXI} would be different even within a single group.

Table 2.4: α_g used to correct individual groups for the difference between the \overline{R} in a group's ensemble of OXI targets and the \overline{R} in all OXI targets on the wheel

Analysis Date	Group	α_g	No. OXI
11/17/2003	1	1.0005	6
	2	1.0000	7
	3	0.9992	8
12/28/2003	1	1.0002	7
	2	1.0000	6
	3	0.9999	7
	4	1.0000	9
2/12/2004	1	1.0000	7
	2	0.9995	6
	3	1.0004	7
2/13/2004	1	0.9998	8
	2	0.9999	6
	3	0.9997	7
Continued on next page			

Table 2.4 – continued from previous page

Analysis Date	Group	α_g	No. OXI
	4	1.0008	3
2/15/2004	1	1.0002	7
	2	1.0004	7
	3	0.9999	7
	4	0.9999	6
	5	0.9992	6
2/4/2005	1	1.0003	6
	2	1.0002	6
	3	0.9997	6
6/3/2005	1	1.0006	7
	2	1.0005	6
	3	0.9981	6
	4	0.9982	6
6/5/2005	1	1.0004	7
	2	0.9999	7
	3	0.9988	6
8/18/2005	1	0.9994	7
	2	1.0006	6
	3	1.0003	5
	4	1.0002	5
8/19/2005	1	1.0006	7
	2	0.9995	5
	3	0.9996	5
	4	0.9993	5
8/21/2005	1	1.0004	6
	2	0.9996	6
	3	1.0002	6
	4	1.0001	5
8/23/2005	1	1.0008	7
	2	1.0003	5
	3	0.9991	5
	4	0.9987	5
3/6/2006	1	1.0006	8
	2	0.9999	8
	3	0.9993	8

Using the α_g calculated for each group, the measured R was corrected in each sputtering period of each target in that group according to:

$$R_{corr} = R/\alpha_g \quad (2.40)$$

The correction to $\Delta^{14}\text{C}$ caused by applying Equation 2.40 was between -1.7 to +3.9 ‰ in the CO_2 samples analyzed in groups on the first 15 wheels. The adjustment to σ_{Int} for these samples was between -0.8 to +0.4 ‰. Average corrections were less than a 0.5 ‰ absolute change in $\Delta^{14}\text{C}$ and near a 0 ‰ change in σ_{Int} .

2.16.2 Definition of wheel factors (α_w)

In addition to the correction for the differences in mean raw $^{14}\text{C}/^{13}\text{C}$ ratio of a group's particular ensemble of OXI targets, another correction is required to eliminate the differences in mean $^{14}\text{C}/^{13}\text{C}$ ratios of the entire ensemble of OXI targets on each wheel. As Table 2.2 and Figure 2.7 showed, significant differences were observed in the average r_{OXI} on different wheels, relative to r_{Cyl-1} and r_{Cyl-2} . These differences caused systematic biases in the $\Delta^{14}\text{C}$ of CO_2 samples and the reproducibility of Cyl-1 and Cyl-2 targets was poorer as a result of these biases.

For those wheels where Cyl-1 or Cyl-2 could not be used for normalization, we calculated a “wheel factor,” or α_w , for each wheel to be used in a similar manner as α_g to correct all targets in that wheel for the biases resulting from the normalization by OXI targets. α_w was calculated by 3 different methods. The following sections outline the procedure in which α_w was calculated for each of the first 15 wheels, and how α_w was applied as a correction.

2.16.3 Calculation of α_w using Cyl-1 and Cyl-2

For the wheels analyzed from 2/4/2005 to 3/6/2006, between 1 to 19 Cyl-1 and Cyl-2 targets were analyzed on each wheel. The number of Cyl-1 and Cyl-2 targets on each wheel is listed in Table 2.5. Though most of these wheels did include 2 or more Cyl-1 or Cyl-2 targets, these targets cannot easily be used for normalization because they were separated into groups and some groups did not include a Cyl-1 or Cyl-2 target.

Instead, the Cyl-1 and Cyl-2 targets can be used to diagnose α_w by comparing the average in \bar{R} for all Cyl-1 or Cyl-2 targets on a wheel to the overall

Table 2.5: Number of Cyl-1 and Cyl-2 targets analyzed on wheels between 2/4/2005 and 3/6/2006

Analysis Date	No. Cyl-1	No. Cyl-2
2/4/2005	10	9
2/5/2005	5	4
4/22/2005	9	9
6/3/2005	1	2
6/5/2005	1	1
8/18/2005	0	2
8/19/2005	1	2
8/21/2005	0	1
8/23/2005	0	3
3/6/2006	2	3

average in \bar{R} for Cyl-1 or Cyl-2 targets analyzed on all wheels. The overall mean \bar{R} of Cyl-1 and Cyl-2 to OXI are:

$$\overline{R_{Cyl-1}} = 1.03818 \quad (2.41)$$

$$\overline{R_{Cyl-2}} = 0.98829 \quad (2.42)$$

The calculation of α_w proceeds by:

$$\alpha_w = \frac{1}{N_{Cyl-1} + N_{Cyl-2}} \left(\sum_{i=1}^{N_{Cyl-1}} \frac{(\overline{R_{Cyl-1}})_i}{1.03812} + \sum_{i=1}^{N_{Cyl-2}} \frac{(\overline{R_{Cyl-2}})_i}{0.98826} \right) \quad (2.43)$$

When α_w is greater than 1, the average $\Delta^{14}\text{C}$ of Cyl-1 and Cyl-2 is consistently high. α_w is less than 1 on wheels where the average $\Delta^{14}\text{C}$ of Cyl-1 and Cyl-2 is consistently low.

2.16.4 Calculation of α_w using replicate La Jolla samples

Five early wheels did not contain any Cyl-1 and Cyl-2 targets, necessitating an alternative means to characterize α_w . To estimate α_w for the first four wheels, we consider replicate flask samples from La Jolla that were measured on separate wheels. As the replicate flask samples contain CO_2 with identical $\Delta^{14}\text{C}$, they provide a similar reference as the Cyl-1 and Cyl-2.

Table 2.6: Number of CO₂ samples from La Jolla replicated from early wheels

Wheel	Replicate Wheel	N_{rep}
11/17/2003	5/8/2006b	4
	10/26/2006	2
12/28/2003	6/5/2005	1
	5/7/2006a	1
	5/8/2006b	1
	10/26/2006	1
	10/28/2006	2
2/12/2004	6/5/2005	1
	5/7/2006a	1
	5/8/2006b	1
	7/22/2006	2
	10/26/2006	1
2/13/2004	5/5/2006a	2

To calculate α_w using replicate samples, we first calculate α_w using Cyl-1 and Cyl-2 according to Equation 2.43 for all 43 wheels analyzed in 2005 and later. Then, we compare the \bar{R} measured in La Jolla samples from the first four wheels, to one or more replicate samples measured in 2005 or later. The calculation of α_w then proceeds by:

$$\alpha_w = \frac{1}{N_{rep}} \sum_{i=1}^{N_{rep}} \frac{(\bar{R})_i}{(\overline{R_{rep}})_i} (\alpha_{w,rep})_i \quad (2.44)$$

$(\bar{R})_i$ indicates the mean normalized ratio in the i^{th} sample measured on 11/17/2003, 12/28/2003, 2/12/2004 or 2/13/2004. $(\overline{R_{rep}})_i$ refers to the mean normalized ratio in the replicate of the i^{th} sample measured on a later wheel. N_{rep} is the number of La Jolla samples analyzed on that wheel which were replicated in later wheels. $\alpha_{w,rep}$ is the α_w calculated for the replicate wheel, according to Equation 2.43.

Table 2.6 lists each of the 4 earliest wheels, the later wheels on which replicate La Jolla samples were analyzed, and the number of replicate pairs on each of the later wheels. Each early wheel had 6 La Jolla CO₂ samples which were replicated in later wheels, except for 2/13/2004, which had 2 replicate samples.

2.16.5 Estimation of α_w for wheel analyzed on 2/15/04

The wheel analyzed on 2/15/2004 did not contain any Cyl-1 or Cyl-2 targets, or any samples from La Jolla. We cannot use either of the methods from the previous sections to estimate α_w for this wheel. Instead, we examine measurements of \bar{R} in CO₂ samples from Samoa and from Mauna Loa.

At Samoa, the 6 samples that were analyzed on 2/15/2004 spanned the period October 2001-August 2002 (Figure 2.9). Over this sampling period, there were also 7 samples measured on 8/23/2005. We used these overlapping samples to calculate α_w for 2/15/2004.

We fit both sets of \bar{R} to a straight line, and evaluated the fit of the two lines at the midpoint of the overlapping period: April 1, 2002. Then, α_w was estimated in a similar manner as in Equation 2.44, using the evaluation of the fit to the 2/15/2004 measurements on April 1, 2002 for \bar{R} in Equation 2.44 and the evaluation of the fit to the 8/23/2005 measurements on April 1, 2002 for \bar{R}_{rep} in Equation 2.44. $\alpha_{w,rep}$ in Equation 2.44 is the α_w calculated for the wheel analyzed on 8/23/2005. The method of evaluating the offset between the two fitted lines at the midpoint is equivalent to averaging the offset over the period of overlap.

Similarly, at Mauna Loa, the 4 samples that were analyzed on 2/15/2004 spanned the period January 2002-August 2002 (Figure 2.9). This period also included 6 samples that were analyzed on 5/21/2006. We used these overlapping samples to make a second estimate of α_w for 2/15/2004. This time, the midpoint of the overlapping period was May 10, 2002. Here we used the evaluation of the fit to the 2/15/2004 measurements on May 10, 2002 for \bar{R} in (2.44) and the evaluation of the fit to the 5/21/2006 measurements on May 10, 2002 for \bar{R}_{rep} in (2.44). $\alpha_{w,rep}$ in (2.44) is the α_w calculated for the wheel analyzed on 5/21/2006.

We use the average of these two estimates of α_w for the 2/15/2004 wheel.

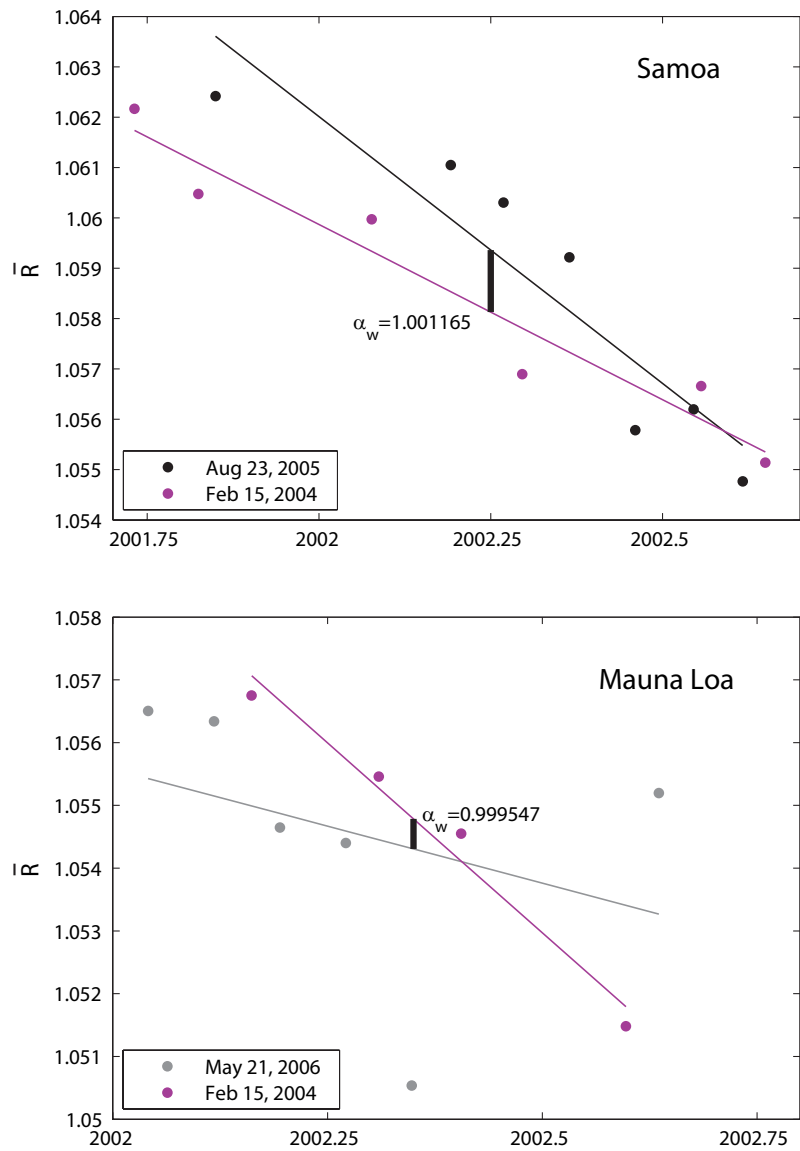


Figure 2.9: Estimation of α_w for wheel analyzed 2/15/04. The upper panel shows \bar{R} in CO_2 samples from Samoa. Samples analyzed on 8/23/2005 are shown in black, with a fitted line. Samples analyzed on 2/15/2004 are shown in purple, with a fitted line. The ratio of the fitted lines at April 1, 2002 estimates α_w for 2/15/2004. The lower panel shows \bar{R} in CO_2 samples from Mauna Loa. Samples analyzed on 5/21/2006 are shown in gray, with a fitted line. Samples analyzed on 2/15/2004 are shown in purple, with a fitted line. The ratio of the fitted lines at May 10, 2002 provides a second estimate of α_w for 2/15/2004.

Table 2.7: α_w and $(\sigma_{BW})_w$ calculated for the first 15 wheels of CO₂ samples analyzed at LLNL.

Analysis Date	α_w	$(\sigma_{BW})_w$
11/17/2003	0.999681	1.7
12/28/2003	1.003594	1.7
2/12/2004	0.998589	1.7
2/13/2004	1.005762	1.7
2/15/2004	1.000356	1.7
2/4/2005	1.003588	0.6
2/5/2005	1.000863	0.4
4/22/2005	0.998160	0.5
6/3/2005	1.001433	1.2
6/5/2005	0.998810	0.7
8/18/2005	1.001790	1.3
8/19/2005	0.999699	0.8
8/21/2005	1.000961	1.3
8/23/2005	1.002889	0.6
3/6/2006	0.999872	1.3

2.16.6 Application of α_w and calculation of total uncertainty

The values of α_w calculated for the first 15 wheels are listed in Table 2.7. α_w was applied to each target according to:

$$\overline{R_{Adj}} = \overline{R_{corr}} / \alpha_w \quad (2.45)$$

$\overline{R_{corr}}$ indicates the \overline{R} that results from applying values of R_{corr} from each sputtering period of a target to Equation 2.6. The calculation of $\Delta^{14}\text{C}$ for each target then proceeds by Equations 2.9 and 2.10, using $\overline{R_{Adj}}$ instead of \overline{R} in 2.9.

For the samples that were measured in the first 15 wheels and corrected using α_g and α_w , we use a quadrature sum to estimate total uncertainty:

$$(\sigma_{Tot})_i^2 = (\sigma_{Int})_i^2 + (\sigma_{BW})_w^2 \quad (2.46)$$

The quadrature sum incorporates the internal uncertainty as well as the between-wheel uncertainty. A different $(\sigma_{Tot})_i$ is calculated for each individual target, i .

$(\sigma_{Int})_i$ is calculated as in Equation 2.11, using $\overline{R_{Adj}}$ instead of \overline{R} . Here we assume that most of the between-wheel uncertainty comes from the OXI normalization and that σ_{IW} is zero. $(\sigma_{BW})_w$ represents the particular between wheel uncertainty for each wheel, w , estimating how well we have been able to correct for the uncertainty from OXI using α_w .

For wheels measured 2/4/2005-3/6/2006, we measure $(\sigma_{BW})_w$ for each wheel as the standard error in Cyl-1 and Cyl-2 $\Delta^{14}\text{C}$ after the correction α_w was applied. For each wheel, the standard error in Cyl-1 and Cyl-2 $\Delta^{14}\text{C}$ gives an estimate of the uncertainty in the mean values of Cyl-1 and Cyl-2 $\Delta^{14}\text{C}$ on that wheel. As such, the standard error in Cyl-1 and Cyl-2 $\Delta^{14}\text{C}$ is a suitable measure of the elimination of uncertainty from the OXI normalization since the uncertainty from the OXI normalization is expressed by differences in mean Cyl-1 and Cyl-2 $\Delta^{14}\text{C}$ on different wheels.

Two wheels included only 1 Cyl-2 target, 8/18/2005 and 8/21/2005. For these two wheels, we use the maximum standard error in Cyl-1 and Cyl-2 $\Delta^{14}\text{C}$ observed over 2/4/2005-3/6/2006 for $(\sigma_{BW})_w$. For wheels that did not contain any Cyl-1 or Cyl-2 samples (11/17/2003-2/15/2004), we use the pooled standard deviation in $\Delta^{14}\text{C}$ of all La Jolla replicate samples, as normalized by OXI and divided by $\sqrt{2}$: 1.7 ‰. Table 2.7 lists $(\sigma_{BW})_w$ for each wheel.

If the total uncertainty calculated according to Equation 2.46 was less than 1.7 ‰ for a particular target, 1.7 ‰ was specified as the total uncertainty for that target. The maximum value of $(\sigma_{Tot})_i$ in CO_2 samples measured on the first 15 wheels was 2.7 ‰.

2.17 Fractionation caused by incomplete graphitization

Ensuring that graphitization proceeds to completion is a key component to achieving high precision measurements. The chemical reduction that transforms

the CO₂ sample to graphite is a fractionating process, selecting the lighter isotope preferentially. CO₂ samples that have not been completely graphitized will result in a measured $\Delta^{14}\text{C}$ that is too low.

When graphitization has not completed, the residual pressure in the reactor will be higher than expected from the initial stoichiometric excess of H₂ gas. Therefore, the reactor pressure can serve as an indicator of the extent of graphitization. Indeed, the pressure in the reactors declines exponentially as the reaction proceeds. After 1-2 hours, the pressure will reach a steady level indicating that the reaction has stopped. Sometimes at this point the pressure will be recognized as being too high and the reactor will be tapped to expose fresh iron to try to restart the reaction. This frequently succeeds in reducing the remaining CO₂ in the reactor. However, at times a sample which has achieved a steady pressure yet has not achieved completion is not recognized. The main cause of this oversight is the poor quality of the pressure sensors used to monitor the graphitization reactors.

Inexpensive pressure sensors from Omega are used in the graphitization reactors. These sensors are both imprecise and very sensitive to temperature, where higher temperatures increase the pressure indicated. Because the reactors are exposed to liquid nitrogen when adding the H₂ gas and then exposed to heaters at 570°C during the reaction, it is difficult to compare the pressure read at these two stages of the procedure.

Incomplete graphitization is not usually recognized until after a sample has been analyzed on the AMS, resulting in a large amount of time wasted analyzing compromised samples. The imprecision in the pressure sensors also leads to a reliance on comparing neighboring measurements in the time series to identify fractionated samples. Therefore, a measurement must be substantially different than its neighbors to be identified as an outlier.

To better quantify the magnitude of the fractionation that occurs during graphitization, I conducted an experiment on Cyl-1 reference samples. I purposely stopped the reaction at different stages of completion (roughly 60 %, 75 % and

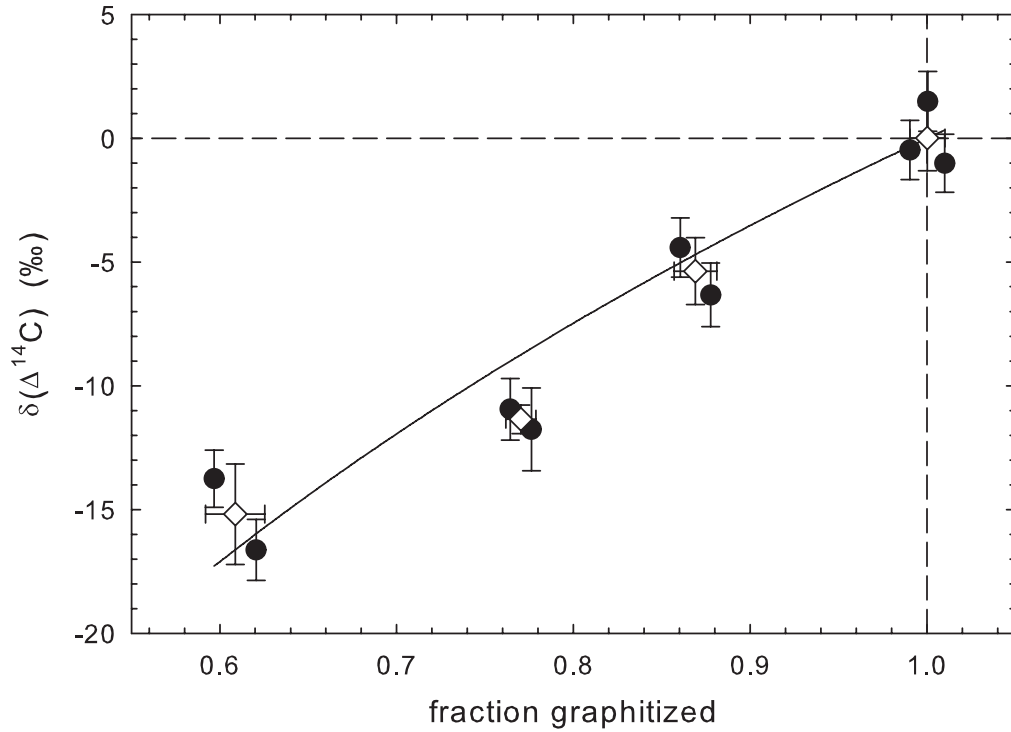


Figure 2.10: Results of fractionation experiment. Fraction graphitized is an estimate of the extent of completion of the graphitization reaction, using the reactor pressure before and after graphitization. $\delta(\Delta^{14}\text{C})$ is the difference from the mean $\Delta^{14}\text{C}$ of the 3 Cyl-1 samples which were allowed to proceed to completion.

90 %) and compared the resulting $\Delta^{14}\text{C}$ to the fraction of CO_2 remaining. The results of this experiment are shown in Figure 2.10 and Table 2.8.

The $\Delta^{14}\text{C}$ in the Cyl-1 samples that were stopped before completion is substantially lower than the samples that graphitized completely. The decrease in $\Delta^{14}\text{C}$ compared to the average of the completed samples was 4.1 ± 0.5 ‰ for each 10% of initial CO_2 gas remaining. This experiment indicates that at least 97 % of the CO_2 sample must be graphitized to achieve a bias that is smaller than -1.5 ‰.

Concerning the background CO_2 measurements included in this thesis, 102 of 699 (15%) samples were fractionated during graphitization. Samoa had the greatest share of fractionated samples where 18 of 76 (24%) had to be rejected. In February 2004, 2 sets of CO_2 samples graphitized on the same rig were all

Table 2.8: Results of fractionation experiment. Fraction graphitized is an estimate of the extent of completion of the graphitization reaction, using the reactor pressure before and after graphitization. $\delta(\Delta^{14}\text{C})$ is the difference from the mean $\Delta^{14}\text{C}$ of the 3 Cyl-1 samples which were allowed to proceed to completion. Mean $\delta(\Delta^{14}\text{C})$ is the average of $\delta(\Delta^{14}\text{C})$ in samples with similar fractions remaining.

Fraction graphitized	$\delta(\Delta^{14}\text{C})$	Mean $\delta(\Delta^{14}\text{C})$
1.01	-1.0	0 ± 1.3
1.00	1.5	
0.99	-0.5	
0.88	-6.3	-5.4 ± 1.4
0.86	-4.4	
0.78	-11.8	-11.4 ± 0.6
0.76	-10.9	
0.62	-16.6	-15.2 ± 2.0
0.60	-13.8	

identified to be fractionated. This wholesale contamination of samples prepared together presents an argument for preparing and analyzing samples in random orders rather than in sets from a certain location or year.

The equipment used to graphitize CO_2 samples for this thesis represents a deficiency that needs to be addressed in future pursuit of high precision measurements at CAMS. I recommend that a graphitization system with pressure sensors of significantly higher quality is constructed that will be used solely for high precision CO_2 samples. I also recommend that extra care is taken in ensuring complete graphitization by tapping all reactors during graphitization or after the preconditioning step and that the reaction is allowed to proceed for several hours rather than being stopped shortly after a steady pressure is achieved.

It is important to note that almost all (85 %) CO_2 samples complete the graphitization reaction and that fractionated samples have been carefully identified through examining residual reactor pressures and by examining the $\Delta^{14}\text{C}$ time series at each station for outliers. Fractionation during graphitization is therefore not a serious concern for errors or uncertainties in measurements of $\Delta^{14}\text{C}$ in CO_2 . The advantage gained by improving the graphitization equipment is in avoiding

the contamination of archived CO₂ samples.

2.18 Special handling of flasks from Palmer Station

In order to capture the outstanding features of the latitudinal profile of $\Delta^{14}\text{C}$, we realized it would be important to obtain samples from a station along the Southern Ocean to augment the six other background sampling sites contained in the Scripps archive. Palmer Station is situated on the coast of Antarctica, at the tip of the Antarctic Peninsula. The Atmospheric Oxygen Research Group (AORG) at Scripps, run by Ralph Keeling, collects whole air samples in triplicate biweekly at Palmer Station.

The AORG air samples are used to characterize O₂/N₂ ratios with either a custom interferometer or a MicroMass IsoPrime mass spectrometer and to characterize CO₂ concentrations with a Siemens infrared gas analyzer (IRGA). Analysis on the interferometer utilizes approximately 2 L STP of sample gas and dilutes the remaining air with a reference gas. Analysis on the mass spectrometer uses only 150 ml and does not inject any reference air thus preserving a 4.85 L air sample after analysis for O₂/N₂ and CO₂. Analysis on the mass spectrometer also enables the measurement of Ar/N₂ ratios. Under usual procedures, all three flasks in a triplicate sample from Palmer Station are analyzed on the interferometer.

We were able to adjust the usual procedure to analyze 2 of 3 flasks from Palmer Station on the interferometer and 1 flask on the mass spectrometer, which allowed the CO₂ remaining in the flask analyzed on the mass spectrometer to be extracted for isotopic analysis. The third flask was not analyzed on the mass spectrometer until after the other two had undergone interferometric analysis which agreed within 7 per meg in $\delta(\text{O}_2/\text{N}_2)$ and 0.2 ppm in CO₂ concentration. If the two flasks did not agree within these thresholds, then the third flask was also analyzed on the interferometer and a CO₂ sample from that set was not extracted.

The AORG whole air samples are collected in 5 L glass flasks, similar to the flasks used by the Scripps CO₂ Program. The AORG flasks have two stopcocks which are sealed with Viton® O-rings whereas the Scripps CO₂ Program's flasks use a single stopcock sealed with high vacuum grease. The AORG flasks are designed to eliminate potential fractionation from large changes in pressure by allowing air to flow through the flask (Keeling et al., 2004).

2.18.1 Comparison of $\Delta^{14}\text{C}$ of air in different flasks

To ensure that the sampling or extraction of air stored in AORG flasks did not introduce any error or bias in ^{14}C in comparison to flasks sampled by the Scripps CO₂ Program, we performed experiments by simultaneously sampling flasks of both types. In La Jolla, flasks of both the AORG and the Scripps CO₂ Program are usually sampled concurrently from the Scripps Pier when clean air conditions are identified. To identify any differences in $\Delta^{14}\text{C}$ measured in different flasks, we conducted analysis on CO₂ samples extracted from both types of flasks that were sampled concurrently on January 26, 2005 and on March 23, 2005. The results from these analyses are listed in Table 2.9. Performing an "Analysis of Variance" (Winer, 1971), similar to a "t-test," on the set sampled on 1/26/2005 resulted in a p value of 0.98, indicating that the mean value of $\Delta^{14}\text{C}$ measured in the AORG flasks is statistically indistinguishable from that measured in the CO₂ flasks. The set of samples from March 23, 2005 included 2 samples from AORG flasks and 1 sample from a CO₂ flask that were flagged during graphitization. Only one measurement from an AORG flask for this set does not allow statistical comparison of the two flask types; however the measured $\Delta^{14}\text{C}$ in the AORG flask lies in between the $\Delta^{14}\text{C}$ measured in the 2 CO₂ flasks. These tests do not indicate that there is any significant difference in measurements of $\Delta^{14}\text{C}$ from AORG flask samples compared to CO₂ flask samples, with respect to the total measurement uncertainty.

Table 2.9: Comparison $\Delta^{14}\text{C}$ in different flask types. Flasks were sampled concurrently on two dates, 1/26/2005 and 3/23/2005, and analyzed for $\Delta^{14}\text{C}$ on 2/4/2005 and 6/3/2005. Flask type “CO₂” refers to the single-valve flask used by the Scripps CO₂ Program; Flask type “O₂” refers to the double-valve flask used by AORG.

Flask Type	Sample ID	Sample Date	Analysis Date	$\Delta^{14}\text{C}$
CO ₂	CDRG247	1/26/2005	2/4/2005	63.1
CO ₂	CDRG248	1/26/2005	2/4/2005	60.1
CO ₂	CDRG249	1/26/2005	2/4/2005	59.3
CO ₂	CDRG250	1/26/2005	2/4/2005	60.4
O ₂	AORG126	1/26/2005	2/4/2005	61.7
O ₂	AORG338	1/26/2005	2/4/2005	61.7
O ₂	AORG416	1/26/2005	2/4/2005	58.4
O ₂	AORG420	1/26/2005	2/4/2005	61.0
CO ₂	CDRG219	3/23/2005	6/3/2005	61.8
CO ₂	CDRG222	3/23/2005	6/3/2005	58.7
O ₂	AORG262	3/23/2005	6/3/2005	60.6

2.18.2 Experiments on $\delta^{13}\text{C}$ in second extraction

To maximize the utility of an air sample, it would be advantageous to measure several different species from one flask. The current procedure for the Scripps CO₂ Program is to analyze CO₂ concentration in each flask sample, then extract one CO₂ sample. Therefore, each flask that is extracted will provide a measure of CO₂ concentration and one of either stable isotopic composition or $\Delta^{14}\text{C}$. In order to investigate the potential for acquiring CO₂ concentration, and O₂/N₂, Ar/N₂, stable isotope and $\Delta^{14}\text{C}$ ratios all from a single sample, I performed several tests to compare the difference between two consecutive CO₂ extractions out of one flask.

The analysis of flask air for CO₂ concentration in the Scripps CO₂ program removes about 1 L STP of air from the flask. As mentioned in Section 2.18 above, analysis of O₂/N₂ and Ar/N₂ by mass spectrometry and CO₂ concentration by the Siemens IRGA in the AORG laboratory uses only 0.15 L STP of air. Extraction of a CO₂ sample using the automated extraction rack of the Scripps CO₂ Program then removes roughly 2 L STP of air. There is potentially 2 L of air

left in a Scripps CO₂ flask sample and 2.85 L in an AORG flask sample after one extraction.

To determine whether the remaining air might be usable for isotopic analysis of CO₂, I sampled 6 CO₂ flasks and 4 AORG flasks concurrently on the Scripps Pier on April 9, 2007. All flasks were analyzed for CO₂ concentration and AORG flasks were analyzed for $\delta(\text{O}_2/\text{N}_2)$ and $\delta(\text{Ar}/\text{N}_2)$ ratios by mass spectrometry. I then performed 2 consecutive extractions on the remaining air. The second extraction of CO₂ (sample B) did not produce as large a CO₂ sample as the first extraction (sample A), where the size ratio B/A averaged 0.36 for the CO₂ flasks and 0.74 for the AORG flasks. The second extraction is smaller from the CO₂ flasks because more air is used in the measurement of CO₂ concentration. All CO₂ samples were analyzed for stable isotope composition using a MicroMass Optima dual-inlet mass spectrometer in the Scripps CO₂ laboratory (Guenther et al., 2001).

Figure 2.11 shows the deviation in $\delta^{13}\text{C}$ in the CO₂ samples against sample size, which was measured as the pressure in mbar of the sample expanded into the fully extended bellows of the mass spectrometer. The results are also listed in Table 2.10. All of the smaller extractions had $\delta^{13}\text{C}$ that was lower than the full-sized extraction, with the difference in $\delta^{13}\text{C}$ increasing with decreasing size. The largest difference in $\delta(\delta^{13}\text{C})$, -0.145 ‰, was observed in sample B of the smallest size. The second extraction evidently results in a fractionation of the remaining flask air. It is unlikely that the difference in $\delta^{13}\text{C}$ and $\delta^{18}\text{O}$ in the smaller samples is caused within the mass spectrometer, as the CO₂ samples are still large enough to control sample gas pressure by adjusting the bellows.

Fractionation probably begins to occur when the pressure in the sample flask drops below a certain level during the second extraction. At this point, the upstream pressure is too low for the flow control valve to control the air flow, which must then drop quite dramatically. The low air flow rate then allows the lighter CO₂ isotopomers to proceed more quickly to the spiral trap, resulting in a CO₂

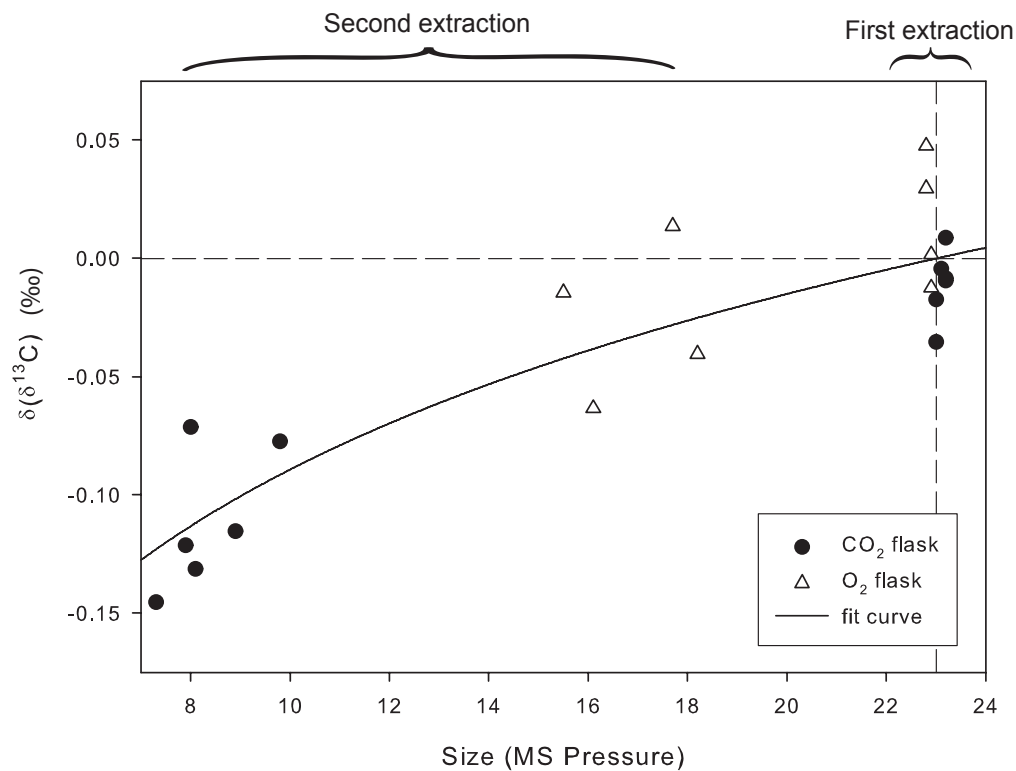


Figure 2.11: $\delta^{13}\text{C}$ in first and second extractions. $\delta(\delta^{13}\text{C})$ shows the difference from mean $\delta^{13}\text{C}$ of all 10 first extractions. Size is the CO_2 sample pressure measured inside the mass spectrometer in mbar. Circles show samples collected with the single-valve flask used by the Scripps CO_2 Program; triangles show samples collected with the double-valve flask used by AORG. The solid line shows the equation used to correct for fractionation (Equation 2.47)

Table 2.10: $\delta^{13}\text{C}$ in first and second extractions. $\delta(\delta^{13}\text{C})$ shows the difference from mean $\delta^{13}\text{C}$ of all 10 first extractions. Flask type “CO₂” refers to the single-valve flask used by the Scripps CO₂ Program; Flask type “O₂” refers to the double-valve flask used by AORG. Size is the CO₂ sample pressure measured inside the mass spectrometer in mbar.

Flask Type	Extraction	Size	$\delta(\delta^{13}\text{C})$
CO ₂	First (A)	23.2	0.009
CO ₂	First (A)	23.2	-0.009
CO ₂	First (A)	23	-0.035
CO ₂	First (A)	23	-0.017
CO ₂	First (A)	23.1	-0.004
CO ₂	First (A)	23.2	-0.008
CO ₂	Second (B)	7.3	-0.145
CO ₂	Second (B)	8.9	-0.115
CO ₂	Second (B)	8.1	-0.131
CO ₂	Second (B)	8	-0.071
CO ₂	Second (B)	9.8	-0.077
CO ₂	Second (B)	7.9	-0.121
O ₂	First (A)	22.9	0.002
O ₂	First (A)	22.8	0.03
O ₂	First (A)	22.8	0.048
O ₂	First (A)	22.9	-0.012
O ₂	Second (B)	18.2	-0.04
O ₂	Second (B)	15.5	-0.014
O ₂	Second (B)	17.7	0.014
O ₂	Second (B)	16.1	-0.063

sample that is isotopically lighter than the original composition.

This observation does not signify that there is any fractionation affecting the sample A that is routinely used for isotopic analysis at Scripps. Rather, the fractionating process probably begins during the second extraction and results in an unequal separation of the sample B from the remaining flask air.

It is possible that this effect could be eliminated by stopping the second extraction early, before the pressure in the flask drops low enough to allow the fractionating process to initiate. Simply adjusting the program to run the extraction for 5 minutes rather than 10 would likely result in a smaller, yet unfractionated sample of CO₂ that could be analyzed for stable isotopic composition.

Alternatively, the fractionation may be corrected for as the magnitude of the fractionation appears to be predictable from the size of the sample. From the results of the experiment shown in Figure 2.11 and Table 2.10, I fit equations to calculate $\delta(\delta^{13}\text{C})$ and $\delta(\delta^{18}\text{O})$ from the sample size measured as the bellows pressure inside the mass spectrometer using a Rayleigh fractionation model.

$$\delta(\delta^{13}\text{C}) = 0.1071 \ln(p/23) \quad (2.47)$$

$$\delta(\delta^{18}\text{O}) = 0.2177 \ln(p/23) \quad (2.48)$$

These equations were fit using a least squares approach in Matlab. The r^2 values for both equations are 0.8.

I applied Equations 2.47 and 2.48 to measurements of $\delta^{13}\text{C}$ and $\delta^{18}\text{O}$ in B samples from Palmer Station. I then subtracted the $\delta(\delta^{13}\text{C})$ and $\delta(\delta^{18}\text{O})$ from the measured values to correct for fractionation during extraction. The corrected measurements of $\delta^{13}\text{C}$ are shown as a time series in Figure 2.12 (black circles). Also shown in Figure 2.12 are measurements of $\delta^{13}\text{C}$ at Palmer Station conducted by the Institute for Arctic and Alpine Research (INSTAAR) at the University of Colorado, Boulder (gray circles). The top panel shows the INSTAAR measurements as reported, and the bottom panel shows the INSTAAR measurements with an addition of 0.13 ‰. The 0.13 ‰ offset is an arbitrary value used to better compare the variability in the two records.

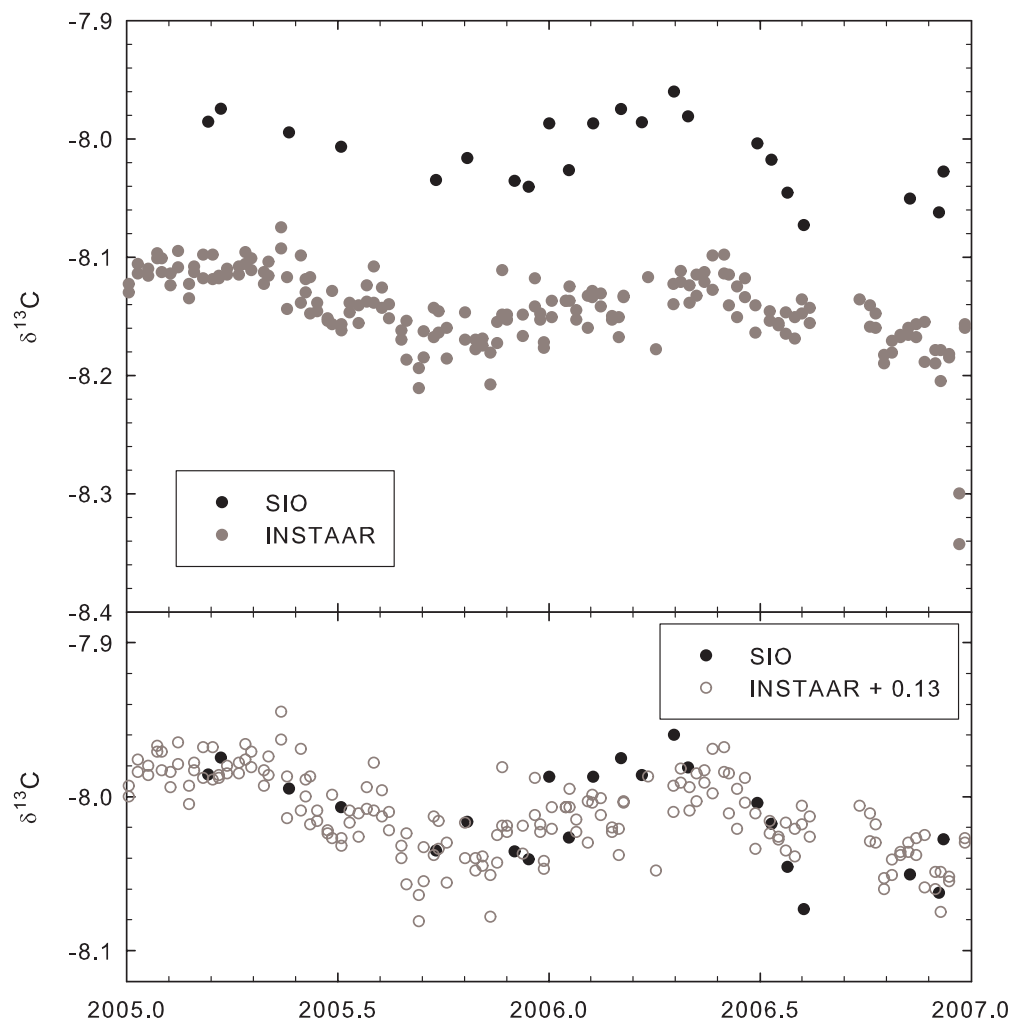


Figure 2.12: Corrected $\delta^{13}\text{C}$ measurements at Palmer Station and $\delta^{13}\text{C}$ in CO_2 measured at INSTAAR. The bottom panel includes an addition of 0.13 ‰ to the INSTAAR data.

After adjusting the INSTAAR measurements by 0.13 ‰, the agreement with the corrected Scripps measurements of $\delta^{13}\text{C}$ is very good at Palmer Station. The records seem to reflect similar seasonal variability over 2005-2007 and show similar levels of scatter in the measurements.

To ensure that the agreement found at Palmer Station is not merely an artifact of the arbitrary constant offset applied to the INSTAAR data, I compared routine Scripps $\delta^{13}\text{C}$ measurements with INSTAAR data at another station: Mauna Loa. The reported data are shown in the top panel of Figure 2.13; the bottom panel of Figure 2.13 shows the INSTAAR data with the 0.13 ‰ offset added. Again, we find excellent comparability between the two records.

The 0.13 ‰ offset used here was an estimate of the laboratory offset based on comparing the $\delta^{13}\text{C}$ measurements conducted at SIO and at INSTAAR, not on an official laboratory intercomparison activity. The actual $\delta^{13}\text{C}$ offset between several stable isotope measurement laboratories is under consideration by the community of scientists conducting the measurements (Miller, 2006). The SIO measurements have been compared in detail to the instrument and calibration procedures of the Centrum voor Isotopen Onderzoek (CIO) at the University of Groningen, The Netherlands, where SIO CO_2 samples were analyzed for $\delta^{13}\text{C}$ and $\delta^{18}\text{O}$ during the period 1977-1992. Measurements conducted at CIO were 0.112 ‰ more negative, on average, than the corresponding SIO measurements. To provide consistency throughout the entire period of $\delta^{13}\text{C}$ measurement, published measurements conducted at SIO have been adjusted by adding a -0.112 ‰ offset (Keeling et al., 1989, 1995; Gruber et al., 1999; Keeling et al., 2005b). The Scripps measurements shown in Figures 2.12 and 2.13 have not been adjusted with the CIO-SIO offset, suggesting that the laboratory offset between INSTAAR and CIO is small. The $\delta^{13}\text{C}$ values reported in the following chapters and appendices are adjusted by -0.112 ‰.

These comparisons suggest that the corrections applied to the smaller B samples from Palmer Station sufficiently correct for the effect of the fractionation

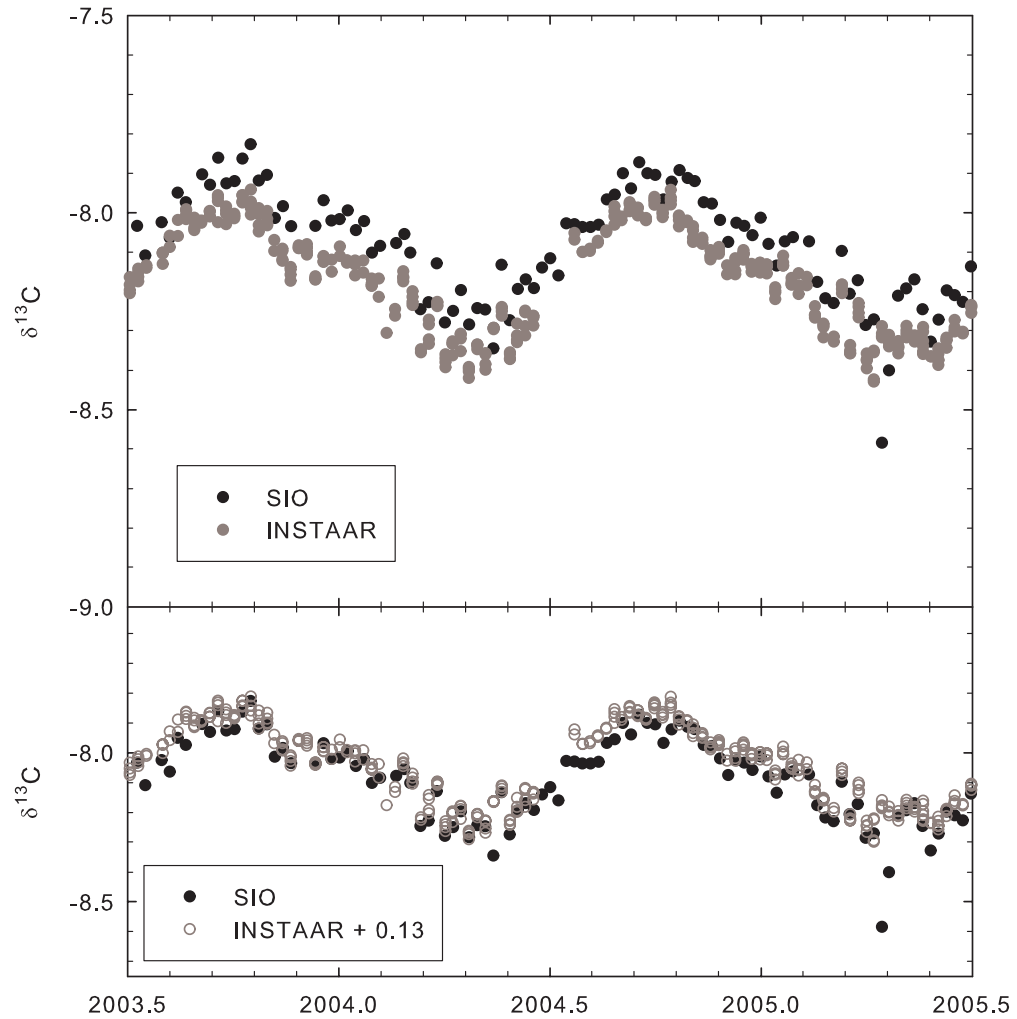


Figure 2.13: Scripps $\delta^{13}\text{C}$ measurements at Mauna Loa and $\delta^{13}\text{C}$ in CO_2 measured at INSTAAR. The bottom panel includes an addition of 0.13 ‰ to the INSTAAR data.

during extraction. This result is noteworthy because it indicates that CO₂ concentration and ratios of $\delta(\text{O}_2/\text{N}_2)$, $\delta(\text{Ar}/\text{N}_2)$, $\delta^{13}\text{C}$, $\delta^{18}\text{O}$ and $\Delta^{14}\text{C}$ can all be analyzed on the same air sample. By analyzing 5 L AORG flasks for O₂/N₂ and Ar/N₂ on the mass spectrometer, we retain enough air to complete two CO₂ extractions that provide CO₂ samples for both $\Delta^{14}\text{C}$ and stable isotopic analysis. As long as the size of the second (B) CO₂ sample is measured, it appears that we can correct for fractionation using Equations 2.47 and 2.48. We may be able to eliminate the need for a correction on the $\delta^{13}\text{C}$ and $\delta^{18}\text{O}$ measurements by adjusting the CO₂ extraction procedures.

The ability to measure so many species in a single sample is an important consideration in planning future sampling activities where the number of flasks may be limited. The ability to perform analyses of multiple species could be especially useful for short-term field campaigns by maximizing the utility of each flask sample. It may also enable regular time series of more species, particularly $\Delta^{14}\text{C}$, to be performed at more background sampling sites.

Expanding the analysis of CO₂, $\delta(\text{O}_2/\text{N}_2)$, $\delta(\text{Ar}/\text{N}_2)$, $\delta^{13}\text{C}$, $\delta^{18}\text{O}$ and $\Delta^{14}\text{C}$ within a single background AORG air sample does necessitate significant changes to the usual practice in AORG. While currently most samples undergo interferometric analysis, the samples designated for CO₂ extractions would have to be analyzed only on the mass spectrometer. Such a change in analytical procedure has implications for the long-term $\delta(\text{O}_2/\text{N}_2)$ records that form the basis of AORG activities. Nevertheless, the measurement of this set of 6 different tracers from within a single air sample is a capability that is unique to Scripps and that provides new opportunities for future carbon cycle studies.

2.19 ¹⁴CO₂ Laboratory Intercomparison

In order to expand the interpretation of our $\Delta^{14}\text{C}$ measurements, it is desirable to combine our data sets with those measured by other laboratories. To

do so, we need to examine the possibility of offsets in $\Delta^{14}\text{C}$ from sampling or analysis by different laboratories. Offsets are not expected to be large in $\Delta^{14}\text{C}$ as there have been ongoing intercomparison activities carried out by the radiocarbon dating community for many years.

We are currently participating in a $^{14}\text{CO}_2$ inter-laboratory comparison activity to diagnose any laboratory offsets. This activity was initiated during the 13th WMO Meeting of CO_2 Experts, where T. Guilderson and I were present to assist in the planning of the intercomparison. The comparison activity is being carried out at the Earth System Research Laboratory (ESRL) of the National Oceanic and Atmospheric Administration (NOAA), where flasks from each laboratory are filled with air from 2 different reference cylinders. The flasks are returned to the respective laboratories for CO_2 extraction and measurement by AMS. The participants of this intercomparison are: Scripps/LLNL; NOAA/University of California, Irvine; Tohoku University, Japan; the University of Groningen Center for Isotope Research (CIO), the Netherlands; and the Commonwealth Scientific and Industrial Research Organisation (CSIRO), Australia. The results of the $^{14}\text{CO}_2$ intercomparison will be reported at the 15th Meeting of CO_2 Experts in 2009.

Several laboratories, including the Heidelberg laboratory in Germany and the Rafter laboratory in New Zealand, are unable to participate in the current intercomparison activity. This is because these laboratories use counting techniques to measure $\Delta^{14}\text{C}$ and require high volume samples of CO_2 . It would be advantageous to establish any offsets between these laboratories and Scripps/LLNL by other means. One possibility for comparison would be to expand the CO_2 sample collection for $\Delta^{14}\text{C}$ to include two sites that AORG or the Scripps CO_2 Program has in common with the Heidelberg network: Alert, Canada and Cape Grim, Australia, and one site that the Scripps CO_2 Program has in common with the Rafter network: Baring Head, New Zealand. The overlapping time series that would result at these stations would enable laboratory offsets to be well quantified. An alternative means of comparison could split a single, integrated high volume CO_2

sample collected by Heidelberg scientists into several CO₂ samples that could be dispersed to several laboratories.

We have already overlapping time series at Point Barrow, Alaska with the University of California, Irvine’s AMS facility. Though these data have not yet been statistically examined for offsets, it appears as though the two time series are very similar.

2.20 Summary

This chapter described the methodology developed while pursuing improvements in measurement uncertainty of $\Delta^{14}\text{C}$ in Scripps CO₂ samples at LLNL. Other than the Poisson counting uncertainty, the main source of uncertainty in $\Delta^{14}\text{C}$ of CO₂ was shown to be added when samples are analyzed in several batches, or wheels. This added “between-wheel” uncertainty was identified by a larger overall scatter than the “within-wheel” scatter in Cyl-1 and Cyl-2 and is also reflected by differences in the average $\Delta^{14}\text{C}$ of Cyl-1 and Cyl-2 on different wheels. The difference in average Cyl-1 and Cyl-2 between wheels is partly caused by small differences in the composition of oxalic acid standard samples that are used in normalization. The oxalic acid samples are prepared differently and show a larger “within-wheel” scatter than the Cyl-1 and Cyl-2 samples.

We eliminated the uncertainty contributed by OXI targets by adopting a new procedure of normalizing the CO₂ sample targets using Cyl-1 targets. For several wheels analyzed before 2006 that could not utilize the Cyl-1 normalization procedure, we implemented corrections to OXI-normalized ratios. Incomplete graphitization was found to result in low values of $\Delta^{14}\text{C}$, indicating that the identification of incompletely graphitized samples is important for eliminating low outliers. Figure 2.14 shows an example of the decreased scatter and the reduction of wheel-to-wheel biases in the $\Delta^{14}\text{C}$ time series when the above modifications were incorporated into the data processing for Samoa. We also found that CO₂ samples

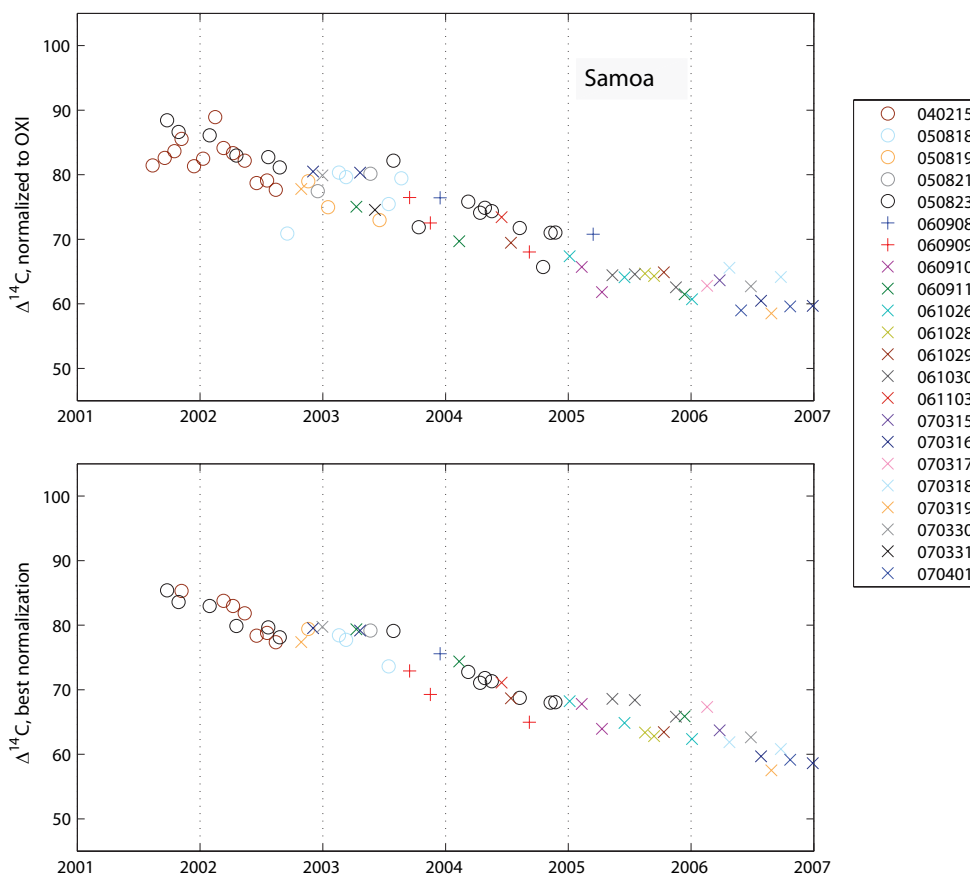


Figure 2.14: $\Delta^{14}\text{C}$ at Samoa, calculated by OXI normalization (upper panel). $\Delta^{14}\text{C}$ at Samoa, calculated by Cyl-1 normalization and adjustments to OXI normalization as described in sections 2.15 and 2.16 (lower panel). Samples flagged for incomplete graphitization were removed from the lower plot.

from Atmospheric Oxygen Research Group flasks were statistically indistinguishable in $\Delta^{14}\text{C}$ as CO_2 samples from the Scripps CO_2 Program and that AORG flask samples allow two CO_2 samples to be extracted, enabling measurement of CO_2 concentration, $\delta(\text{O}_2/\text{N}_2)$, $\delta(\text{Ar}/\text{N}_2)$, $\Delta^{14}\text{C}$, $\delta^{13}\text{C}$ and $\delta^{18}\text{O}$ from a single flask.

Measurements of Cyl-1 and Cyl-2 were integral to achieving high precision $^{14}\text{CO}_2$ measurements at LLNL. The Cyl-1 and Cyl-2 targets provide a means of quantifying the total measurement uncertainty in $\Delta^{14}\text{C}$ of CO_2 samples. After it was revealed that the OXI normalization procedure added considerable uncertainty

to the $^{14}\text{CO}_2$ measurements, the Cyl-1 targets also provided an alternative reference material to use in normalization. Use of Cyl-1 targets for normalizing measured $^{14}\text{C}/^{13}\text{C}$ ratios in CO_2 samples was shown to improve measurement uncertainty to a level of 1.7 ‰ in $\Delta^{14}\text{C}$.

We intend to use the results of this thesis chapter for a journal article providing guidelines to other laboratories wishing to incorporate measurements of CO_2 extracted from whole air cylinders in their data normalization. In addition, at the 14th WMO/IAEA Meeting of Experts on Carbon Dioxide, Other Greenhouse Gases, and Related Tracer Measurement Techniques in September 2007, Dr. Ingeborg Levin and I wrote the expert recommendations for $^{14}\text{CO}_2$ measurements. As part of the recommendations, we advised the use of CO_2 extracted from whole air cylinders as a reference material for $^{14}\text{CO}_2$ measurements.

2.21 Future measurements from the Scripps archive

Though the methodological improvements made in this thesis have enabled substantial enhancements in measurement precision and reproducibility of CO_2 samples, we recommend several more improvements for future measurements of CO_2 from the Scripps Archive.

First, the equipment at CAMS needs to be improved to better identify incompletely graphitized samples. Our experiments showed that the graphitization reaction fractionates the CO_2 sample, producing lower $\Delta^{14}\text{C}$ in the resulting graphite. Graphitization needs to achieve at least 96 ‰ completion to ensure the fractionation error is less than 2 ‰. Presently, low resolution pressure sensors in the vacuum manifold at CAMS make it difficult to identify CO_2 samples that have not completed graphitization. Replacing the current pressure sensors with better quality sensors that are also less temperature-sensitive will allow the user to actively monitor the extent of the graphitization reaction. Then, the user can

try to agitate samples to encourage the graphitization to proceed to completion, or correct the measured $\Delta^{14}\text{C}$ for a calculable amount of fractionation.

Second, the preparation of OXI targets needs to be changed to improve their reproducibility. Measurements of OXI targets show larger scatter than the Cyl-1 and Cyl-2 targets. We believe that the usual procedure of splitting OXI CO_2 gas into several reactors by individual aliquots introduces differences in the resulting OXI targets. Preliminary tests on an alternative method of splitting OXI by expanding OXI CO_2 into several reactors at once suggested that this method may reduce the scatter. Further tests on OXI preparation need to be performed. Stable isotope analysis of the split OXI CO_2 gas, using both methods to split the CO_2 , would tell how much fractionation was introduced by splitting. Better reproducibility in OXI would improve the determination of absolute $\Delta^{14}\text{C}$ of Cyl-1 and Cyl-2.

As the LLNL AMS system measures only $^{14}\text{C}^{4+}$ and $^{13}\text{C}^{4+}$ ions, we are currently unable to detect any target-to-target differences in fractionation that may occur in the ion source as the targets are sputtered, or any target-to-target differences in electron stripping efficiency inside the accelerator. Measurement of all three carbon isotopes would allow correction of fractionation inside the instrument, further improving the detection capabilities at LLNL. The implementation of $^{12}\text{C}^-$ detection in the low-energy section and $^{12}\text{C}^{4+}$ detection in the high-energy section of the AMS has been discussed and may be possible in the next few years. Alteration of the existing setup is a risk to the normal operation of the AMS and therefore must be highly beneficial to the instrument performance. The proposed modification for $^{12}\text{C}^-$ and $^{13}\text{C}^-$ detection in the low-energy section is estimated to enable a precision of 2 ‰ in $\delta^{13}\text{C}$. Such a low precision would only be useful in detecting equivalent target-to-target differences in mass-dependent fractionation of 4 ‰ in $\Delta^{14}\text{C}$. As our current reproducibility is 1.7 ‰ in $\Delta^{14}\text{C}$, this modification would not appear to provide much benefit to the measurement precision in $\Delta^{14}\text{C}$. Installing $^{12}\text{C}^{4+}$ detection in the high-energy section would require sub-

stantial modification, as the injection of the highly abundant $^{12}\text{C}^-$ ion into the accelerator would make it difficult to sustain 6.5 MV at the center. ^{12}C detection at LLNL therefore has not yet been pursued in earnest.

Acknowledgment

Chapter 2, in part, contains some material as it appears in Radiocarbon 2007. Graven, Heather D.; Guilderson, Thomas P., Keeling, Ralph F., University of Arizona, 2007. The dissertation author was the primary investigator and author of this paper.

Chapter 2, in part, is being prepared for publication. Graven, Heather D.; Guilderson, Thomas P.; Keeling, Ralph F. The dissertation author is the primary investigator and author of this paper.

Chapter 3:

A 15-year record of variability in $\Delta^{14}\text{C}$ of CO_2 at La Jolla, California

ABSTRACT

Monthly observations of $\Delta^{14}\text{C}$ in CO_2 at La Jolla, California from 1992 through 2006 are presented in this chapter. A decreasing trend is observed, which averages $-5.5 \pm 0.1 \text{ ‰ yr}^{-1}$ yet shows significant interannual variability. The most prominent excursion from a linear trend occurs in 1998-2000, when relatively high levels of $\Delta^{14}\text{C}$ drop rapidly in 2000. This feature could be explained by enhanced ventilation of the North Pacific in 2000 or by more intense fluxes of stratospheric air across the tropopause during the 1998 El Niño. The amplitude of the seasonal cycle varies from year to year, though maxima in $\Delta^{14}\text{C}$ are consistently observed in October. The phasing of seasonal maximum at La Jolla is similar to yet slightly later than the maxima observed in other Northern Hemisphere midlatitude stations since the 1960s. We find that atmospheric dynamics driving stratosphere-troposphere exchange and vertical mixing in the troposphere are likely to regulate the seasonal variation of $\Delta^{14}\text{C}$ at La Jolla. The record from La Jolla exhibits

close correspondence with observations at Jungfraujoch, Switzerland by the Heidelberg Laboratory and Niwot Ridge, Colorado by the University of Colorado and the University of California, Irvine. During 1992-2006, $\Delta^{14}\text{C}$ at Jungfraujoch was slightly higher, on average, than La Jolla ($+2.2\pm 4.6$ ‰) however since 2003 the measurements at La Jolla, Jungfraujoch and Niwot Ridge appear to be statistically indistinguishable.

3.1 Introduction

Atmospheric measurements of ^{14}C in CO_2 began in 1954 (Rafter, 1955; Rafter and Fergusson, 1957; Manning et al., 1990). A few stations have continued $\Delta^{14}\text{C}$ measurements in CO_2 for several decades, producing long time series that captured the addition of bomb-derived ^{14}C and the atmospheric response to the exchange of this bomb ^{14}C . These stations include Wellington, New Zealand (Manning et al., 1990), Fruholmen, Norway (Nydal and Lovseth, 1983) and Vermunt, Austria (Levin et al., 1985). In the mid-1980s, the Vermunt station was replaced by sample collection at Jungfraujoch, Switzerland (Levin and Kromer, 2004).

These time series have provided valuable records of the atmospheric history of ^{14}C following the massive perturbation of the nuclear weapons tests in the 1950s and 1960s. The response of the earth system to the additional ^{14}C has been an extremely useful measure of the exchange time between different carbon reservoirs. Our understanding of mixing between different parts of the atmosphere and between the troposphere and the land biosphere and surface ocean has been greatly enhanced by the records of ^{14}C in CO_2 during the 20th century (e.g. Goudriaan 1992; Lal and Rama 1966; Naegler et al. 2006).

Long term records will continue to provide a measure of the secular changes in $\Delta^{14}\text{C}$ in CO_2 caused by evolving oceanic and biospheric ^{14}C fluxes and fossil fuel CO_2 emissions. Here we contribute to previous atmospheric records by initiating measurement of $\Delta^{14}\text{C}$ in CO_2 collected by the Scripps CO_2 Program.

We were able to produce a 15-year record at La Jolla by utilizing an archive of CO₂ samples that were saved for retrospective stable isotopic analyses.

Observations of $\Delta^{14}\text{C}$ in CO₂ from the Scripps CO₂ Program use advancements in AMS measurement precision at Lawrence Livermore National Laboratory. High precision measurements allow small anomalies to be distinguished and investigated, leading to a more robust characterization of $\Delta^{14}\text{C}$ variability in the atmosphere. Improved understanding of ¹⁴C dynamics will provide insight on internal cycling of carbon in the ocean and the terrestrial biosphere.

Long term background ¹⁴CO₂ measurements from the Scripps CO₂ Program will also enable the expansion of ¹⁴C in regional studies of carbon cycling (Levin and Hesshaimer, 2000). One of the applications of interest for $\Delta^{14}\text{C}$ measurements is their utility quantifying fossil fuel CO₂. To identify local additions of fossil fuel derived CO₂ with high precision, an accurate characterization of background levels of $\Delta^{14}\text{C}$ is critical. Our measurements reveal substantial and unpredictable variability in $\Delta^{14}\text{C}$ in air sampled at La Jolla under clean air conditions, demonstrating that clean air measurements of $\Delta^{14}\text{C}$ are necessary to define the background $\Delta^{14}\text{C}$ endmember in regional studies.

This chapter presents measurements of $\Delta^{14}\text{C}$ in CO₂ samples from the Scripps CO₂ Program collected at La Jolla, California between 1992 and 2006 and discussions of potential influences on observed variability at multiple timescales.

3.2 Sampling and analysis of clean air samples at La Jolla

CO₂ sampling at La Jolla, California is conducted at the Scripps Pier on the campus of the Scripps Institution of Oceanography. The Scripps Pier extends 320 m from the coast at an elevation of approximately 9 m above the sea surface. The pier is located at 32°52'N and 117°15'W. Six evacuated 5 L round glass flasks are filled with whole air when meteorological conditions are favorable for sampling

clean marine air. These conditions occur in the afternoon when a steady, strong wind is blowing onshore in a westerly or southwesterly sector. Continuous measurements of CO₂ concentration are additionally used to identify clean air conditions suitable for flask sampling, based on short-term stability of CO₂ levels.

Whole air samples are measured for CO₂ concentration by non-dispersive infrared gas analysis. Mixing ratios of CO₂ are measured as $\mu\text{mol CO}_2 \text{ mol}^{-1}$ dry air, which is equivalent to parts per million (ppm). Measurement uncertainty is 0.1 ppm, based on extensive calibration activities (Keeling et al., 2002). Measurements of replicate samples must agree within 0.4 ppm, and measured CO₂ must fall within $3\text{-}\sigma$ from the concentration predicted by an exponential trend, 4 harmonics and smoothing spline fit to previous measurements. Otherwise, the data is rejected and the remaining flask air is discarded.

After analyzing CO₂ concentration in whole air samples, the air remaining in the flask is used to produce a pure CO₂ sample. The cryogenic extraction of CO₂ proceeds by the description provided in Section 2.4.

Pure CO₂ samples are either archived or used for analysis of stable isotope composition. Measurement of $\delta^{13}\text{C}$ and $\delta^{18}\text{O}$ is conducted at Scripps by isotope ratio mass spectrometry using a MicroMass Optima dual-inlet mass spectrometer (Guenther et al., 2001). Precision in $\delta^{13}\text{C}$ is $\pm 0.03 \text{ ‰}$. Values are reported on the PDB scale and include the addition of an offset of -0.112 ‰ . This offset represents the calibration difference between SIO instruments and procedures and those in practice at the Centrum voor Isotopen Onderzoek (CIO) at the University of Groningen, The Netherlands where $\delta^{13}\text{C}$ analyses were conducted on Scripps CO₂ samples during 1977-1992.

3.3 The Scripps CO₂ archive

The Scripps CO₂ Program began archiving samples of atmospheric CO₂ from La Jolla in 1992. Archived samples were initially kept for retrospective mea-

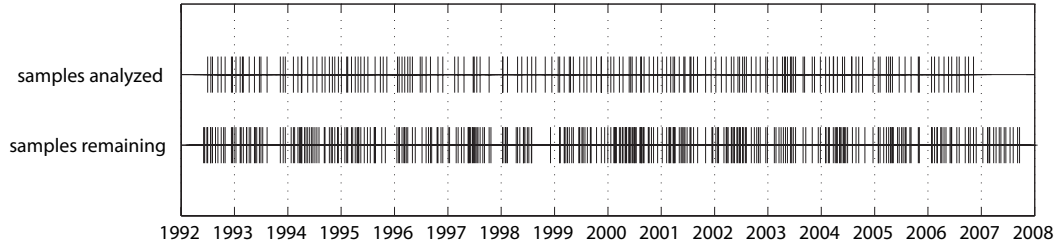


Figure 3.1: Status of the Scripps CO₂ archive from La Jolla. The first row shows sample dates of CO₂ samples which were analyzed for $\Delta^{14}\text{C}$ at LLNL; the second row shows sample dates of CO₂ samples remaining in the Scripps archive.

measurements of stable isotopic composition. In 2003, the archived CO₂ samples began to be used for $\Delta^{14}\text{C}$ analysis as part of this thesis research. A subset of the archived samples was allocated for $\Delta^{14}\text{C}$ analysis at this time, and CO₂ samples produced since are also continually set aside for $\Delta^{14}\text{C}$.

The archive of CO₂ samples from La Jolla designated for $\Delta^{14}\text{C}$ analysis comprised a total of 842 samples through the end of 2007. A diagram showing the sample dates of CO₂ samples that have been analyzed for $\Delta^{14}\text{C}$ and CO₂ samples that remain in the archive is shown in Figure 3.1. For most sample dates at La Jolla 2-3 replicate samples have been saved for $\Delta^{14}\text{C}$ analysis.

Samples were selected from the archive for analysis to produce time series spanning the length of the archive at roughly monthly resolution. Only 35 % of the total archived samples have been utilized: 293 of 842 samples. The record presented here can be augmented by additional measurements in the future that could improve the uncertainty in measured values and increase the temporal resolution.

3.4 $\Delta^{14}\text{C}$ analysis

High precision measurements of ^{14}C in atmospheric CO₂ by Accelerator Mass Spectrometry at Lawrence Livermore National Laboratory were developed as a main part of this thesis work. The methods described in Chapter 2 and

Graven et al. (2007) were employed to analyze $\Delta^{14}\text{C}$ in CO_2 samples from La Jolla. Measurement uncertainty in $\Delta^{14}\text{C}$ was 1.7 ‰ for recently analyzed samples, however 156 samples analyzed prior to 2006 had slightly higher uncertainties of 1.7-2.7 ‰. A total of 256 CO_2 samples from La Jolla were analyzed, which included 73 sample dates for which 2 or more replicate samples were analyzed. The ability to measure replicate samples from La Jolla improved the accuracy of $\Delta^{14}\text{C}$ reported here.

3.5 $\Delta^{14}\text{C}$ observations

The entire set of $\Delta^{14}\text{C}$ observations from La Jolla is plotted in Figure 3.2. Errorbars indicate the total measurement uncertainty for each sample, calculated as in Section 2.15.2 or Section 2.16.6. Replicate measurements have been averaged, and, in the cases where the standard deviation of replicate measurements was greater than the total measurement uncertainty, the errorbars show the standard deviation of replicate measurements. The line in Figure 3.2 shows a cubic smoothing spline.

Measurements from La Jolla are listed in Appendix B.1.1, together with the CO_2 concentration measured in the same flask air and the $\delta^{13}\text{C}$ measured in a concurrent sample. Replicate samples are listed singly, with the total measurement uncertainty for individual samples.

Overall, the record shows a decreasing trend of $\Delta^{14}\text{C}$ at La Jolla. Annual variation can also be detected, though the seasonality is not consistent from year to year. Periodic changes in $\Delta^{14}\text{C}$ over timescales of several years are also suggested in the time series.

The derivative of the cubic smoothing spline shown in Figure 3.2, is plotted in Figure 3.3. The continuous derivative is shown by the solid line, annual averages are shown with circles and the average annual change is represented by the dotted line. This figure is included mostly for descriptive purposes, emphasizing

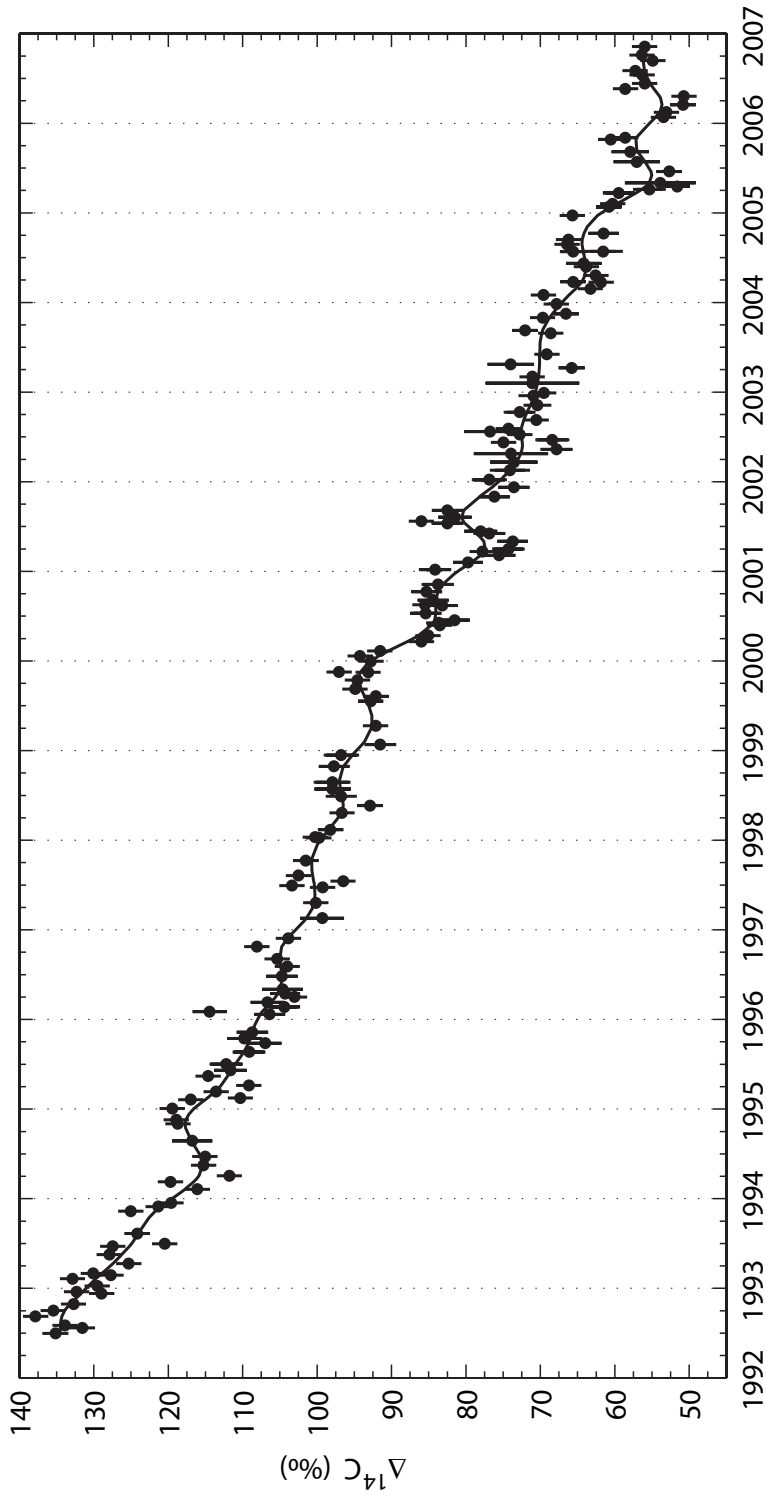


Figure 3.2: $\Delta^{14}\text{C}$ measured in CO_2 sampled at La Jolla. Errorbars show measurement uncertainty of 1.7-2.7 ‰ or standard deviation in $\Delta^{14}\text{C}$ of replicate samples, whichever is larger. The line shows a cubic smoothing spline fit to the data.

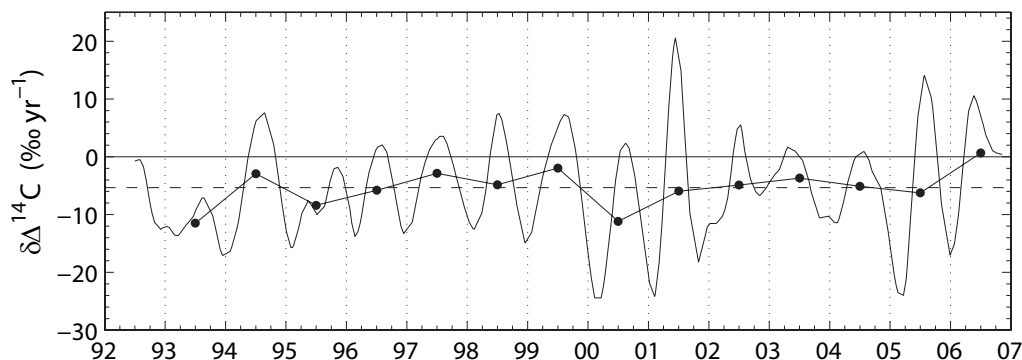


Figure 3.3: Derivative of the cubic smoothing spline fit to $\Delta^{14}\text{C}$ at La Jolla and shown in Figure 3.2. Circles show annual averages in the $\Delta^{14}\text{C}$ derivative and the dashed line shows the average annual change in $\Delta^{14}\text{C}$ at La Jolla: 5.5 ‰ yr^{-1} .

ing that variability in $\Delta^{14}\text{C}$ is apparent on several timescales in the measurements at La Jolla.

3.5.1 Comparison with $\Delta^{14}\text{C}$ at Jungfraujoch and Niwot Ridge

Records have been published for two other clean air stations in the northern mid-latitudes that overlap with the measurement period at La Jolla (1992–2006): Jungfraujoch, Switzerland (Levin and Kromer, 2004) and Niwot Ridge, Colorado (Turnbull et al., 2007). Comparing measurements from these stations to the La Jolla data can provide an indication of the tropospheric variability within clean air in the midlatitudes of the Northern Hemisphere.

CO_2 samples have been collected at Jungfraujoch, Switzerland (46.5°N , 8.0°E , 3.6 km ASL) by I. Levin of the Institut für Umweltphysik, University of Heidelberg, Germany since 1986. These samples are collected by the absorption of CO_2 from many liters of air into a alkaline solution over several days. $\Delta^{14}\text{C}$ has been measured by decay counting techniques with an average measurement uncertainty of 2.7 ‰ .

At Niwot Ridge, Colorado (40.1°N , 105.6°W , 3.5 km ASL), whole air sam-

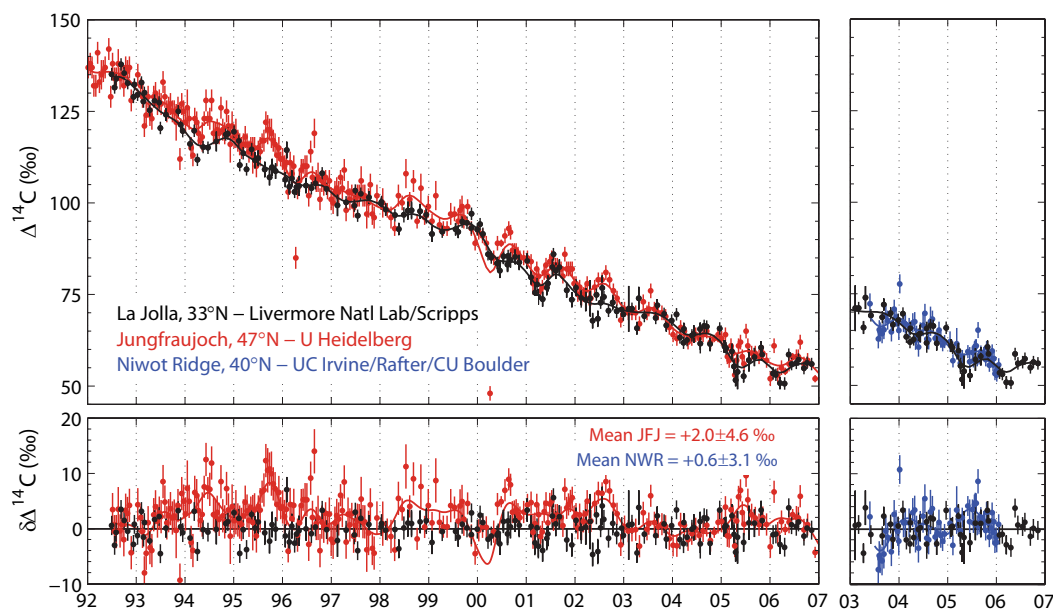


Figure 3.4: Comparison of $\Delta^{14}\text{C}$ measured at La Jolla (black), Jungfraujoch (red, left) and Niwot Ridge (blue, right). The upper panels show measured $\Delta^{14}\text{C}$ with uncertainties expressed as error bars and lines showing cubic smoothing spline curves fit to each time series. The lower panels show the difference from the smooth curve fit to measurements from La Jolla (black line in upper panels).

ples are collected as part of the National Oceanic and Atmospheric Administration (NOAA) Global Monitoring Division (GMD) program. These samples are used to measure concentrations and isotopic composition of several trace gases. Subsequent to analysis of trace gases and stable isotopes, the remaining air samples from 2 flasks collected simultaneously are combined to produce one CO_2 sample for $\Delta^{14}\text{C}$ analysis. Collection of remaining air for ^{14}C analysis began in May 2003. $\Delta^{14}\text{C}$ was measured initially by AMS at the Rafter Radiocarbon Laboratory in New Zealand for samples collected prior to mid-2004, with measurement uncertainty of approximately 2.6 ‰. Since 2004 $\Delta^{14}\text{C}$ has been measured by AMS at the University of California, Irvine (UCI). Measurement uncertainty at UCI is comparable to LLNL: 1.8 ‰.

Comparison of $\Delta^{14}\text{C}$ measurements from these different laboratories requires that any instrument or calibration offsets must be small; close correspon-

dence between records could result from compensation of laboratory offsets by real atmospheric differences. Because of a long history of intercalibration activities between these labs for purposes of radiocarbon dating, laboratory offsets are not expected to be large. Potential offsets are in the process of being diagnosed in the first intercomparison activity specific to ^{14}C in CO_2 , described in Section 2.19.

$\Delta^{14}\text{C}$ records from the three stations, La Jolla, Jungfraujoch and Niwot Ridge, are shown in Figure 3.4. Jungfraujoch data has been updated from Levin and Kromer (2004) through personal communication with I. Levin. Data from each station is plotted in a different color with errorbars denoting measurement uncertainty on each sample and a line showing the fit to a cubic smoothing spline. The bottom panels show the residuals calculated by subtracting the smoothing spline fit to the La Jolla measurements.

Comparison of the three Northern Hemisphere records of $\Delta^{14}\text{C}$ in Figure 3.4 suggests that the differences between stations are small. The average in the residuals from Jungfraujoch is $+2.0\text{‰}$, with a standard deviation of 4.6‰ . The apparent offset of Jungfraujoch from La Jolla is small, yet the excursions are mostly positive. Performing an ‘‘Analysis of Variance’’ (Winer, 1971) on the residuals from La Jolla and Jungfraujoch (shown in the bottom panel of Figure 3.4) results in a p value that is near zero ($p = 1.3 \times 10^{-7}$) indicating that there is a statistically significant difference between the two records. The agreement seems to improve since 2003; an Analysis of Variance for the 2003-2006 period produced a p value of 0.4 which does not refute the hypothesis that the residuals from each station have the same mean (i.e. 0). Correspondence between La Jolla and Niwot Ridge was very close, the residuals at Niwot Ridge had a mean value of $+0.6 \pm 3.1\text{‰}$ and the p value from an Analysis of Variance was 0.4.

The seasonal cycle seems to be variable at all three sites, and also seems to vary between sites in an individual year. For example, 1995 exhibited a strong seasonal cycle at Jungfraujoch whereas $\Delta^{14}\text{C}$ at La Jolla for that year showed no discernable seasonal changes. In 2005, a strong seasonal cycle was observed at

La Jolla but Niwot Ridge and Jungfraujoch did not show unusually large annual variation.

Comparison of $\Delta^{14}\text{C}$ records at La Jolla, Jungfraujoch and Niwot Ridge suggests that there is little difference between the stations despite their spatial and vertical separation. Jungfraujoch is 2 ‰ higher than La Jolla, on average, which was found to be significant, however this difference is not apparent in the last 4 years. It appears that all three stations enable the sampling of air that is representative of background $\Delta^{14}\text{C}$ levels in the midlatitudes of the Northern Hemisphere.

The differences observed in $\Delta^{14}\text{C}$ between La Jolla and Jungfraujoch prior to 2003 may reflect variability in atmospheric transport or regional exchanges of ^{14}C associated with climatic patterns. Further examination of the temporally varying gradient between these two stations using atmospheric transport modeling could provide valuable insights to the transport and exchange of ^{14}C and CO_2 in the Northern Hemisphere.

3.5.2 $\Delta^{14}\text{C}$, CO_2 and $\delta^{13}\text{C}$

Measurements of $\Delta^{14}\text{C}$, CO_2 and $\delta^{13}\text{C}$ at La Jolla are plotted together in Figure 3.5. $\Delta^{14}\text{C}$ is shown as circles in the top panel, where replicate measurements have been averaged. Measurement uncertainty is plotted as errorbars where replicate measurements show the larger of the measurement uncertainty or the standard deviation in all replicates (as in Figure 3.2). The solid curve shows monthly values of $\Delta^{14}\text{C}$ which were calculated from a function incorporating a linear trend ($a+bt$), a single harmonic ($c \cos(2\pi t) + d \sin(2\pi t)$) and a cubic smoothing spline ($s(t)$) fit to the $\Delta^{14}\text{C}$ observations:

$$y = a + bt + c \cos(2\pi t) + d \sin(2\pi t) + s(t) \quad (3.1)$$

The monthly values plotted in Figure 3.5 are listed in Appendix B.2.

The datapoints plotted as circles in the middle panel show the measured

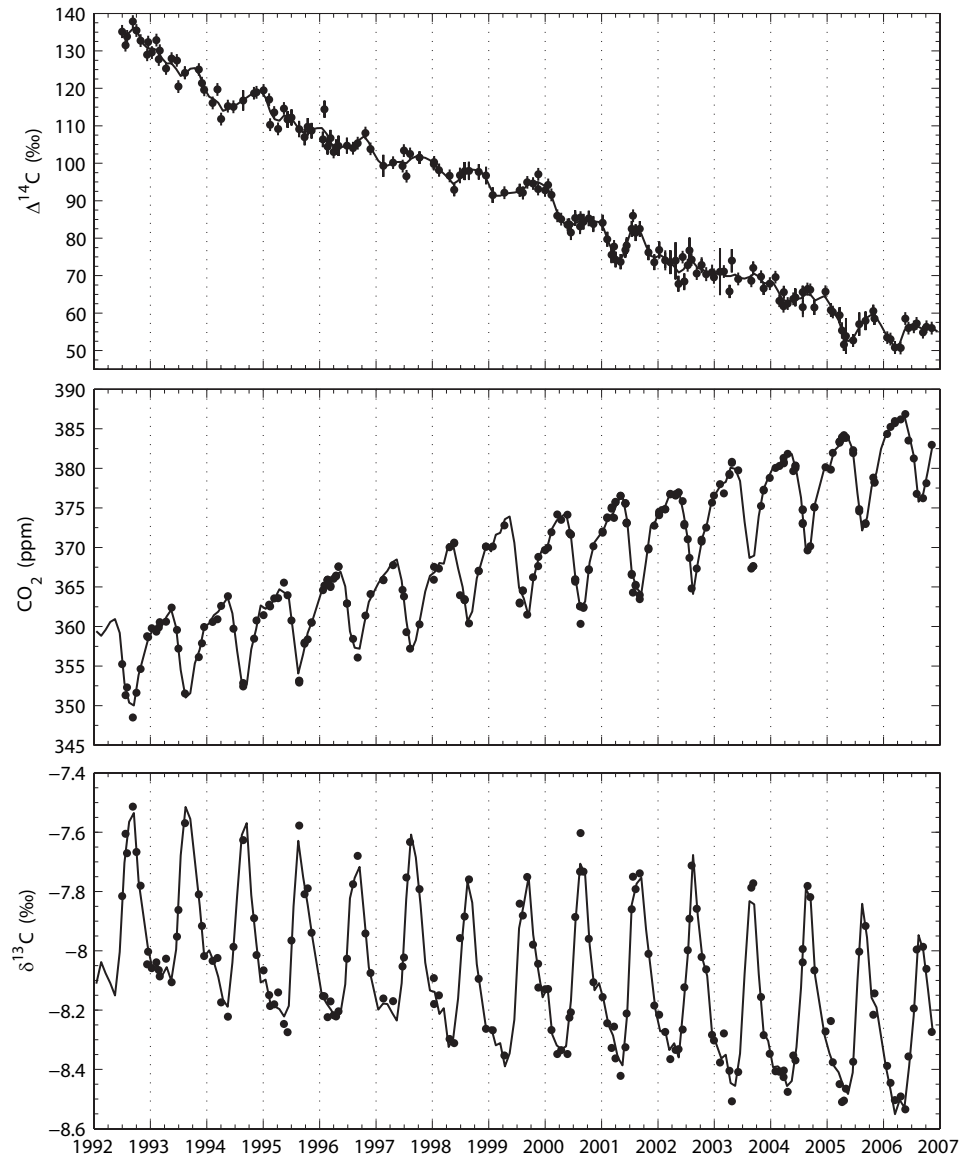


Figure 3.5: Observations of $\Delta^{14}\text{C}$, CO_2 and $\delta^{13}\text{C}$ at La Jolla since 1992. Line in $\Delta^{14}\text{C}$ shows monthly values as calculated by Equation 3.1 and listed in Appendix B.2. For CO_2 and $\delta^{13}\text{C}$, the lines show monthly means and the circles show the sample dates for which $\Delta^{14}\text{C}$ was measured, corresponding to the circles in $\Delta^{14}\text{C}$.

CO₂ concentration in the flask samples where the extracted CO₂ sample was used for $\Delta^{14}\text{C}$ analysis. The lines connect monthly values as reported in Keeling and Whorf (2005).

The datapoints plotted as circles in the bottom panel show the measured $\delta^{13}\text{C}$ ratios in CO₂ samples that were collected concurrently with CO₂ samples used for $\Delta^{14}\text{C}$ analysis. The lines show monthly values as reported in Keeling et al. (2005a).

Plotting $\Delta^{14}\text{C}$, CO₂ and $\delta^{13}\text{C}$ together enables the comparison of variability in the concentration of CO₂ and its isotopic composition. Each parameter shows a secular trend and seasonal cycle. Seasonal variation in CO₂ and $\delta^{13}\text{C}$ are caused by intensive photosynthetic activity of the terrestrial biosphere in the Northern summer, where opposite cycles can be explained by the preferential assimilation of ¹²CO₂ by the land plants. $\Delta^{14}\text{C}$ exhibits seasonal phasing that is not unlike $\delta^{13}\text{C}$ though the dominant process driving the seasonality of $\Delta^{14}\text{C}$ is probably not biospheric exchange, as discussed in Section 3.8.3. This figure also suggests that slight outliers in $\Delta^{14}\text{C}$ are not correlated with unusual deviations in CO₂ or $\delta^{13}\text{C}$, providing confidence that the CO₂ samples represent clean air and that $\Delta^{14}\text{C}$ reflects real atmospheric variability with random errors from measurement uncertainty.

3.6 Secular trend of $\Delta^{14}\text{C}$

The record of $\Delta^{14}\text{C}$ at La Jolla exhibits a trend toward more negative values. Over the recent decades, including the period of observation at La Jolla: 1992-2006, the trend of $\Delta^{14}\text{C}$ was regulated by several processes. Net fluxes of ¹⁴C related to the relaxation of the bomb perturbation interacted with the enhanced dilution of atmospheric ¹⁴C through ever-increasing fossil fuel emissions. Oceanic exchange continued to take up bomb ¹⁴C, on average, whereas the shorter average residence time probably converted the terrestrial biosphere into a source of ¹⁴C

(Caldeira et al., 1998; Randerson et al., 2002) between 1985 and 2000. The rate of decrease of $\Delta^{14}\text{C}$ is sensitive to the annual emissions of fossil fuel CO_2 and the evolving disequilibrium between biospheric and oceanic carbon exchanging with the atmosphere.

We have begun work quantifying the sensitivity of atmospheric $\Delta^{14}\text{C}$ to these processes, specifically with respect to fossil fuel emissions, using simulations of a simple box diffusion model, as in Oeschger et al. (1975) and Joos et al. (1997). The results of this work are preliminary and therefore are not included here.

Figures 3.6 and 3.7 demonstrate the fit of the $\Delta^{14}\text{C}$ record at La Jolla to linear, exponential and polynomial models. For comparison, the trend in atmospheric $\Delta^{14}\text{C}$ exhibited a fairly linear trend during 1900-1950 (Stuiver and Quay, 1981): $\Delta^{14}\text{C}$ declined steadily by $\sim 4 \text{‰ decade}^{-1}$ over 1900-1950. In the 1950s, $\Delta^{14}\text{C}$ rose sharply in response to the nuclear weapons tests. After the nuclear test ban treaty in 1963, $\Delta^{14}\text{C}$ began to decline quasi-exponentially.

A simple linear least squares fit the La Jolla data resulted in a trend of $-5.5 \pm 0.1 \text{‰ yr}^{-1}$. 0.1 represents the 1-sigma uncertainty (68.3 % confidence interval) in fitted slope. The fitted line is plotted in Figure 3.6a, with the residual $\Delta^{14}\text{C}$ after subtraction of the fitted line plotted in Figure 3.6b.

The linear model shows a reasonable fit to the long term change in $\Delta^{14}\text{C}$. Interannual variability in the trend is also suggested by the residuals as there are consecutive years with consistently high $\delta\Delta^{14}\text{C}$ (e.g. 1995-96) or consistently low $\delta\Delta^{14}\text{C}$ (e.g. 1998-99 and 2003-04). Deviations from the fitted line are less than 10 ‰; the standard deviation in the residuals is $\pm 3.5 \text{‰}$. The presence of irregular annual variations is evident in the residuals.

Fitting an exponential function to the La Jolla $\Delta^{14}\text{C}$ record, plotted in Figure 3.6c, results in a decay constant or e-folding time of 16.4 ± 0.2 years. This fitted parameter is in remarkable agreement with the exponential trend observed in earlier records. Measurements at Shauinsland, Germany during 1977-1996 exhibited a decay constant of 16.3 ± 0.2 years (Levin and Kromer, 1997). Observations

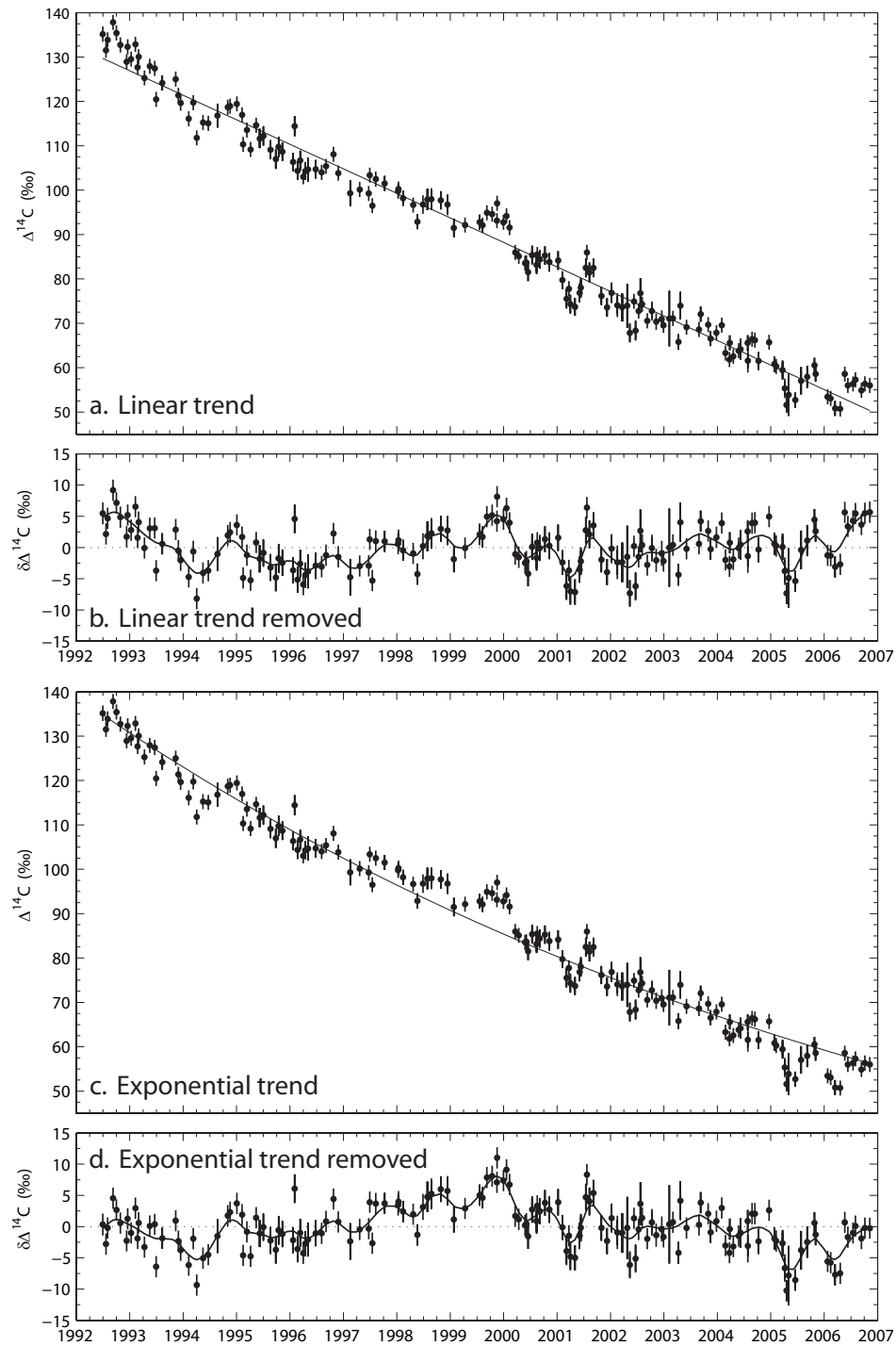


Figure 3.6: $\Delta^{14}\text{C}$ observations from La Jolla fit to linear and exponential models (solid curves in a. and c., respectively). Residual $\Delta^{14}\text{C}$ after subtraction of linear and exponential fits are shown in b. and d., respectively, where the solid curves show cubic smoothing splines through the residuals.

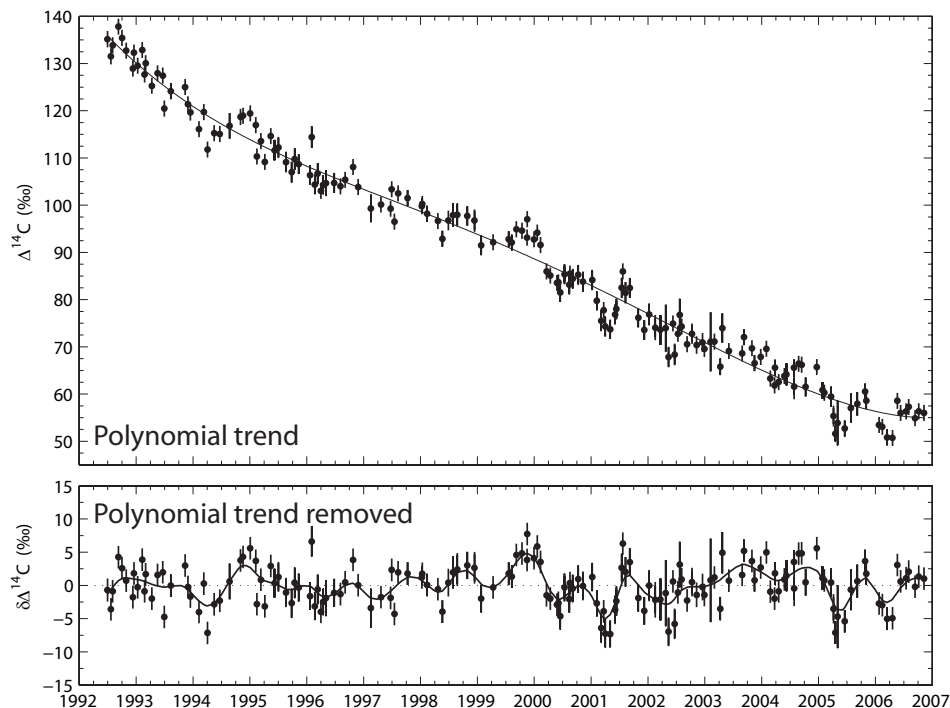


Figure 3.7: $\Delta^{14}\text{C}$ observations from La Jolla fit to a polynomial model (top panel). Residual $\Delta^{14}\text{C}$ after subtraction of polynomial fit is shown in lower panel, where the solid curve shows a cubic smoothing spline through the residuals.

from the South Pacific during the period of the bomb testing through 1987 also show a decay time of roughly 17 years (Manning et al., 1990).

The scatter in residuals of $\Delta^{14}\text{C}$ calculated by subtracting the exponential fit is $\pm 3.7\text{‰}$ (Figure 3.6d), indicating that the exponential fit is slightly poorer than the linear fit to the data. The periods showing the least coherence between the fit exponential and the observations are the middle and the end of the 15-year record. Disagreement in these specific sections of the record might be expected for an exponential fitted to linear data. However, the linear fit also shows excursions in similar periods, suggesting that genuine variability caused interannual anomalies in $\Delta^{14}\text{C}$ at La Jolla.

Finally, the La Jolla measurements were fit to a 4th order polynomial, shown in Figure 3.7 (upper panel) with the residual $\Delta^{14}\text{C}$ after subtracting the fit shown in the lower panel. The polynomial fit shows the best correspondence

to the data. The scatter in the residuals has improved relative to the linear or exponential fits ($\pm 3.1\%$) and multi-year periods of coherent positive or negative excursions are less apparent.

The improvement shown in the polynomial fit indicates that the fluxes of ^{14}C driving changes in $\Delta^{14}\text{C}$ at La Jolla vary on interannual timescales.

3.7 Interannual variability in $\Delta^{14}\text{C}$

In this section, the interannual changes in $\Delta^{14}\text{C}$ at La Jolla are investigated. First, the seasonal variation is removed by the use of cubic smoothing splines (Figure 3.8). The seasonal variation was estimated by subtracting a cubic smoothing spline loosely fit to the $\Delta^{14}\text{C}$ observations at La Jolla, then fitting a stiff spline to the residual $\Delta^{14}\text{C}$. The stiff spline estimating the seasonal variation was evaluated for the sample dates at La Jolla and then subtracted from the original $\Delta^{14}\text{C}$ measurements (shown in top panel of Figure 3.8). The lower panels of Figure 3.8 show the subtraction of both the seasonal variation (annual cycles) and the linear or exponential trend from Figure 3.6a and c.

Removal of the seasonal variation in $\Delta^{14}\text{C}$ at La Jolla reveals interannual anomalies. The anomaly differs slightly whether the linear trend or exponential is assumed, however several features are robust to either assumption. The strongest excursion is the anomalously high $\Delta^{14}\text{C}$ in 1998-1999, followed by a rapid decrease in $\Delta^{14}\text{C}$ in 2000. Shorter periods near 1995 and 2004 also show relatively high levels of $\Delta^{14}\text{C}$.

Figure 3.9 shows the derivative in the apparent $\Delta^{14}\text{C}$ anomaly at La Jolla, calculated with linear (black) and exponential (purple) trends removed. Several climatic indices are also plotted in Figure 3.9; these will be discussed in the following sections.

The anomalies of $\Delta^{14}\text{C}$ shown in Figure 3.8 presumably reflect interannual variability in the fluxes of ^{14}C to the troposphere. As we only have long

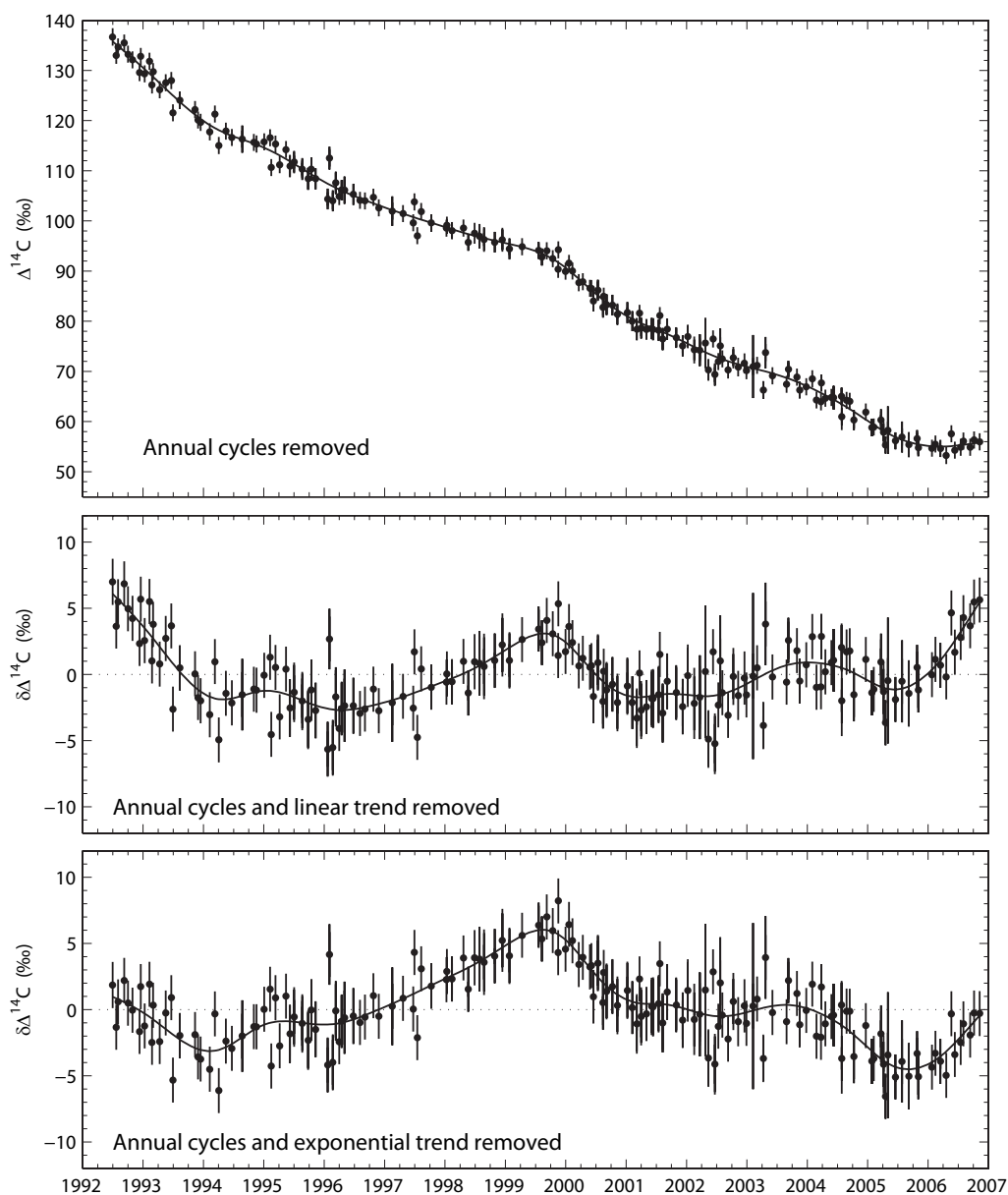


Figure 3.8: $\Delta^{14}\text{C}$ with annual cycles removed (top). Annual cycles were calculated by the use of cubic smoothing splines. The middle panel shows the anomaly in $\Delta^{14}\text{C}$ after removing the annual cycles and the linear trend from Figure 3.6a. The bottom panel shows the anomaly in $\Delta^{14}\text{C}$ after removing the annual cycles and the exponential trend from Figure 3.6c.

records of $\Delta^{14}\text{C}$ at La Jolla, we cannot conclude that the anomalies are global in nature. However, the anomalous changes in $\Delta^{14}\text{C}$ over 1998-2000 are also observed at Jungfraujoch (Levin and Kromer, 2004), suggesting that this feature extended through the Northern Hemisphere midlatitudes. Upcoming publications of Southern Hemisphere measurements by K. Currie and I. Levin will provide important perspective on the extent of recent $\Delta^{14}\text{C}$ anomalies in the atmosphere.

^{14}C fluxes are determined by both the magnitude of the carbon flux and the isotopic disequilibrium between the source and the troposphere. This can be seen in the following equation incorporating an approximation of mass balance in total CO_2 and in ^{14}C :

$$\delta\Delta_{atm} = f(\Delta_a - \Delta_i) \quad (3.2)$$

Here $\delta\Delta_{atm}$ represents the change in $\Delta^{14}\text{C}$ of atmospheric CO_2 resulting from the addition of carbon, f denotes the fraction of CO_2 derived from the carbon source, Δ_a is the $\Delta^{14}\text{C}$ signature in the source of carbon and Δ_i is the initial atmospheric $\Delta^{14}\text{C}$. Carbon reservoirs that have similar $\Delta^{14}\text{C}$ to the atmosphere would have to experience larger anomalies in the mass flux of carbon to produce the same effect on $\Delta^{14}\text{C}$ as flux anomalies from reservoirs that are more disparate from atmospheric $\Delta^{14}\text{C}$.

The following sections investigate possible causes for interannual variability of $\Delta^{14}\text{C}$ observed at La Jolla: air sea gas exchange, land biosphere exchange, stratosphere-troposphere exchange, cosmic ray flux, and fossil fuel emissions.

3.7.1 Interannual variability in air-sea gas exchange

Exchange of CO_2 across the ocean's surface is driven by gradients in partial pressure of CO_2 ($p\text{CO}_2$) between the local atmosphere and the surface water. Strong air-sea gradients can result from the upwelling of deep water to shallow areas. Deep waters can exhibit higher $p\text{CO}_2$ due to the remineralization of organic matter and they also tend to be depleted in ^{14}C , relative to the atmosphere, due to radioactive decay while isolated from the surface.

The El Niño Southern Oscillation (ENSO) is a climatic phenomenon that describes anomalous atmospheric and oceanic circulation in the tropical Pacific (Philander, 1983). During El Niño conditions the predominant trade winds weaken and shift the area of strong convection eastward. Upwelling of deep waters in the eastern equatorial Pacific is greatly reduced and precipitation patterns are altered globally. These effects profoundly influence the net fluxes of carbon to the atmosphere. The reduced upwelling in the eastern tropical Pacific prohibits the exchange of deep, carbon-rich waters with the atmosphere that usually constitute a significant source of CO₂ to the atmosphere (Feely et al., 1999).

Growth rates in CO₂ concentration have been shown to be correlated with ENSO indices (Bacastow et al. 1980; Keeling et al. 1995; Rayner et al. 1999; Bousquet et al. 2000; Figure 3.9), which provide a measure of the presence and intensity of El Niño conditions using observations from the equatorial Pacific. The Multivariate ENSO Index (MEI) incorporates measurements of sea-level pressure, wind, sea surface and surface air temperature, and cloudiness to characterize anomalies associated with El Niño or the opposite, La Niña, conditions. The MEI is plotted in the second panel of Figure 3.9.

El Niño could influence atmospheric $\Delta^{14}\text{C}$ through the suppression of equatorial upwelling. Dutta (2002) found significant coherence between tropospheric $^{14}\text{CO}_2$ and the Multivariate ENSO Index during the period 1651-1950 recorded in tree rings in Washington, USA and during the period 1970-1994 measured with atmospheric CO₂ sampling at Wellington, New Zealand. The correlation between the records was observed to be highest with zero lag or with atmospheric $\Delta^{14}\text{C}$ leading the MEI by several months. As a similar lead in tropical oceanic CO₂ flux anomalies was found by Rayner et al. (1999), Dutta concluded that the positive $\Delta^{14}\text{C}$ anomalies are caused mainly by the reduction in oceanic CO₂ exchange. Observation of reduced atmospheric $\Delta^{14}\text{C}$ in Aychapicho, Ecuador in 1992-93 was attributed to local oceanic CO₂ exchange by Rozanski et al. (1995). The modulation of air-sea fluxes of ^{14}C during El Niño can also be inferred from

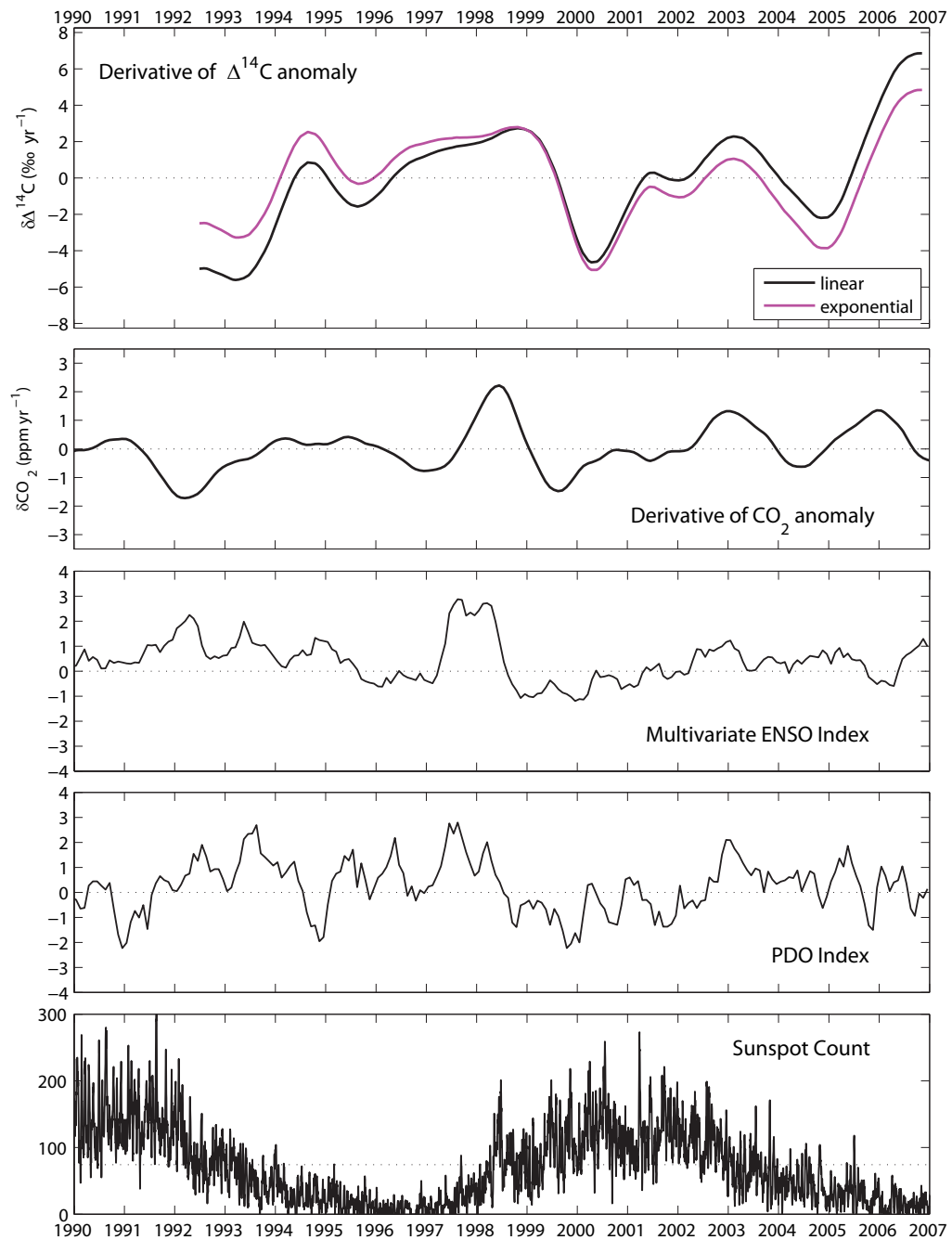


Figure 3.9: Derivative in the $\Delta^{14}\text{C}$ anomaly at La Jolla, calculated with linear (black) and exponential (purple) trends removed. Also shown are the CO_2 anomaly at La Jolla, monthly values of the Multivariate El Niño Southern Oscillation Index, monthly values of the Pacific Decadal Oscillation Index and the daily count of visible sunspots.

ENSO-related variation of $\Delta^{14}\text{C}$ in corals growing in shallow tropical Pacific waters (Guilderson and Schrag, 1998; Guilderson et al., 2004).

The dissolved inorganic carbon in surface waters of the equatorial Eastern Pacific had $\Delta^{14}\text{C}$ of approximately 70 ‰ during 1997-98, as recorded by shallow corals at Wolf Island measured by T. Guilderson. The air-sea gradient in $\Delta^{14}\text{C}$ was then approximately 30 ‰, with surface waters slightly depleted in ^{14}C compared to the atmosphere. This air-sea gradient for the equatorial Eastern Pacific in 1997-98 is much smaller than the gradient would have been previously, due to the uptake and transport of excess ^{14}C by the ocean after the nuclear weapons tests. Performing a calculation similar to Equation 3.2 suggests that a change in $\Delta^{14}\text{C}$ of +2 ‰ yr^{-1} could only be caused by the removal of a 26 Pg C yr^{-1} tropical CO_2 outgassing flux, when estimating that this CO_2 source is well-mixed through the tropics. A 26 Pg C yr^{-1} tropical CO_2 outgassing flux is an order of magnitude larger than the estimated negative flux anomaly associated with the early stages of the 1997-98 El Niño (Rayner et al., 1999), indicating that variation in tropical upwelling cannot explain interannual variability in $\Delta^{14}\text{C}$ at La Jolla over 1998-2000.

Upwelling of deep waters also occurs in the higher latitudes. The Pacific Decadal Oscillation (PDO) is a pattern of interdecadal climatic variability in the North Pacific (Mantua and Hare, 2002; Miller et al., 1994). The phase of the PDO is determined by anomalies in sea surface temperature, which form the basis of a PDO index (plotted in Figure 3.9 and available at <http://jisao.washington.edu/pdo/PDO.latest>). The PDO exhibits abrupt shifts which affect wind stress and mixing in the upper ocean and lead to dramatic impacts on marine ecosystems (Mantua and Hare, 2002; Miller et al., 1994). Such shifts were observed in 1925, 1947 and 1977 (Mantua and Hare, 2002). Investigation of the mechanisms causing the PDO and descriptions of its climatic effects are still in the early stages as the climatic pattern was only identified in the 1990s.

The PDO index suggests that changes in the pattern of sea surface tem-

perature occurred in the North Pacific in 1999-2000. The PDO may have shifted from the “warm” phase to the “cool” phase at this time (Chavez et al., 2003), though definitive identification of a phase shift will not be possible until a longer period of time has elapsed (Mantua and Hare, 2002).

Climatic variability may influence the air-sea exchange of CO₂ in the North Pacific due to changes in ventilation of deep waters (Patra et al., 2005b; McKinley et al., 2006). In their inversion study, Patra et al. (2005b) estimate a ~ 1 Pg C yr⁻¹ net CO₂ flux anomaly occurred in the North Pacific in 2000, and that the fluxes in the North Pacific have significant negative correlation with the PDO. Hamme and Keeling (manuscript in review) have observed a shift in atmospheric potential oxygen during 1999-2001 which seems to be explained by enhancements in the ventilation of deep, O₂-depleted waters. Hamme and Keeling note that the winter of 2000-01 exhibited the coldest SSTs observed in the Pacific north of 40° over the period 1992-2008, which can indicate anomalously deep mixing.

Enhanced ventilation of the North Pacific could cause a negative anomaly in atmospheric $\Delta^{14}\text{C}$ if the ventilated waters were significantly depleted in $\Delta^{14}\text{C}$ relative to the atmosphere. Results from the World Ocean Circulation Experiment (WOCE) in the 1990s show that $\Delta^{14}\text{C}$ age is positively correlated with apparent oxygen utilization in the Pacific (Key et al., 2002). This relationship is expected as O₂ is removed during remineralization of organic carbon and $\Delta^{14}\text{C}$ is removed by decay as a water mass ages, as long as the water mass is old enough that intrusion of bomb excess ¹⁴C has not elevated $\Delta^{14}\text{C}$. WOCE data from section P13 collected along 164°E in 1992 showed $\Delta^{14}\text{C}$ of -30 to +4.6 ‰ in surface samples, which corresponds to an air-sea gradient of 130-160 ‰. If the $\Delta^{14}\text{C}$ of surface waters in this area of the Northwest Pacific near the Kamchatka Peninsula in 2000 was similar to or more depleted than $\Delta^{14}\text{C}$ observed in 1992 because of enhanced upwelling, an increase of ≤ 3 Pg C yr⁻¹ in the gross flux of CO₂ from this area could explain the observed $\Delta^{14}\text{C}$ anomaly in 2000. This estimate is based on a simple calculation, assuming atmospheric $\Delta^{14}\text{C}$ in 2000 was 85 ‰, average $\Delta^{14}\text{C}$

in surface waters was -11‰ and that the anomalous gross CO_2 flux was mixed into the Northern Hemisphere troposphere, north of 30° . As Patra et al. (2005b) estimate a net CO_2 flux anomaly of $\sim 1\text{ Pg C yr}^{-1}$ in the North Pacific in 2000, it is possible that anomalous gross exchange of $\leq 3\text{ Pg C yr}^{-1}$ from the Kamchatka area provide an explanation for the decline in $\Delta^{14}\text{C}$ at La Jolla in 2000.

Changes in North Pacific air-sea CO_2 exchange need to be investigated further to estimate more accurately how large of an effect could be expected in atmospheric $\Delta^{14}\text{C}$. As described in the previous section, the influence of oceanic fluxes of CO_2 on atmospheric $\Delta^{14}\text{C}$ is highly dependent on the level of $\Delta^{14}\text{C}$ in the surface water, our knowledge of which would be aided by more recent observations of $\Delta^{14}\text{C}$ in the North Pacific surface ocean. Continued observation of $\Delta^{14}\text{C}$ at La Jolla will enable more robust identification of interdecadal variability and potential correlation with ventilation of the ocean at mid- to high latitudes of the Northern Hemisphere.

3.7.2 Interannual variability in land biosphere exchange

The exchange of carbon between the atmosphere and the land biosphere varies interannually in response to climatic and anthropogenic influences. Variation in the gross terrestrial flux of CO_2 to the atmosphere may therefore contribute to anomalies in $\Delta^{14}\text{C}$ of CO_2 at La Jolla.

Significant interannual changes in atmospheric CO_2 concentration can be attributed to El Niño periods, with the largest perturbation caused by an anomalous terrestrial source of CO_2 (Rayner et al., 1999; Bousquet et al., 2000). Altered atmospheric circulation patterns produce warmer, drier conditions, on average, that enhance respiration fluxes from the terrestrial biosphere and promote the release of carbon through wildfires (Van der Werf et al., 2004). For the 1998 El Niño, the anomalous land flux may have been $2\text{--}6\text{ Pg C yr}^{-1}$ (Patra et al., 2005a), where most of the source was caused by biomass burning.

While the net biospheric CO_2 flux to the atmosphere was anomalously

high because of the 1998 El Niño, the gross fluxes influencing $\Delta^{14}\text{C}$ changed by a smaller percentage ($<5\%$). As the average $\Delta^{14}\text{C}$ disequilibrium between the biosphere and the atmosphere was probably less than 30 ‰ in 1998 (Randerson et al., 2002), the influence of enhancements in biospheric fluxes of 2-6 Pg C yr⁻¹ on atmospheric $\Delta^{14}\text{C}$ would be less than 0.5 ‰ yr⁻¹.

However, El Niño could have a substantial influence on atmospheric $\Delta^{14}\text{C}$ by releasing long-lived biospheric carbon with high $\Delta^{14}\text{C}$ during biomass burning. Van der Werf et al. (2004) estimate that fire activity accounted for $66 \pm 24\%$ of the CO₂ growth rate anomaly during the 1998 El Niño. Fires could increase the average age of biospheric carbon released to the atmosphere, which could mean that the isotopic disequilibrium between the atmosphere and the mean biospheric signature could have been larger than average. This would enhance any perturbation that may be effected on $\Delta^{14}\text{C}$ by the terrestrial biosphere during El Niño.

To estimate the possibility for respiration and biomass burning to drive the observed $\Delta^{14}\text{C}$ anomaly at La Jolla, the disequilibrium between the atmosphere and the average $\Delta^{14}\text{C}$ in the anomalous biospheric carbon source required to explain increases of +2 ‰ yr⁻¹ was calculated. Assuming the additional biospheric flux of 2-6 Pg C yr⁻¹ was mixed into the Northern Hemisphere troposphere, this carbon would have to have been at least 100 ‰ or as much as 300 ‰ higher than atmospheric $\Delta^{14}\text{C}$ to account for a 2 ‰ yr⁻¹ positive anomaly. These calculations suggest it is unlikely that the variability in $\Delta^{14}\text{C}$ at La Jolla can be solely attributed to biospheric fluxes, however, carbon released from wildfires probably did cause a small increase in atmospheric $\Delta^{14}\text{C}$ in 1998.

3.7.3 Interannual variability in stratosphere-troposphere exchange

Mixing of air from the stratosphere increases $\Delta^{14}\text{C}$ in the troposphere as stratospheric air is enriched in $\Delta^{14}\text{C}$ from cosmogenic production of ¹⁴C and because it is isolated from exchanges that deplete $\Delta^{14}\text{C}$ at the surface. The mag-

nitude of stratosphere-troposphere exchange (STE) is influenced by El Niño (Zeng and Pyle, 2005; James et al., 2003). More intense STE is observed during the positive phase of El Niño, which may be driven by changes in the subtropical jet (Langford, 1999). Using a coupled climate-chemistry model, Zeng and Pyle (2005) found extratropical STE increased by 10 % over the mean value in 1998, then dropped to 10 % below the mean value in 1999. Appenzeller et al. (1996) estimate the extratropical STE is 3.5×10^{17} kg yr⁻¹. The effect on tropospheric $\Delta^{14}\text{C}$ of a 10 % increase in STE over one year would be ~ 2 ‰ higher $\Delta^{14}\text{C}$, assuming the stratospheric air was 50 ‰ more enriched than the troposphere and initially mixed into the troposphere north of 30°N. This simple estimate corresponds reasonably well with the observed $\Delta^{14}\text{C}$ anomaly at La Jolla, suggesting that enhancements in STE exchange caused by El Niño may drive interannual variability of ± 2 -3 ‰ in Northern Hemisphere $\Delta^{14}\text{C}$.

The Quasi-Biennial Oscillation (QBO) is a periodic variation in the tropical stratospheric winds which regulate tropical upwelling of tropospheric air into the stratosphere (Baldwin et al., 2001). The QBO influences extratropical planetary waves that regulate surface weather patterns and stratosphere-troposphere exchange. Through mass continuity, tropospheric upwelling rates in the tropics also influence the large scale overturning circulation in the atmosphere. The QBO has an average period of 28 months.

Hamilton and Fan (2000) investigated a potential QBO effect in long-lived trace gases through modeling of atmospheric dynamics associated with the QBO. Transport effects related to the QBO were found to be a significant influence on simulated atmospheric growth rates of atmospheric N₂O and CH₄.

Through the modulation of ¹⁴C-enriched stratospheric air input to the troposphere, the QBO could also influence tropospheric levels of $\Delta^{14}\text{C}$. Though not apparent in Figures 3.8 and 3.9, spectral analysis of the detrended monthly values of $\Delta^{14}\text{C}$ at La Jolla suggested regular variability with a period of 28 months exists in the data. This period is also a mode of variability in the QBO index

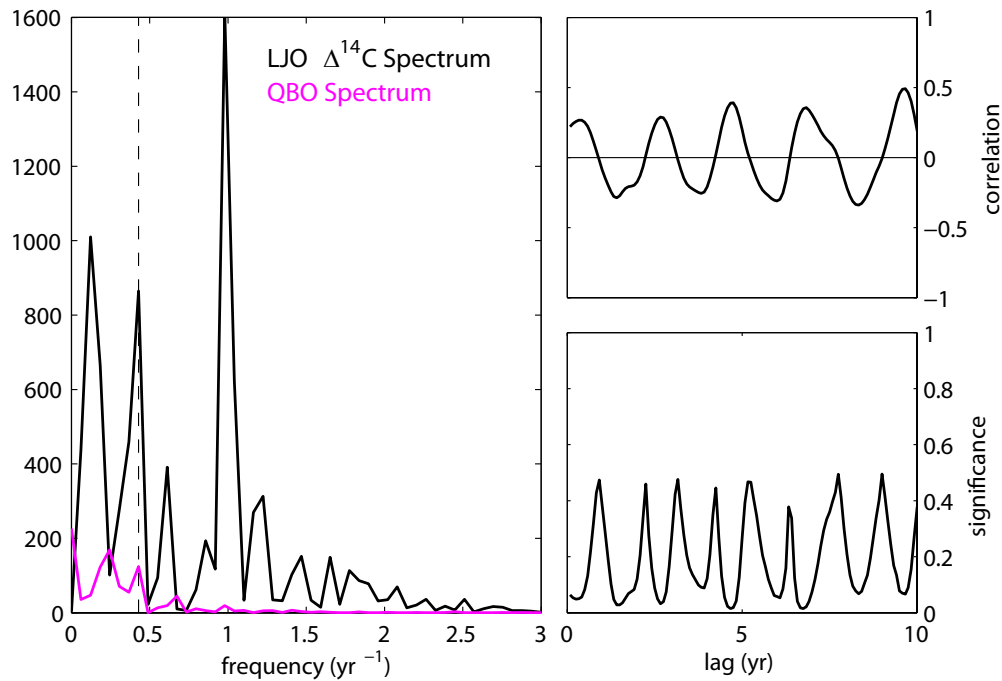


Figure 3.10: Power spectra of $\Delta^{14}\text{C}$ at La Jolla (black) and the Quasi-Biennial Oscillation Index (purple) in left panel. The dashed line shows the frequency corresponding to a period of 28 months. The results of a random phase test between $\Delta^{14}\text{C}$ at La Jolla and the QBO Index for different lags are shown at right, with correlation in the upper panel and significance in the lower panel.

over 1992-2006, which is measured as the anomaly in stratospheric tropical zonal wind strength (available at <http://www.cpc.noaa.gov/data/indices/>). The power spectra of monthly $\Delta^{14}\text{C}$ at La Jolla and the QBO index are shown in Figure 3.10. The two records do not show significant correlation for any lag time in a random phase test (also shown in Figure 3.10), which is a test of time series correlation appropriate to use when there is high serial correlation expected in the data (Ebisuzaki, 1997). However, it is possible that transport effects related to the QBO may be a small influence on extratropical ^{14}C that could become detectable in the next few years.

3.7.4 Interannual variability in cosmic ray flux

The production of ^{14}C is regulated by the flux of cosmic ray particles entering the Earth's atmosphere. During periods of intense solar activity, cosmic rays are deflected from entering the atmosphere and ^{14}C production is reduced. When solar activity is diminished, more cosmic radiation penetrates the atmosphere causing enhanced production of ^{14}C .

Solar activity varies on an 11 year cycle, as well as on longer timescales. The activity of the sun has historically been estimated by counting the number of spots visible on the face of the sun. Counts of the number of sunspots are plotted in Figure 3.9 with data from NOAA's National Geophysical Data Center (available at <http://www.ngdc.noaa.gov/stp/SOLAR/getdata.html>).

Several observations of $\Delta^{14}\text{C}$ in tree rings, wines, whiskies and plant seeds have suggested the occurrence of an 11-year cycle with ~ 10 ‰ peak-to-peak variation in atmospheric $\Delta^{14}\text{C}$ during the early 1900s that may be correlated with the solar cycle (Burchuladze et al., 1980, 1993; Baxter and Walton, 1971; Stuiver and Quay, 1981). Stuiver and Quay (1981) calculate that the modulation of ^{14}C production caused by the 11-year solar cycle would have a small effect on atmospheric $\Delta^{14}\text{C}$ of only 1 ‰. Though the production varies by a substantial amount, ~ 10 % (Lowe and Allan, 2002), production anomalies are not sustained for very long and changes in $\Delta^{14}\text{C}$ are buffered by exchanges with the biospheric and oceanic reservoirs of ^{14}C . Baxter and Walton (1971) propose that the observed variation in $\Delta^{14}\text{C}$ in the early 1900s could be influenced by the climatic effects of solar intensity on the exchange of air between the stratosphere and troposphere, rather than the variation in total inventory of ^{14}C in the atmosphere.

The $\Delta^{14}\text{C}$ record at La Jolla extends from the end of solar cycle 22 through solar cycle 23. Comparing the derivative of the anomaly in $\Delta^{14}\text{C}$ at La Jolla shown in Figure 3.9 to the sunspot cycle plotted in the bottom panel does not reveal any obvious relationship. In the records of the early 20th century, atmospheric $\Delta^{14}\text{C}$ was positively correlated with the sunspot number. In the record

from La Jolla, $\Delta^{14}\text{C}$ is not consistently high when solar activity is high. As the 15-year record does not provide a long enough time series to clearly identify decadal variations, we cannot conclude whether solar activity has a significant impact on atmospheric $\Delta^{14}\text{C}$ in recent decades.

3.7.5 Interannual variability in fossil fuel emissions

Over the period of $\Delta^{14}\text{C}$ observation at La Jolla global emissions of fossil fuel CO_2 rose by approximately 2 % per year, ranging between -0.8 to 5.4 % growth each year (Marland et al., 2007; Canadell et al., 2007). The influence of fossil fuel emissions on global $\Delta^{14}\text{C}$ increased over this period. While fossil fuel emissions are a major determinant of the long-term trend in $\Delta^{14}\text{C}$, growth in emissions has been mainly been steady and does not show temporal variability that is coherent with interannual $\Delta^{14}\text{C}$ variability at La Jolla nor large enough to expect positive and negative anomalies of several ‰.

3.7.6 Conclusions about secular trend of $\Delta^{14}\text{C}$

The most outstanding feature in the record of $\Delta^{14}\text{C}$ in CO_2 at La Jolla is a relative maximum in 1998-1999 which rapidly changes to a negative anomaly in 2000. Through examining potential influences on $\Delta^{14}\text{C}$ at interannual time scales, we find that this anomaly is likely to be caused by changes in oceanic ventilation in the North Pacific or by modulation of stratosphere-troposphere exchange related to the 1998 El Niño. Release of long-lived carbon with enriched $\Delta^{14}\text{C}$ by biomass burning during El Niño may also explain a portion of the relatively high $\Delta^{14}\text{C}$ in 1998-1999.

We suggest that $\Delta^{14}\text{C}$ is sensitive to climatic variability and that examination of $\Delta^{14}\text{C}$ anomalies could provide new information on gross CO_2 fluxes across the ocean surface. Further investigation of the anomaly in 1998-2000 would be aided by atmospheric $\Delta^{14}\text{C}$ measurements from the Southern Hemisphere over

this period as well as simulations of atmospheric transport including stratosphere-troposphere exchange.

3.8 Seasonal cycle

3.8.1 Observation of seasonal cycle

The $\Delta^{14}\text{C}$ observations from La Jolla show substantial variability at sub-annual timescales. The following sections characterize the seasonal variation at La Jolla and discuss the potential influences driving the changes in $\Delta^{14}\text{C}$ during the year.

The seasonal cycle at La Jolla can be examined by subtracting the trend of $\Delta^{14}\text{C}$ and overlaying the detrended $\Delta^{14}\text{C}$ from all years onto a single calendar year, as shown in Figure 3.11. Here, the linear trend from Section 3.6 was subtracted. Each year of data is shown with a different symbol and monthly means and standard deviations are shown by black circles and error bars.

Figure 3.11 indicates that $\Delta^{14}\text{C}$ at La Jolla is lower in the first half of the year, and higher the second half. Highest values tend to occur in September and October, whereas the lowest $\Delta^{14}\text{C}$ is found in April. The difference between the seasonal minimum and maximum is approximately 5 ‰, on average. Comparison of all 15 years shows substantial scatter, where deviation around the monthly means shown in black is $\pm 3\text{--}5$ ‰. Part of this scatter is caused by excursions from the linear trend investigated in the previous section. Part of the scatter also arises from year-to-year variability in the seasonal cycle at La Jolla.

Another estimate of the average seasonal variation at La Jolla can be obtained by fitting a linear trend and single harmonic to observed $\Delta^{14}\text{C}$. The components of this function are the first 4 terms of Equation 3.1. The fit is plotted in Figure 3.12 together with the $\Delta^{14}\text{C}$ observations. The lower panel shows the residuals after subtracting the fitted function. Comparison to the removal of only the linear trend (Figure 3.6b) shows that most of the subannual variability has

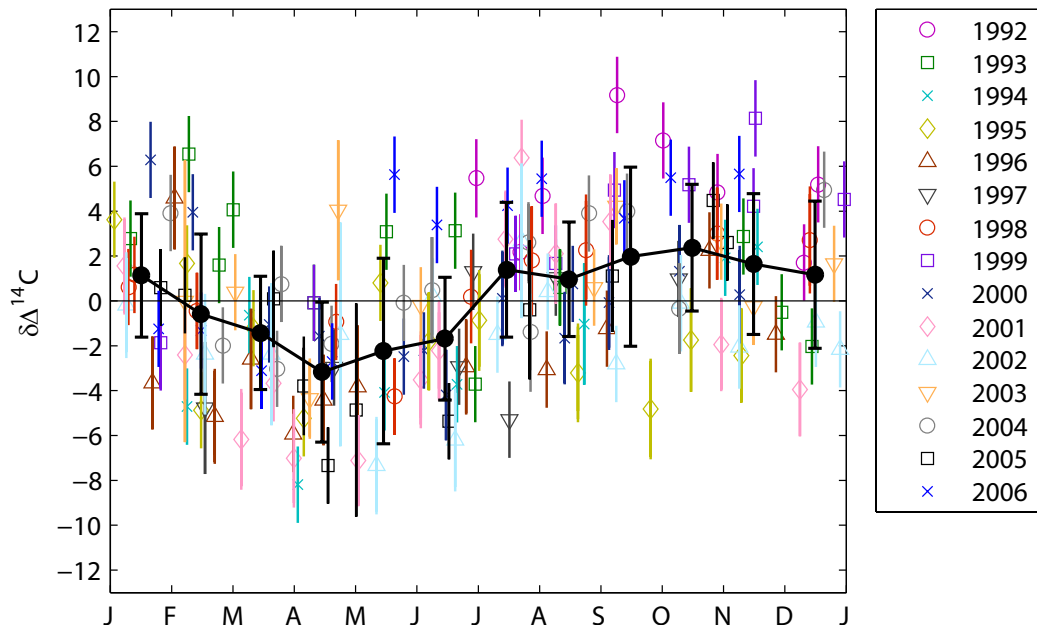


Figure 3.11: Seasonal variation in detrended $\Delta^{14}\text{C}$ observations from all years. Symbols represent measurements from different years and black circles and error-bars show mean and standard deviation for each month.

been removed. Seasonal variation remains in the residuals of some years which show substantial scatter ($\pm 3.1\text{‰}$) overall, reflecting the interannual variation in the seasonality of $\Delta^{14}\text{C}$ at La Jolla.

To better examine the fitted harmonic, the cycle for each year is shown in Figure 3.13 with the trend removed. The fitted parameters of the harmonic suggest the average seasonal cycle has a peak-to-peak amplitude of $5.0 \pm 0.5\text{‰}$, which is twice the amplitude of the sinusoid in Figure 3.13. The seasonal amplitude calculated by the harmonic and by overlaying detrended $\Delta^{14}\text{C}$ from each year (Figure 3.11) are similar. The maximum $\Delta^{14}\text{C}$ in the fitted harmonic occurs on October 19, ± 11 days. The trend fitted to this function ($-5.5 \pm 0.1\text{‰ yr}^{-1}$) is not statistically different from the slope calculated by fitting a linear trend alone.

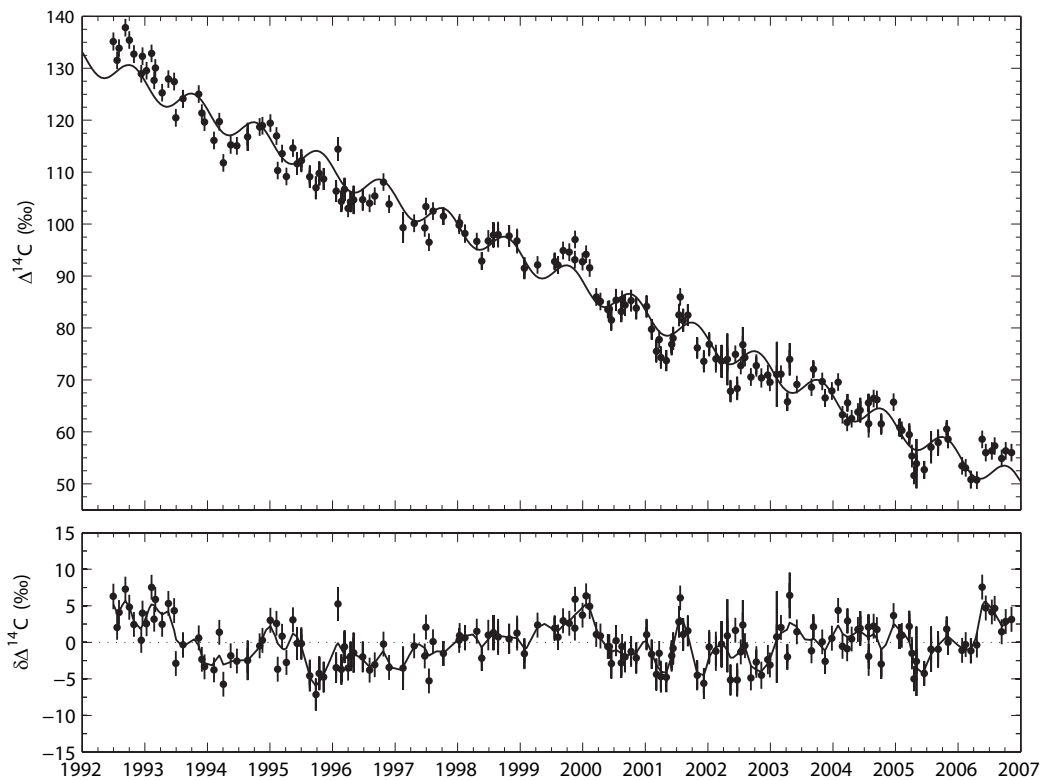


Figure 3.12: $\Delta^{14}\text{C}$ observations from La Jolla fit with linear trend and one harmonic (top panel). Residuals in $\Delta^{14}\text{C}$ after subtracting the fitted function are shown in the lower panel with a smoothing spline.

3.8.2 Variation in amplitude and phase of seasonal cycle

To examine the variability in the annual cycle at La Jolla, a single harmonic was fit to each calendar year of data after removing the polynomial function shown in Figure 3.7.

The time of year when $\Delta^{14}\text{C}$ reaches a maximum is plotted in Figure 3.14 for each year where the uncertainty in the fitted timing of the maximum was less than 4 months. The omitted years did not have well-resolved seasonal cycles, which could be due to measurement uncertainty, reduced sampling frequency in a particular year or a low seasonal amplitude.

Results from La Jolla are shown in black. The process of removing a polynomial trend and fitting each year of data to a single harmonic was repeated

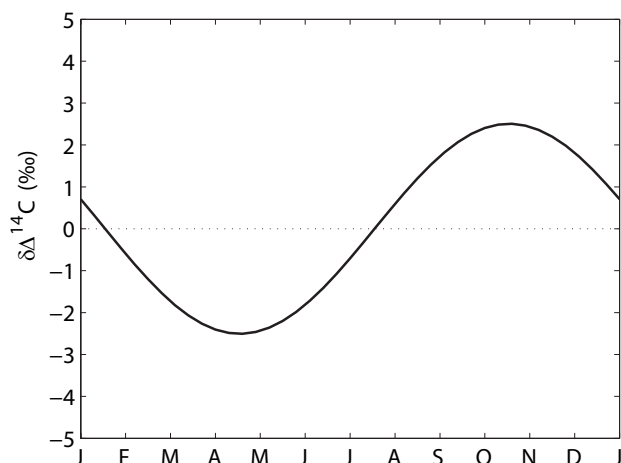


Figure 3.13: Average annual cycle of $\Delta^{14}\text{C}$ at La Jolla, calculated by fitting a linear trend and single harmonic to observed $\Delta^{14}\text{C}$. The harmonic component is plotted here. Minima occurs in mid-April; maxima occurs in mid-October. The difference between maximum and minimum is 5.0 ‰.

for other long time series in the Northern Hemisphere: Jungfrauoch (shown as red circles in Figure 3.14, Levin and Kromer 2004), Fruholmen (gray circles, Nydal and Lövseth 1996) and Vermunt (blue circles, Levin and Kromer 2004). The placement of the station names on the right axis reflects the average value observed at each station.

Figure 3.14 shows that the maximum $\Delta^{14}\text{C}$ in the Northern Hemisphere records has always occurred in the second half of the year. The maximum occurs later in the year at La Jolla in comparison to the more northerly stations. Trends in the timing of the maximum are not apparent at any station, indicating that the phasing of $\Delta^{14}\text{C}$ has not changed appreciably since the years directly following the period of intense weapons testing. During that period (1964-70), the seasonal cycle was driven by the annual mixing of stratospheric air to the troposphere, as most of the ^{14}C from the nuclear weapons was injected into the stratosphere.

Variation in the peak-to-peak amplitude of the fitted harmonic for each year is shown in Figure 3.15. Here, single harmonics were fit to individual years of data defined as January-December and again as single years from July-June. Black

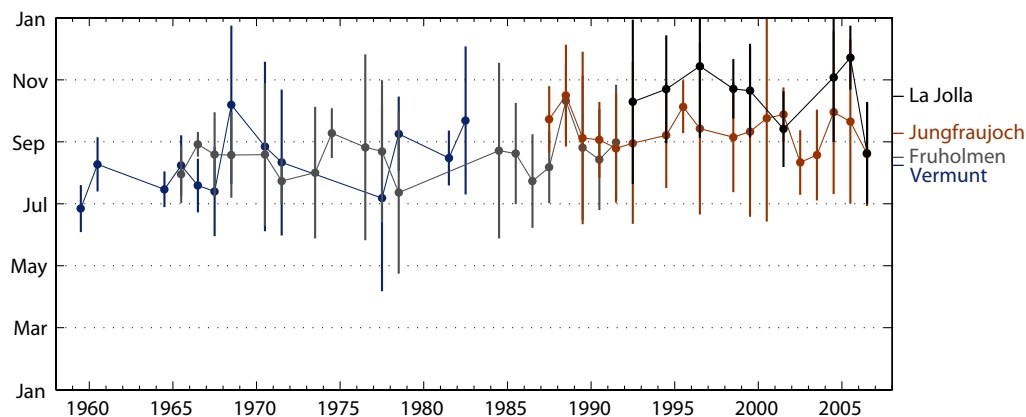


Figure 3.14: Timing of maximum annual $\Delta^{14}\text{C}$ in the Northern Hemisphere, calculated by detrending $\Delta^{14}\text{C}$ observations with a polynomial curve then fitting each calendar year to a single harmonic. Errorbars reflect uncertainty in the maximum of the fitted harmonic. Years where uncertainty was greater than 4 months were omitted. Shown for La Jolla (33 °N, black), Jungfrauoch (47 °N, red), Fruholmen (71 °N, gray) and Vermont (47 °N, blue). The station labels on the right axis indicate mean timing of maximum $\Delta^{14}\text{C}$ at each station.

circles show results from years specified as January-December and gray circles show results from years specified as July-June. Errorbars represent uncertainty ($1-\sigma$) in the peak-to-peak amplitude of the harmonic fit.

Several years with very large amplitudes are evident in Figure 3.15: 1994, 2005 and 2000 or 2001, depending on the designation of the beginning and end of a year. Outstanding seasonal cycles in these years are also easily identified by eye from the original measurements (e.g. in Figure 3.2).

Also plotted in Figure 3.15 is the derivative of the $\Delta^{14}\text{C}$ anomaly at La Jolla, shifted forward by 2 years. The $\Delta^{14}\text{C}$ anomaly was calculated by removing the seasonal cycles by cubic smoothing splines, and subtracting the linear or exponential fit to the entire record (Section 3.7). This parameter provides an indication of the rate of change of $\Delta^{14}\text{C}$ at La Jolla in comparison to that expected by a long-term linear or exponential trend, where positive values indicate that the $\Delta^{14}\text{C}$ anomaly was increasing.

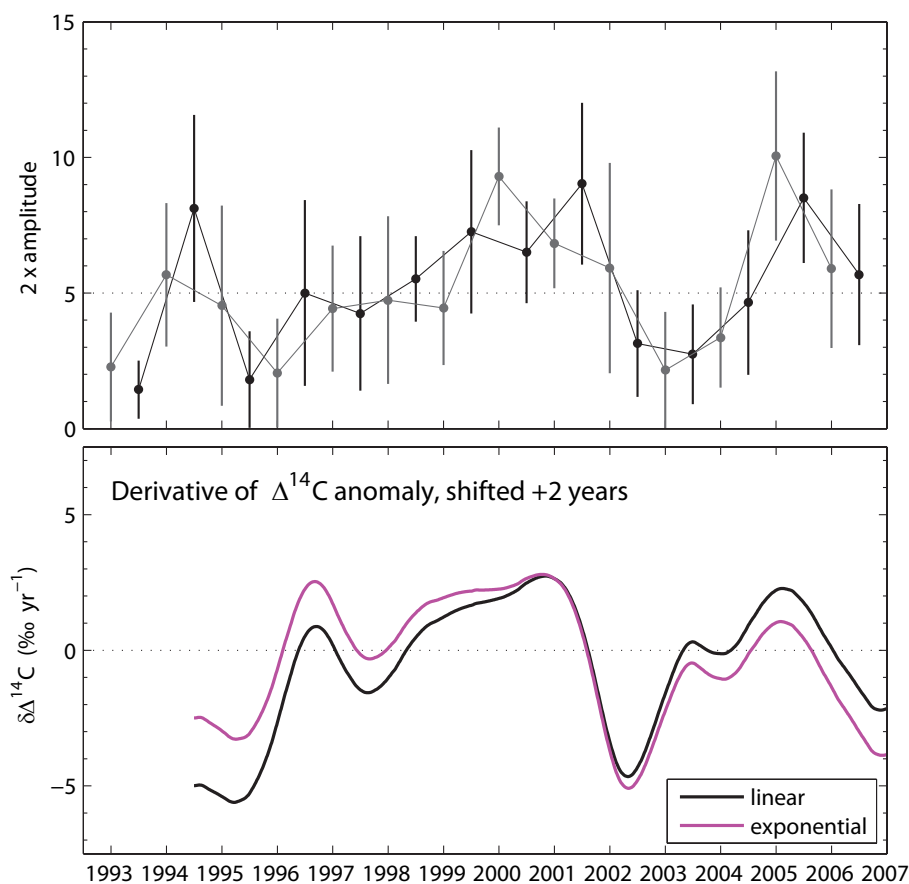


Figure 3.15: Yearly amplitude of the seasonal cycle of $\Delta^{14}\text{C}$ at La Jolla (top panel) calculated for years defined as January-December (black) and as July-June (gray). Derivative of the $\Delta^{14}\text{C}$ anomaly (described and shown in Figure 3.9, Section 3.7), shifted forward by 2 years (bottom panel).

The derivative of the $\Delta^{14}\text{C}$ anomaly seems to express maxima 2 year prior to maxima in the seasonal amplitude (Figure 3.15). This observation suggests that the magnitude of seasonal variation is larger when the atmospheric $\Delta^{14}\text{C}$ anomaly at La Jolla was increasing 2 years earlier. This effect could be influenced by the exchange of ^{14}C with a short-term reservoir that stores carbon for only a few years. Another explanation could be that periods experiencing little change in the tropospheric $\Delta^{14}\text{C}$, which therefore have relatively higher $\Delta^{14}\text{C}$ levels, are less sensitive to the processes driving seasonal variation in $\Delta^{14}\text{C}$.

3.8.3 Discussion of seasonal cycle

Exchanges of carbon that could cause variability in $\Delta^{14}\text{C}$ on seasonal timescales include fossil fuel emissions, biospheric respiration and stratosphere-troposphere exchange. Seasonal changes in atmospheric transport and mixing may also influence $\Delta^{14}\text{C}$ observed at La Jolla. The following sections describe the potential influence from each of these sources.

The average seasonal cycle at La Jolla was shown in Figure 3.13. La Jolla experiences maxima in $\Delta^{14}\text{C}$ in October, on average. This phasing is similar to or slightly later than other Northern Hemisphere stations, none of which have shown a measurable trend in phase since the 1960s. The peak-to-peak amplitude of $\Delta^{14}\text{C}$ at La Jolla is marked by high variability, ranging from near zero to 10 ‰ and averaging 5.0 ± 0.5 ‰. The seasonal amplitude may be higher when the derivative of the $\Delta^{14}\text{C}$ anomaly was positive 2 years prior.

3.8.4 Biospheric exchange

Because the seasonal cycle of $\Delta^{14}\text{C}$ has a similar phase as the seasonal cycle of $\delta^{13}\text{C}$ (Figure 3.5), it is suggestive that biospheric exchange is the dominant influence on the seasonal variation in $\Delta^{14}\text{C}$. However, the process that drives seasonal variation in $\delta^{13}\text{C}$, i.e. the photosynthetic discrimination against heavy isotopes during intensive assimilation of CO_2 during the growing season, is corrected for by the mass-dependent fractionation correction in $\Delta^{14}\text{C}$.

Atmospheric $\Delta^{14}\text{C}$ could be influenced on seasonal timescales by the respiration of carbon with a different $\Delta^{14}\text{C}$ signature than atmospheric $\Delta^{14}\text{C}$. $\Delta^{14}\text{C}$ in respiration reflects a weighted average of the turnover time of biospheric carbon being respired. Approximately half of the respiratory flux is from autotrophic respiration, which releases freshly assimilated carbon with $\Delta^{14}\text{C}$ that is very similar to atmospheric levels (Gamnitzer et al., 2006).

Randerson et al. (2002) found that seasonality in respiration served to counteract a substantial portion of the observed annual cycle forced by strato-

spheric mixing in the first few years after the bomb testing. At this time, the disequilibrium between biospheric and atmospheric $\Delta^{14}\text{C}$ was large and negative as much of the biospheric mass was fixed prior to the addition of bomb ^{14}C . Modeling of biospheric exchanges with the atmosphere indicates that average $\Delta^{14}\text{C}$ in terrestrial vegetation increased after the bomb tests, and should have matched atmosphere $\Delta^{14}\text{C}$ at some point over the period 1985-2000 (Caldeira et al., 1998; Randerson et al., 2002). Since that time, the biosphere should be slightly enriched in $\Delta^{14}\text{C}$.

Estimates of the biospheric influence on $\Delta^{14}\text{C}$ seasonality of recent periods indicates that the effect should be small. Based on the results of Randerson et al. (2002) and Naegler (2005), the biosphere-atmosphere disequilibrium over the period 1992-2006 is not large. Randerson et al. (2002) simulated a negligible biospheric contribution to seasonality of $\Delta^{14}\text{C}$ at Fruholmen, Norway during 1985-1990. Global simulations by Randerson et al. for 2000 suggested that respiration would produce a seasonal cycle of no more than 3 ‰ in continental regions of the Northern Hemisphere and probably less than 1 ‰ for marine stations. We believe that biospheric exchange is not likely to be the main influence to the seasonal cycle of $\Delta^{14}\text{C}$ at La Jolla over the period of 1992-2006.

Biospheric fluxes also cannot explain the year-to-year variability observed in the seasonal cycle at La Jolla. The $\Delta^{14}\text{C}$ disequilibrium should be larger in recent years as compared to the early measurements at La Jolla, suggesting that a dominant influence from the biosphere would cause increasing amplitude in $\Delta^{14}\text{C}$ which is not apparent. It is not probable that sufficient year-to-year variation in the seasonality of the gross respiration flux or in the average $\Delta^{14}\text{C}$ of the respired carbon could occur without causing measurable impacts on CO_2 concentration or $\delta^{13}\text{C}$.

3.8.5 Fossil fuel emissions

Estimates of monthly fossil fuel emissions for the United States based on production, consumption and trade of fuels show a “double-peaked” seasonal cycle with relatively high emissions in the winter and in the summer (Blasing et al., 2004b). These high emissions correspond to the energy use required for heating and cooling of buildings during seasonal extreme warm and cold temperatures. Inventories suggest that CO₂ emissions vary by only $\pm 5\%$ over the year (Rotty, 1987; Blasing et al., 2004b).

Observations of CO₂ and $\Delta^{14}\text{C}$ in continental Europe suggest that seasonal variation in emissions in this region may be as large as $\pm 50\%$. Levin et al. (2003) sampled continental air in Heidelberg and Schauinsland, Germany for CO₂ and $\Delta^{14}\text{C}$ and found that seasonality of local fossil fuel emissions contributed to a 10-50 ‰ seasonal variation in $\Delta^{14}\text{C}$. Using these observations, Levin et al. estimated the monthly variation in fossil emissions. Figure 3.16 shows the seasonality of fossil fuel CO₂ emissions, normalized over the year, for the Blasing et al. (2004b) estimates averaged over 1993-2003 for the US and for the Levin et al. (2003) estimates for Heidelberg.

We used both these estimates to calculate the seasonality of $\Delta^{14}\text{C}$ in background air of the Northern Hemisphere resulting from variable fossil fuel emissions. These calculations were performed using atmospheric $\Delta^{14}\text{C}$ of 85 ‰, 370 ppm CO₂ and 7 Gt C fossil fuel emissions, which are approximate values for the year 2000. Seasonality was calculated by assuming all fossil fuel emissions were released into the troposphere north of 30°N. The results, plotted in Figure 3.16 after detrending, indicate that the seasonality in the economic inventories produces a seasonal variation of less than 1 ‰ in Northern Hemisphere $\Delta^{14}\text{C}$ (shown in black in the right panel). Levin et al.’s estimate produces a significant cycle, with a 4 ‰ difference between minimum and maximum values (shown in purple in the right panel). Both estimates result in minimum values in April or May, and Levin et al. produce a maximum in October, similar to the phasing observed at La Jolla. It can be seen

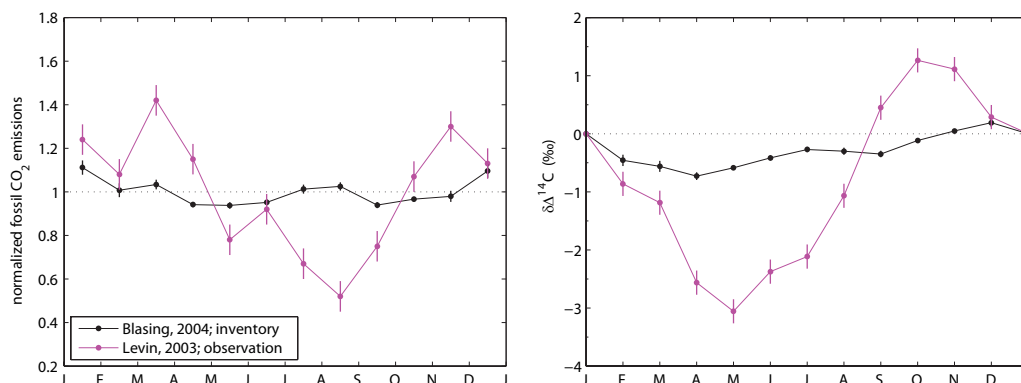


Figure 3.16: Seasonality of fossil fuel emissions and amplitude of the $\Delta^{14}\text{C}$ seasonal cycle in the Northern Hemisphere estimated from fossil fuel emissions. Normalized monthly fossil CO_2 emissions for the US from economic inventories (black, Blasing et al. 2004a) and for Heidelberg, Germany (purple, Levin et al. 2003) are shown on the left panel. Resulting seasonality in $\Delta^{14}\text{C}$ for each estimate was calculated with approximate tropospheric CO_2 and $\Delta^{14}\text{C}$ observed in 2000 (right panel).

that, for background levels of $\Delta^{14}\text{C}$, seasonality in fossil fuel emissions is not as important as for continental measurements.

The results of Levin et al. are for a specific location in Germany and certainly overestimate of the seasonality of emissions in the entire hemisphere. It is possible that their results are also influenced by variations in atmospheric mixing which may not have been sufficiently accounted for by using measurements of Radon-222. However, the results of Levin et al. (2003) are included here to provide an upper limit to the simple estimate of the influence of seasonal changes in fossil fuel emissions on background levels of $\Delta^{14}\text{C}$ in the Northern Hemisphere. The actual seasonal variation of fossil fuel emissions over the entire Northern Hemisphere midlatitudes (which represents most of the total emissions (Marland et al., 2007)) is probably between the two estimates of Blasing et al. and Levin et al..

Emissions of fossil fuel-derived CO_2 are not likely to change seasonality from year to year by a large enough amount to explain the variation in seasonal amplitude observed at La Jolla. Additionally, increases in fossil fuel emissions would tend to drive an small increase ($<1\text{‰}$) in the seasonal cycle of $\Delta^{14}\text{C}$ over

the 15-year record at La Jolla.

We conclude that seasonal variability in fossil fuel emissions are likely to account for a portion of the seasonal cycle at La Jolla but are not sufficient to explain all features of the observed annual variation.

3.8.6 Stratosphere-troposphere exchange

Stratosphere-troposphere exchange (STE) refers to the transport of air across the tropopause and plays an important role in the distribution of many gases in the atmosphere (Holton et al., 1995; Appenzeller et al., 1996; Gettelman and Sobel, 2000). The large scale overturning circulation of the lower atmosphere occurs through the upwelling of tropospheric air in the tropics and return of stratospheric air to the troposphere in the extratropics. In the following discussion, we discuss STE as the net stratosphere-to-troposphere transport that occurs in the extratropics.

In the 1960s, enormous seasonal variation in $\Delta^{14}\text{C}$ was driven by input of stratospheric air that was highly enriched in bomb-produced ^{14}C . In recent years, the stratospheric $\Delta^{14}\text{C}$ enrichment is caused mainly by local cosmogenic ^{14}C production and the decreasing trend of tropospheric ^{14}C . As the residence time of air in the stratosphere is on the order of less than 10 years, it is unlikely there is a residual excess of ^{14}C from bomb testing.

Most reported measurements of the stratosphere-troposphere gradient of $\Delta^{14}\text{C}$ come from the early 1990s (Nakamura et al., 1992; Brenninkmeijer et al., 1995; Zahn et al., 2000). Nakamura et al. (1992) and T. Nakazawa (personal communication) report gradients of ~ 80 ‰ across the tropopause over Japan in 1989 and 1994. However, weak gradients of only ~ 10 ‰ were observed by Zahn et al. (2000) over the midlatitudes of the Northern Hemisphere during winter sampling between 1991-95. Brenninkmeijer et al. (1995) report a “considerable $^{14}\text{CO}_2$ increase” over the midlatitudes of the Southern Hemisphere in 1993, measuring a range of 50 ‰ in samples collected in the upper troposphere and the stratosphere.

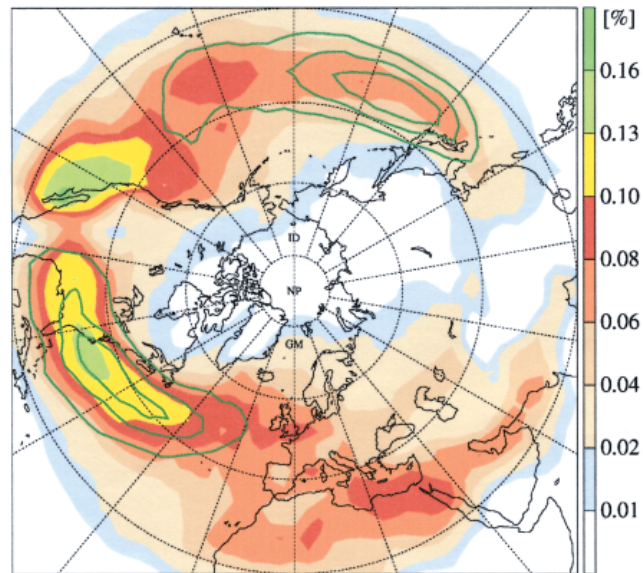


Figure 3.17: Winter climatology (Dec-Feb) of tropospheric destinations of deep stratospheric intrusions. Figure 3a from Stohl et al. (2003). Values are in % and indicate the probability that a low-tropospheric air parcel ($P > 700$ hPa) was transported downward from the lower stratosphere.

Most of the STE in the Northern Hemisphere occurs in the subtropics and midlatitudes, with particularly intense fluxes over the eastern subtropical Pacific (Stohl et al., 2003; Langford, 1999; James et al., 2003). Figure 3.17, reproduced from Stohl et al. (2003), shows the regions experiencing the most frequent occurrences of rapidly descending air from the stratosphere. STE occurs mainly by episodic intrusions related to atmospheric eddies and tropopause folds.

STE is highly seasonal, where most downward mixing occurs in the winter and spring. Figure 3.18 shows the seasonal variation of STE in the Northern and Southern midlatitudes, reproduced from Appenzeller et al. (1996). There is very strong seasonality in the Northern Hemisphere, with mass fluxes varying by ± 40 %. Annual variation in the Southern Hemisphere is not as pronounced.

The air in the northern mid-latitude lower stratosphere that enters the troposphere during STE has an age of 1-3 years (Andrews et al., 2001). The age refers to the average residence time of air in the stratosphere or the time

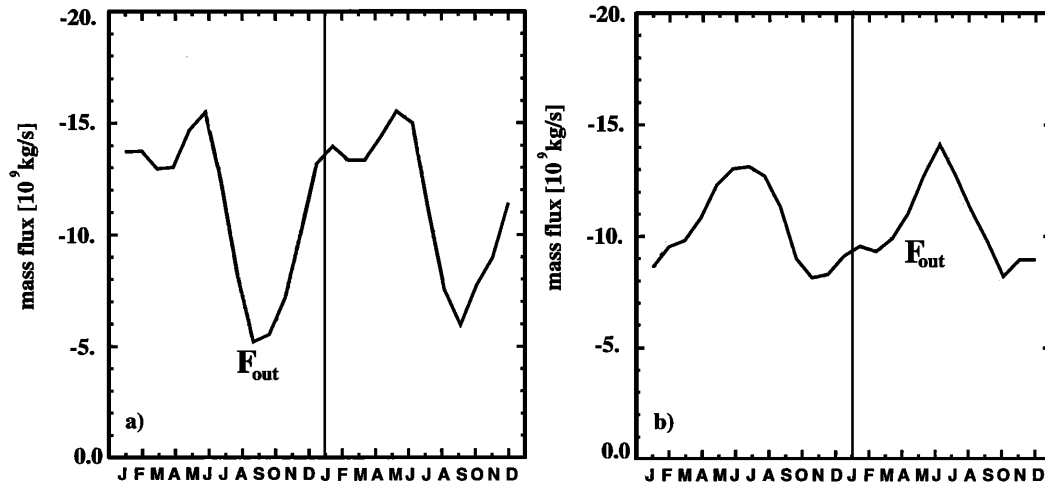


Figure 3.18: Annual variation of the net downward mass transport across the extratropical tropopause in the a. Northern Hemisphere and b. Southern Hemisphere for 1992 and 1993. Figure 8 from Appenzeller et al. 1996. Values are given in 10^9 kg s^{-1} ; negative values denote downward mass flux.

since isolation from mixing with tropospheric air. Integrated over a year, the stratosphere-to-troposphere mass flux replaces 18 % of the air in the Northern troposphere, or 36 % of the tropospheric air north of 30° .

Fluxes shown in 3.18 indicate the rate that stratospheric air is added to the troposphere. To estimate the effect of this seasonal flux on tropospheric $\Delta^{14}\text{C}$, a simple calculation was conducted. Beginning with an initial tropospheric $\Delta^{14}\text{C}$ of 85 ‰, monthly values of $\Delta^{14}\text{C}$ were calculated with a simple mixing equation where the fraction of stratospheric air equals the flux given in Figure 3.18, integrated over 30 days, divided by the mass of the Northern Hemisphere extratropical troposphere ($\sim 10^{18} \text{ kg}$) which remained constant. A slight correction for lower CO_2 concentrations in the stratosphere was included, but the seasonal variation in tropospheric CO_2 was neglected. Shown in Figure 3.19 after detrending, the estimated seasonal cycle caused by STE was calculated for two scenarios, one where the stratosphere is 30 ‰ more enriched than the troposphere and one where the enrichment is 75 ‰. These scenarios bracket expected values for the 1992-2006 period.

Figure 3.19 shows that the maximum in $\Delta^{14}\text{C}$ arising from seasonal fluxes of stratospheric air occurs in July-August. A maximum enrichment of 1.5-4 ‰ is calculated for the two scenarios.

This calculation represents an idealized scenario where the monthly input of stratospheric air is mixed into the entire northern extratropical troposphere in a month. As discussed above, STE occurs in specific regions of the tropopause. Mixing of the troposphere results in a lag of 1-2 months for the propagation of surface signals to the upper troposphere (Gerbig et al., 2003; Nakazawa et al., 1991), which is also a reasonable estimate for average downward propagation time for stratospheric signals. Therefore, the seasonal cycle depicted in Figure 3.19 is likely to underestimate the amplitude and the timing of maximum $\Delta^{14}\text{C}$ at ground level. Adjusting the cycle in Figure 3.19 with a lag of 2 months and an enhancement in amplitude could result in good agreement with the observed cycle at La Jolla. The influence of STE on surface $\Delta^{14}\text{C}$ would be better quantified by the use of an atmospheric transport model. We hope to pursue such a study in the future.

Figure 3.19 indicates the determination of the significance of STE for $\Delta^{14}\text{C}$ requires an accurate characterization of $\Delta^{14}\text{C}$ in stratospheric air. The laboratory of T. Nakazawa is continuing measurements of stratospheric samples and K. Boering of the University of California, Berkeley has initiated new measurements. Publication of these results will aid the definition of a stratospheric component to the seasonal cycle of Northern Hemisphere $\Delta^{14}\text{C}$.

Another indication of the effect of STE on tropospheric composition can be derived from observations of nitrous oxide (N_2O) and chlorofluorocarbons (CFCs). Nevison et al. (2004) examined the influence of stratospheric air on the seasonal cycles of N_2O and CFCs. These gases are destroyed in the stratosphere by photolysis and oxidation so stratospheric concentrations are lower than tropospheric concentrations. STE therefore influences N_2O and CFCs in an opposite manner as expected in $\Delta^{14}\text{C}$.

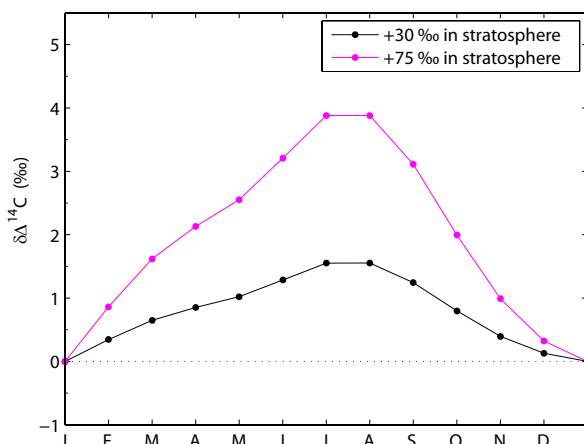


Figure 3.19: Estimated seasonal influence of stratosphere-troposphere exchange on $\Delta^{14}\text{C}$ in the extratropical Northern Hemisphere. Calculated using seasonal cross-tropopause mass flux from Appenzeller et al. (1996) mixed into the Northern Hemisphere extratropical troposphere ($> 30^\circ\text{N}$) with approximate tropospheric CO_2 and $\Delta^{14}\text{C}$ observed in 2000 (85 ‰ and 370 ppm). Stratospheric $\Delta^{14}\text{C}$ was estimated to be enriched by +30 and +75 ‰ in black and purple, respectively.

Observations of the seasonal cycle in N_2O and CFCs are shown in Figure 3.20, which is reproduced from Figure 1a and c in Nevison et al. (2004). Nevison et al. note that minimum concentrations occur in the Northern Hemisphere summer. The authors conclude that the summer minima can be explained by the propagation of stratospheric air to the ground-based sampling sites with a lag of roughly 4 months. Additionally, a smaller seasonal amplitude is observed in N_2O and CFCs in the Southern Hemisphere that agrees with a reduced seasonality of STE over the southern midlatitudes (Figure 3.18, Appenzeller et al. 1996).

Variation in $\Delta^{14}\text{C}$ as compared to N_2O and CFCs is not exactly anticorrelated, indicating that the seasonal cycle for $\Delta^{14}\text{C}$ and/or N_2O and CFCs is also influenced by other processes. Another factor could be the more northerly location of the AGAGE monitoring stations compared to La Jolla. The seasonal cycle of $\Delta^{14}\text{C}$ at Jungfraujoch tends to experience maxima earlier than La Jolla (shown in Figure 3.14), corresponding more closely to the phasing of minima observed in Northern Hemisphere N_2O and CFCs.

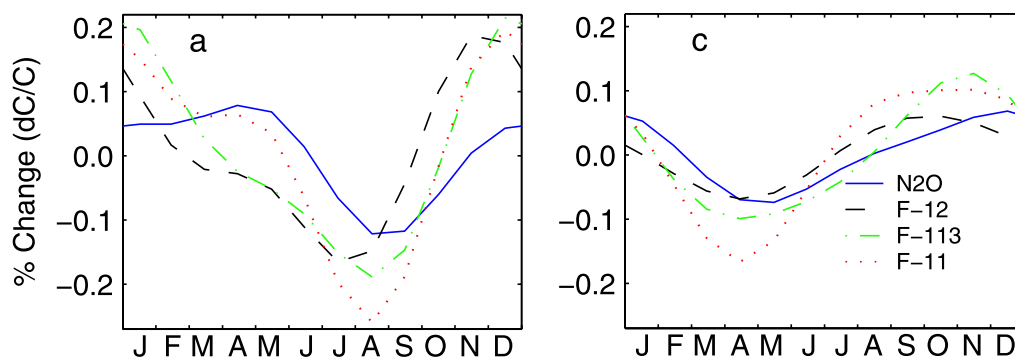


Figure 3.20: Seasonal cycle of N_2O , CFC-11, CFC-12 and CFC-113 concentrations at a. Mace Head and c. Cape Grim. Figure 1a and c from Nevison et al. (2004). Seasonal cycles are represented by detrended harmonic fits to 8-12 years of monthly mean data from the Advanced Global Atmospheric Gases Experiment (AGAGE).

The episodic nature of STE provides a possible explanation for the variability observed in the seasonal cycle of $\Delta^{14}\text{C}$ at La Jolla. It is likely that there is significant year-to-year differences in the areas experiencing most episodes of air descending from the stratosphere as well as differences in the seasonal intensity of STE.

From the inspection of the seasonality of stratosphere-troposphere exchange in the Northern Hemisphere, we conclude that STE is likely to drive a significant portion of the seasonal cycle at La Jolla. The timing of the maximum $\Delta^{14}\text{C}$ predicted from STE matches that observed when a 2 month lag is included for vertical mixing in the troposphere, and the seasonal cycle of $\Delta^{14}\text{C}$ is largely opposite to the cycle observed for N_2O and CFCs in the Northern Hemisphere. Further, the phasing of $\Delta^{14}\text{C}$ in the Northern Hemisphere is similar to that observed in the 1960s when the bomb-derived ^{14}C flux from the stratosphere was undoubtedly driving the seasonal cycle. Episodic and localized STE events provide a possible explanation for the variation in the annual cycle at La Jolla. Our conclusion agrees with the ^{14}C modeling study of Randerson et al. (2002), which indicated that STE was a significant component of the seasonal cycle of $\Delta^{14}\text{C}$ at Fruholmen, Norway over 1985-1990.

3.8.7 Vertical mixing in the troposphere

Vertical mixing of air in the troposphere could be a substantial influence on the seasonal cycle of $\Delta^{14}\text{C}$ via variable dilution of CO_2 emitted by fossil fuel emissions and/or transport of stratospheric air to the surface. Over land, the depth of the well-mixed atmospheric boundary layer is larger in the summer and shallower in the winter months. This variability enhances the seasonal cycle of CO_2 in the Northern Hemisphere by the coherence of net summer CO_2 uptake with deep boundary layer depth and winter CO_2 release into shallow boundary layers (Keeling et al., 1989; Denning et al., 1995). While the air sampled at La Jolla is mainly of oceanic origin, which experiences seasonality in boundary layer depth that is opposite to the land, the composition at La Jolla may reflect the larger scale seasonal mixing of air in the Northern Hemisphere (Keeling et al., 1989).

Boundary layer depth could be an important factor in the depletion of $\Delta^{14}\text{C}$ caused by fossil fuel emissions. Shallowing of the boundary layer in the winter months decreases the effective mixing volume of emitted CO_2 , which would proportionally increase the resulting change in $\Delta^{14}\text{C}$.

As discussed briefly in the previous section, the effect of stratospheric air entering the troposphere on ground level composition depends on the transport of this air to the surface. The vertical mixing occurs over 1-2 months on average, however significant regional variability could have a measurable effect on seasonality of $\Delta^{14}\text{C}$ by regulating the local fraction of stratospheric air.

Vertical transport in the atmosphere is likely to play a fundamental role in the seasonal cycle of $\Delta^{14}\text{C}$ in the Northern Hemisphere by modulating the expression of seasonal inputs of stratospheric air and fossil fuel CO_2 . This suggests that atmospheric transport modeling is necessary for investigating of fluxes of ^{14}C in background air on subannual timescales. Atmospheric transport modeling would also provide information on year-to-year variability in horizontal mixing, which would improve our understanding of the fluctuating differences in $\Delta^{14}\text{C}$ observed

between La Jolla and Jungfraujoch.

3.8.8 Conclusions about the seasonal cycle at La Jolla

We conclude that the seasonal cycle of $\Delta^{14}\text{C}$ at La Jolla is driven by atmospheric mixing, which causes seasonality in the input of $\Delta^{14}\text{C}$ -enriched stratospheric air, modulates the vertical transport of stratospheric air to the surface and regulates the dilution of fossil fuel CO_2 emissions. Estimates of the timing of the maximum $\Delta^{14}\text{C}$ caused by STE and by fossil emissions are consistent with the observations. Variability in atmospheric mixing and/or localized, episodic STE provides a reasonable explanation for changes in seasonal amplitude at La Jolla.

In their modeling investigation of the temporal evolution of the seasonal cycle of $\Delta^{14}\text{C}$, Randerson et al. (2002) estimated that the stratospheric and fossil fuel components contributed the most to the seasonal cycle at Fruholmen, Norway during 1985-1990. A figure showing the seasonality in $\Delta^{14}\text{C}$ caused by fossil fuel emissions, oceanic exchange, stratosphere-troposphere transport, and respiration computed by Randerson et al. is shown in 3.21. Though the model results seem to underestimate the seasonal cycle at Fruholmen and do not show any interannual variability in the amplitude, the phasing in the model is consistent with the observations.

Our conclusions are consistent with the findings of Randerson et al. (2002) that stratospheric and fossil fuel seasonality provide significant contributions to the Northern Hemisphere seasonal cycle of $\Delta^{14}\text{C}$. It is possible that the main cause for disagreement between Randerson et al.'s results and the observations at Fruholmen could be due to imperfect representation of vertical mixing, which we believe is also an important determinant of the annual variation in $\Delta^{14}\text{C}$.

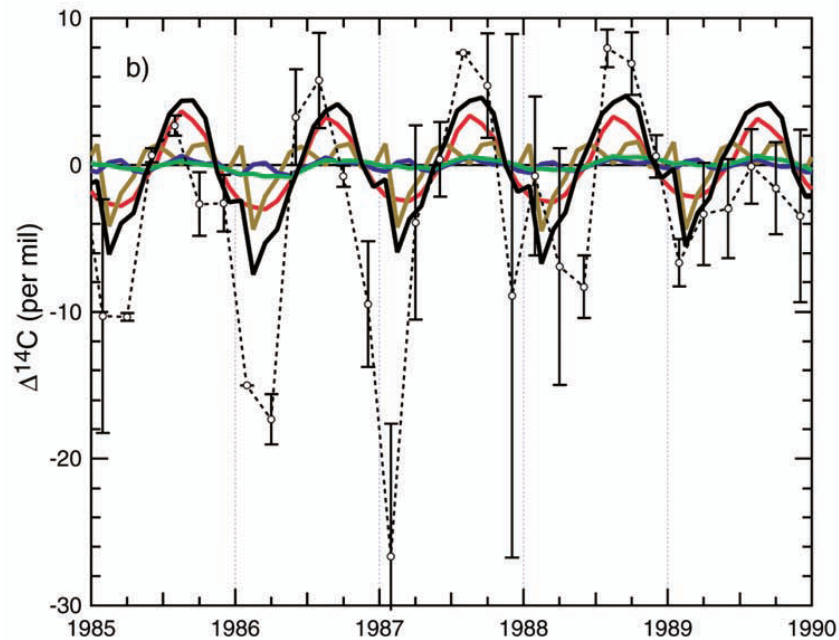


Figure 3.21: Components of the seasonal cycle at Fruholmen, Norway 1985-1990. Figure 11b from Randerson et al. (2002). The sum of fossil fuel (brown), ocean (blue), stratosphere (red), and terrestrial biosphere (green) components is represented by the solid black line.

3.9 Summary

Measurements of $\Delta^{14}\text{C}$ in CO_2 were conducted on monthly samples from La Jolla, California. The long-term $\Delta^{14}\text{C}$ decrease fits a linear trend of -5.5 ± 0.1 ‰ yr^{-1} and an exponential decay curve with e-folding time of 16.4 ± 0.2 yr, similar to the decay constant of $\Delta^{14}\text{C}$ in observations in the two decades following nuclear weapons testing. The trend of $\Delta^{14}\text{C}$ is influenced by carbon fluxes from the surface ocean, terrestrial biosphere and fossil fuel emissions and it appears to be sensitive to interannual variability in climate. Anomalies in the secular trend of $\Delta^{14}\text{C}$ over 1998-2000 were observed and could be related to changes in North Pacific ventilation or the modulation of stratosphere-troposphere exchange by El Niño conditions. Stratosphere-troposphere exchange was also found to be a dominant source of seasonal variation, where tropospheric mixing is also important for seasonality by regulating the transport of stratospheric air to the surface and the

dilution of fossil fuel emissions. We have begun to investigate the sensitivity of the secular trend of $\Delta^{14}\text{C}$ to carbon exchanges, particularly fossil fuel emissions, using a box diffusion model.

3.10 Recommendations for future $\Delta^{14}\text{C}$ measurements at La Jolla

The archive of CO_2 samples from La Jolla kept by the Scripps CO_2 Program enabled the production of a 15-year time series over only 4 years of sample analyses. Sample archiving provides an enormous benefit to environmental measurements. In addition to the valuable information that can be gleaned from a long time series of measurements, archives provide additional means of evaluating measurement accuracy and reproducibility.

The archive from La Jolla is particularly advantageous because of the inclusion of 2-3 replicate samples. These replicate samples were instrumental to the development of corrections to early measurements of $\Delta^{14}\text{C}$ in CO_2 . La Jolla replicates provided an additional measure of analytical reproducibility at LLNL. Finally, the ability to average several samples reduced random noise in the final time series.

As shown in Figure 3.1, 549 CO_2 samples from La Jolla through 2007 remain in the archive. This is a very large number of samples, as only 293 were utilized in the production of the $\Delta^{14}\text{C}$ time series reported here. Future analysis of unique sample dates will enhance the resolution of the monthly time series while measurement of replicate samples can improve uncertainty and serve as a diagnostic of measurement drift or bias.

For samples collected before 1998, the amount of CO_2 contained in each archived sample is twice as much as those samples processed after 1998. The shift in sample size occurred as the use of an automated system which extracts approximately half of the remaining flask air replaced a manual system which extracted all

remaining air. The pre-1998 sample size allows the CO₂ sample to be split into 2 separate samples. The 2 samples can both be graphitized and analyzed on the same wheel or in subsequent wheels, or one of the split samples can be stored for future analysis. Measurement of stable isotopic composition on five such split samples shows that the splitting procedure causes depletions in $\delta^{13}\text{C}$ ($-0.07 \pm 0.03 \text{ ‰}$) and $\delta^{18}\text{O}$ ($-0.32 \pm 0.06 \text{ ‰}$) which indicates that samples are slightly fractionated and not suitable for $\delta^{13}\text{C}$ and $\delta^{18}\text{O}$ analysis after splitting. The fractionation in $\delta^{18}\text{O}$ is greater than 2 times the fractionation in $\delta^{13}\text{C}$, suggesting that $^{18}\text{O}/^{16}\text{O}$ in the CO₂ sample is altered by another process inside the graphitization manifold other than mass-dependent thermal fractionation. The fractionation in $\delta^{13}\text{C}$ is insignificant for $\Delta^{14}\text{C}$, however, and no consistent difference has been observed in $\Delta^{14}\text{C}$ for split samples. Therefore, pre-1998 CO₂ samples can be split into two different samples for $\Delta^{14}\text{C}$ analysis which means that the sample archive is essentially twice as large for the period 1992-1997. Splitting of these samples is also advantages for AMS analysis, as the split samples are more consistent with the amount of CO₂ in later samples and in the Cyl-1 and Cyl-2 reference materials.

I recommend, as more recent samples from La Jolla are analyzed to extend the record, regular and continual analysis of archived samples should be conducted simultaneously. For each wheel of samples measured in the future, 1-2 archived samples from La Jolla should be included in the analysis. This practice will gradually utilize a portion of remaining archived samples, improve the resolution and scatter in the time series, and ensure that temporary instrument biases will not provide a significant source of error in the record.

Another recommendation concerns the designation of flask samples to extract and store in the Scripps archive. While it is extraordinary to have such a large archive of samples at La Jolla and preservation of these samples for potential future applications is undoubtedly of great value, it may be preferable to archive fewer samples from La Jolla to enable the collection of CO₂ samples for $\Delta^{14}\text{C}$ from other stations in the Scripps CO₂ or AORG sampling networks. As included in the

recommendations from the next chapter, analysis of $\Delta^{14}\text{C}$ from additional stations will improve the characterization of global variability in $\Delta^{14}\text{C}$ as well as provide the opportunity for intercomparisons through concurrent measurements with other ^{14}C laboratories. Samples collected at more stations could provide more scientific value, as well as a greater chance of support for the expensive AMS analysis, than the accumulation of vast numbers of samples from La Jolla. Presuming that the total number of CO_2 extractions that can be conducted in the Scripps laboratory is fixed because of personnel and time constraints, performing fewer extractions on CO_2 samples from La Jolla would enable more extractions of flasks collected at different sites.

Acknowledgment

Chapter 3, in part, is being prepared for publication. Graven, Heather D.; Guilderson, Thomas P.; Keeling, Ralph F. The dissertation author is the primary investigator and author of this paper.

Chapter 4:

Recent patterns of $\Delta^{14}\text{C}$ in CO_2 at 7 global sampling sites

ABSTRACT

Measurements of $\Delta^{14}\text{C}$ in CO_2 were conducted on monthly samples from 7 global stations in the Scripps flask sampling network. Records of 2-7 years at Point Barrow, Kumukahi, Mauna Loa, Samoa, Palmer Station and the South Pole are combined with records from La Jolla presented in Chapter 3 to describe the latitudinal gradient of $\Delta^{14}\text{C}$ in recent years. A shift to lower values in the Northern Hemisphere is observed between 1987-89 and 2005-06 by comparison to observations from Levin et al. (1992) and Meijer et al. (2006). The observed change in the latitudinal profile of $\Delta^{14}\text{C}$ is only partly explained by the rise in fossil fuel emissions over this period, indicating that ^{14}C fluxes to the Southern Ocean have diminished, mostly in response to the >100 ‰ decline in atmospheric $\Delta^{14}\text{C}$ between 1987-89 and 2005-06. Further investigation of the atmospheric gradients of $\Delta^{14}\text{C}$ and continued observation of the evolving gradient promise to improve our understanding of the turnover of carbon in the Southern Ocean and in northern ecosystems.

4.1 Introduction

Global sampling networks provide information on the distribution of atmospheric gases that is crucial for understanding the magnitude and location of sources and sinks in the atmosphere. In the years following the nuclear weapons testing, many stations were set up to collect CO₂ for measurements of $\Delta^{14}\text{C}$ (Nydal and Lovseth, 1983; Manning et al., 1990), yet the majority of these stations operated for only a few years. Published measurements of $\Delta^{14}\text{C}$ in CO₂ with global coverage and consistent frequency after 1980 are not readily available to the community.

The global distribution of $\Delta^{14}\text{C}$ in CO₂ is sensitive to regional exchanges of carbon by fossil fuel emissions, respiration and oceanic upwelling. Accurate observation of the gradients of $\Delta^{14}\text{C}$ in the atmosphere are likely to provide insights on these fluxes (Levin and Hesshaimer, 2000; Randerson et al., 2002).

The Scripps CO₂ Program has conducted whole air flask sampling in global networks for precise analysis of atmospheric CO₂ concentration and stable isotopic composition for decades. Since 1992, CO₂ samples have been archived for future isotopic analyses. The locations of sampling stations where CO₂ samples have been archived for $\Delta^{14}\text{C}$ analysis are listed in Table 4.1 and shown on a map in Figure 4.1. One site, Palmer Station, is part of the Scripps Atmospheric Oxygen sampling network rather than the Scripps CO₂ network. We began to collect CO₂ samples at Palmer Station in 2005 to enable observations of $\Delta^{14}\text{C}$ in air that is influenced by carbon exchanges in the Southern Ocean.

This chapter reports measurements of $\Delta^{14}\text{C}$ in CO₂ at these stations. Discussions of the seasonal cycles and mean gradients in $\Delta^{14}\text{C}$ incorporate measurements from La Jolla that were presented in Chapter 3. The gradients of $\Delta^{14}\text{C}$ observed between the Scripps stations in 2005-06 are then compared to previous observations.

Table 4.1: Clean air sampling stations in the Scripps CO₂ Program where samples were collected for $\Delta^{14}\text{C}$ analysis

Station Name	Code	Latitude	Longitude	Elevation
Point Barrow, Alaska	PTB	71.38°N	156.47°W	3397m ASL
La Jolla, California	LJO	32.87°N	117.25°W	
Mauna Loa, Hawaii	MLO	19.53°N	155.58°W	
Kumukahi, Hawaii	KUM	19.52°N	154.82°W	
Cape Matatula, Samoa	SAM	14.25°S	170.57°W	
Palmer Station, Antarctica	PSA	64.92°S	64.00°W	2810m ASL
South Pole, Antarctica	SPO	89.98°S	24.80°W	

4.2 The Scripps CO₂ archive

In 1992, the Scripps CO₂ Program began archiving samples of atmospheric CO₂ from La Jolla. Samples from Point Barrow and the South Pole have been saved since 1999, with a year-long interruption from mid-2000 through mid-2001 at Point Barrow. The tropical stations Mauna Loa, Kumukahi and Samoa have sample archives beginning in 2001. The Scripps archive contains replicate samples only for La Jolla. In 2003, the archived CO₂ samples began to be used for $\Delta^{14}\text{C}$ analysis as part of this thesis research and a subset of all archived samples was allocated for $\Delta^{14}\text{C}$ analysis.

The entire archive of CO₂ samples from all stations other than La Jolla designated for $\Delta^{14}\text{C}$ analysis comprised 1111 samples through the end of 2007 (1953 including La Jolla). Figure 3.1 shows a diagram of the archived samples. Sample dates of the CO₂ that has been analyzed and of the CO₂ samples remaining in the archive are shown.

Samples were selected from the archive spanning the length of the archive at roughly monthly resolution. Only 34 % of the total archived samples have been utilized (not counting samples at La Jolla): 381 of 1111 samples. Mauna Loa has the most archived samples (243 remaining out of a total of 322); Point Barrow has the least (66 remaining out of 139 total).

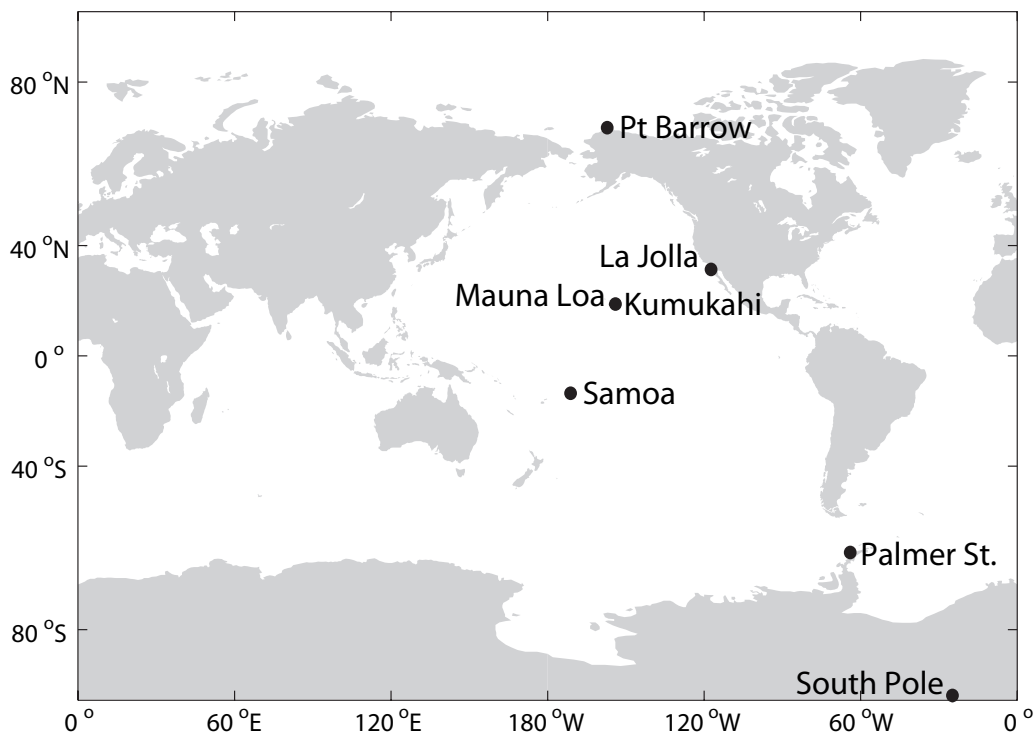


Figure 4.1: Map of clean air sampling stations in the Scripps CO₂ Program and Atmospheric Oxygen Research Group networks where samples were collected for $\Delta^{14}\text{C}$ analysis

4.3 Analysis of clean air samples

As described in sections 2.3 and 3.2, whole air flask samples are first measured for CO₂ concentration by infrared gas analysis (Keeling et al., 2002). Subsequently, the remaining air is extracted to produce a pure CO₂ sample for $\Delta^{14}\text{C}$ analysis. Concurrently sampled CO₂ is used to measure $\delta^{13}\text{C}$ by isotope ratio mass spectrometry (Guenther et al., 2001).

Special handling procedures were developed for air samples collected at Palmer Station by the Scripps Atmospheric Oxygen Research Group. Processing of flask air collected at Palmer Station is outlined in Section 2.18.

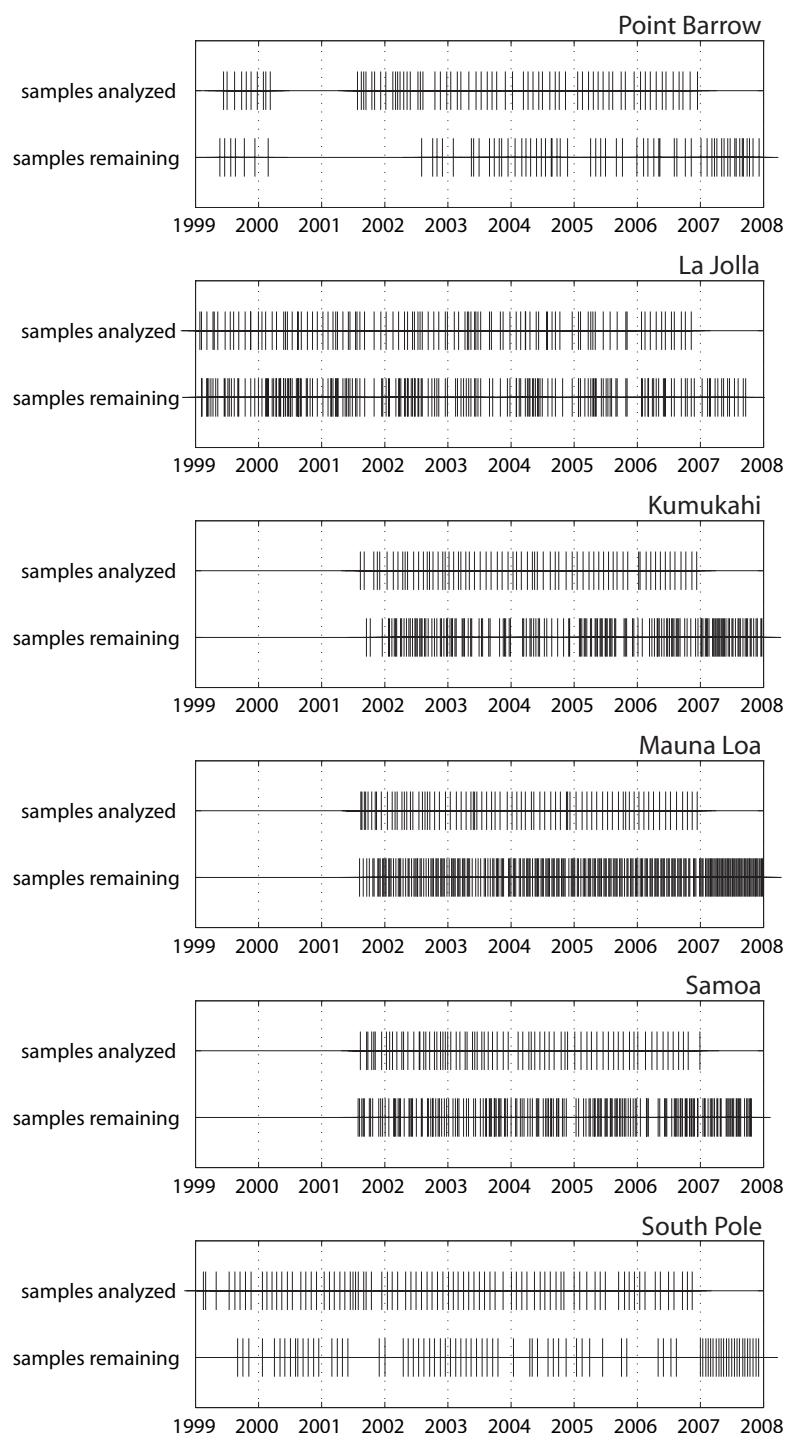


Figure 4.2: Status of the Scripps CO₂ archive from all stations, 1999-2007. For each station, the first row shows sample dates of CO₂ samples which were analyzed for $\Delta^{14}\text{C}$ at LLNL; the second row shows sample dates of CO₂ samples remaining in the Scripps archive.

4.4 $\Delta^{14}\text{C}$ observations

$\Delta^{14}\text{C}$ analysis was conducted on archived CO_2 samples at the Center for Accelerator Mass Spectrometry (CAMS) at Lawrence Livermore National Laboratory (LLNL) as described in Chapter 2. Uncertainty in $\Delta^{14}\text{C}$ was 1.7 ‰ for most samples; analyses conducted prior to 2006 had slightly higher uncertainties of 1.7-2.7 ‰.

Figures 4.3, 4.4 and 4.5 show $\Delta^{14}\text{C}$ observations at each station. Network stations are shown by latitude; Figure 4.3 includes the northern stations Point Barrow and La Jolla, 4.4 shows the tropical stations Kumukahi, Mauna Loa and Samoa, and 4.5 includes the southern stations Palmer Station and the South Pole. Each figure shows measured $\Delta^{14}\text{C}$ and uncertainty, as well as a cubic smoothing spline.

At Point Barrow, there is a gap in the record between mid-2000 and mid-2001. No samples exist in the archive for this period. At the South Pole, the period of mid-2001 to mid-2002 includes only 2 samples and also comprises something of a gap in the record. There were samples analyzed from this period, but they were found to be contaminated during sample processing. There are 5 samples remaining in the archive that will be measured to fill this gap, but were not able to be completed in time to be included in this thesis.

$\Delta^{14}\text{C}$ measurements and uncertainties are listed in Appendix B together with the CO_2 concentration measured in the same flask air and the $\delta^{13}\text{C}$ measured in a concurrent sample.

4.4.1 $\Delta^{14}\text{C}$, CO_2 and $\delta^{13}\text{C}$

Observations of $\Delta^{14}\text{C}$ are shown together with CO_2 and $\delta^{13}\text{C}$ for each station in Figures 4.6, 4.7, 4.8, 4.9, 4.10 and 4.11, as in the analogous plot for La Jolla, Figure 3.5. The solid curve shows monthly values of $\Delta^{14}\text{C}$ which were calculated from a function incorporating a linear trend ($a + bt$), a single harmonic

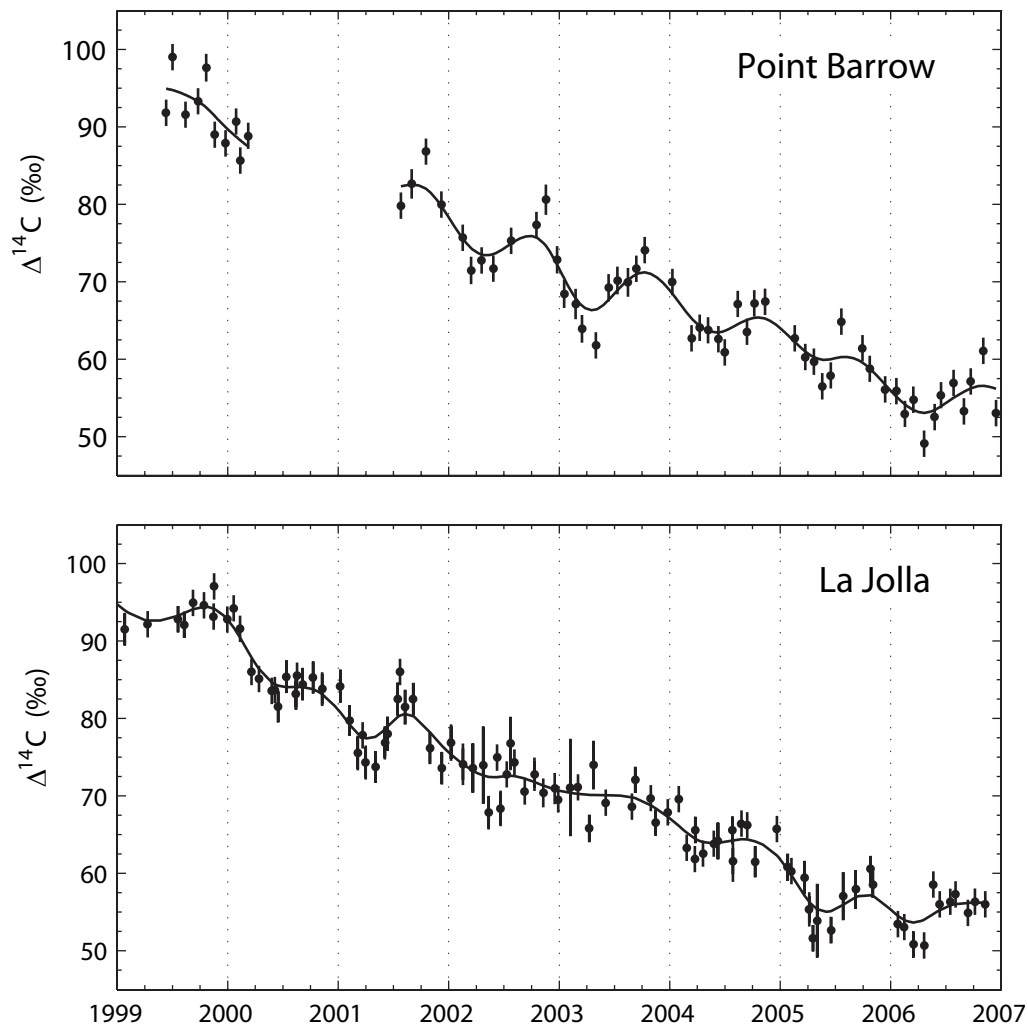


Figure 4.3: $\Delta^{14}\text{C}$ measured in CO_2 sampled in the Northern Hemisphere at Point Barrow (top) and La Jolla (bottom). La Jolla measurements are shown as in Figure 3.2, zoomed in to the period 1999-2006. Error bars show measurement uncertainty of 1.7-2.7 ‰. The lines show cubic smoothing splines.

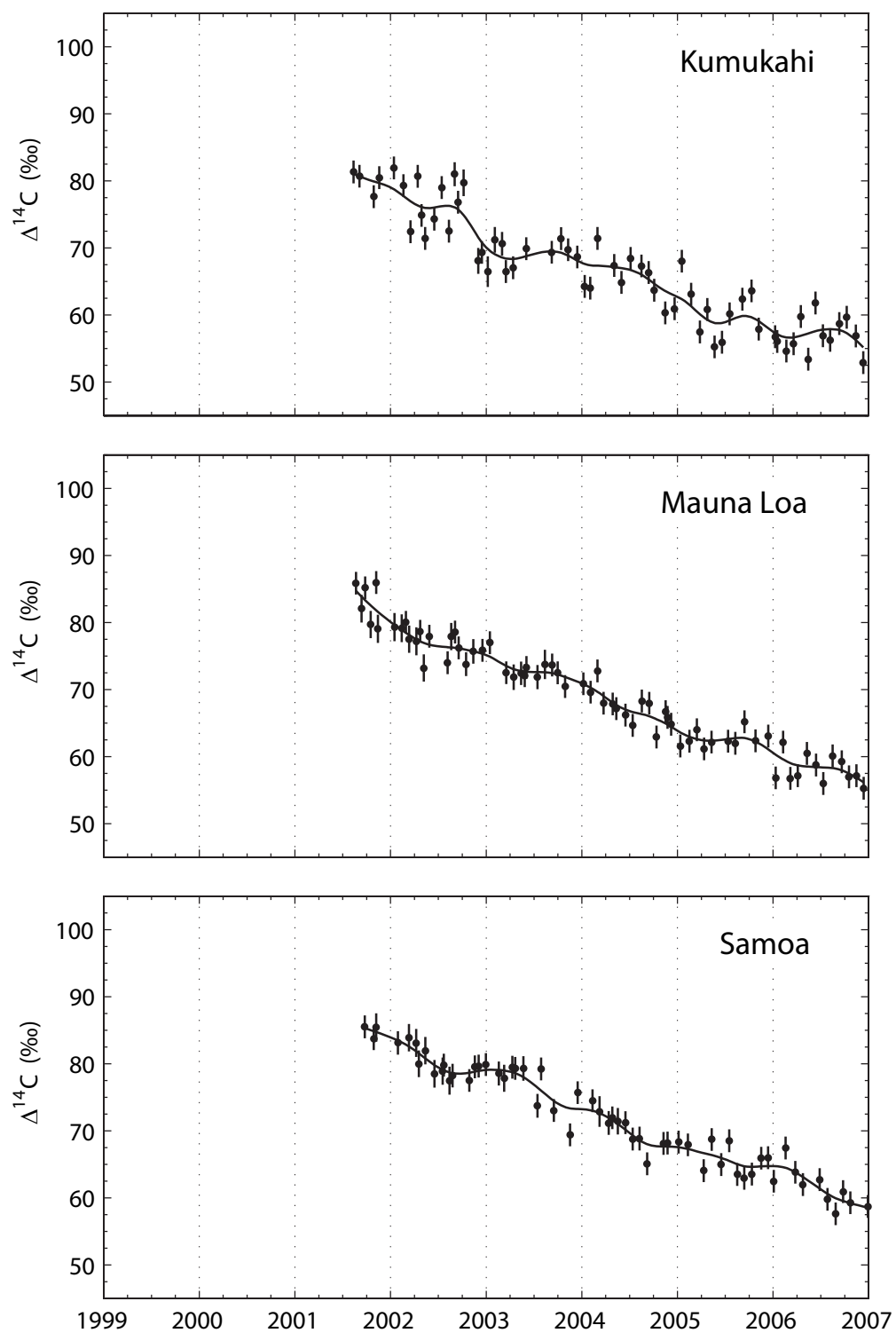


Figure 4.4: $\Delta^{14}\text{C}$ measured in CO_2 sampled in the Tropics at Kumukahi (top), Mauna Loa (middle) and Samoa (bottom). Error bars show measurement uncertainty of 1.7-2.3 ‰. The lines show cubic smoothing splines.

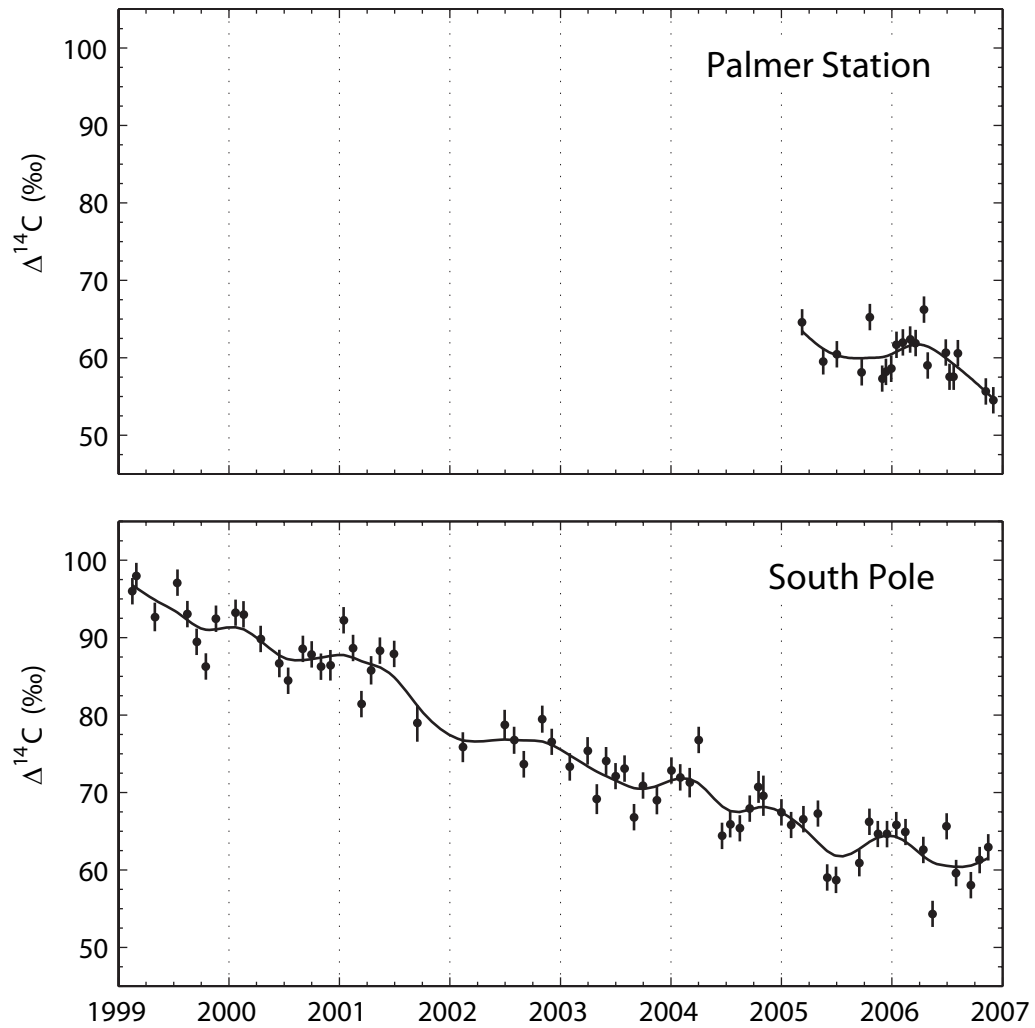


Figure 4.5: $\Delta^{14}\text{C}$ measured in CO_2 sampled in the Southern Hemisphere at Palmer Station (top) and the South Pole (bottom). Error bars show measurement uncertainty of 1.7-2.6 ‰. The lines show cubic smoothing splines.

$(c \cos(2\pi t) + d \sin(2\pi t))$ and a smoothing spline $(s(t))$ fit to the $\Delta^{14}\text{C}$ observations:

$$y = a + bt + c \cos(2\pi t) + d \sin(2\pi t) + s(t) \quad (4.1)$$

The monthly values for each station plotted in the following figures are listed in Appendix B.2. For CO_2 and $\delta^{13}\text{C}$, the curves connect monthly means of biweekly measurements and the circles show measured values on the sample dates for which $\Delta^{14}\text{C}$ was measured, corresponding to the circles in $\Delta^{14}\text{C}$.

For $\delta^{13}\text{C}$ at Palmer Station the solid line denoting monthly mean values is omitted, as the $\delta^{13}\text{C}$ measurements were conducted specifically for the $\Delta^{14}\text{C}$ analysis of this work. $\delta^{13}\text{C}$ measured in Palmer Station samples was not conducted as part of the rigorous procedures of the long term measurements of the other gases measured at Scripps. These measurements required a correction as described in Section 2.18 and are likely to have more uncertainty than $\delta^{13}\text{C}$ measured at the other stations. Greater uncertainty in $\delta^{13}\text{C}$ does not contribute greater uncertainty to $\Delta^{14}\text{C}$ at Palmer Station.

Photosynthetic activity drives strong seasonal cycles of CO_2 and $\delta^{13}\text{C}$ in the Northern Hemisphere, whereas little seasonality is observed in CO_2 and $\delta^{13}\text{C}$ in the south owing to the minimal land cover in the extratropics and correspondingly, small terrestrial biosphere (Keeling, 1960; Bolin and Keeling, 1963). Seasonality in $\Delta^{14}\text{C}$ does not show the same patterns: significant seasonal variation is observed at the South Pole and suggested at Palmer Station.

4.5 Trends of $\Delta^{14}\text{C}$ at each station

All stations show decreasing trends in $\Delta^{14}\text{C}$ (Figure 4.12). Trends were quantified with simple linear least squares fit. The fitted slopes are listed in Table 4.2. Also shown are the 1-sigma uncertainties (68.3 % confidence interval) in fitted slope.

The linear trend at all of the stations is approximately -5 ‰ yr^{-1} . The linear fit to the measurements at Palmer Station seems to exhibit a smaller trend,

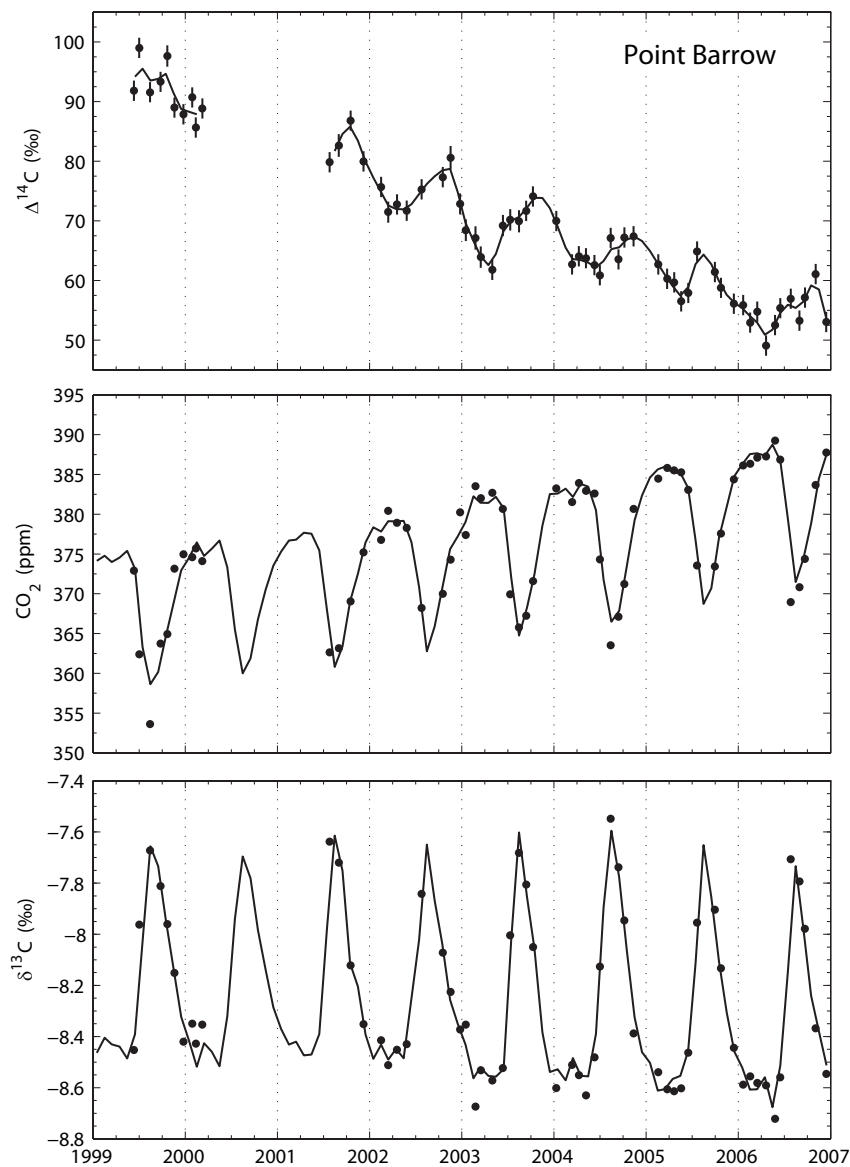


Figure 4.6: Observations of $\Delta^{14}\text{C}$, CO_2 and $\delta^{13}\text{C}$ at Point Barrow. The line in $\Delta^{14}\text{C}$ shows monthly values calculated by fitting a linear trend, single harmonic and cubic smoothing spline to the observations, listed in Appendix B.2. For CO_2 and $\delta^{13}\text{C}$, the lines show monthly values and the circles show the sample dates for which $\Delta^{14}\text{C}$ was measured, corresponding to the circles in $\Delta^{14}\text{C}$.

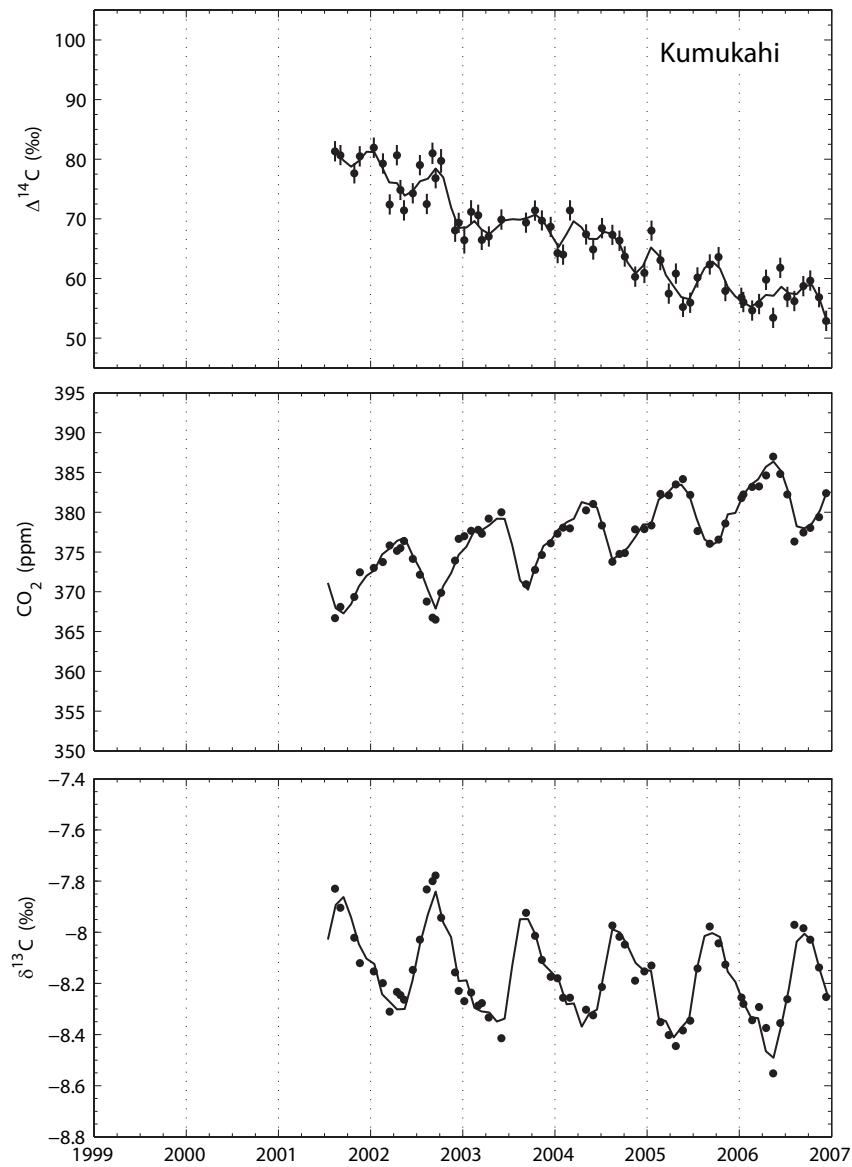


Figure 4.7: Observations of $\Delta^{14}\text{C}$, CO_2 and $\delta^{13}\text{C}$ at Kumukahi. The line in $\Delta^{14}\text{C}$ shows monthly values calculated by fitting a linear trend, single harmonic and cubic smoothing spline to the observations, listed in Appendix B.2. For CO_2 and $\delta^{13}\text{C}$, the lines show monthly values and the circles show the sample dates for which $\Delta^{14}\text{C}$ was measured, corresponding to the circles in $\Delta^{14}\text{C}$.

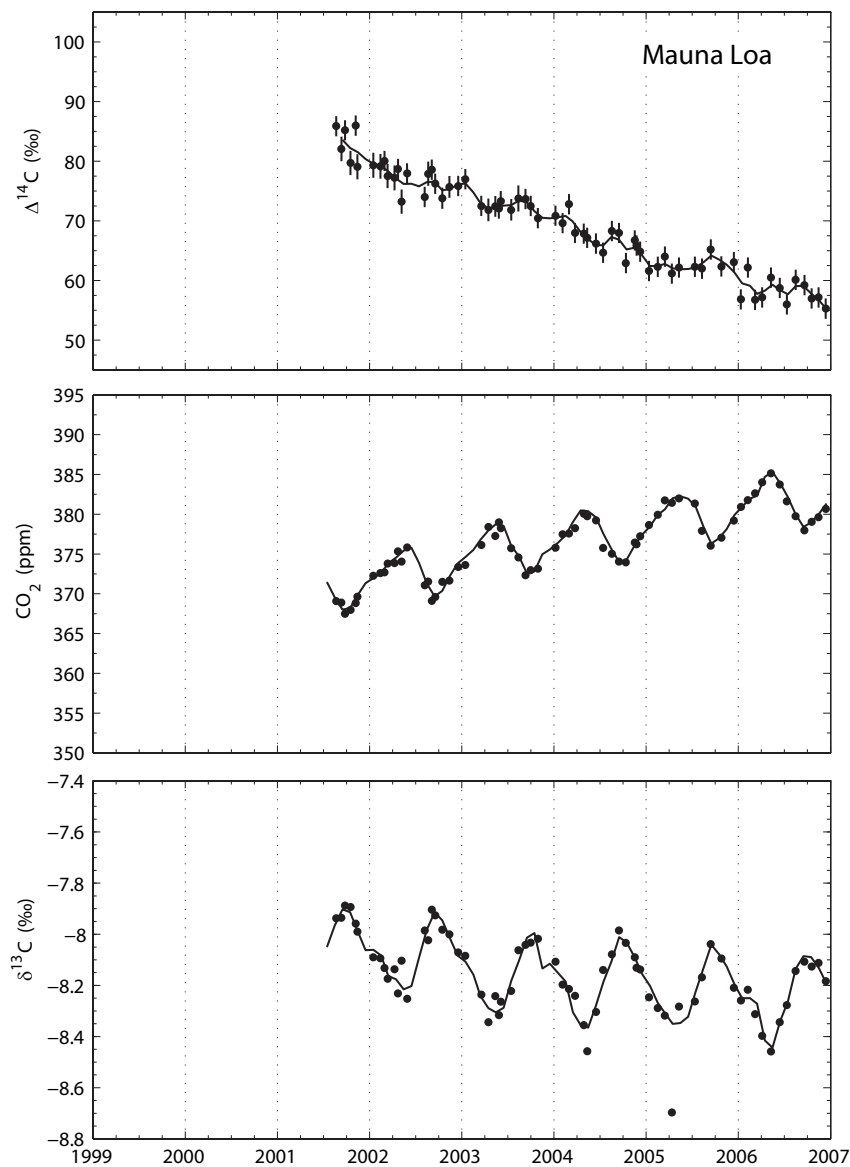


Figure 4.8: Observations of $\Delta^{14}\text{C}$, CO_2 and $\delta^{13}\text{C}$ at Mauna Loa. The line in $\Delta^{14}\text{C}$ shows monthly values calculated by fitting a linear trend, single harmonic and cubic smoothing spline to the observations, listed in Appendix B.2. For CO_2 and $\delta^{13}\text{C}$, the lines show monthly values and the circles show the sample dates for which $\Delta^{14}\text{C}$ was measured, corresponding to the circles in $\Delta^{14}\text{C}$.

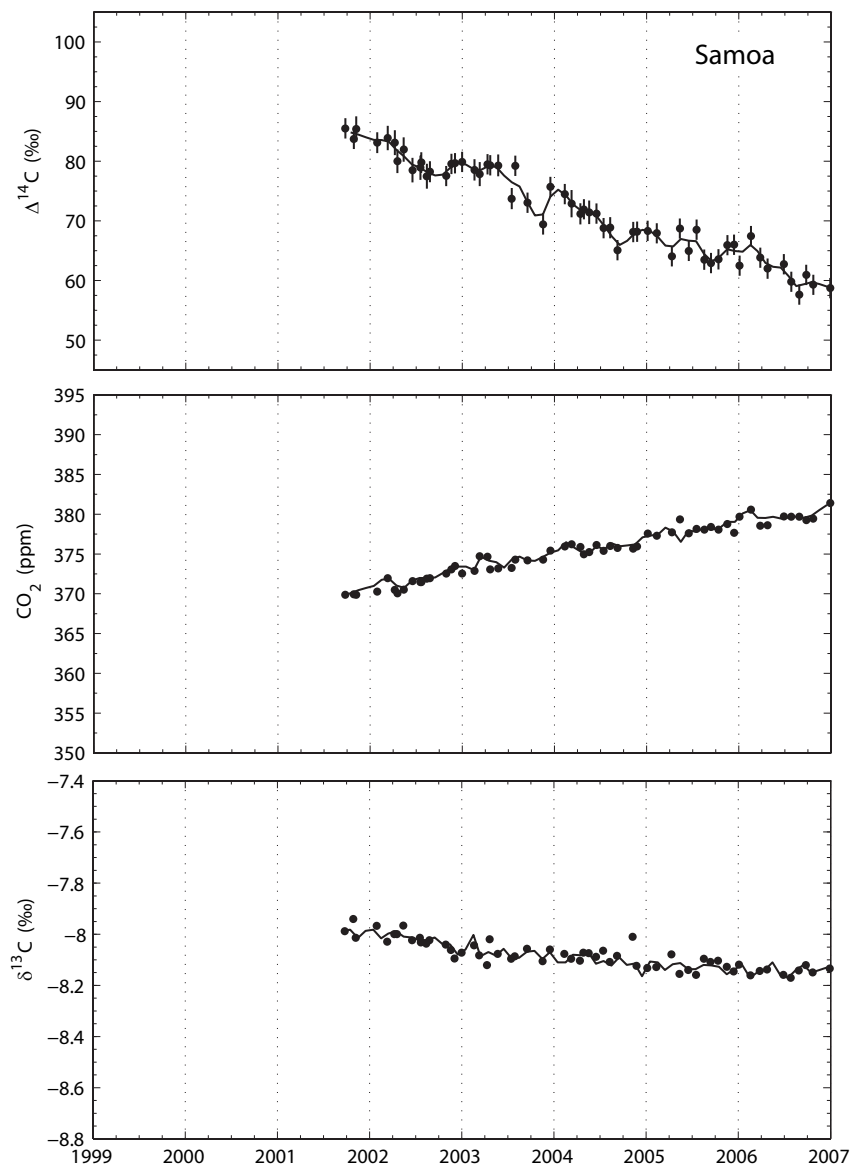


Figure 4.9: Observations of $\Delta^{14}\text{C}$, CO_2 and $\delta^{13}\text{C}$ at Samoa. The line in $\Delta^{14}\text{C}$ shows monthly values calculated by fitting a linear trend, single harmonic and cubic smoothing spline to the observations, listed in Appendix B.2. For CO_2 and $\delta^{13}\text{C}$, the lines show monthly values and the circles show the sample dates for which $\Delta^{14}\text{C}$ was measured, corresponding to the circles in $\Delta^{14}\text{C}$.

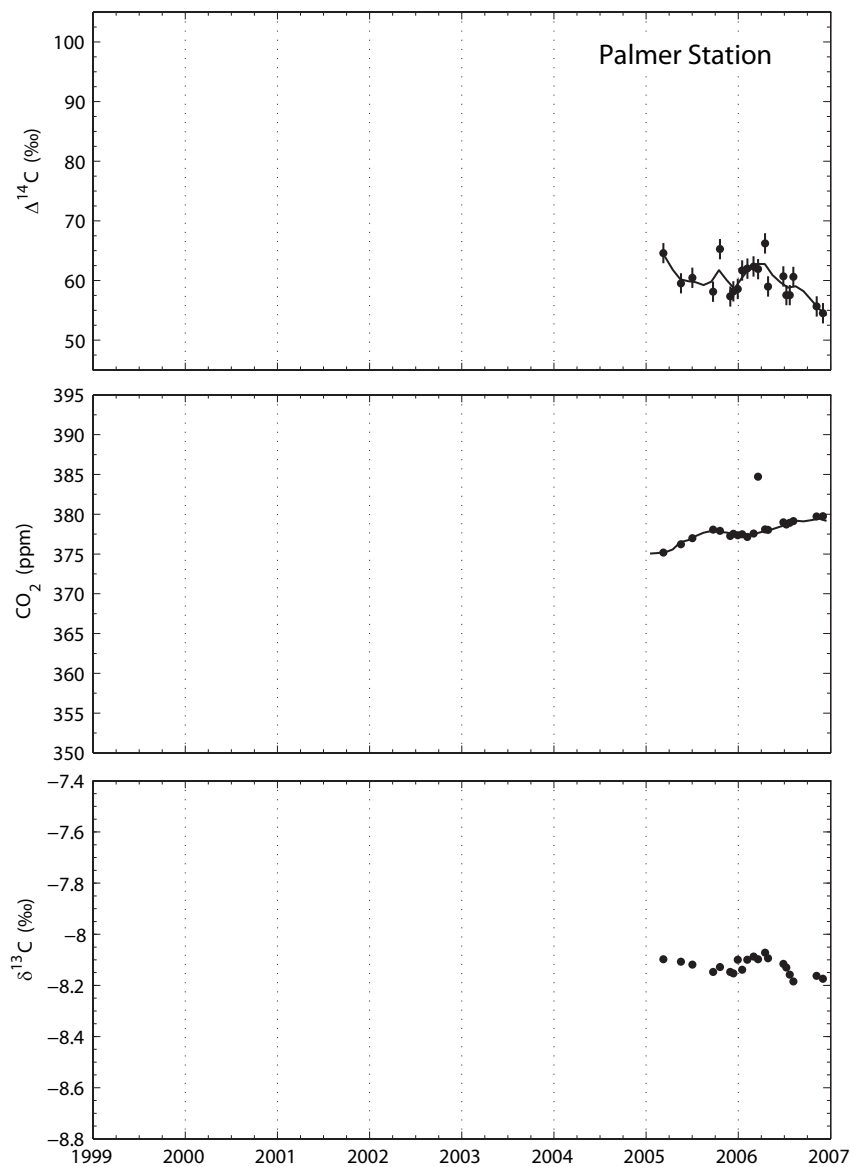


Figure 4.10: Observations of $\Delta^{14}\text{C}$, CO_2 and $\delta^{13}\text{C}$ at Palmer Station. The line in $\Delta^{14}\text{C}$ shows monthly values calculated by fitting a linear trend, single harmonic and cubic smoothing spline to the observations, listed in Appendix B.2. For CO_2 and $\delta^{13}\text{C}$, the lines show monthly values and the circles show the sample dates for which $\Delta^{14}\text{C}$ was measured, corresponding to the circles in $\Delta^{14}\text{C}$.

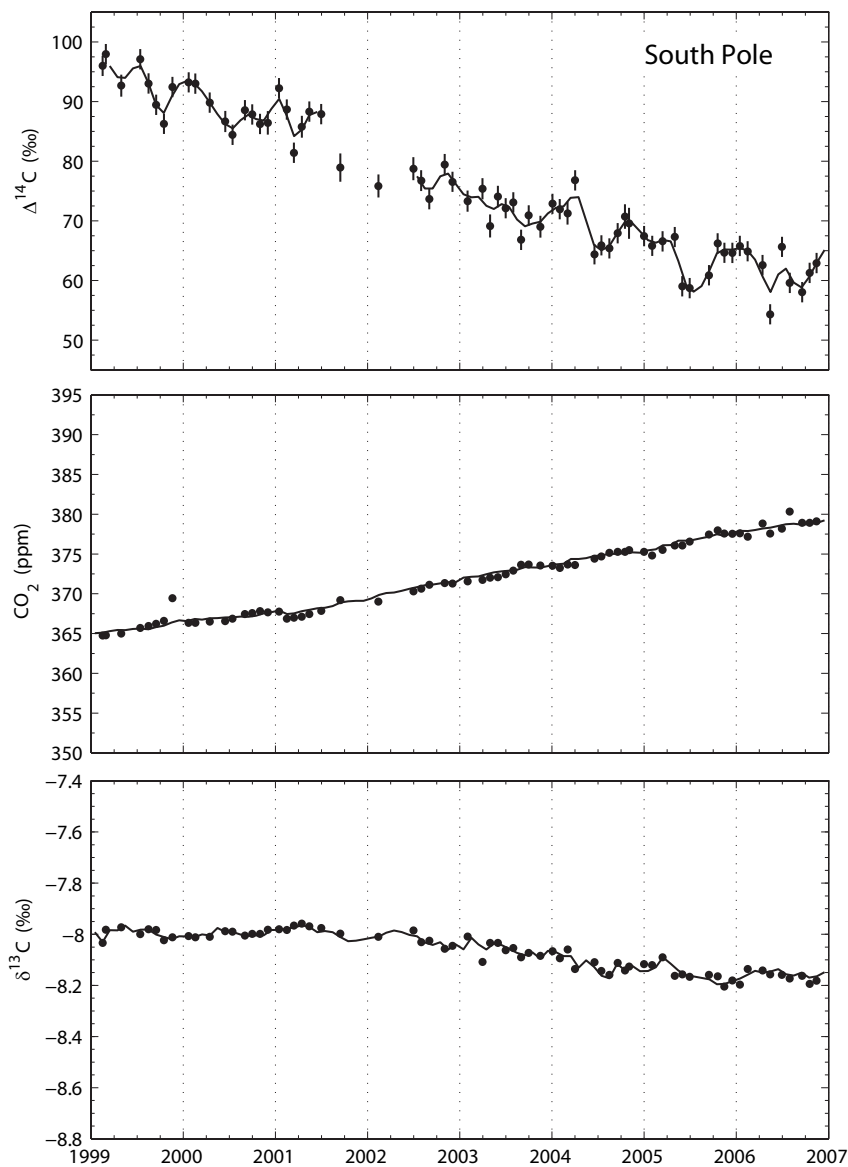


Figure 4.11: Observations of $\Delta^{14}\text{C}$, CO_2 and $\delta^{13}\text{C}$ at the South Pole. The line in $\Delta^{14}\text{C}$ shows monthly values calculated by fitting a linear trend, single harmonic and cubic smoothing spline to the observations, listed in Appendix B.2. For CO_2 and $\delta^{13}\text{C}$, the lines show monthly values and the circles show the sample dates for which $\Delta^{14}\text{C}$ was measured, corresponding to the circles in $\Delta^{14}\text{C}$.

however the period of less than 2 years of records does not allow a representative trend to be resolved. La Jolla and Point Barrow may have slightly steeper trends than the rest of the stations, however the measurement period at La Jolla, Point Barrow and the South Pole includes several years before the initiation of measurements at the tropical stations. As the trend of atmospheric $\Delta^{14}\text{C}$ since the 1960s has shown an exponential character (Chapter 3, Manning et al. 1990, Levin and Kromer 1997), earlier records would be expected to show more rapid decline. In addition, the inclusion of partial years of measurements could skew the calculated trend if a substantial seasonal cycle is present.

Trends were also calculated using measurements only from 2002-2006 (shown as Trend ($y > 2002$) in Table 4.2), in order to incorporate only whole years of records and allow a consistent time period for all stations. For trends fitted to measurements after 2002, the stations show excellent correspondence to the trends fit to the entire record, within regression error, except for the South Pole. Since 2001, $\Delta^{14}\text{C}$ at the South Pole may have declined less rapidly.

The σ_{Det} column in Table 4.2 shows the standard deviation of residuals calculated by subtracting the fitted linear trend from the $\Delta^{14}\text{C}$ data at each station. Mauna Loa and Samoa exhibit very low σ_{Det} ; σ_{Det} is nearly the same as the measurement uncertainty in $\Delta^{14}\text{C}$ at Mauna Loa and Samoa. These two stations do not appear to have a significant annual cycle or short term variability. The other stations show $\sigma_{Det} \geq 3 \text{ ‰}$, suggesting that regular seasonal or other variability is present.

Table 4.2 also includes the p value calculated from a “runs test” on the detrended time series from each station. A runs test compares the number of sign changes in a sequence of data to the number of sign changes expected from a random sequence (Gibbons and Chakraborti, 2003). A low value of p indicates the time series contains few sign changes and shows significant temporal coherence. Point Barrow, La Jolla, Kumukahi and the South Pole show small p values, indicating the hypothesis that the detrended time series is randomly ordered can

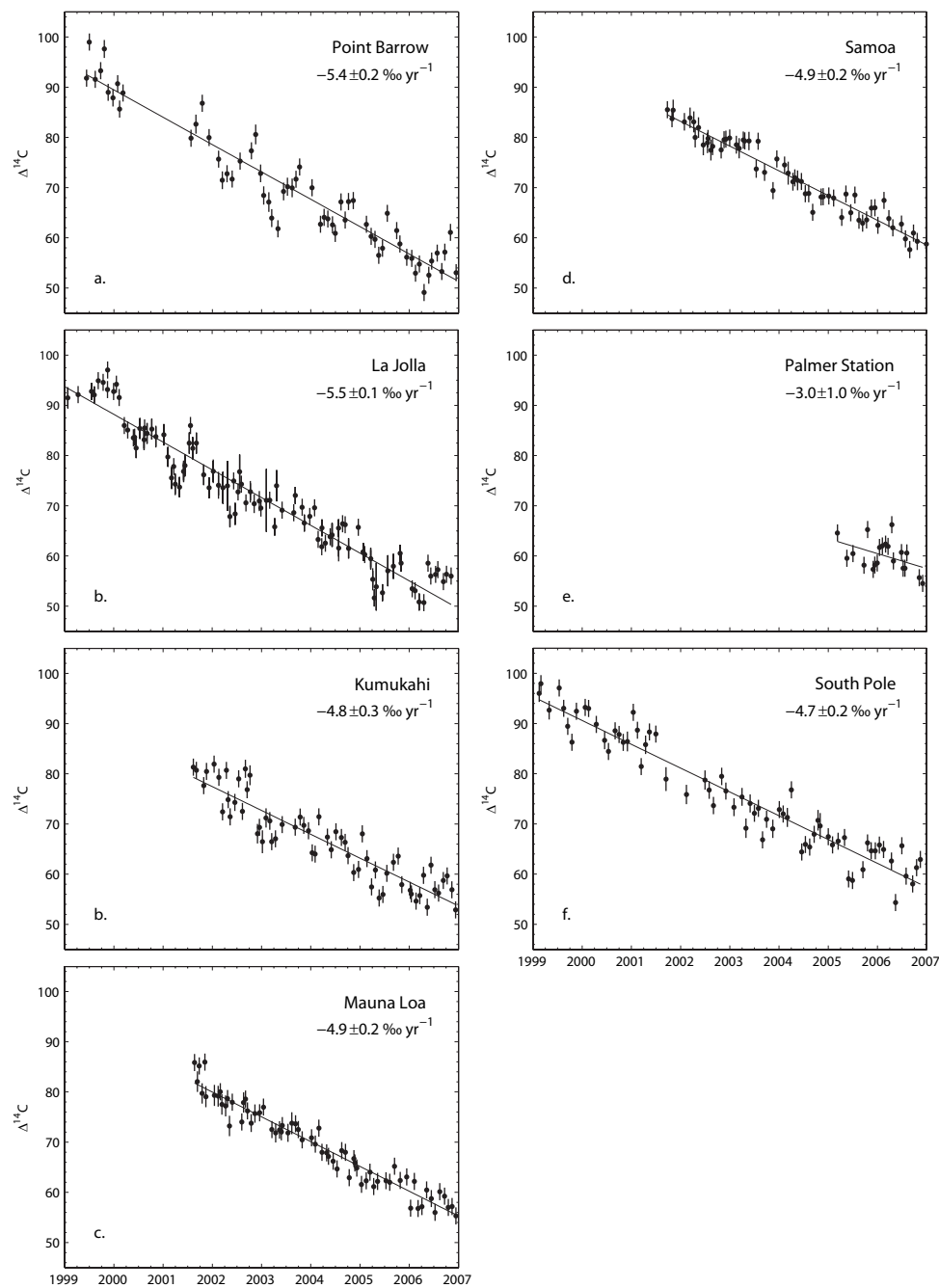


Figure 4.12: Trends calculated by fitting a linear equation to the observations at a. Point Barrow, b. La Jolla, c. Kumukahi, d. Mauna Loa, e. Samoa, f. Palmer Station and g. the South Pole. Fitted slopes are listed for each station with 1-sigma uncertainties.

Table 4.2: Observed trends at each station. Trend was fitted for the entire period of measurements at each station, and for the period including whole years of measurement after 2002. σ_{Det} shows the standard deviation of observed $\Delta^{14}\text{C}$ at each station after subtracting the fitted linear trend. The results of a test of randomness of the detrended records are also listed (p value), where low p values signify greater regularity in the zero-crossing of the detrended data.

Station	Trend (‰ yr ⁻¹)	Trend (y>2002) (‰ yr ⁻¹)	σ_{Det} (‰)	p value
PTB	-5.4±0.2	-4.6±0.4	3.8	0.005
LJO	-5.5±0.1	-4.7±0.3	3.5	2.25e-6
KUM	-4.8±0.3	-4.6±0.3	3.3	0.06
MLO	-4.9±0.2	-4.7±0.3	2.0	0.6
SAM	-4.9±0.2	-4.9±0.2	1.9	0.8
PSA	-3.0±1.0		2.9	0.6
SPO	-4.7±0.2	-3.8±0.4	3.2	0.07

be rejected. Mauna Loa and Samoa do not exhibit significant temporal coherence ($p \gg 0.1$). While Palmer Station also does not express regularity in positive or negative residuals, the record is not long enough for statistically significant seasonal variability to be expected.

Whereas variation in the trend of $\Delta^{14}\text{C}$ was observed at La Jolla at 5-8 year timescales (Section 3.7), the $\Delta^{14}\text{C}$ records at the other Scripps stations are too short to observe changes in the secular trend that would be evident through coherent variability in $\Delta^{14}\text{C}$ anomalies at timescales longer than one year.

4.6 Seasonal cycles of $\Delta^{14}\text{C}$ at each station

Using the linear trends calculated in the previous section, the secular decline in $\Delta^{14}\text{C}$ can be removed to show the annual variation at each station. To examine consistencies in annual variation over all years, detrended $\Delta^{14}\text{C}$ are overlain onto a single calendar year in Figure 4.13. Individual years are plotted with different symbols and solid black circles and errorbars show the mean and standard deviation within each month.

Measurements at Point Barrow show the most pronounced annual varia-

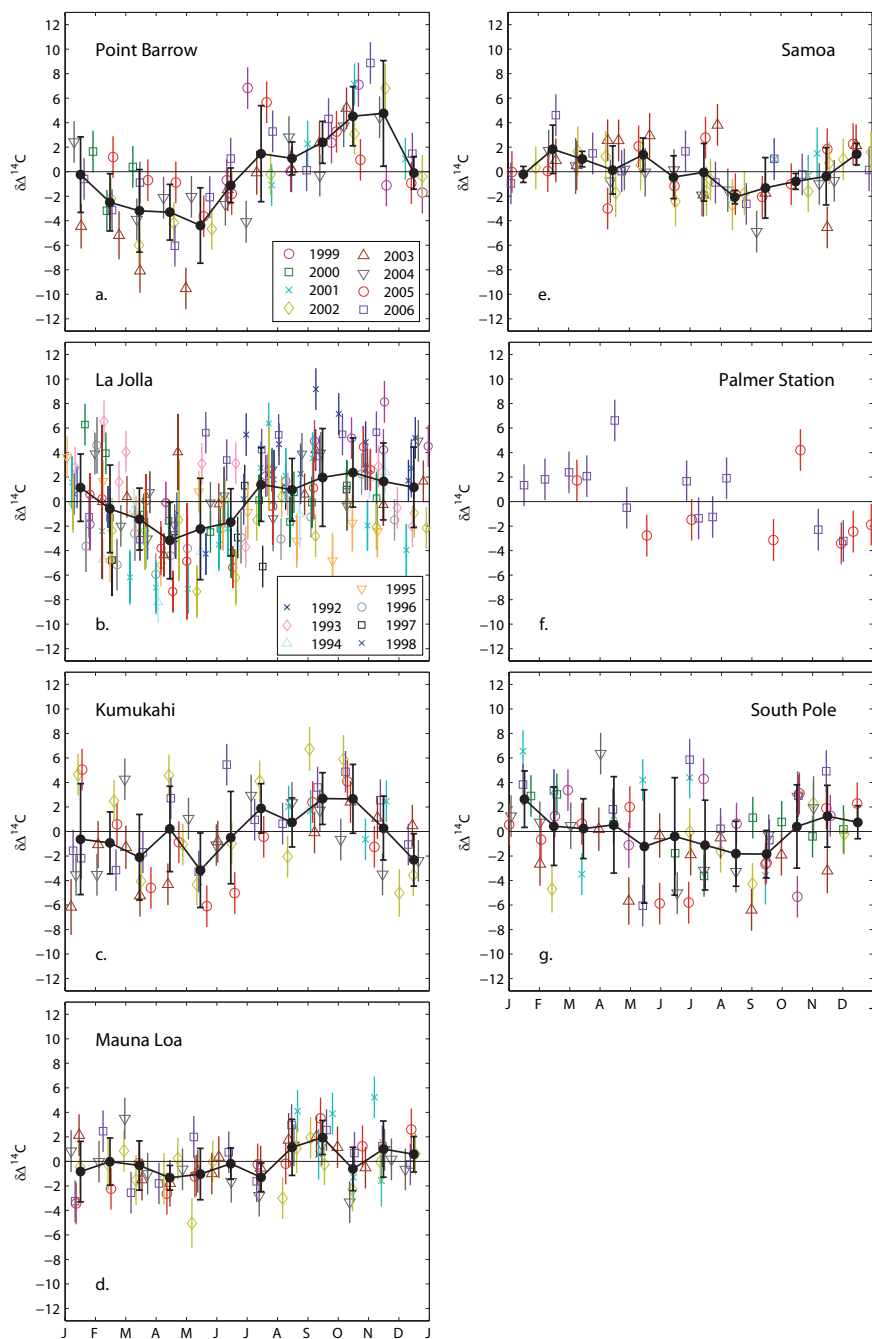


Figure 4.13: Detrended $\Delta^{14}\text{C}$ at a. Point Barrow, b. La Jolla, c. Kumukahi, d. Mauna Loa, e. Samoa, f. Palmer Station and g. South Pole. Individual years are overlain and marked with different symbols; Panel a. shows the legend for all stations while Panel b. shows the legend for additional years observed at La Jolla. Monthly averages and standard deviations are shown with black circles and errorbars.

tion of $\Delta^{14}\text{C}$. At Point Barrow, $\Delta^{14}\text{C}$ is distinctly higher in the second half of the year with maximum values observed in October, on average. Examination of six years of data between 1999 and 2006 suggests that the range of seasonal variation is approximately 8 ‰.

Described in Section 3.8.1, annual cycles at La Jolla show similar phasing to Point Barrow, with a reduced and highly variable amplitude. Kumukahi shows the same phasing with smaller amplitude: ± 3 ‰. There appears to be more scatter in the record at Kumukahi, especially showing excursions of high $\Delta^{14}\text{C}$. The sites at sea level in the Northern Hemisphere show similar phasing, with the seasonal amplitude and regularity being highest at the most northerly station and increasing as one progresses northward from Kumukahi to La Jolla to Point Barrow.

Mauna Loa and Samoa show very little variation over the year. As indicated by the σ_{Det} and p value in Table 4.2, the records at Mauna Loa and Samoa are not significantly different than expected from random variation around a linear trend. However, visual inspection of Figure 4.13d and e suggests that a consistent annual variation of ± 1 -2 ‰ may exist at the stations, with opposite phase at Samoa than at Mauna Loa. Phasing at Mauna Loa and Samoa is roughly consistent with other sites in the respective hemispheres. The magnitude of seasonal variability at Mauna Loa and Samoa is at nearly the same level as the measurement precision.

As less than 2 years of monthly samples have been measured at Palmer Station, annual patterns of $\Delta^{14}\text{C}$ cannot yet be discerned by overlaying detrended $\Delta^{14}\text{C}$ as in Figure 4.13f.

Detrended $\Delta^{14}\text{C}$ at the South Pole shows the most scatter of all stations. Measurements in the winter are especially variable, with standard deviations of ± 5 ‰ in detrended measurements over May and June. $\Delta^{14}\text{C}$ tends to be slightly enhanced in summer (December and January) and depleted in winter, though a regular seasonal cycle does not seem to exist at the South Pole.

To estimate a mean seasonal cycle at each station, a linear trend and

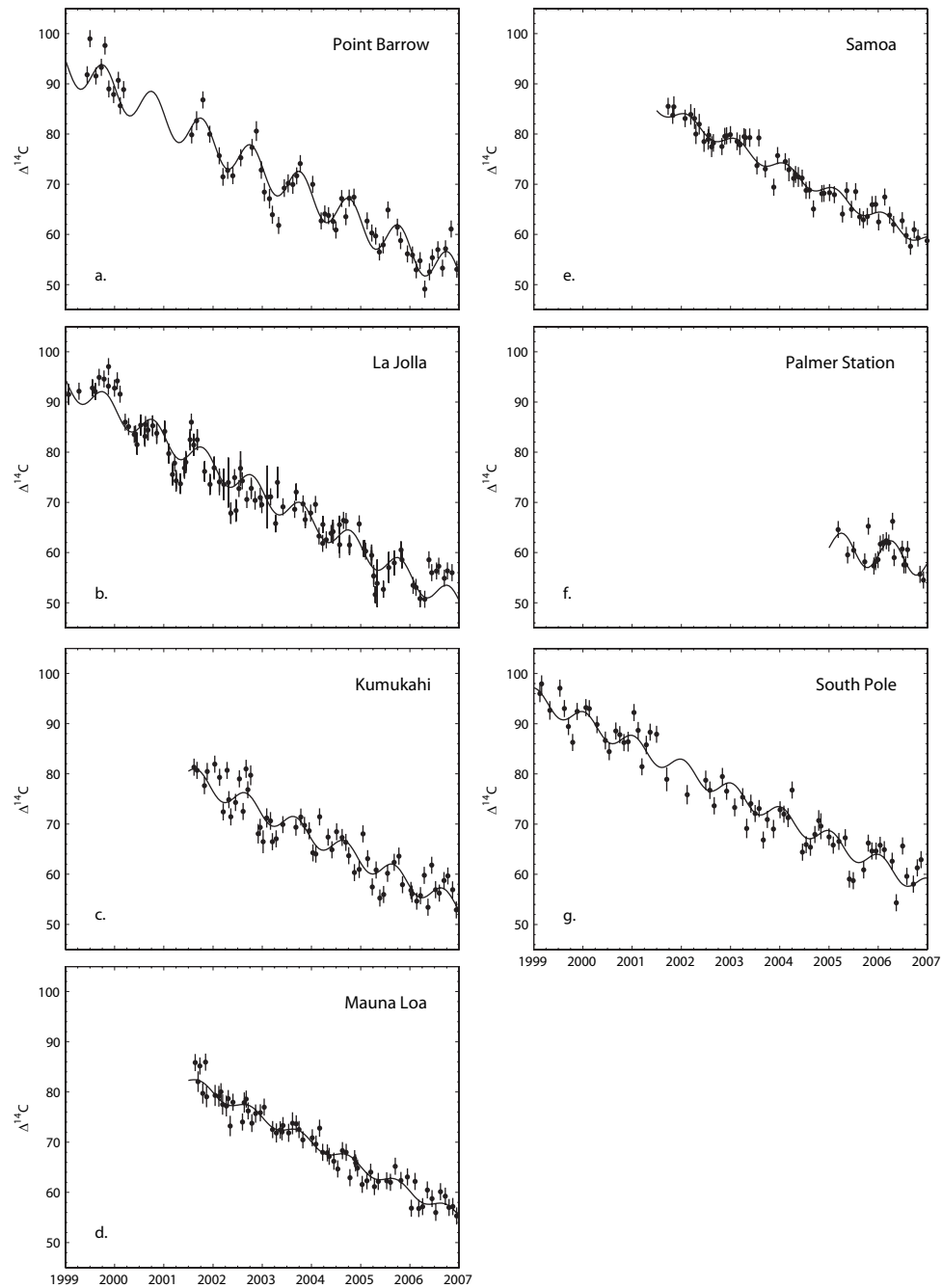


Figure 4.14: $\Delta^{14}\text{C}$ observations fit with a linear trend and one harmonic (Equation 4.2) at a. Point Barrow, b. La Jolla, c. Kumukahi, d. Mauna Loa, e. Samoa, f. Palmer Station and g. the South Pole

Table 4.3: Mean annual cycle and trend at all stations calculated by fitting a linear trend and single harmonic (Equation 4.2) to measurements from each station. The linear slope is given by the fitted parameter “b”, and the timing of maximum $\Delta^{14}\text{C}$ and the difference between minimum and maximum values ($2\times$ amplitude) are given for the fitted harmonic. σ_{Des} shows the standard deviation of residual $\Delta^{14}\text{C}$ after subtracting the curves in Figure 4.14.

Station	Trend (‰ yr ⁻¹)	2× Amplitude (‰)	Timing of Max (day)	σ_{Des} (‰)
PTB	-5.3±0.2	7.4±0.8	Oct 12±9	2.7
LJO	-5.5±0.1	5.0±0.5	Oct 19±11	3.1
KUM	-4.7±0.3	4.1±1.5	Sep 9±22	3.1
MLO	-4.9±0.2	2.1±0.6	Oct 2±27	1.9
SAM	-4.9±0.2	2.7±0.9	Feb 18±19	1.8
PSA	-1.5±1.2	6.1±1.5	Apr 8±19	2.6
SPO	-4.7±0.2	3.8±1.4	Jan 16±170	3.0

single harmonic was fit to the measured $\Delta^{14}\text{C}$ according to:

$$y = a + bt + c \cos(2\pi t) + d \sin(2\pi t) \quad (4.2)$$

This procedure was also performed for observations from La Jolla in Section 3.8.1. Results for all stations are listed in Table 4.3 and plotted in Figure 4.14. Slopes calculated by fitting the measurements with the single harmonic as well as the linear trend agree with the slopes calculated by a linear trend only (Table 4.2), with the exception of Palmer Station. As the record at Palmer Station is less than two years long, we do not expect to produce robust estimates of the fitting parameters. The fitted “c” and “d” were used to estimate the annual variation (“2× Amplitude” in Table 4.3) and day of the year where $\Delta^{14}\text{C}$ is highest (“Timing of Max” in Table 4.3). 1-sigma uncertainties (68.3 % confidence interval) in fitted parameters and resulting phase and amplitude are also listed in Table 4.3.

4.7 Discussion of seasonal cycles of $\Delta^{14}\text{C}$

The average seasonal cycles of $\Delta^{14}\text{C}$ at each station, as calculated by the fitted constants for the last two terms in Equation 4.2, are plotted in different colors

in the right panel of Figure 4.15. The northern stations are shown as warmer colors (PTB: black, LJO: red, KUM: orange, MLO: purple) and the southern stations use cooler colors (SAM: green, PSA: light blue, SPO: dark blue). The offsets in the curves represent differences in annual mean $\Delta^{14}\text{C}$ at each station, which will be discussed in the next section.

The northern stations exhibit consistent phasing in the seasonal cycle, with the maximum $\Delta^{14}\text{C}$ occurring in September-October. In Section 3.8.3, we concluded that the seasonal cycle at La Jolla is mainly driven by atmospheric dynamics. The seasonal flux of stratospheric air across the tropopause with a lag time for vertical transport in the troposphere contributes to high $\Delta^{14}\text{C}$ in the fall. Vertical mixing should also enhance the seasonality of $\Delta^{14}\text{C}$ through variation in the boundary layer depth and ventilation; more vigorous vertical mixing during summer dissipates the negative influence of fossil fuel emissions at the surface and brings down ^{14}C -enriched air from the upper troposphere. It is reasonable that these signals would be enhanced in the more northerly station of Point Barrow, and attenuated in the tropical stations. Greater amplitude in the seasonal variation at Kumukahi as compared to Mauna Loa may indicate that seasonal variability originates in surface level air and seasonality in the northern tropics is attenuated with altitude. This observation does not discredit the idea that stratosphere-troposphere exchange is an important contributor, as the STE signal could be propagated from the midlatitudes in low-level air.

Seasonal variation at Samoa is similar to Mauna Loa, except with nearly opposite phasing. The amplitude at both stations is very low, indicating that seasonal changes in ^{14}C fluxes or transport influencing remote tropical air are small. The slight seasonal cycles that are observed are probably related to atmospheric mixing. The seasonality at Mauna Loa may be attenuated by the presence of a substantial fraction of air with Southern Hemisphere origin in the northern, descending branch of the Hadley circulation (Keeling et al., 1998).

The measurements from Palmer Station suggest a seasonal phasing of

$\Delta^{14}\text{C}$ that is opposite to the midlatitude stations of the north. While this record is too short yet to provide a reliable estimate of the mean annual cycle, it is useful to compare the preliminary results to prior observations in the southern midlatitudes. Manning et al. (1990) reported a seasonal cycle at Wellington, New Zealand with maxima in March and minima in August in $\Delta^{14}\text{C}$ observations before 1980. After 1980, they note the emergence of a different seasonal cycle where maxima shifted to July-August. Our measurements at Palmer appear to agree with the phasing observed in the early period at Wellington rather than the phasing of the period 1981-1987. Closer inspection of the measurements from 1981-1987 at Wellington reveals that several years in this period contain only 5-6 sample dates, there are several $\pm 10\text{-}20\text{ ‰}$ outliers and the average measurement uncertainty ($\pm 4\text{ ‰}$) is close to the seasonal amplitude ($\pm 5\text{ ‰}$). It seems that the phasing of seasonal variation would be difficult to detect with these measurement characteristics (also indicated in Figure 4b of Manning et al. (1990)). It is possible that the seasonal cycle at Wellington became indistinguishable in 1980 and did not experience a phase shift. Randerson et al. (2002) were unable to recreate the shift in seasonal cycle with their ^{14}C model. It will be exciting to observe the seasonal cycle at Palmer Station through several more years of measurements to see whether the seasonal cycle of the southern midlatitudes exhibits a regular seasonal cycle and if it does, whether this cycle is anticorrelated with the northern stations. If the cycle does show opposite phasing, it could suggest that atmospheric mixing and stratosphere-troposphere exchange are most important to seasonal variation in the south, as found for La Jolla (Section 3.8.3). If the maximum $\Delta^{14}\text{C}$ at Palmer Station occurs during another time of year, it could indicate that seasonality in air-sea gas exchange also produces measurable effects on $\Delta^{14}\text{C}$.

The irregularity of $\Delta^{14}\text{C}$ observations at the South Pole led to high uncertainty in the fitted harmonic, where the phasing is almost completely uncertain. However, the years 2004-2006 include less scatter and do show good coherence with the fitted curve (Figure 4.14g), where highest $\Delta^{14}\text{C}$ is observed in January. The

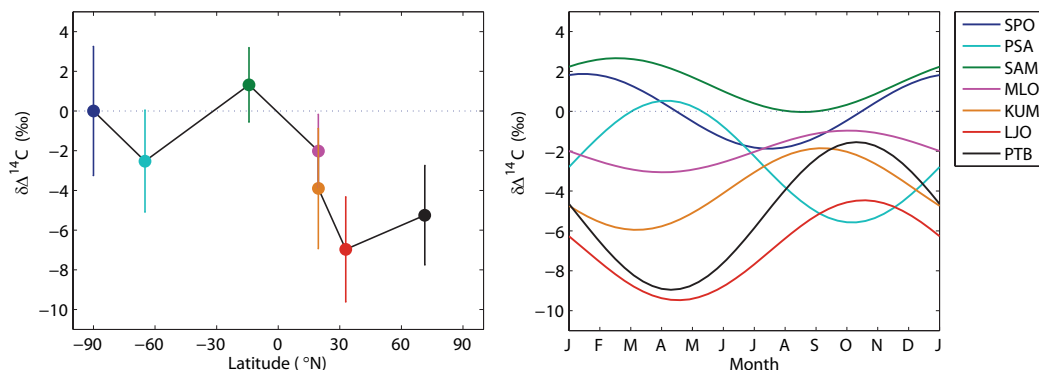


Figure 4.15: Annual means of $\Delta^{14}\text{C}$ at each station for 2005-06, plotted vs station latitude (left panel). Annual means were calculated by evaluating the curves fit to Equation 4.2 at 0.05 yr intervals over 2005 and 2006 and averaging. Errorbars are given by the scatter in residual $\Delta^{14}\text{C}$ during 2005-06 after subtracting the curves fit to Equation 4.2. In the right panel annual cycles of $\Delta^{14}\text{C}$ in the curves fit to Equation 4.2 are shown for one year at each station and offset by the annual mean difference from the South Pole.

$\Delta^{14}\text{C}$ levels at the South Pole are likely to be influenced by the unique Antarctic meteorology. During the long winter night, intense radiative cooling at the surface results in a consistent temperature inversion which restricts vertical mixing with the free troposphere (Harder et al., 2000). In summer the temperature inversion weakens, allowing ventilation of boundary layer air. If the upper tropospheric air above Antarctica contains higher $\Delta^{14}\text{C}$, then seasonal mixing would cause $\Delta^{14}\text{C}$ of boundary layer air to rise. $\Delta^{14}\text{C}$ in surface level air at the South Pole could be depleted relative to the free troposphere by horizontal mixing of low- $\Delta^{14}\text{C}$ air from coastal Antarctica. Air in the upper troposphere could receive enhanced $\Delta^{14}\text{C}$ air from mixing with the polar stratosphere. Further, additional noise in wintertime $\Delta^{14}\text{C}$ at the South Pole may be caused by temporary lifting of the temperature inversion that would enable short term mixing of surface-level air with the free troposphere.

4.8 Latitudinal gradient of $\Delta^{14}\text{C}$

As fluxes of carbon that influence $\Delta^{14}\text{C}$ occur in specific regions of the globe, spatial gradients of $\Delta^{14}\text{C}$ are expected, including gradients across latitudes. To compare the average $\Delta^{14}\text{C}$ at each station in our recent measurements, the curves fit to Equation 4.2 (shown in Figure 4.14) were evaluated at 0.05 yr intervals over the period 2005 through 2006 and averaged. Uncertainty in the estimated annual average for each station is given by the standard deviation of the residuals, similar to the σ_{Des} column in Table 4.3, but specific to the 2005-06 period.

Annual mean $\Delta^{14}\text{C}$ for 2005-06 is plotted against station latitude in the left panel of Figure 4.15. Values are presented relative to the South Pole. Mean $\Delta^{14}\text{C}$ is lower in the Northern Hemisphere than in the South. The highest mean $\Delta^{14}\text{C}$ is observed at Samoa, and the lowest is observed at La Jolla. Midlatitude stations express local minima in $\Delta^{14}\text{C}$, and there is a gradient of -5 ‰ between the northern and southern tropics at sea level.

The interhemispheric difference in $\Delta^{14}\text{C}$ depends on the balance of regional ^{14}C fluxes between the troposphere and the ocean and land biosphere and the rate of addition of fossil fuel CO_2 which continually dilutes ^{14}C in the Northern Hemisphere. The midlatitude depletions in $\Delta^{14}\text{C}$ are caused by the concentration of nearly all of the global emissions of fossil fuel CO_2 in the Northern Hemisphere, and by air-sea gas exchange with aged water masses in the Southern Ocean (Levin and Hesshaimer, 2000; Randerson et al., 2002). Figure 4.15 reveals that the uptake of ^{14}C by the Southern Ocean is a smaller negative influence on $\Delta^{14}\text{C}$ than the emission of fossil fuel CO_2 in 2005-06 since $\Delta^{14}\text{C}$ is lower in the Northern Hemisphere compared to the south. Biospheric release of excess ^{14}C in the Northern Hemisphere also influences the interhemispheric difference of $\Delta^{14}\text{C}$ by counteracting the effect of fossil-derived CO_2 . Release of ^{14}C from tropical ecosystems may additionally strengthen the maximum in $\Delta^{14}\text{C}$ observed in the tropics.

The latitudinal gradient shown in Figure 4.15 contains valuable information about oceanic and biospheric fluxes of ^{14}C which are determined by the

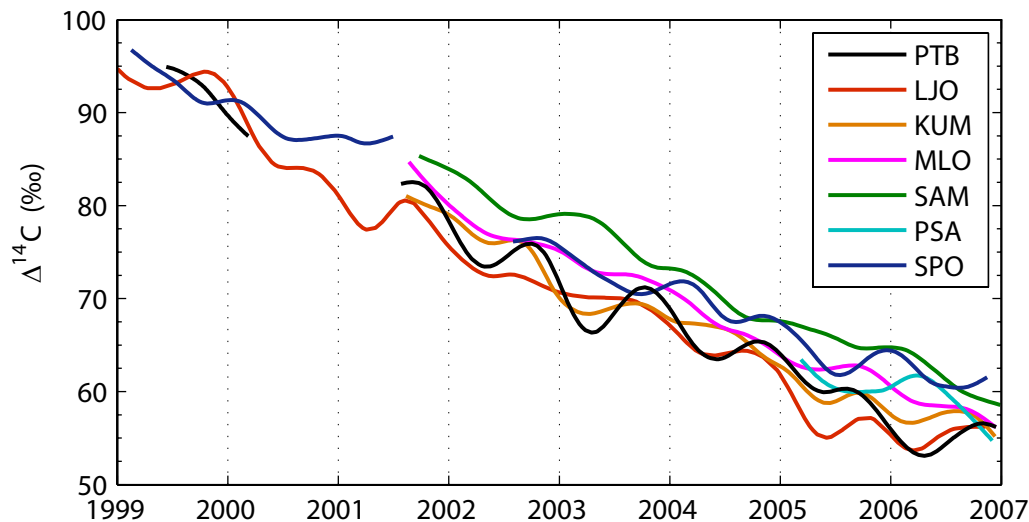


Figure 4.16: Smoothing splines fitted to $\Delta^{14}\text{C}$ observations at each station: Point Barrow (black), La Jolla (red), Kumukahi (orange), Mauna Loa (purple), Samoa (green), Palmer Station (light blue) and the South Pole (dark blue). Curves were also shown individually in Figures 4.3, 4.4 and 4.5.

turnover time of carbon in these reservoirs. As fossil CO_2 emissions grow, gross fluxes of carbon react to rising CO_2 and climate, and levels of atmospheric $\Delta^{14}\text{C}$ evolve, the regional influences on $\Delta^{14}\text{C}$ and the latitudinal $\Delta^{14}\text{C}$ profile will adjust. In the following section (4.10), we examine how the latitudinal profile of $\Delta^{14}\text{C}$ has changed since the nuclear weapons tests, particularly since 1987-89.

The differences in annual mean at each station were also incorporated into the right panel of Figure 4.15, which shows both the mean annual cycle and the mean $\Delta^{14}\text{C}$, relative to the South Pole. Depiction of the seasonal variation in the latitudinal gradient reveals the largest gradients of $\Delta^{14}\text{C}$ in background air are approximately 12 ‰ in March-May, whereas smaller gradients of roughly 7 ‰ exist in September-November. This figure emphasizes the need for high precision measurements in detecting atmospheric gradients in background air across the globe.

Another view of $\Delta^{14}\text{C}$ across latitudes is shown in Figure 4.16. Here, the cubic smoothing splines fit to each station (shown in Figures 4.3, 4.4 and 4.5)

are plotted together as different colors. This enables inspection of the latitudinal profile over the course of the year and over several years. A few features of the global dataset are highlighted by comparing the curves in this way.

1. La Jolla nearly always exhibits the lowest $\Delta^{14}\text{C}$ and Samoa nearly always exhibits the highest $\Delta^{14}\text{C}$, through all years and all seasons
2. Global $\Delta^{14}\text{C}$ gradients are largest in the first half of the year
3. Over the period 2002-06, relative $\Delta^{14}\text{C}$ differences between the stations remained fairly consistent except for the South Pole, where $\Delta^{14}\text{C}$ appeared to increase
4. The gradient in $\Delta^{14}\text{C}$ between Samoa and Kumukahi is always at least 2 ‰, suggesting there is a significant, continual cross-equator gradient in $\Delta^{14}\text{C}$
5. Variations in seasonality at La Jolla does not appear to carry over to Kumukahi or Point Barrow

4.9 Changes in variability at Point Barrow and the South Pole since the 1980s

Between 1978 and 1999, the Centrum voor IsotopenOnderzoek (Center for Isotope Research or CIO) at the University of Groningen, The Netherlands performed stable isotopic analysis on CO_2 samples collected by the Scripps Program. Between 1985 and 1991, Scripps CO_2 samples were “sucked back” after analysis of isotope ratio mass spectrometry to be preserved for $\Delta^{14}\text{C}$ analysis. Samples from two stations were preserved: Point Barrow and the South Pole. The “sucked back” CO_2 samples were analyzed at the Groningen AMS facility and published in 2006 (Meijer et al., 2006).

The early measurements from Point Barrow and the South Pole provide a valuable measure of the changes of $\Delta^{14}\text{C}$ at these stations over the past ~ 20

Table 4.4: Mean annual cycle and trend at Point Barrow and the South Pole for 1985-1991 and 1999-2006. Results from fitting data from Meijer et al. (2006) and this thesis to Equation 4.2, similar to Table 4.3.

Station	Period of record	Trend (‰ yr^{-1})	2x Amplitude (‰)	Timing of Max (year)	Timing of Max (day)
PTB	1985-1991	-10.6 ± 0.3	10.1 ± 1.9	0.73 ± 0.03	Sep 24 \pm 11
SPO	1985-1991	-10.3 ± 0.3	3.8 ± 1.4	0.99 ± 0.45	Dec 30 \pm 166
PTB	1999-2006	-5.3 ± 0.2	7.4 ± 0.8	0.78 ± 0.03	Oct 12 \pm 9
SPO	1999-2006	-4.7 ± 0.2	3.8 ± 1.4	0.04 ± 0.46	Jan 16 \pm 170

years. To investigate such changes, a linear trend and single harmonic were fit to the South Pole and Point Barrow data, as in Equation 4.2 in Section 4.6. The fitted parameters are shown in Table 4.4 for the measurements from Meijer et al. (2006) and from this work.

Figure 4.17 shows the fitted seasonal cycles at Point Barrow and the South Pole for the two measurement periods: 1985-91 in dashed lines and 1999-2006 in solid lines. Blue lines are for the South Pole and black lines are for Point Barrow. The most noticeable change between the two periods is the difference in annual mean $\Delta^{14}\text{C}$ between Point Barrow and the South Pole, indicated by the vertical offset in the Point Barrow curve. In the early period, the annual mean $\Delta^{14}\text{C}$ at Point Barrow was slightly higher than the South Pole ($\sim 2 \text{‰}$), whereas the $\Delta^{14}\text{C}$ at Point Barrow was substantially lower than the South Pole ($\sim 5 \text{‰}$) in 2005-06. Together, our measurements reveal a substantial change in the gradient of $\Delta^{14}\text{C}$ between the South Pole and Point Barrow; annual mean $\Delta^{14}\text{C}$ at Point Barrow decreased by approximately 8‰ between 1987-89 and 2005-06, relative to the South Pole.

The phasing of the seasonal cycles at both Point Barrow and the South Pole do not appear to have changed between 1985-91 and 1999-2006. Point Barrow exhibits maximum $\Delta^{14}\text{C}$ in late September-early October and the South Pole exhibits maximum $\Delta^{14}\text{C}$ in late December-early January. The fitted seasonal cycle at the South Pole for 1985-91 is also uncertain with respect to the phasing, suggesting that $\Delta^{14}\text{C}$ at the South Pole consistently expresses high levels of short-term

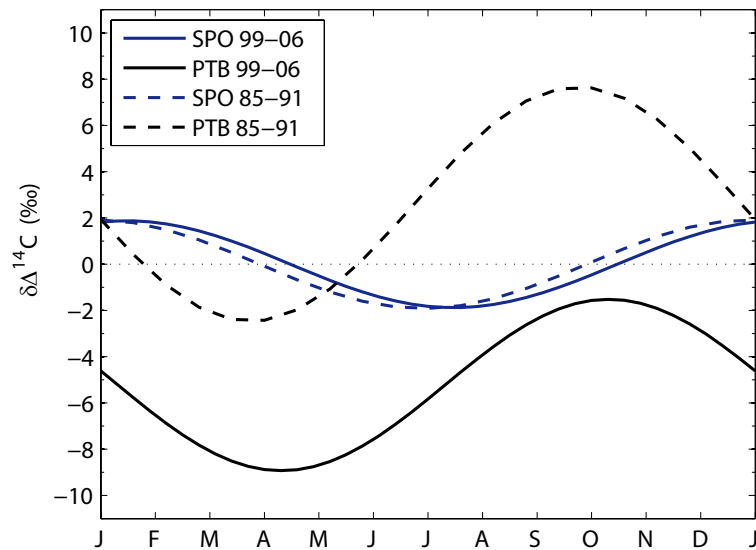


Figure 4.17: Annual cycles at Point Barrow and South Pole, 1985-91 and 1999-2006. The harmonic component to the fit calculated by Equation 4.2 for each record is shown for a single year. The South Pole is shown in blue, Point Barrow is shown in black; dashed lines show results from Meijer et al. (2006), solid lines show results from this thesis. The mean difference, South Pole - Point Barrow, in 1999-2006 and in 1985-91 is indicated by the vertical offset in the sinusoids.

variability.

The amplitude of the seasonal cycle at Point Barrow has decreased by approximately 25 % since 1985-91. For the South Pole, the parameters listed in Table 4.4 and shown in Figure 4.17 indicate that the seasonal amplitude has not changed between the two periods of record. In fact, the amplitude of seasonal variation at the South Pole probably has changed between the CIO and SIO records. Because of the variability in the seasonal cycle at the South Pole, the fitting of a linear trend and single harmonic does not serve to characterize the annual variation as well as for Point Barrow, which has a much more distinct seasonal cycle (see end of Section 4.7). Examination of linearly detrended CIO South Pole data in a way similar to Figure 4.13 suggests the seasonal variation was actually ~ 5 ‰ (Meijer et al., 2006) in 1985-1991. The seasonal amplitude at the South Pole then seems to have been attenuated by a similar amount as Point Barrow between 1985-1991

to 1999-2006: 25 ‰.

4.10 Evolution of the latitudinal profile of $\Delta^{14}\text{C}$

Tree ring evidence of the preindustrial gradient of $\Delta^{14}\text{C}$ between the northern and southern hemispheres suggests that the Northern Hemisphere was 3-5 ‰ more enriched than the South (Braziunas et al., 1995; McCormac et al., 1998). Model investigations of the $\Delta^{14}\text{C}$ gradient suggest that air-sea gas exchange in the Southern Ocean was the main driver of the interhemispheric difference (Braziunas et al., 1995; Levin et al., 1987) before 1890.

During the 20th century, $\Delta^{14}\text{C}$ in the atmosphere experienced massive perturbation by the input of bomb-produced ^{14}C and the increasing emission of fossil fuel CO_2 , both concentrated in the Northern Hemisphere. These regional fluxes caused changes in the the interhemispheric gradient between the northern and southern troposphere.

Estimates of the mean $\Delta^{14}\text{C}$ gradient between sampling stations in the Northern and the Southern Hemisphere for discrete time intervals are shown in Figure 4.18. This figure incorporates measurements from Wellington, New Zealand (Manning et al., 1990), Vermunt, Austria (Levin and Kromer, 2004), Fruholmen, Norway (Nydal and Lövseth, 1996), Jungfrauoch, Switzerland (Levin and Kromer, 2004), the South Pole, Antarctica (Meijer et al. 2006 and this work), and Point Barrow and La Jolla, USA (Meijer et al. 2006 and this work). Annual means were calculated by evaluating a cubic smoothing spline fit to the data and averaging over each calendar year. Mean $\Delta^{14}\text{C}$ at the southern station was subtracted from the mean $\Delta^{14}\text{C}$ at the northern station. Years with poor temporal coverage were omitted. Errorbars in Figure 4.18 indicate the average measurement uncertainty. The average measurement uncertainty may overestimate the uncertainty in the $\Delta^{14}\text{C}$ gradient between sampling stations, though additional sources of uncertainty must be considered when comparing samples measured by different laboratories,

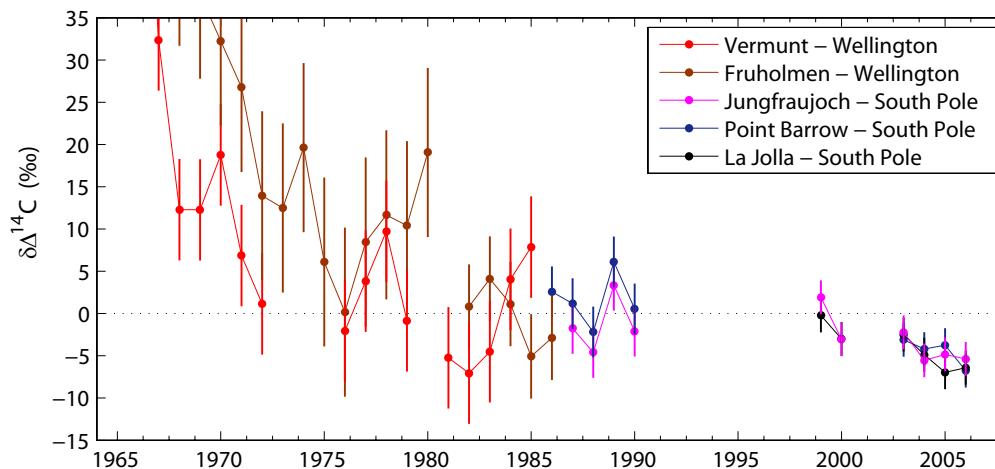


Figure 4.18: Evolution of the $\Delta^{14}\text{C}$ gradient between the Northern and Southern Hemispheres. Datapoints show the difference between the annual mean of $\Delta^{14}\text{C}$ at a northern site minus the annual mean of $\Delta^{14}\text{C}$ at a southern site. For the Southern Hemisphere, measurements from Wellington, New Zealand (Manning et al., 1990) and the South Pole (Meijer et al. 2006 and this work) are used. For the Northern Hemisphere, measurements from Vermunt, Austria and Jungfrauoch, Switzerland (Levin and Kromer, 2004; Levin et al., 2008), Fruholmen, Norway (Nydal and Lövseth, 1996), and Point Barrow and La Jolla, USA (Meijer et al. 2006 and this work) are used. Annual means were calculated by averaging a cubic smoothing spline fit to the measurements. Years with poor temporal coverage are omitted. Errorbars show average measurement uncertainty.

as discussed in Sections 2.19 and 3.5.1, and when estimating an annual mean from discrete observations. Before the mid-1980s, measurement uncertainty was approximately 8 ‰. Precision progressively improved to ± 5 ‰ in the early 1980s, to $\pm 2\text{--}3$ ‰ in the late 1980s and to better than ± 2 ‰ in current analytical techniques (Graven et al., 2007; Turnbull et al., 2007).

The interhemispheric gradient was extremely large and positive in the years following the nuclear weapons tests because of the enormous enrichment of $\Delta^{14}\text{C}$ in the north by excess ^{14}C produced by the detonations. Maximum gradients were several hundred ‰ in 1963–1965 (Nydal and Lovseth, 1983), then decreased quickly as excess ^{14}C was distributed by atmospheric mixing. Gradients were on the order of 20 ‰ during the early 1970s and by 1980, the interhemispheric gradient

had nearly disappeared (Figure 4.18). During the 1980s and perhaps until 2000, there appeared to be little or no difference between $\Delta^{14}\text{C}$ in the Northern and Southern Hemispheres. Published records from the Southern Hemisphere are not readily available for the period 1991-1998, however, (Levin and Hesshaimer, 2000) report a difference of approximately -1 ‰ between Jungfraujoch and Neumayer in 1994.

Our measurements reveal that the sign of the interhemispheric $\Delta^{14}\text{C}$ gradient has switched. $\Delta^{14}\text{C}$ at the northern stations is now more depleted than $\Delta^{14}\text{C}$ at the South Pole. It appears that the change happened between 1990 and 2000, and the gradient is becoming more negative with time. In 2005-06, $\Delta^{14}\text{C}$ at La Jolla was roughly 6.5 ‰ lower than $\Delta^{14}\text{C}$ at the South Pole.

To examine the change in average $\Delta^{14}\text{C}$ across latitudes over the last 20 years, Figure 4.19 compares the latitudinal profile of $\Delta^{14}\text{C}$ observed in 2005-2006 with the profile observed in 1987-89. Plotted is the difference in annual mean of $\Delta^{14}\text{C}$ at each station relative to the annual mean at the South Pole for the same time period. The black circles show the observations from the Scripps stations averaged over 2005-2006; these are the same data from Figure 4.15. The diamonds show results from 1987-89 reported by Levin et al. (1992) and Meijer et al. (2006). Solid diamonds represent measurements by Meijer et al. at Point Barrow and the South Pole (discussed in Section 4.9). Empty diamonds show observations reported by Levin et al.. Stations shown are (from south to north): Neumayer, Antarctica, Wellington, New Zealand, Izaña, Spain and Jungfraujoch, Switzerland. In combining data from Levin et al. (1992) and Meijer et al. (2006), the laboratory offset between CIO and Heidelberg University is assumed to be zero (Meijer et al., 2006). Errorbars for the Scripps stations are estimated by the scatter of residual $\Delta^{14}\text{C}$ at each station after subtracting the fitted linear trend and single harmonic for the 2005-06 data. Errorbars for the 1987-89 measurements are Meijer et al. (2006)'s estimate of the combined uncertainty of the atmospheric variability and calibration uncertainty: ± 1.5 ‰. This value may underestimate the uncertainty

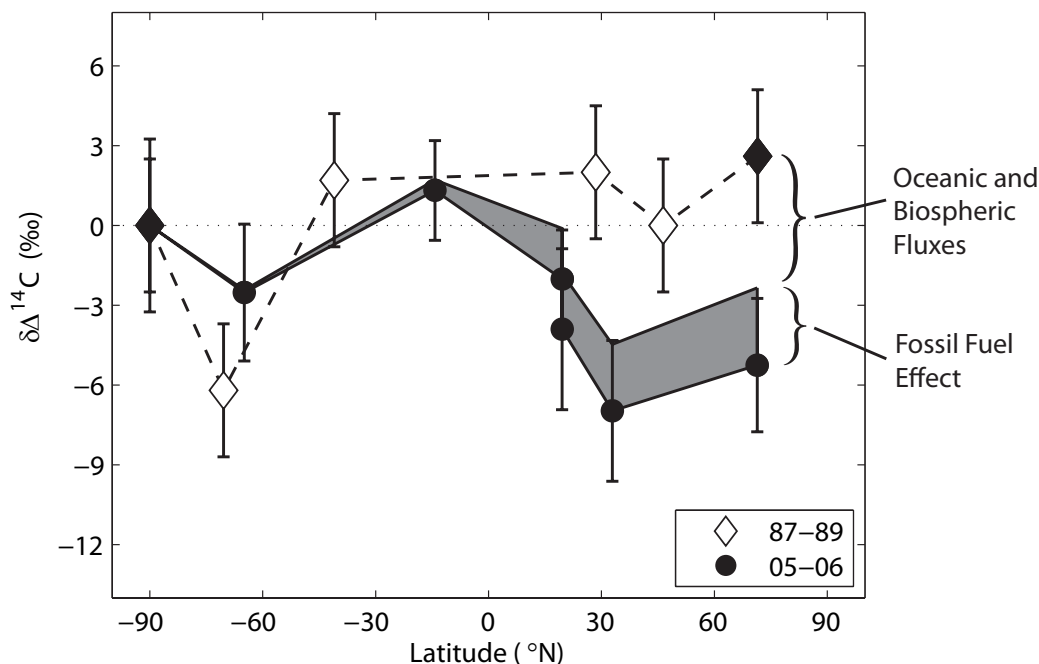


Figure 4.19: Latitudinal profile of mean $\Delta^{14}\text{C}$ in 1987-89 (diamonds, dashed line) and 2005-06 (circles, solid line), referenced to the South Pole. The 2005-06 profile is reproduced from Figure 4.15. The 1987-89 profile was reported in Levin et al. (1992) and Meijer et al. (2006). The solid diamonds show annual means at Point Barrow and the South Pole, measured by CIO, and the empty diamonds show annual means at Neumayer, Wellington, Izaña and Jungfraujoch, measured by the Heidelberg Laboratory. The shaded area represents the change in latitudinal gradients of $\Delta^{14}\text{C}$ caused by increasing fossil fuel emissions, the remaining difference is caused by changes in oceanic and biospheric ^{14}C fluxes.

in annual mean $\Delta^{14}\text{C}$ for 1987-89, particularly at the mid- to high latitude stations which express more annual variation.

The latitudinal profile of $\Delta^{14}\text{C}$ in CO_2 observed in 2005-06 shows substantial differences from the profile observed in 1987-89. The interhemispheric gradient in 1987-89 was very small, with slightly higher $\Delta^{14}\text{C}$ in the Northern Hemisphere (Meijer et al., 2006; Levin et al., 1992). A similar diagram of $\Delta^{14}\text{C}$ levels in 1994 also shows small differences between the hemispheres (Levin and Hesshaimer, 2000). However, in 2005-06, the Northern Hemisphere is significantly depleted in $\Delta^{14}\text{C}$ compared to the south. The interhemispheric gradient is ap-

proximately -6 ‰ in 2005-06. While local minima in the midlatitudes of each hemisphere are evident in both time periods, it appears that the minimum in the southern midlatitudes is not as strong in 2005-06 whereas the northern minimum may have become more prominent. A strong gradient across the tropics of roughly -5 ‰ is revealed in 2005-06. Tropical gradients are not resolved by the 1987-89 profile, however, a difference of approximately -3 ‰ was observed in $\Delta^{14}\text{C}$ from shipboard samples collected at $23.4\text{-}25.9^\circ\text{N}$ and $11.8\text{-}14.2^\circ\text{S}$ in 1995 (Kitagawa et al., 2004).

The shaded area in Figure 4.19 depicts the change in the latitudinal profile of $\Delta^{14}\text{C}$ that is expected from the $\sim 40 \text{ ‰}$ increase in total fossil fuel emissions of CO_2 between 1987-89 and 2005-06. This calculation uses results from a manuscript in preparation by C.D. Keeling, S.C. Piper, T.P. Whorf and R.F. Keeling, which examines the amount of fossil fuel CO_2 present at each sampling site in the Scripps network using atmospheric transport models and regressions of the time series measurements of CO_2 concentration. Their analysis provided estimates of the ppm fossil fuel CO_2 per Gt C emissions at each station, relative to the South Pole, which were scaled by the fossil fuel CO_2 emissions reported for the periods 1987-89 and 2005-06 (Marland et al., 2007; Canadell et al., 2007). As no estimate was available for the AORG site Palmer Station, the fossil fuel CO_2 present at Palmer Station was assumed to be similar to the fossil fuel CO_2 present at Baring Head, New Zealand. Simple mixing calculations were performed using the values of fossil fuel CO_2 present and measured annual mean $\Delta^{14}\text{C}$ and CO_2 concentration at each station. Comparison of the mixing calculation results for the time periods 1987-89 and 2005-06 provided an estimate of the change in latitudinal profile of $\Delta^{14}\text{C}$ caused by fossil fuel emissions, illustrated by the shaded area in Figure 4.19. Adding the estimated change in $\Delta^{14}\text{C}$ gradients caused by fossil fuel emissions to the 2005-06 observations produces the expected latitudinal gradient in 1987-89, shown as the upper line of the shaded area. As this line does not match the observations for 1987-89, it appears the shift in the latitudinal gradient can only

partly be explained by increasing fossil fuel emissions and other fluxes must also have undergone significant changes during this period.

Other than fossil fuel emissions, the main fluxes important to the latitudinal gradient of $\Delta^{14}\text{C}$ are the air-sea gas exchange with ^{14}C -depleted waters in the Southern Ocean and the respiration of ^{14}C -enriched organic material in the terrestrial biota of the Northern Hemisphere. As the atmospheric levels of $\Delta^{14}\text{C}$ decreased by $>100\text{‰}$ over 1987-89 to 2005-06 and the average $\Delta^{14}\text{C}$ in the respiratory and oceanic carbon reservoirs evolved, the ^{14}C disequilibrium driving these regional fluxes changed. The largest influence on the latitudinal gradient, other than fossil fuel emissions, is the weakening of the negative influence of the Southern Ocean on Southern Hemisphere air in recent years. The positive disequilibrium in $\Delta^{14}\text{C}$ of biospheric carbon compared to the atmosphere (Randerson et al., 2002) probably contributed a small positive influence on the north-south latitudinal gradient of $\Delta^{14}\text{C}$, opposite to the shift observed.

Based on modeling of ^{14}C fluxes, Randerson et al. (2002) predicted that the Northern Hemisphere would become more depleted than the Southern Hemisphere after the 1990s because of growing fossil fuel emissions, where the relative difference would be modulated by gross exchange over the Southern Ocean. Randerson et al., as well as Levin and Hesshaimer and others, suggest that measurement of the temporal change in the latitudinal profile of $\Delta^{14}\text{C}$ could be used to investigate CO_2 fluxes in the Southern Ocean, which remain a large uncertainty in budgets of anthropogenic carbon and in projections of future CO_2 concentration. The latitudinal profile is also sensitive to the turnover rate of carbon in northern ecosystems, which comprises another significant uncertainty in CO_2 projections.

The remainder of the observed shift in the $\Delta^{14}\text{C}$ profile that cannot be attributed to fossil fuel emissions (3-4 ‰) corresponds to rough estimates using a global mean oceanic $\Delta^{14}\text{C}$ signature predicted a box diffusion model and specifying 62-67 ‰ of the gross oceanic CO_2 exchange to occur in the Southern Hemisphere. In order to draw conclusions about Southern Ocean ventilation rates and/or vari-

ability, with implications for atmospheric CO₂ levels, we have to know accurately the regional air-sea $\Delta^{14}\text{C}$ gradient and the effect of regional biospheric fluxes in addition to the fossil fuel component calculated above. Further investigation of the latitudinal profile of $\Delta^{14}\text{C}$ using oceanic inventories of $\Delta^{14}\text{C}$ and atmospheric and oceanic transport models are likely to better resolve the regional fluxes contributing to observed $\Delta^{14}\text{C}$ gradients.

In Chapter 3, Section 3.7, we examined anomalies in $\Delta^{14}\text{C}$ at La Jolla reflecting year-to-year variability in the secular trend and examined potential climatic influences on ^{14}C fluxes from the ocean, the biosphere and the stratosphere. The latitudinal profile of $\Delta^{14}\text{C}$ is likely to be sensitive to interannual variation in these fluxes as well.

We have observed a shift in the latitudinal gradient of $\Delta^{14}\text{C}$ since 1987-89, where average $\Delta^{14}\text{C}$ in the Northern Hemisphere is approximately 6 ‰ more depleted than average $\Delta^{14}\text{C}$ in the Southern Hemisphere. Increased fossil fuel emissions between 1987-89 and 2005-06 explain ~ 3 ‰ of the shift, suggesting that adjustments in regional fluxes of ^{14}C from the ocean and the land biosphere are responsible for an additional ~ 3 ‰ decrease in the interhemispheric gradient of $\Delta^{14}\text{C}$.

4.11 Summary

Monthly time series of $\Delta^{14}\text{C}$ in CO₂ at 6 global sampling stations in the Scripps networks were produced in collaboration with Lawrence Livermore National Laboratory, augmenting the long record of $\Delta^{14}\text{C}$ in CO₂ at La Jolla reported in Chapter 3. The records are of varying length: Palmer Station has the shortest record of 2 years and the South Pole has the longest record of 7 years. The strongest and most consistent seasonal cycle is observed at Point Barrow, while the tropical stations Samoa and Mauna Loa exhibit very little seasonality in $\Delta^{14}\text{C}$. Comparison of seasonal cycles measured at Point Barrow and the South Pole

in 1985-91 by Meijer et al. (2006) reveals that seasonal amplitudes have shrunk by 25 % but phasing has not changed at these stations. The latitudinal profile of annual mean $\Delta^{14}\text{C}$ in 2005-06 reveals the Northern Hemisphere is depleted in $\Delta^{14}\text{C}$ compared to the south. This profile is a significant shift from 1987-89 and 1994, when little to no difference was apparent between the two hemispheres (Levin et al., 1992; Levin and Hesshaimer, 2000; Meijer et al., 2006). We find that increases in fossil fuel emissions drive a -3 ‰ shift in the Northern Hemisphere; the remaining -3 ‰ difference must be due to changes in the ^{14}C fluxes from the ocean or terrestrial biosphere. Further examination and continued observation of the latitudinal profile of $\Delta^{14}\text{C}$ will provide important information about regional fluxes of ^{14}C and CO_2 that should improve our understanding of the global response to fossil fuel emissions of CO_2 .

4.12 Recommendations for future $\Delta^{14}\text{C}$ measurements in the Scripps CO_2 Program

This thesis may initiate a long term, global measurement program for $\Delta^{14}\text{C}$ measurements in CO_2 collected by the Scripps CO_2 Program and analyzed at Lawrence Livermore National Laboratory. The recommendations of the previous chapter (Section 3.10) for future measurements of $\Delta^{14}\text{C}$ in Scripps CO_2 samples are extended here for the other stations.

Archived samples that remain from the stations reported in this chapter should continue to be measured periodically. Analysis of the remaining archived samples will provide two important benefits: resolution of the records will be improved and comparability between different analysis batches will be insured. Archived samples from other stations should not be analyzed as frequently as samples from La Jolla, perhaps 1-2 samples per 4 wheels measured. Then, archived samples would compose $\sim 15\%$ of the analyses. The first priority in analysis of archived samples should be the period mid-2001 to mid-2002 at the South Pole

where there is a gap in measurement because of the incomplete graphitization of several samples. There are 5 samples remaining from the South Pole for this period which should help to improve the continuity of the record through this period.

Currently, CO₂ samples from 6 sampling stations in the Scripps CO₂ Program are archived for $\Delta^{14}\text{C}$. The Scripps CO₂ sampling network collects flasks from several other stations which are not extracted for $\Delta^{14}\text{C}$ analysis because of personnel and time constraints. Expansion of the number of stations where CO₂ samples are extracted for $\Delta^{14}\text{C}$ analysis would enable the observation of more detail in the global distribution of $\Delta^{14}\text{C}$. It would also enable long term comparison with measurements from other laboratories. Of particular interest are the sampling stations Alert, Canada at 82°N and Baring Head, New Zealand at 41°S. I. Levin of the Heidelberg Laboratory collects CO₂ samples for $\Delta^{14}\text{C}$ at Alert, and K. Currie and others are continuing long records of $\Delta^{14}\text{C}$ in New Zealand. Both of these laboratories have conducted $\Delta^{14}\text{C}$ measurements for over 50 years and both utilize counting techniques on large volume CO₂ samples collected over several days. Co-located sampling would enable valuable comparisons with these two laboratories which are unable to participate in the current intercomparison activity because of the large volumes of CO₂ required for counting measurements. It would also be of great interest to compare instantaneous flask samples with integrated CO₂ absorption samples.

Additionally, we have developed procedures to collect CO₂ samples from Palmer Station, a sampling site within the network of the Scripps Atmospheric Oxygen Research Group, for $\Delta^{14}\text{C}$ analysis (Section 2.18). More sites within this network could also be added. With more development, better extraction techniques could enable high precision measurements of $\delta^{13}\text{C}$ and $\delta^{18}\text{O}$ to be conducted from the AORG flask air as well. It would be remarkable to have a global network of time series measurements of CO₂, O₂/N₂, $\Delta^{14}\text{C}$, $\delta^{13}\text{C}$ and $\delta^{18}\text{O}$ from the same sampling stations, utilizing the expertise and quality assurance of the Scripps laboratories. Such a coordinated global measurement program would be likely to

provide immense scientific value to carbon cycle research.

Acknowledgment

Chapter 4, in part, is being prepared for publication. Graven, Heather D.; Guilderson, Thomas P.; Keeling, Ralph F. The dissertation author is the primary investigator and author of this paper.

Chapter 5:

Vertical profiles of biogenic and fossil fuel-derived CO₂ from airborne measurements of $\Delta^{14}\text{C}$ and CO₂ above Colorado

ABSTRACT

In areas that may be influenced by emissions from urban regions, measurements of $\Delta^{14}\text{C}$ in atmospheric CO₂ are the best method of separating CO₂ additions from fossil fuel and biogenic sources. We demonstrate the use of this technique with detailed vertical profiles of CO₂ and $\Delta^{14}\text{CO}_2$ analyzed in whole air flask samples collected during the Airborne Carbon in the Mountains Experiment (ACME) above Colorado in May and July of 2004. By comparing lower tropospheric composition to cleaner air at higher altitudes, we estimate the relative magnitude of vegetative and combustion sources of CO₂ in urban and mountainous rural locations at different times of day and season. Considerable additions from respiration were observed in the morning in both urban and rural locations. Afternoon concentrations were mainly governed by fossil fuel emissions and boundary

layer depth, also showing net biospheric CO₂ uptake in some cases. Using *in situ* measurements of CO concentration we estimate local industrial CO₂:CO emission ratios. Observed CO₂:CO ratios are found to vary by almost 100% and average 56 CO₂:CO, higher than expected from the US national and Colorado state emissions inventories. This study highlights the unique capability of $\Delta^{14}\text{C}$ observations to precisely separate fossil fuel-derived and biospheric CO₂. Uncertainty in CO₂ derived from different sources is 0.8-3.6 ppm, limited by $\Delta^{14}\text{C}$ measurement precision and uncertainty in background $\Delta^{14}\text{C}$ and CO₂ levels. Similar estimation of CO₂ sources with airborne measurements of $\Delta^{14}\text{CO}_2$ in regional studies that include atmospheric transport modeling could be employed to investigate rates of vertical mixing, to examine diurnal rectification of fossil and vegetative CO₂ fluxes and to estimate local CO₂ emissions from fossil fuel combustion.

5.1 Introduction

Atmospheric observations of CO₂ concentration that are utilized to investigate surface exchanges of CO₂ reflect a mixture of CO₂ from different sources. The relative contribution from each source depends on the magnitude of a surface CO₂ flux and on the transport or mixing of air interacting with the surface source. When additions of CO₂ from fossil fuel combustion may be present in a study area for biospheric CO₂ exchanges, multiple strategies can be employed to correct for the presence of fossil fuel-derived CO₂.

Radiocarbon, or ¹⁴C, is a nearly perfect tracer of fossil fuel-derived CO₂, as the combustion of million year old fossil carbon produces CO₂ containing only the stable isotopes ¹²C and ¹³C. Addition of CO₂ from fossil sources dilutes the concentration of ¹⁴CO₂ in the local atmosphere, which is measured as $\Delta^{14}\text{C}$ in part per thousand deviation from a standard concentration (Stuiver and Polach, 1977). Conversely, biotic exchange of CO₂ does not substantially alter $\Delta^{14}\text{C}$ in local CO₂ because respiratory fluxes involve carbon that has been recently fixed, on average,

and $\Delta^{14}\text{C}$ notation corrects for mass-dependent fractionation. Measurements of $\Delta^{14}\text{C}$ and CO_2 concentration can be used together to distinguish CO_2 added from fossil fuel or biospheric sources (Meijer et al., 1996; Takahashi et al., 2002; Levin et al., 2003; Gamnitzer et al., 2006; Turnbull et al., 2006).

While $\Delta^{14}\text{C}$ is currently the most accurate tracer for fossil fuel CO_2 , measurements of $\Delta^{14}\text{C}$ are expensive and require discrete samples of air. Other trace gases related to combustion, mainly CO but also SF_6 and C_2Cl_4 , can be measured with reduced expense and the possibility of continuous observation. To quantify fossil CO_2 present in an air sample these gases require the application of emission ratios which are uncertain and can be highly variable ($>300\%$) depending on the type of fuel and combustion (Environmental Protection Agency (EPA), 2006; Rivier et al., 2006). Other techniques combine a priori assumptions of the distribution of surface fossil fuel emissions with transport models to calculate the amount of fossil fuel-derived CO_2 present at a sampling location (e.g. Gurney et al. 2002; Campbell et al. 2007). A priori assumptions of the distribution of fossil fuel emissions use data on fuel production, consumption, and trade for national or other political regions and data on the distribution of human population (e.g. Andres et al. 1996).

Uncertainties in estimates of local fossil fuel-derived CO_2 can present a significant limitation to the precision attainable in CO_2 flux estimates for investigations on subannual and subcontinental scales (Gerbig et al., 2003; Gibert et al., 2007). Reliable techniques for estimating fossil fuel CO_2 or fossil fuel CO_2 emissions are necessary to serve the expansion of CO_2 flux investigations at these scales (Wofsy and Harriss, 2002). Estimates of CO_2 emitted by fossil fuel combustion based on atmospheric observations that are independent of economic inventories could additionally provide an important method of verifying government-mandated emissions reductions on regional scales. As $\Delta^{14}\text{C}$ allows accurate estimation of fossil fuel-derived CO_2 , expanded measurement of $\Delta^{14}\text{C}$ would provide a unique and much needed capability to carbon cycle studies.

To investigate the use of $\Delta^{14}\text{C}$ for estimating fossil fuel-derived CO_2 in airborne measurement campaigns, we collected whole air samples for $\Delta^{14}\text{C}$ analysis during the Airborne Carbon in the Mountains Experiment (ACME) in May and July of 2004. The ACME study conducted airborne profiling of the lower troposphere in rural and urban areas of Colorado.

The collection of airborne samples during ACME for $\Delta^{14}\text{C}$ analysis was an exploratory study. Our main goal was to sample detailed vertical profiles of $\Delta^{14}\text{C}$ in the lower troposphere (3-6 samples per profile) and use measured $\Delta^{14}\text{C}$ and CO_2 concentration to define a simple mixture of background, biogenic and fossil fuel-derived CO_2 in each sample. The detailed profiles offered the potential to observe changes in the relative fraction of CO_2 from fossil fuel and biospheric sources with altitude, implying that $\Delta^{14}\text{C}$ can provide a unique tool for investigating temporal changes in surface CO_2 sources and/or the transport of air with different CO_2 flux history, both vertically and horizontally. Measurements of $\Delta^{14}\text{C}$ therefore have the potential to improve the representation of vertical mixing of surface fluxes in atmospheric transport models that currently contributes large uncertainties to regional and global CO_2 budgeting (Gurney et al., 2002; Stephens et al., 2007).

We also aimed to assess the reliability of the CO tracer of fossil fuel emissions by observing the fossil fuel emission ratio $\text{CO}_2:\text{CO}$ and its variability. Stable isotope measurements additionally allowed the comparison of measured $\delta^{13}\text{C}$ signatures in surface sources to those expected from the $\Delta^{14}\text{C}$ -determined mixture of CO_2 source components.

5.2 Methods

The ACME campaign was conducted onboard the National Center for Atmospheric Research/National Science Foundation C-130 aircraft in May and July 2004. We sampled flasks on 4 flights in May and 5 flights in July with 6 flasks collected on each flight. Flask sampling was performed mainly in two areas. One

area was a mountainous rural setting near Kremmling, Colorado, a town with a population of approximately 1500 located at 40.06°N, 106.38°W and 2252 m elevation. The other sampling location was an urban setting near Broomfield, Colorado, located at 39.91°N, 105.12°W and 1728 m elevation in the Denver metropolitan area which has a population of approximately 2.5 million people. Flasks were collected during vertical profiles during which the aircraft descended and/or ascended between a cruising altitude of approximately 5.5 or 7 km above sea level (ASL) to less than 100 m above ground level (AGL).

Whole air samples were taken onboard the aircraft using evacuated 5-liter round glass flasks. A schematic of the flask sampling apparatus is shown in Figure 5.1. Outside air was sampled from a forward-facing 1/2" stainless steel inlet and flushed through Synflex® tubing. The tubing was flushed without pumps, simply using the pressure gradient between the inlet and exhaust, which was located beneath and to the rear of the cabin. To sample, a valve was closed downstream of the flask and the evacuated flask was opened for approximately 30 seconds until it reached the ambient pressure at the altitude of the aircraft.

Each flask was measured for CO₂ concentration at Scripps using a non-dispersive infrared gas analyzer with a precision of ±0.1 ppm (Keeling et al., 2002). CO₂ was then cryogenically extracted in a glass vacuum manifold by passing all of the remaining air in the flask over a ball trap filled with liquid nitrogen. Each CO₂ sample was frozen and sealed into a Pyrex® tube. Sizes of CO₂ samples ranged from 0.25 mg C in flasks sampled above 5 km to 0.55 mg C in flasks sampled near the surface.

A set of the CO₂ samples were split approximately in half to enable both stable isotope ratio mass spectrometry (IRMS) and ¹⁴C measurement by accelerator mass spectrometry (AMS) in the same sample. Other samples were used entirely for IRMS or AMS analysis. IRMS was conducted at Scripps using a Micro Mass Optima dual-inlet mass spectrometer with a precision of ±0.03 ‰ (Guenther et al., 2001). For ¹⁴C measurements, CO₂ samples were converted to

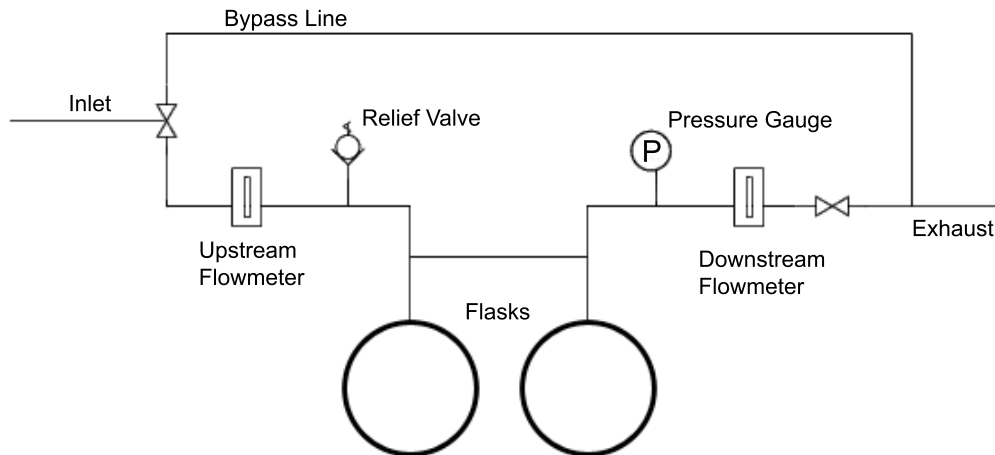


Figure 5.1: Schematic of the airborne flask sampling apparatus used in the ACME campaign

graphite and analyzed with AMS at Lawrence Livermore National Laboratory using procedures that have a precision of $\pm 1.7\text{--}2.4\text{‰}$, similar to Graven et al. (2007). We report $^{14}\text{C}/^{12}\text{C}$ ratios using $\Delta^{14}\text{C}$ notation, where the ratios have been corrected for decay and mass-dependent fractionation using $\delta^{13}\text{C}$ measurements (Stuiver and Polach, 1977). To calculate $\Delta^{14}\text{C}$ in the samples that were used only for AMS analysis, we interpolated $\delta^{13}\text{C}$ from other samples taken on the same flight, assuming that the air throughout the sample profile was influenced by CO_2 sources with the same average $\delta^{13}\text{C}$.

In situ measurements of CO were performed with an Aero-Laser vacuum ultraviolet resonance fluorescence instrument, after Gerbig et al. (1999). The CO measurements have a 1 second time resolution with a detection limit of 3 ppbv. Accuracy is estimated to be $\pm(3\text{ ppbv} + 5\%)$ based on in-flight intercomparisons over 5 years. Meteorological and positioning variables were measured onboard the aircraft and recorded as 1 second averages.

To assess the reproducibility of $\Delta^{14}\text{C}$ and CO_2 in our sampling and anal-

ysis methods, we collected pairs of flasks in rapid succession while cruising at 5.5 km ASL. Because air at higher altitudes generally has much lower variability in CO₂, the rapid collection of two flasks at high altitude results in two samples with roughly the same composition. The pair agreement then primarily indicates the amount of uncertainty added in the sample handling and analysis. The first pair was sampled within 2 minutes on May 20, 2004 and the second pair was sampled within 1.5 minutes on July 20, 2004. Combining the results for both pairs, the pooled standard deviation was 1.9 ‰ in $\Delta^{14}\text{C}$ and 0.3 ppm in CO₂, slightly higher than or comparable to the established instrument precision in both $\Delta^{14}\text{C}$ and CO₂. The agreement in these pairs implies that the amount of uncertainty added in processing the samples was negligible.

5.3 CO₂ Source Partitioning

5.3.1 Calculating Sources

CO₂ sources from vegetation and fossil fuel emissions were calculated with simple mass balances. For CO₂, we take the measured value (C_{meas}) to be a sum of sources from vegetative exchange (C_{veg}) and fossil fuel combustion (C_{ff}) added to background levels (C_{bg}): $C_{meas} = C_{veg} + C_{ff} + C_{bg}$. To approximate a mass balance for ¹⁴C, we sum the product of the $\Delta^{14}\text{C}$ signature (represented as Δ) and the amount of CO₂ from each source: $C_{meas}\Delta_{meas} \cong C_{veg}\Delta_{veg} + C_{ff}\Delta_{ff} + C_{bg}\Delta_{bg}$.

Using the two mass balance equations, we solve for the two unknown variables C_{veg} and C_{ff} . C_{meas} , Δ_{meas} , C_{bg} and Δ_{bg} were measured in the flask samples and Δ_{ff} and Δ_{veg} are assigned according to assumptions about the $\Delta^{14}\text{C}$ signature of fossil fuels and of terrestrial respiration.

Since ¹⁴C is absent from fossil fuel carbon, Δ_{ff} is -1000 ‰. This treatment calculates only CO₂ sources from fossil fuel combustion. Fuels derived from plant material (biofuels) have an isotopic concentration that is similar to the modern

atmosphere and to respired CO₂. A significant source of CO₂ from biofuel combustion would increase the average $\Delta^{14}\text{C}$ in all combustion-derived CO₂. Presently, this effect is very small; biofuels accounted for only 3 % of the total energy consumption in the United States in 2004 (Energy Information Administration (EIA), 2007).

Δ_{veg} , the $\Delta^{14}\text{C}$ level in CO₂ respired by terrestrial vegetation, is not well known and may be quite heterogeneous over different species and ecosystems. In previous studies, Δ_{veg} has been treated as a constant estimated with a mean ecosystem residence time of approximately 10 years (Turnbull et al., 2006) or presumed to be equal to Δ_{bg} because most of the ecosystem flux comes from a rapidly overturning reservoir (Levin et al., 2003; Gamnitzer et al., 2006). As in Levin et al. and Gamnitzer et al., we assume that respired CO₂ has a $\Delta^{14}\text{C}$ content that is the same as the background air, $\Delta_{veg} = \Delta_{bg}$. This assumption allows the simple aggregation of respiratory and photosynthetic activity of the local vegetation into C_{veg} .

Combining the two mass balance equations, we solve for the two unknowns, C_{veg} and C_{ff} :

$$C_{ff} = C_{meas} \frac{\Delta_{bg} - \Delta_{meas}}{\Delta_{bg} + 1000} \quad (5.1)$$

$$C_{veg} = C_{meas} - C_{bg} - C_{ff} \quad (5.2)$$

In order to distinguish the sources of CO₂ using Equations 5.1 and 5.2, we must define background concentrations of CO₂ and background levels of $\Delta^{14}\text{C}$ using measured values. Accurate definition of background concentrations is essential as any error in the background specification will be incorporated into the calculated CO₂ sources. Here, we consider two possible definitions: the concentrations measured at clean air stations or the concentrations measured in the high-altitude ACME flasks sampled in the free troposphere.

Figure 5.2 shows CO₂ and $\Delta^{14}\text{C}$ measured in ACME flasks sampled above 5 km ASL and in flasks sampled at three clean air sampling stations during 2004. Data shown are from the Scripps CO₂ Program at La Jolla, California and Point

Barrow, Alaska and by the National Oceanic and Atmospheric Administration's Global Monitoring Division (NOAA/GMD) at Niwot Ridge, Colorado (Conway and Tans, 2004; Turnbull et al., 2007). Flasks from the Scripps CO₂ Program and NOAA/GMD were sampled in the afternoon; replicate measurements were averaged in Figure 5.2.

High altitude measurements during ACME appear to be slightly higher (~ 3 ‰) in $\Delta^{14}\text{C}$ than the values observed at the clean air stations over the same time period. One sample exhibited exceptionally high $\Delta^{14}\text{C}$ (May 20, 5.5 km ASL, 76.8 ‰). $\Delta^{14}\text{C}$ in this sample was over 5 ‰ higher than any other sample collected during the ACME campaign. This sample may have been influenced by high- $\Delta^{14}\text{C}$ air from the stratosphere. A similar excursion was observed at Niwot Ridge on Jan 5, 2004. CO₂ concentrations in upper air are similar to the clean air stations, showing most coherence with concentrations observed at Niwot Ridge.

The high altitude and clean air station measurements both show short term or synoptic scale variability which is likely to influence the expression of daily surface sources. We use the high altitude measurements on each vertical profile to define C_{bg} and Δ_{bg} for that profile in order to account for the short term changes in background air. The high altitude sample from May 20 that exhibited very high $\Delta^{14}\text{C}$ is not used as the background for that profile; instead we use the sample taken at the next highest altitude, 3.7 km ASL.

The uncertainty in background CO₂ and $\Delta^{14}\text{C}$ may be estimated by the scatter in high altitude measurements over each section of the campaign. For May the standard deviation is 1.5 ‰ and 0.5 ppm, for July the standard deviation is 2.0 ‰ and 2.3 ppm. If the enhancement of ~ 3 ‰ in the high altitude samples compared to the clean air stations is not representative of the actual background level of $\Delta^{14}\text{C}$ in the airborne samples, calculated C_{ff} will be ~ 1 ppm too high and the calculated C_{veg} will be ~ 1 ppm too low. As the scatter in $\Delta^{14}\text{C}$ of the high altitude samples seems to overlap the scatter of the clean air observations, this potential bias is incorporated into the background uncertainty.

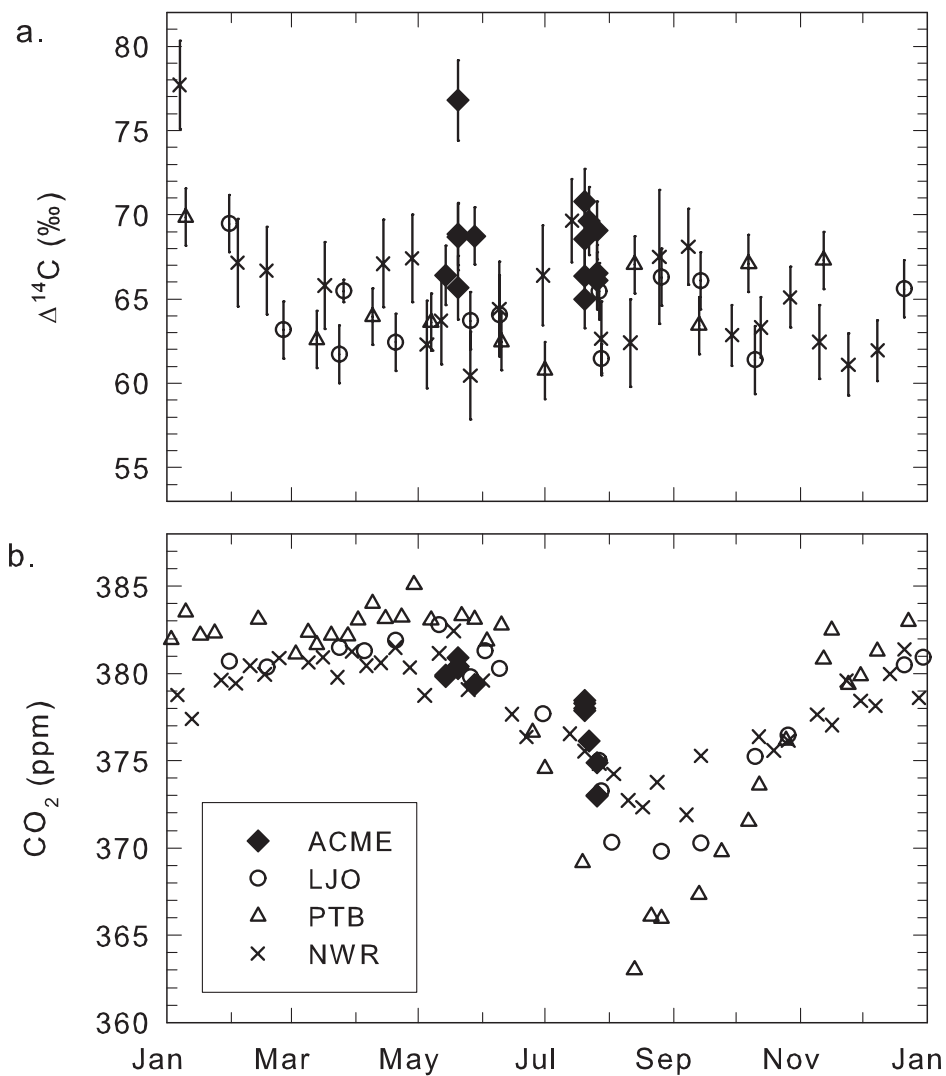


Figure 5.2: $\Delta^{14}\text{C}$ and CO_2 concentration in ACME flasks sampled above 5 km ASL (solid diamonds) and in clean air flasks sampled at La Jolla, California (LJO, circles), Point Barrow, Alaska (PTB, triangles) and Niwot Ridge, Colorado (NWR, crosses) for 2004. LJO and PTB data from the Scripps CO_2 Program and this thesis; NWR CO_2 data from Conway and Tans 2004 and NWR $\Delta^{14}\text{C}$ data from Turnbull et al. 2007.

Measurement uncertainty of $\pm 1.7\text{--}2.4\text{ ‰}$ in $\Delta^{14}\text{C}$ contributes $\pm 0.6\text{--}0.8$ ppm to the uncertainty in calculated CO_2 sources. The assignment of Δ_{veg} also contributes uncertainty which scales with the influence of vegetation. When estimated as the standard deviation between C_{veg} calculated by $\Delta_{veg} = \Delta_{bg}$ or by $\Delta_{veg} = 150\text{ ‰}$, the uncertainty from Δ_{veg} may be as large as 2.6 ppm for the sample with the greatest influence of respiration (53 ppm) but averages to 0.2 ppm in May and 0.8 ppm in July. If Δ_{veg} was actually higher than Δ_{bg} , our calculations of C_{veg} are too high and C_{ff} is, correspondingly, too low.

Overall, the background definition and AMS measurement precision contribute the most uncertainty to C_{veg} and C_{ff} . We estimate total uncertainty in C_{veg} and C_{ff} for each flask as a quadrature sum between the uncertainty in the background composition, the measurement uncertainty, and the average uncertainty from Δ_{veg} (Ellison et al., 2000). The total uncertainty in calculated CO_2 sources averaged 0.9 ppm in May and 2.5 ppm in July.

5.3.2 Rural and Urban Patterns

Vertical profiles were conducted in the mornings around 7 a.m. in the rural area near Kremmling and 10 a.m. in the urban location near Denver. Afternoon profiles were sampled at approximately 2 p.m.

Profiles sampled in the morning in the rural area are shown in Figure 5.3. Figure 5.3a shows the profile sampled on May 20, 2004, 5.3b shows the profile from July 22, 2004 and 5.3c shows the profile from July 26. In each plot, the left panel shows measured CO_2 concentration (flask data in black circles; *in situ* data in gray circles). $\Delta^{14}\text{C}$ (diamonds) is plotted in the center panel. The right panel shows the amount of CO_2 added (ΔCO_2) as C_{veg} (black bars) and C_{ff} (hatched bars).

The rural area near Kremmling exhibited very high CO_2 concentration near the surface in the morning, with enhancements as large as 55 ppm on July 22. At the same time, $\Delta^{14}\text{C}$ showed very little change from the surface to higher

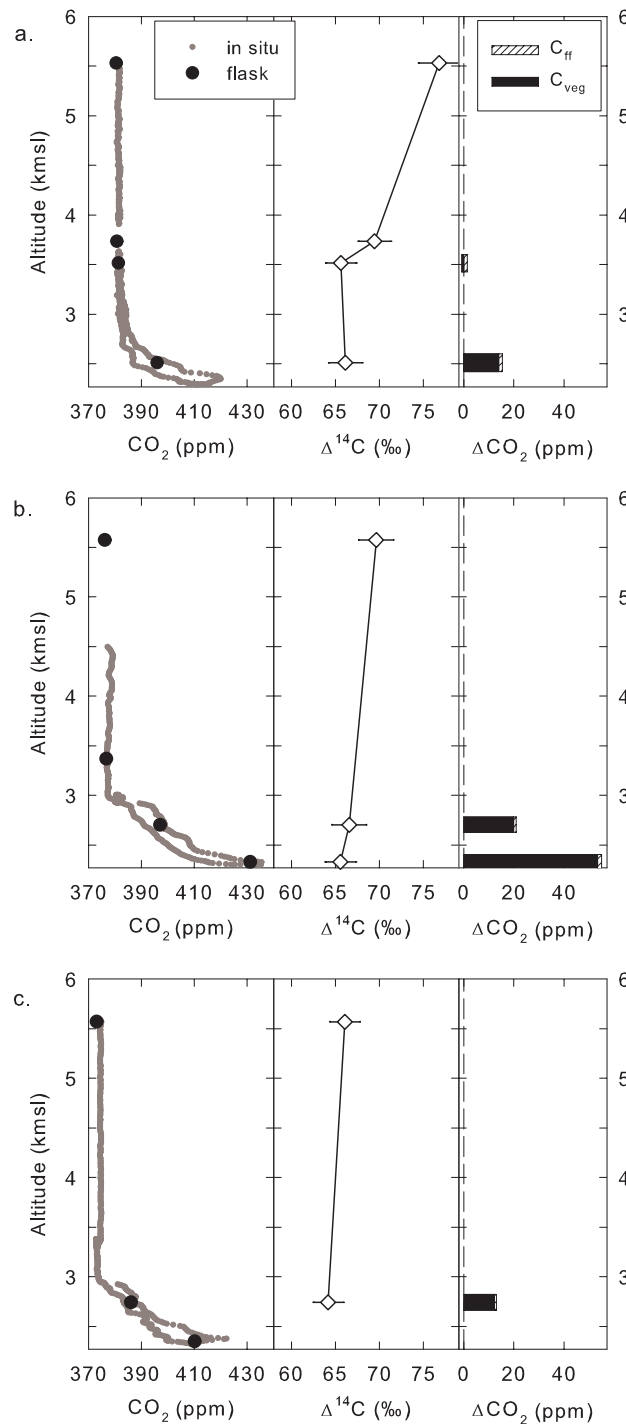


Figure 5.3: Profiles sampled near 7 a.m. in the rural area on a. May 20, 2004, b. July 22, 2004 and c. July 26, 2004. Measured CO_2 concentration (flask data in black circles; *in situ* data in gray circles), $\Delta^{14}\text{C}$ (diamonds), and the amount of CO_2 added (ΔCO_2) as C_{veg} (black bars) and C_{ff} (hatched bars). Altitude is given in km ASL, where the ground level is at the base of the plot (2.27 km ASL).

altitude. Calculated sources from $\Delta^{14}\text{C}$ measurements reveal that the source of this CO_2 is almost entirely of biospheric origin. For air sampled closest to the surface, CO_2 derived from vegetation comprised 14.1 ± 1.1 , 53.3 ± 3.6 and 12.3 ± 2.5 ppm (for a., b., and c., respectively) whereas only 1.2 ± 1.1 , 1.6 ± 3.6 and 0.7 ± 2.5 ppm was attributed to fossil sources. CO_2 from fossil sources was comparable to uncertainty in each of these profiles. The sample collected at the lowest altitude on July 26 was lost during laboratory processing, however the results from other samples suggest that the 37 ppm elevation observed in CO_2 concentration was almost entirely from biogenic CO_2 .

The consistent observation of high concentrations of biosphere-derived CO_2 near the surface reflects the accumulated respiration of CO_2 into a stable nocturnal boundary layer, part of the rectifier effect that enhances diurnal variation in surface CO_2 concentration (Keeling, 1958; Wofsy et al., 1988). In the mountainous rural area sampled during the ACME campaign, the near-surface concentrations were likely enhanced by surface drainage flows in surrounding mountain valleys (Staebler and Fitzjarrald, 2004; Pypker et al., 2007). While the signature of nighttime respiration is expected to be the dominant influence on CO_2 concentration in vegetated rural areas in the morning, the $\Delta^{14}\text{C}$ -calculated source attribution provide validation that fossil emissions added only a small contribution to the natural surface level CO_2 enrichment. This information is pertinent to the use of ACME *in situ* CO_2 measurements for model calculations of biospheric CO_2 fluxes by local montane ecosystems, one of the primary goals of the ACME field campaign. By verifying the dominant source of CO_2 by respiration in this area, the $\Delta^{14}\text{C}$ measurements provide confidence in modeled fluxes.

Figure 5.4 shows profiles sampled near 10 a.m. above the large urban area of Denver, Colorado on a. May 20 and b. July 20. The data is presented in a similar manner to Figure 5.3. There were more modest enhancements in CO_2 near the surface in comparison to the rural profiles sampled earlier in the morning; near-surface elevations in CO_2 totaled 7.5 and 15.9 ppm on May 20 and July 20

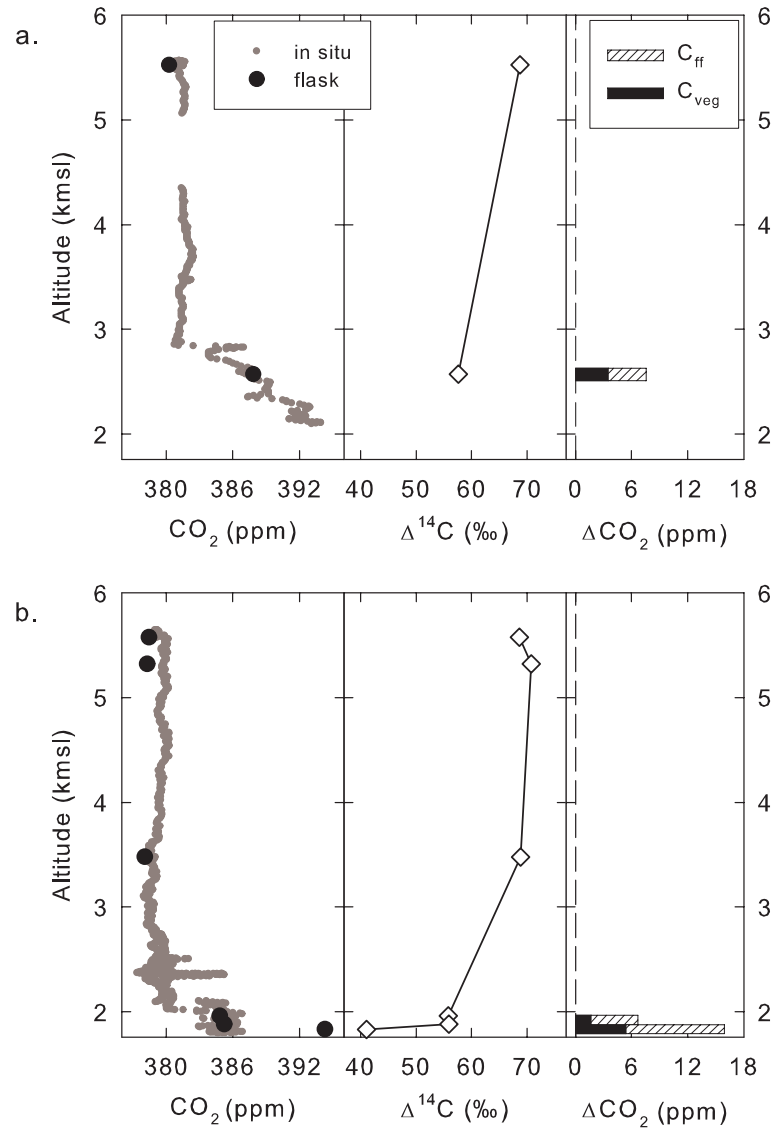


Figure 5.4: Profiles near 10 a.m. sampled in the urban area on a. May 20, 2004 and b. July 20, 2004. Measured CO_2 concentration (flask data in black circles; *in situ* data in gray circles), $\Delta^{14}C$ (diamonds), and the amount of CO_2 added (ΔCO_2) as C_{veg} (black bars) and C_{ff} (hatched bars). Altitude is given in km ASL, where the ground level is at the base of the plot (1.76 km ASL).

respectively. Here, we observe a mixture of biospheric and industrial sources. On May 20 (Figure 5.4a) there were roughly equal contributions to the elevated CO₂ with 4.0 ± 1.0 ppm due to fossil fuel combustion and 3.5 ± 1.0 ppm to vegetation in the sample taken at the lowest altitude. July 20 (Figure 5.4b) showed a larger source of fossil fuel-derived CO₂ (10.5 ± 2.4 ppm) than biotically-derived CO₂ (5.4 ± 2.4 ppm).

These samples demonstrate that, in the mornings, biogenic sources of CO₂ are substantial and comparable in magnitude to industrial sources in the urban Denver region during the growing season. These observations reflect the complexity of carbon cycling in urban regions where land conversion, urban vegetation and soils and anthropogenic emissions may all be important (Pataki et al., 2006). Similar results were observed in Salt Lake City, Utah, using ground-based measurements of $\delta^{13}\text{C}$ and $\delta^{18}\text{O}$ in CO₂. There, up to 60 % of the nighttime CO₂ enhancement above background levels was attributed to biogenic respiration (Pataki et al., 2003a).

Figures 5.6 and 5.5 show profiles sampled above the urban region in the afternoon. These figures are presented in a similar manner as 5.3 and 5.4, with the addition of a fourth panel. This panel shows the potential temperature (Θ) measured during the sampling of the profile. Θ provides a measure of the vertical extent of the turbulent planetary boundary layer. Within the boundary layer, Θ is steady or decreases with height. The top of the planetary boundary layer is indicated by the altitude where the potential temperature begins increasing with height (Henne et al., 2004). Boundary layer height has been estimated to be 0.4 km AGL for May 14 (Figure 5.5a), 0.5 km AGL for July 26 (5.5b), 1.3 km AGL for May 20 (5.6a) and 2.5 km AGL for July 20 (5.6b), shown as the gray horizontal line in each plot.

Profiles sampled in shallow boundary layers of approximately 500 m depth are shown in Figure 5.5. In 5.5a, the profile sampled on May 14 shows a steady decrease in CO₂ concentration while $\Delta^{14}\text{C}$ steadily increases with height. Higher

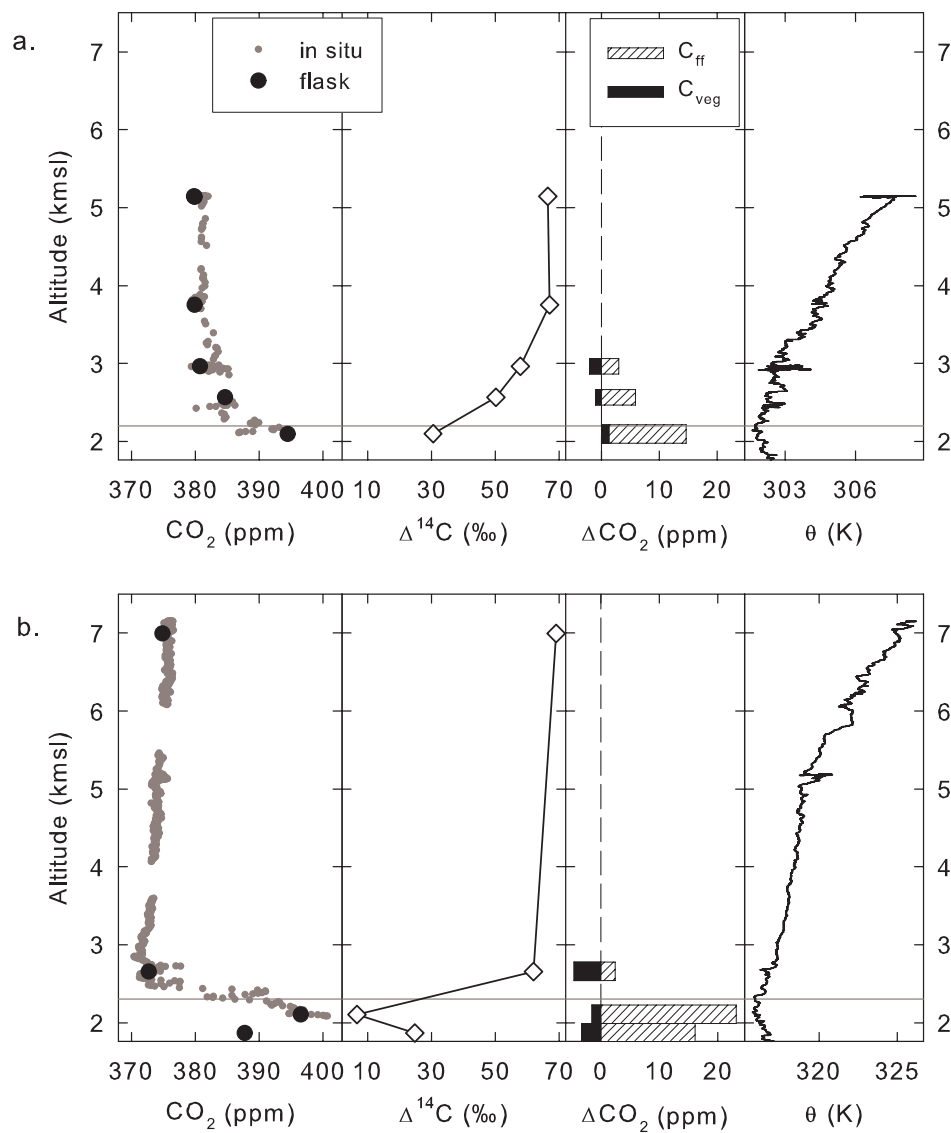


Figure 5.5: Profiles sampled near 2 p.m. in the urban area in a shallow boundary layer on a. May 14, 2004 and b. July 26, 2004. Measured CO₂ concentration (flask data in black circles; *in situ* data in gray circles), Δ¹⁴C (diamonds), the amount of CO₂ added (ΔCO₂) as C_{veg} (black bars) and C_{ff} (hatched bars), and potential temperature (Θ). The gray horizontal line shows boundary layer height. Altitude is given in km ASL, where the ground level is at the base of the plot (1.76 km ASL).

concentrations of CO_2 appear to be mainly caused by fossil fuel emissions, yet a small influence of vegetative exchange also appears to be present up to >1 km above ground level. Above the top of the boundary layer, C_{veg} is negative, indicating that this air experienced net photosynthetic uptake of CO_2 , whereas C_{veg} is positive within the boundary layer, indicating a net source of biospheric CO_2 near the surface. In the lowest sample, collected within the boundary layer, C_{ff} was 13.3 ± 0.8 ppm and C_{veg} was 1.3 ± 0.8 ppm.

The profile sampled on July 26 (Figure 5.5b) also shows a dominant influence from fossil fuel emissions with smaller biospheric influences, yet the character of the profile is very different than that observed on May 14. Here, the CO_2 concentration increases by ~ 10 ppm from near-surface concentration to a maximum around 250 m, then decreases to a minimum at 1-1.5 km above ground level. The $\Delta^{14}\text{C}$ profile shows features that are opposite to CO_2 , indicating that fossil fuel emissions are the main source of CO_2 in the sampled air. C_{ff} is quite large in these samples, up to 23 ± 2.4 ppm for the sample collected 250 m AGL. C_{veg} is negative in all samples, ranging from -1.5 to -4.6 ± 2.4 ppm.

Afternoon profiles sampled during conditions where the boundary layer was deeper (1.3-2.5 km AGL) show much smaller variability in CO_2 and $\Delta^{14}\text{C}$ and much smaller amounts of C_{ff} and C_{veg} . On May 20 (Figure 5.6a) $\Delta^{14}\text{C}$ was lowest at mid-levels of 1-1.5 km AGL and CO_2 concentration showed a small decrease in the sample collected nearest the surface. On July 20 (Figure 5.6b) the lowest $\Delta^{14}\text{C}$ was observed near the surface together with a slight elevation CO_2 concentration.

Lower variability in CO_2 concentration is expected as a deeper boundary layer allows more mixing and the surface sources of CO_2 are diluted with a larger volume of air (Wofsy et al., 1988). Our $\Delta^{14}\text{C}$ measurements indicate that compensation of fossil fuel emissions and biospheric CO_2 uptake additionally contribute to the uniformity of CO_2 concentration in these profiles.

On May 20, C_{veg} is consistently -3.6 ± 0.9 ppm and C_{ff} is between 2.5 to 4.2 ± 0.9 ppm for the 3 samples collected within the boundary layer. The

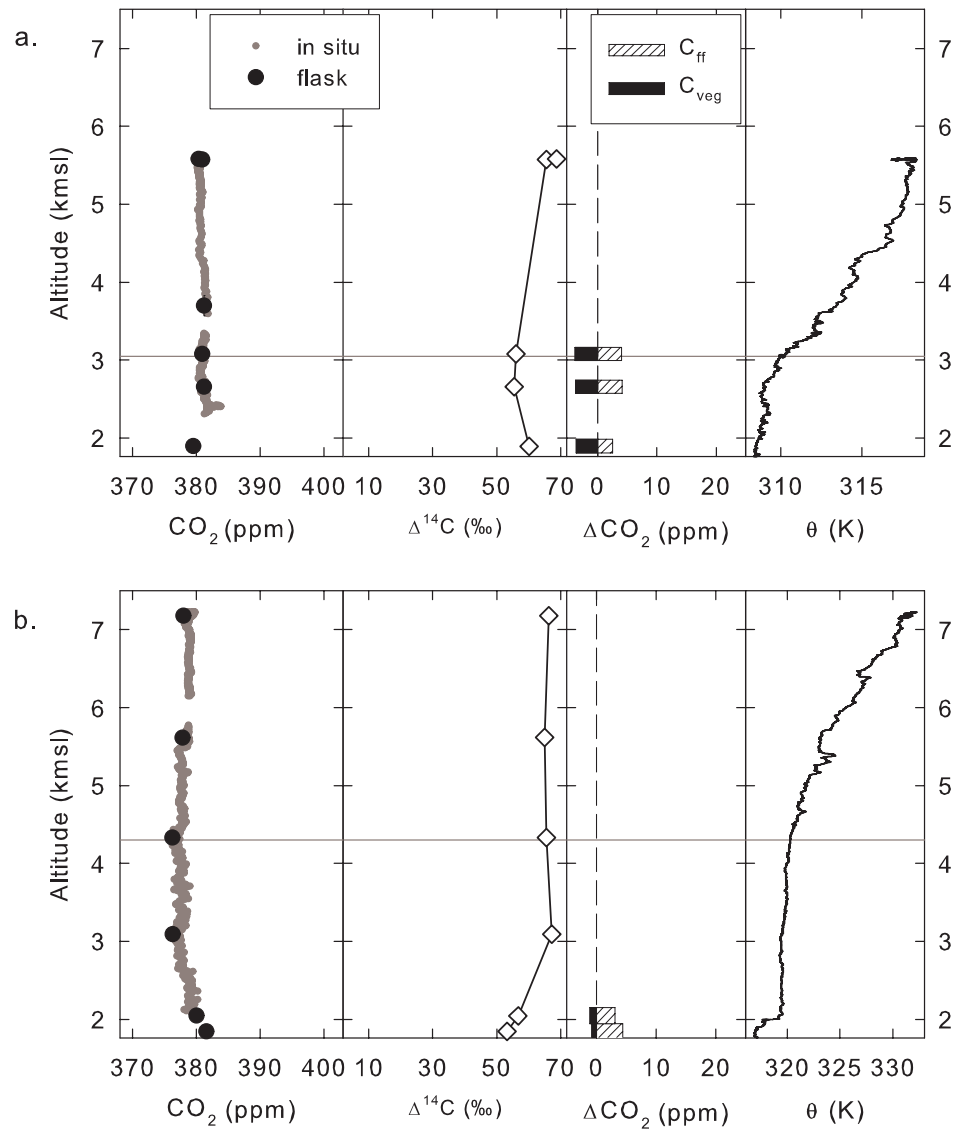


Figure 5.6: Profiles sampled near 2 p.m. in the urban area in a deep boundary layer on a. May 20, 2004 and b. July 20, 2004. Measured CO_2 concentration (flask data in black circles; *in situ* data in gray circles), $\Delta^{14}\text{C}$ (diamonds), the amount of CO_2 added (ΔCO_2) as C_{veg} (black bars) and C_{ff} (hatched bars), and potential temperature (θ). The gray horizontal line shows boundary layer height. Altitude is given in km ASL, where the ground level is at the base of the plot (1.76 km ASL).

expression of biospheric uptake of CO_2 is robust, as background $\Delta^{14}\text{C}$ would have to be >5 ‰ lower than the upper air to eliminate the necessity of compensating fluxes in Equations 5.1 and 5.2.

Low altitude samples collected on July 20 show C_{ff} of 4.4 ± 2.4 ppm and 3.2 ± 2.4 ppm. As $\Delta^{14}\text{C}$ decreases toward the surface, C_{ff} is slightly larger than the difference $C_{meas}-C_{bg}$. Biospheric uptake in these samples is small, -0.8 ± 2.4 ppm and -1.1 ± 2.4 ppm, and within uncertainty.

The profiles sampled in the afternoon demonstrate that $\Delta^{14}\text{C}$ measurements provide unique insight into the vertical propagation and mixing of surface fluxes of CO_2 . Measurement of $\Delta^{14}\text{C}$ greatly augments observations of CO_2 concentration as the components C_{veg} and C_{ff} can be characterized, not only at the surface but further into the troposphere. Similar collection of airborne CO_2 samples for $\Delta^{14}\text{C}$ measurements could be employed in future studies to test models of CO_2 exchange and atmospheric transport, providing valuable measures of the uncertainty and potential bias in modeled vertical mixing (Stephens et al., 2007).

5.3.3 $\delta^{13}\text{C}$ source signatures

Measurement of $\delta^{13}\text{C}$ was conducted on a subset of 34 CO_2 samples. We calculated the average $\delta^{13}\text{C}$ of source CO_2 using a Keeling Plot regression technique (Keeling, 1958) to compare to the CO_2 sources characterized from the ^{14}C analysis. Geometric mean regressions between $\delta^{13}\text{C}$ and $1/\text{CO}_2$ were performed for each profile with 2 or more $\delta^{13}\text{C}$ observations. The intercept of the linear regression indicates the average $\delta^{13}\text{C}$ in CO_2 added from surface sources.

Respired CO_2 ranges from approximately 11.2 to 25.5 ‰ in $\delta^{13}\text{C}$ depending on the dominant photosynthetic pathway in the local vegetation (Bender, 1971; Pataki et al., 2003b). The $\delta^{13}\text{C}$ signature of carbon stored in fossil reservoirs varies by fuel type, but is generally more depleted than the carbon respired from vegetation (Blasing et al., 2004b). Therefore, fossil-derived CO_2 tends to decrease the average $\delta^{13}\text{C}$ of added CO_2 as compared with a source dominated by respiration

(Pataki et al., 2003a).

Keeling Plot regressions for samples in rural areas indicate source signatures in $\delta^{13}\text{C}$ of -23.4, -24.4 and -22.7 ‰ on May 20, July 22 and July 26, respectively. Only 2 stable isotope measurements were conducted on these rural profiles so we cannot characterize the regression error. However, the calculated $\delta^{13}\text{C}$ sources are consistent with a mixed respiration source from both C3 and C4 type photosynthetic plants, dominated by C3. These $\delta^{13}\text{C}$ source signatures are similar to or slightly more enriched in ^{13}C than observations from the Niwot Ridge Ameriflux tower (Pypker et al., 2007). Similar and slightly lower $\delta^{13}\text{C}$ source signatures were also observed by separate $\delta^{13}\text{C}$ measurements conducted on flasks sampled in different rural locations during ACME (C.-T. Lai, private communication).

The urban morning profile on July 20 included 5 $\delta^{13}\text{C}$ measurements and exhibited a source signature of -29.3 ± 1.6 ‰. The sample collected at the lowest altitude was found to contain 16 ppm of added CO_2 , of which 65 % was fossil-derived and 35 % was biogenic. As expected, the urban $\delta^{13}\text{C}$ source signature is lower in comparison to the rural $\delta^{13}\text{C}$ source because of the presence of industrially-derived CO_2 with depleted $\delta^{13}\text{C}$. Similarly, the two urban afternoon profiles sampled in shallow boundary layers also showed average source $\delta^{13}\text{C}$ that was relatively depleted: -31.3 (only 2 samples analyzed) and -25.7 ± 0.2 ‰ for May 14 and July 26, respectively.

5.4 Correlation of C_{ff} with CO

Measurements of the concentration of CO, another product of fossil fuel combustion, are often used to estimate fossil-produced CO_2 (Bakwin et al., 1998; Gerbig et al., 2003; Turnbull et al., 2006; Gamnitzer et al., 2006; Levin and Karstens, 2007). To calculate C_{ff} , an emission ratio factor (R_{ff}) must be multi-

plied by the excess CO concentration above background levels:

$$C_{ff} = R_{ff} (CO_{meas} - CO_{bg}) \quad (5.3)$$

Relative production of CO compared to CO₂ greatly depends on the type of fuel and the type of combustion. For the same amount of CO₂ production, CO emissions from automobiles are roughly 300 times larger than emissions from stationary sources using solid, liquid or gaseous fuels (Environmental Protection Agency (EPA), 2006). Therefore, an accurate estimate of the type of oxidation and the resulting CO₂:CO emission ratio is essential for the use of CO to determine fossil fuel-derived CO₂.

Here, we examine the correlation between C_{ff} calculated with $\Delta^{14}\text{C}$ and CO concentration measured *in situ*. By determining the slope of CO vs C_{ff} , we estimate the emission ratio for several profiles and compare it to prior observations and inventory values. Direct observation of R_{ff} can validate or discredit emission inventory values, reveal seasonal or spatial trends in fuel use and assess the reliability of C_{ff} estimated by Equation 5.3 by characterizing the variability of R_{ff} .

To compare *in situ* data with flask samples, we averaged the *in situ* CO concentration over the ~ 30 second period during which a flask was sampled. A similar estimate of *in situ*-averaged CO₂ concentration using a pressure- and temperature-controlled Licor CO₂ analyzer compared reasonably well with CO₂ measured in the flasks, exhibiting a pooled standard deviation of 0.7 ppm. The Licor system was under development during the campaign but is estimated to have precision of ± 0.3 ppm and an accuracy of ± 0.3 ppm, based on in-flight intercomparisons over 3 years.

Ratios of C_{ff} :CO were calculated by performing geometric mean regressions. There were 5 vertical profiles which had least 3 measurements of both C_{ff} and CO and spanned a range of 30 ppb or more in CO. C_{ff} and CO pairs and regressions are shown in Figure 5.7 for the 5 vertical profiles. Table 5.1 lists the time and location of the sampled profile, the R_{ff} ratio in ppm CO₂: ppm CO

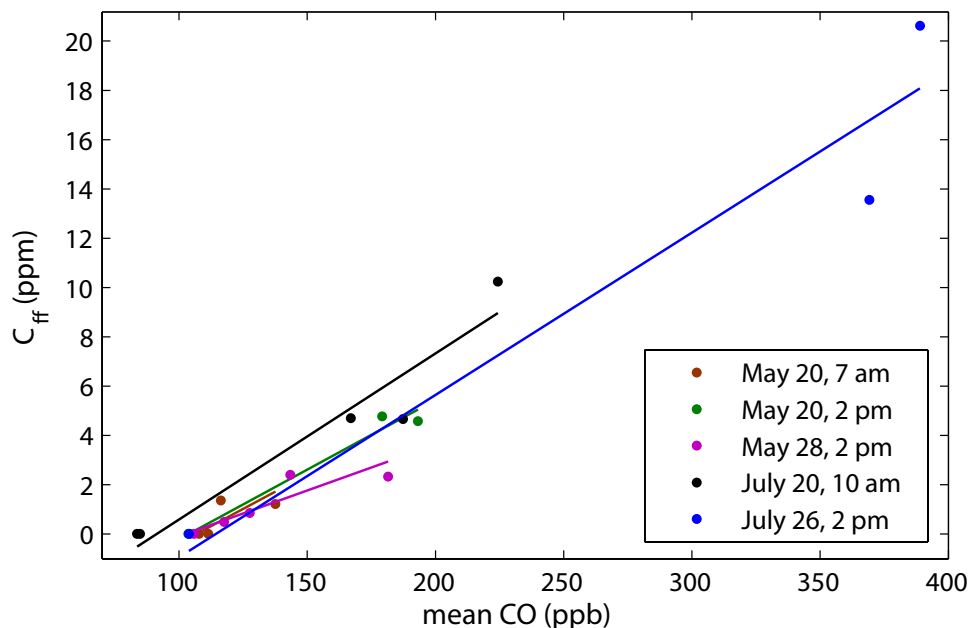


Figure 5.7: C_{ff} versus mean CO concentration measured *in situ* during the ~ 30 second period during which the corresponding flask was sampled. C_{ff} and CO pairs are shown for 5 vertical profiles: May 20, 2004, 7 am (brown), May 20, 2004, 2 pm (green), May 28, 2004, 2 pm (purple), July 20, 2004, 10 am (black) and July 26, 2004, 7 am (blue). The lines resulting from geometric mean regressions on the C_{ff} and CO pairs are shown in corresponding colors.

with the regression uncertainty and the reciprocal CO: C_{ff} , including a factor of 10^3 (equivalent to ppb CO:ppm CO₂). Table 5.1 also summarizes ratios observed in previous studies and reported in emissions inventories.

R_{ff} observed in the airborne samples ranges from 37 to 67. Observed ratios were highly consistent on May 20 (56 ± 31 and 56 ± 6) and between July 20 and 26 (67 ± 11 and 66 ± 18), while R_{ff} for May 28 was much lower (37 ± 11).

These observations broadly agree within their regression uncertainties though the values span nearly a factor of two. Observed C_{ff} :CO ratios overlap with the US inventory average for 2004, 43 (Environmental Protection Agency (EPA), 2006), yet 4 of 5 observations were higher than 43. The inventory estimate for Colorado for 2001, 31 (Blasing et al., 2004a), is lower than all observed ratios

Table 5.1: Emission ratios from observations and inventories for several locations in the US, including observations from ACME. Ratios are given in units of ppm:ppm.

Date	Location	$C_{ff}:CO$	$CO:C_{ff}$ ($\times 10^3$)	Reference
May 20, 7 am	Kremmling, CO	56 ± 31	18 ± 10	This study
May 20, 2 pm	Denver, CO	56 ± 6	18 ± 2	This study
May 28, 2 pm	Denver, CO	37 ± 11	27 ± 8	This study
July 20, 10 am	Denver, CO	67 ± 11	15 ± 2	This study
July 26, 2 pm	Denver, CO	66 ± 18	15 ± 4	This study
Avg 94-96, May	Harvard Forest, MA	45 ± 3	22 ± 2	Potosnak, 1999
Avg 94-96, July	Harvard Forest, MA	34 ± 6	29 ± 5	Potosnak, 1999
Jan. 20, 2004	Niwot Ridge, CO	147 ± 48	7 ± 2	Turnbull, 2006
March 2, 2004	Niwot Ridge, CO	85 ± 40	12 ± 6	Turnbull, 2006
August 2000	North American Survey	30 ± 9	33 ± 10	Gerbig, 2003
2004 average	EPA inventory, US average	43	23	EPA, 2006
2001 average	Dept. of Energy inventory, Colorado average	31	32	Blasing, 2004

and lower than the US inventory average.

While 5 discrete observations provide limited scope for inference, the $\Delta^{14}C$ measurements suggest that actual $C_{ff}:CO$ in these sampling locations is higher than the inventory estimates. The inventories may have errors in the relative fraction of different fuel types or combustion methods used in Colorado, or the combustion sources may be too heterogeneous to be represented by a state-wide or nation-wide average. The underestimation of inventory $C_{ff}:CO$ ratios in Colorado has been suggested previously by Turnbull et al. (2007) in a study that observed very large values of R_{ff} . Studies utilizing inventory estimates of $C_{ff}:CO$ together with CO measurements to estimate C_{ff} could overestimate C_{ff} and resultingly overestimate biospheric uptake of CO_2 .

$C_{ff}:CO$ emitted depends on the type of fuel and type of combustion. Most CO is produced in mobile combustion, resulting in lower $C_{ff}:CO$ in areas where automobiles contribute more to C_{ff} . CO is also emitted in biomass burning and is created and removed via photochemical reactions involving the hydroxyl radical, $\cdot OH$. In simply calculating the slope between CO and C_{ff} , we did not

account for either of these processes in the reported $C_{ff}:\text{CO}$ ratios in Table 5.1. These effects should be small as we did not appear to sample air that was influenced by forest fires and photochemical production and consumption occurs on longer timescales than the daily variation of boundary layer depth that dilutes surface emissions. To ensure that photochemical effects were not significant, we computed the influence of oOH photochemistry on CO concentrations at locations where flasks were sampled in July, as in Campbell et al. (2007). Results indicate the photochemical effect on CO in these samples was consistently small and negative, averaging -3 ± 3 ppb. Photochemical effects of this magnitude are negligible.

The observed ratios increase slightly in July compared to May, with the average value shifting from 50 to 67. This change is opposite to that observed in Harvard Forest over 1994-1996, where the average ratios decreased from 45 in May to 34 in July (Potosnak et al., 1999). Differences in the seasonal change in $C_{ff}:\text{CO}$ between these two areas may be due to differing local pollution sources, photochemical effects in Harvard Forest or unrepresentative sampling.

Two observations of $C_{ff}:\text{CO}$ in ground-based flask samples at Niwot Ridge, Colorado in winter 2004 showed much higher ratios, 147 ± 48 and 85 ± 40 (Turnbull et al., 2006). These ratios were calculated from single observations with estimates of background concentration and have substantial uncertainties. Still, the large discrepancy between the airborne ratios observed in this study and those observed by Turnbull et al. earlier in the year could reflect the difference in combustion and fuel type between winter and summer in Colorado, perhaps due to changes in the relative proportion of transportation to total emissions.

Observations and inventories of $C_{ff}:\text{CO}$ in Europe are generally higher than the U.S. Using $\Delta^{14}\text{C}$, average measured ratios were 114 ± 40 in 1994-96 in Kollumerwaard, Netherlands (Meijer et al., 1996) and 91 ± 9 in 2002-03 in Heidelberg, Germany, similar to the inventory value of 98 ± 2 for the Heidelberg region (Gamnitzer et al., 2006). Regressions between continuous CO_2 and CO measurements in Paris indicated an average ratio of 91 ± 58 (Braud et al., 2004).

Higher European $C_{ff}:\text{CO}$ ratios reflect the smaller proportion of CO_2 emissions contributed by automobiles and the greater prevalence of diesel combustion engines.

The $C_{ff}:\text{CO}$ ratios summarized in Table 5.1 span a factor of 4 for several dates and locations within the U.S., demonstrating that the use of CO to trace C_{ff} is highly uncertain when the $C_{ff}:\text{CO}$ ratio is not known accurately. While ^{14}C measurements carry more limitations than CO, a useful application would combine *in situ* CO measurements with regular observation of $\Delta^{14}\text{C}$ to characterize local R_{ff} (Gamnitzer et al., 2006). In this way, C_{ff} estimates based on CO could be “calibrated” by $\Delta^{14}\text{C}$ to account for temporal or spatial variability in emission sources.

5.5 Summary

Observation of $\Delta^{14}\text{C}$ in CO_2 in vertical profiles of the lower troposphere revealed patterns of CO_2 sources in urban and rural locations that were influenced by vertical mixing. Early morning samples collected in rural Colorado exhibited large enhancements in CO_2 concentration near the surface that were characterized by $\Delta^{14}\text{C}$ to be almost entirely biospheric in origin. Samples collected in urban areas showed varying mixtures of C_{veg} and C_{ff} .

Uncertainty in C_{veg} and C_{ff} by $\Delta^{14}\text{C}$ is limited mainly by measurement precision and by the uncertainty in characterizing background levels of CO_2 and $\Delta^{14}\text{C}$. Variability in CO_2 source components of 0.8 ppm can presently be detected with $\Delta^{14}\text{C}$ measurement uncertainty of 1.7 ‰ when background levels of $\Delta^{14}\text{C}$ and CO_2 concentration are known to ± 1.5 ‰ and ± 0.5 ppm.

Airborne $\Delta^{14}\text{C}$ measurements have great potential to contribute to future studies of CO_2 dynamics. Together with atmospheric transport modeling, $\Delta^{14}\text{C}$ could be applied to augment investigation of biospheric exchange rates, vertical mixing of surface fluxes and observation-based estimation of industrial CO_2

emissions.

Acknowledgment

Chapter 5, in part, is being prepared for publication. Graven, Heather D.; Stephens, Britton B.; Guilderson, Thomas P.; Campos, Teresa L.; Schimel, David S.; Keeling, Ralph F. The dissertation author is the primary investigator and author of this paper.

Chapter 6:

Conclusions

This thesis has made progress in advancing measurement precision of $\Delta^{14}\text{C}$ in CO_2 , it has produced multi-year time series of $\Delta^{14}\text{C}$ in background air at 7 global stations, and it has demonstrated the use of $\Delta^{14}\text{C}$ for separating biospheric and industrial additions of CO_2 in regional studies.

Analytical methods were developed specifically to measure $\Delta^{14}\text{C}$ in CO_2 samples from the Scripps CO_2 Program at the Center for Accelerator Mass Spectrometry of Lawrence Livermore National Laboratory. Through the introduction of new reference materials, improvements were made in sample handling, AMS analysis procedures and data processing. The new techniques exhibit reproducibility of 1.7 *permil*, which is at the forefront of AMS measurement precision for $\Delta^{14}\text{C}$ in CO_2 . The improved analytical methods enable the detection of small gradients of atmospheric $\Delta^{14}\text{C}$, expanding the potential for $\Delta^{14}\text{C}$ observations to contribute to carbon cycle studies at global and regional scales.

One such application was demonstrated by the measurement of $\Delta^{14}\text{C}$ in CO_2 collected by aircraft in vertical profiles above urban and rural areas of Colorado. The observed $\Delta^{14}\text{C}$ was used with measurements of CO_2 concentration to separate local CO_2 additions from biospheric or fossil fuel sources with 0.8 ppm uncertainty. CO_2 sources were found to vary with altitude depending on the boundary layer depth, indicating that airborne $\Delta^{14}\text{C}$ measurements could be used

to investigate vertical mixing of surface exchanges as well as estimating biospheric fluxes and fossil fuel CO₂ emissions.

High precision measurements of $\Delta^{14}\text{C}$ in CO₂ at 7 background stations produced monthly time series of 2-15 years. Records at La Jolla from 1992 through 2006 revealed significant year-to-year variability in the seasonal cycle and in the trend of $\Delta^{14}\text{C}$, suggesting atmospheric $\Delta^{14}\text{C}$ may be sensitive to climatic influences on fluxes of ¹⁴C and CO₂. Anomalies in $\Delta^{14}\text{C}$ observed at La Jolla in 1998-2000 may have been caused by changes in North Pacific oceanic ventilation or by fluctuations in stratosphere-troposphere exchange. The latitudinal profile of $\Delta^{14}\text{C}$ averaged over 2005-06 showed that the Northern Hemisphere is approximately 6 ‰ more depleted than the Southern Hemisphere. This profile is substantially different from 1987-89, when the Northern Hemisphere was similar to or slightly higher than the Southern Hemisphere (Levin et al., 1992; Meijer et al., 2006). The change in atmospheric gradients of $\Delta^{14}\text{C}$ is only partly explained by increases in fossil fuel emissions, suggesting that further investigation and observation of the latitudinal gradient of $\Delta^{14}\text{C}$ will provide insights on evolving regional ¹⁴C fluxes.

The observations of atmospheric $\Delta^{14}\text{C}$ in the Scripps network form a rich dataset that has only begun to be examined in this thesis. By utilizing the progress achieved here, sustained measurements of $\Delta^{14}\text{C}$ in CO₂ collected by the Scripps CO₂ Program and analyzed at Lawrence Livermore National Laboratory can provide precise, regular and extensive records of global variability in $\Delta^{14}\text{C}$. The new ¹⁴C measurement activities developed in this thesis can augment existing programs of the Scripps CO₂ Program and Atmospheric Oxygen Research Group and may lead to new discoveries about the global carbon cycle.

Appendix A:

MATLAB Scripts for Data Processing

A.1 Normalization

```

function [Names NNumbers avgRtoStd CntErr StdErr]=...
    bracketingNorm(filename,stdtype,flagcyl)

% bracketingNorm.m
% function to normalize raw 14C/13C data from CAMS, LLNL
% Heather Graven, 11/14/2007
% Input data is "clean" file generated by Fudger software at
% CAMS and type of standard desired to use for normalization -
% 'OXI', 'Cyl-1' or 'Cyl-2'
% A list of Cyl-1 and Cyl-2 targets that have been flagged is also
% used to ensure the flagged targets are not used in
% normalization
% Output is normalized ratio, counting and standard error in
% norm ratio

% Open text file
fid = fopen(filename, 'r');
% Read header line
HeaderText = textscan(fid, '%s', 23, 'delimiter', '\t');
InputText=textscan(fid, ...
    '%n %n %s %s %n %n %n %n %n %n %n %n %n %n %n %n %n %n ...
    %n %s %n %s %s %n',...
    'delimiter', '\t'); % Read data block
fclose(fid);
clear fid

% assign relevant data to variables
Firing=InputText{1};
Loc=InputText{2};
SampleName=InputText{3};
Ident=InputText{4};
Gated=InputText{5};
Ratio=InputText{7};
Kind=InputText{21};
clear InputText HeaderText

% Check if cylinder targets have been flagged
Flag=zeros(length(Loc),1);
for r=1:length(flagcyl)
    for s=1:length(Loc)
        if strcmp(flagcyl(r),SampleName(s))==1
            Flag(s)=1;
        end
    end
end

```

```

        end
    end
end

% Perform bracketing normalization
for i = min(Loc):max(Loc) % for each target
    % find all indices for the target at Loc i
    allfired = find(Loc==i);
    repts(i)=length(allfired);
    totalgate=0;
    if length(find(Loc==i))>0
        Names(i,:)=SampleName(min(allfired),:);
        NNumbers(i,:)=Ident(min(allfired),:);
    end

    if strcmp(stdtype,'OXI')==1
        %find all indices of OXI targets
        if length(find(strcmp(Kind, 'U')==0 & Loc~=i))>0
            allstds=find(strcmp(Kind, 'U')==0 & Loc~=i);
        else
            disp('No OXI standards available');
            return
        end
    elseif strcmp(stdtype,'Cyl-1')==1
        % find all indices of Cyl-1 targets
        if length(find((strcmp(SampleName,'326',3)==1 ...
            & Loc~=i) & Flag~=1)))>0
            allstds=find((strcmp(SampleName,'326',3)==1 ...
            & Loc~=i) & Flag~=1);
        else
            disp('No Cyl-1 standards available');
            continue
        end
    elseif strcmp(stdtype,'Cyl-2')==1
        % find all indices of Cyl-2 targets
        if length(find((strcmp(SampleName,'55280',5)==1 ...
            & Loc~=i) & Flag~=1)))>0
            allstds=find((strcmp(SampleName,'55280',5)==1 ...
            & Loc~=i) & Flag~=1);
        else
            disp('No Cyl-2 standards available');
            continue
        end
    else

```



```

        disp('Type of standard is not specified correctly');
        return
    end

% calculate number of standard targets
stdlocs=length(find(diff(sort(Loc(allstds)))~=0))+1;

for j=1:length(allfired) % for each firing of target i
    target=(allfired(j)); % index of firing number j
    % compare indices of (target i, firing j) to
    % indices of stds
    compstd=allstds-target;

    % find std fired right after firing j of target i
    if length(min(find(compstd>0)))>0
        % index of allstds of of first 0X1 after target
        middle=min(find(compstd>0));
    else
        % if there are no stds after firing j of target i,
        % then compare to last std index
        middle=length(compstd);
    end

    % for an even number of standard targets
    if rem(stdlocs,2)==0
        ref0X=middle-stdlocs/2:1:middle+stdlocs/2-1;
    else
        %for an odd number of standard targets
        if middle>1
            if abs(compstd(middle))<abs(compstd(middle-1))
                ref0X=middle-(stdlocs-1)/2:1:middle+...
                    (stdlocs-1)/2;
            else
                ref0X=middle-(stdlocs+1)/2:1:middle+...
                    (stdlocs-3)/2;
            end
        else
            ref0X=middle-(stdlocs+1)/2:1:middle+(stdlocs-3)/2;
        end
    end

    if length(find(ref0X<=0))>0
        ref0X=1:stdlocs;
    elseif length(find(ref0X>length(compstd)))>0

```

```

        refOX=length(compstd)-stdlocs+1:length(compstd);
    end

    % check that length(refOX) and number of standard
    % targets are the same
    if length(refOX)~=stdlocs
        disp('Wrong number of standard targets used');
        return
    end

    mid(i,j)=middle;
    midtdiff(i,j)=allstds(middle)-target;
    clear middle

    ratioOX=Ratio(allstds(refOX));

    avgOX(i,j)=mean(ratioOX(:));
    stdOX(i,j)=std(ratioOX);

    rawRatio(i,j)=Ratio(target);

    % calculate normalized ratio
    normRatio(i,j)=Ratio(target)/avgOX(i,j);

    % counting error on raw ratio
    deltah(i,j)=Ratio(target)/sqrt(Gated(target));

    % calculate 2 types of error on ratios used for
    % normalization
    deltastdratio1(i,j)=sqrt(var(ratioOX)/length(ratioOX));
    deltastdratio2(i,j)=sqrt(sum((Ratio(allstds(refOX))./.
        sqrt(Gated(allstds(refOX))))).^2)/length(ratioOX);

    % use greater of 2 types of error to calculate error
    % on normed ratio
    if deltastdratio1(i,j) > deltastdratio2(i,j)
        deltanorm(i,j)=normRatio(i,j)*...
            sqrt((deltah(i,j)/rawRatio(i,j))^2+...
                (deltastdratio1(i,j)/avgOX(i,j))^2);
        which(i,j)=1;
    else
        deltanorm(i,j)=normRatio(i,j)*...
            sqrt((deltah(i,j)/rawRatio(i,j))^2+...
                (deltastdratio2(i,j)/avgOX(i,j))^2);
    end

```

```

        which(i,j)=2;
    end

    clear ratioOX compstd sorted refOX
end
clear allstds
end

% Now calculate mean ratio, counting and standard error
for i = min(Loc):max(Loc) % for each target
    sputs=find(normRatio(i,*)>0);
    % weighted average over all sputtering periods
    avgRtoStd(i)=sum(normRatio(i,sputs)./...
        (deltanorm(i,sputs)).^2)/sum(1./deltanorm(i,sputs).^2);

    % counting error combined over all sputtering periods
    CntErr(i)=sqrt(1/sum(1./deltanorm(i,sputs).^2));

    % standard error between all sputtering periods
    StdErr(i)=sqrt(sum((normRatio(i,sputs)-avgRtoStd(i)).^2)/...
        (length(sputs)*(length(sputs)-1)));
    clear sputs
end

avgRtoStd=avgRtoStd';
CntErr=CntErr';
StdErr=StdErr';

```

A.2 Calculation of $\Delta^{14}\text{C}$

```

function [D14C IntErr]=...
    CalcDeltafromCyl1Norm(avgRtoStd, CntErr, StdErr, d13C, ys, ya)

% CalcDeltafromCyl1Norm.m
% function to calculate D14C from normalized 14C/13C ratios
% Heather Graven, 11/14/2007
% Input data is normalized ratio, counting and standard error in
% norm ratio, d13C, sampling date and analysis date in units of
% years
% Output is D14C and internal error

% calculate Fraction Modern, incorporating fractionation correction
% coefficient is 1.0589 for Cyl-1
% coefficient is 1.0080 for Cyl-2
% coefficient is 1.02 for OXI
FM=1.0589./(1+d13C/1000).*((avgRtoStd-.0015)/(1-.0015));

% calculate D14C, correcting for age
D14C= (FM.*exp((1950-ys)/8267).*exp(-(ya-ys)./8267)-1)*1000;

% calculate internal error, using larger of counting
% or standard error
IntErr=1000*FM.*sqrt((max(CntErr,StdErr)./avgRtoStd).^2+...
    (.0005*(avgRtoStd-1)./(avgRtoStd-.0015)/(1-.0015)).^2);

```

Appendix B:

$\Delta^{14}\text{CO}_2$ Data from 7 Scripps Stations

B.1 Observations of $\Delta^{14}\text{C}$

The following tables list $\Delta^{14}\text{C}$ in CO_2 samples collected by the Scripps CO_2 Program and measured at Lawrence Livermore National Laboratory. Measurements were conducted at 7 clean air sites: La Jolla, California, Point Barrow, Alaska, Kumukahi and Mauna Loa, Hawaii, Cape Matatula, Samoa and Palmer Station and South Pole, Antarctica. The CO_2 concentration listed is specific to the flask sample used for $\Delta^{14}\text{C}$ analysis; $\delta^{13}\text{C}$ is an average of all measurements with the same sample date. Starred $\delta^{13}\text{C}$ values are estimates of $\delta^{13}\text{C}$, based on the average of neighboring samples, when measurements of $\delta^{13}\text{C}$ in concurrently sampled CO_2 was not available. CO_2 concentrations were measured on the '03A' Calibration Scale. $\delta^{13}\text{C}$ values are relative to the international PDB standard and include the addition of a -0.112 ‰ offset for consistency with earlier measurements at the Center for Isotope Research, University of Groningen. The date of $\Delta^{14}\text{C}$

analysis by accelerator mass spectrometry at LLNL is listed as AMS Date. Procedures for calculating $\Delta^{14}\text{C}$ and total measurement uncertainty, σ_{Tot} , are described in Sections 2.15 and 2.16. Flagged samples have been removed.

B.1.1 Measurements from La Jolla

Table B.1: Measurements from La Jolla

Sample ID	Sample Date	CO ₂ (ppm)	$\delta^{13}\text{C}$ (‰)	AMS Date	$\Delta^{14}\text{C}$ (‰)	σ_{Tot} (‰)
K92-418	07/01/1992	355.26	-7.815	06/05/2005	135.2	1.7
K92-487	07/23/1992	351.32	-7.605	05/05/2006a	131.5	1.7
K92-496	08/03/1992	352.30	-7.671	06/05/2005	133.9	1.7
K92-840	09/09/1992	348.50	-7.514	06/05/2005	137.8	1.7
K93-004	10/02/1992	351.63	-7.667	06/05/2005	135.4	1.7
K93-023	10/29/1992	354.64	-7.780	06/05/2005	132.7	1.7
K93-059	12/11/1992	358.77	-8.046	06/05/2005	128.9	1.7
K93-081	12/18/1992	358.63	-8.003	05/23/2006b	132.3	1.7
K93-141	01/11/1993	359.77	-8.058	06/05/2005	129.5	1.7
K93-149	02/09/1993	359.35	-8.039	06/05/2005	132.9	1.7
K93-208	02/24/1993	359.87	-8.065	05/23/2006b	127.7	1.7
K93-237	03/03/1993	360.55	-8.087	06/05/2005	130.1	1.7
K93-245	04/12/1993	360.62	-8.027	06/05/2005	125.3	1.7
K93-356	05/18/1993	362.38	-8.106	06/05/2005	127.9	1.7
K93-431	06/21/1993	359.57	-7.952	06/05/2005	127.5	1.7
K93-502	07/01/1993	357.21	-7.862	05/05/2006a	120.5	1.7
K93-612a	08/12/1993	351.52	-7.569	10/28/2006	123.4	1.7
K93-612b	08/12/1993	351.52	-7.569	10/29/2006	124.8	1.7
K93-979	11/11/1993	356.12	-7.810	03/31/2007	125.0	1.7
K94-107	11/30/1993	357.90	-7.917	05/23/2006a	121.4	1.7
K94-253a	12/15/1993	359.95	-8.018	03/15/2007	119.6	1.7
K94-298	02/08/1994	360.60	-8.034	05/21/2006b	116.1	1.7
K94-355	03/11/1994	360.92	-8.024	03/18/2007	119.7	1.7
K94-402	04/04/1994	362.60	-8.174	05/05/2006a	111.8	1.7
K94-675	05/17/1994	363.82	-8.222	05/05/2006a	115.2	1.7
K94-729	06/22/1994	359.71	-7.987	05/05/2006a	115.1	1.7

Continued on next page

Table B.1 – continued from previous page

Sample ID	Sample Date	CO ₂ (ppm)	$\delta^{13}\text{C}$ (‰)	AMS Date	$\Delta^{14}\text{C}$ (‰)	σ_{Tot} (‰)
K94-951	08/24/1994	352.86	-7.627	06/05/2005	118.7	1.7
K94-952	08/24/1994	352.42	-7.627	05/05/2006a	114.9	1.7
K95-006	11/02/1994	358.47	-7.890	05/05/2006b	118.7	1.7
K95-018	11/18/1994	360.74	-8.014	06/05/2005	118.9	1.7
K95-179	01/03/1995	361.42	-8.066	06/05/2005	119.5	1.7
K95-581	02/08/1995	362.75	-8.150	06/05/2005	117.0	1.7
K95-587	02/15/1995	362.56	-8.186	05/05/2006b	110.3	1.7
K95-724	03/13/1995	363.56	-8.181	06/05/2005	113.6	1.7
K95-755	04/07/1995	363.60	-8.141	06/05/2005	109.2	1.7
K95-846	05/15/1995	365.55	-8.247	06/05/2005	114.6	1.7
K95-850	06/08/1995	363.96	-8.275	12/28/2003	111.3	2.2
K95-851	06/08/1995	363.96	-8.275	02/12/2004	109.7	2.2
K95-852	06/08/1995	363.96	-8.275	06/05/2005	114.0	1.7
K95-A48	07/03/1995	360.77	-7.966	12/28/2003	111.3	2.2
K95-A49	07/03/1995	360.76	-7.966	02/12/2004	113.1	2.1
K95-C86	08/21/1995	353.10	-7.578	12/28/2003	109.1	2.2
K95-C87	08/21/1995	352.92	-7.578	02/12/2004	110.4	2.1
K95-C89	08/21/1995	353.17	-7.578	05/07/2006a	107.9	1.7
K95-E07	09/26/1995	357.84	-7.809	12/28/2003	105.5	2.2
K95-E08	09/26/1995	357.97	-7.809	02/12/2004	108.5	2.1
K96-022	10/16/1995	358.39	-7.790	12/28/2003	111.4	2.2
K96-023	10/16/1995	358.38	-7.790	02/12/2004	108.1	2.2
K96-034	11/10/1995	360.51	-7.939	12/28/2003	108.7	2.1
K96-035	11/10/1995	360.49	-7.939	02/12/2004	108.7	2.1
K96-131	01/22/1996	364.60	-8.153	02/13/2004	107.3	2.0
K96-132	01/22/1996	364.60	-8.153	02/13/2004	105.4	2.1
K96-149a	02/02/1996	365.19	-8.154	05/23/2006b	112.8	1.7
K96-149b	02/02/1996	365.19	-8.154	05/23/2006b	116.1	1.7
K96-185	02/22/1996	365.90	-8.224	02/13/2004	104.4	2.1
K96-186	02/22/1996	365.93	-8.224	02/13/2004	104.7	2.0
K96-187	02/22/1996	365.82	-8.224	05/05/2006a	104.1	1.7
K96-296	03/11/1996	365.01	-8.171	02/13/2004	108.3	2.0
K96-297	03/11/1996	365.15	-8.171	02/13/2004	105.1	2.0
K96-321	04/01/1996	366.04	-8.217	05/07/2006a	103.0	1.7
K96-377	04/16/1996	366.36	-8.222	02/13/2004	105.7	2.0

Continued on next page

Table B.1 – continued from previous page

Sample ID	Sample Date	CO ₂ (ppm)	$\delta^{13}\text{C}$ (‰)	AMS Date	$\Delta^{14}\text{C}$ (‰)	σ_{Tot} (‰)
K96-378	04/16/1996	366.43	-8.222	02/13/2004	102.9	2.0
K96-450	05/03/1996	367.55	-8.204	02/13/2004	102.7	2.0
K96-451	05/03/1996	367.61	-8.204	02/13/2004	106.6	2.0
K96-518	06/26/1996	362.92	-8.027	02/13/2004	104.6	2.1
K96-519	06/26/1996	362.90	-8.027	02/13/2004	104.8	2.1
K96-711	08/05/1996	358.44	-7.775	05/07/2006a	104.0	1.7
K96-837	09/04/1996	356.07	-7.680	05/23/2006a	105.4	1.7
K96-921	10/25/1996	361.39	-7.942	03/31/2007	108.1	1.7
K96-938	11/27/1996	364.12	-8.075	05/07/2006b	103.9	1.7
K97-150	02/17/1997	365.91	-8.161	05/07/2006b	97.2	1.7
K97-151	02/17/1997	365.83	-8.161	05/23/2006a	101.4	1.7
K97-213	04/22/1997	367.76	-8.170	03/18/2007	100.2	1.7
K97-375	06/23/1997	364.64	-8.053	05/07/2006b	99.3	1.7
K97-381	06/30/1997	363.79	-8.022	05/23/2006b	103.4	1.7
K97-465	07/18/1997	359.28	-7.752	05/07/2006b	96.5	1.7
K97-569	08/10/1997	357.21	-7.634	04/01/2007	102.5	1.7
K97-660a	10/10/1997	360.25	-7.792	10/26/2006	101.7	1.7
K97-660b	10/10/1997	360.25	-7.792	10/28/2006	101.3	1.7
A98-005	01/10/1998	365.93	-8.092	05/07/2006b	99.8	1.7
A98-011	01/13/1998	367.54	-8.180	05/21/2006b	100.3	1.7
K98-102a	02/13/1998	367.31	-8.150	09/08/2006	99.0	1.7
K98-102b	02/13/1998	367.31	-8.150	09/09/2006	97.4	1.7
A98-183	04/23/1998	370.02	-8.297	07/23/2006	96.6	1.7
A98-197	05/22/1998	370.50	-8.312	05/08/2006b	92.5	1.7
A98-198	05/22/1998	370.61	-8.312	05/23/2006a	93.3	1.7
A98-272	06/29/1998	363.94	-7.958	02/12/2004	96.8	2.1
A98-472	07/29/1998	363.35	-7.884	02/12/2004	99.5	2.1
A98-473	07/29/1998	363.46	-7.884	02/12/2004	99.1	2.1
A98-474	07/29/1998	363.34	-7.884	07/22/2006	95.1	1.7
A98-480	08/25/1998	360.40	-7.759	02/12/2004	97.0	2.5
A98-481	08/25/1998	360.41	-7.759	02/12/2004	98.9	2.2
A99-040	10/29/1998	366.98	-8.094	02/12/2004	97.3	2.1
K99-029	10/29/1998	367.05	-8.094	02/12/2004	98.1	2.0
A99-046	12/14/1998	370.08	-8.264	02/12/2004	98.2	2.0
K99-035	12/14/1998	370.12	-8.264	02/12/2004	95.3	2.4

Continued on next page

Table B.1 – continued from previous page

Sample ID	Sample Date	CO ₂ (ppm)	$\delta^{13}\text{C}$ (‰)	AMS Date	$\Delta^{14}\text{C}$ (‰)	σ_{Tot} (‰)
A99-130	01/26/1999	370.12	-8.268	02/12/2004	92.4	2.0
K99-044	01/26/1999	370.12	-8.268	02/12/2004	90.6	2.1
A99-243	04/12/1999	372.81	-8.353	05/07/2006b	92.1	1.7
A99-511	07/21/1999	362.92	-7.842	07/23/2006	91.8	1.7
A99-512	07/21/1999	363.03	-7.842	05/08/2006b	93.8	1.7
A99-551	08/10/1999	364.58	-7.881	07/23/2006	90.9	1.7
A99-552	08/10/1999	364.52	-7.881	07/24/2006	93.3	1.7
A99-760	09/08/1999	361.51	-7.751	05/23/2006b	94.9	1.7
A99-766	10/15/1999	366.25	-7.979	09/10/2006	94.6	1.7
A00-009	11/16/1999	367.64	-8.044	05/07/2006b	93.1	1.7
A00-014	11/17/1999	368.82	-8.125	05/21/2006b	97.0	1.7
A00-122	12/31/1999	369.65	-8.130	07/22/2006	92.8	1.7
A00-128	01/21/2000	369.94	-8.129	09/11/2006	94.2	1.7
A00-185	02/11/2000	371.90	-8.267	07/22/2006	91.6	1.7
A00-288	03/20/2000	374.16	-8.348	05/23/2006a	86.0	1.7
A00-304	04/14/2000	373.48	-8.335	05/08/2006b	85.1	1.7
A00-412	05/26/2000	374.15	-8.348	05/08/2006b	83.5	1.7
A00-419	06/05/2000	371.85	-8.225	05/08/2006b	83.7	1.7
A00-447	06/16/2000	371.61	-8.208	11/17/2003	81.8	2.0
A00-448	06/16/2000	371.65	-8.208	11/17/2003	81.2	2.0
A00-567	07/14/2000	365.97	-7.886	11/17/2003	85.0	2.0
A00-568	07/14/2000	365.91	-7.886	11/17/2003	85.8	2.1
A00-571	07/14/2000	365.68	-7.886	05/08/2006b	85.4	1.7
A00-606	08/14/2000	362.54	-7.733	11/17/2003	83.3	2.0
A00-607	08/14/2000	362.58	-7.733	11/17/2003	82.6	2.1
A00-609	08/14/2000	362.58	-7.733	05/08/2006b	83.5	1.7
A00-615	08/18/2000	360.32	-7.603	05/07/2006b	85.5	1.7
A00-718	09/05/2000	362.34	-7.733	11/17/2003	83.0	2.0
A00-719	09/05/2000	362.47	-7.733	11/17/2003	85.8	2.1
A00-730	10/10/2000	367.25	-7.960	11/17/2003	84.9	2.1
A00-731	10/10/2000	367.14	-7.960	11/17/2003	85.6	2.0
A01-085	11/09/2000	370.15	-8.106	11/17/2003	83.2	2.2
A01-086	11/09/2000	370.15	-8.106	11/17/2003	84.4	2.0
A01-121	01/08/2001	372.01	-8.156	11/17/2003	83.4	2.1
A01-122	01/08/2001	371.87	-8.156	11/17/2003	84.9	2.2

Continued on next page

Table B.1 – continued from previous page

Sample ID	Sample Date	CO ₂ (ppm)	$\delta^{13}\text{C}$ (‰)	AMS Date	$\Delta^{14}\text{C}$ (‰)	σ_{Tot} (‰)
A01-127	02/07/2001	373.69	-8.244	11/17/2003	80.0	2.0
A01-128	02/07/2001	373.81	-8.244	11/17/2003	79.5	2.0
A01-187	03/07/2001	374.91	-8.328	11/17/2003	75.9	2.2
A01-188	03/07/2001	375.06	-8.328	11/17/2003	75.2	2.1
A01-217	03/23/2001	373.73	-8.256	05/21/2006b	77.8	1.7
A01-232	04/02/2001	375.69	-8.363	11/17/2003	75.4	2.2
A01-233	04/02/2001	375.77	-8.363	11/17/2003	73.2	2.0
A01-308	05/04/2001	376.50	-8.422	11/17/2003	73.2	2.0
A01-309	05/04/2001	376.54	-8.422	11/17/2003	74.2	2.0
A01-298	06/04/2001	375.54	-8.326	10/26/2006	78.2	1.7
A01-302	06/04/2001	375.62	-8.326	11/17/2003	76.2	2.0
A01-303	06/04/2001	375.55	-8.326	11/17/2003	76.2	2.2
A01-358	06/13/2001	373.17	-8.212	10/28/2006	76.8	1.7
A01-362	06/13/2001	373.11	-8.212	12/28/2003	78.9	2.1
A01-363	06/13/2001	373.01	-8.212	12/28/2003	78.3	2.2
A01-382	07/16/2001	366.68	-7.860	12/28/2003	83.6	2.2
A01-383	07/16/2001	366.54	-7.860	12/28/2003	81.4	2.1
A01-574	07/24/2001	364.29	-7.750	05/08/2006a	86.0	1.7
A01-584	08/10/2001	365.15	-7.792	12/28/2003	79.9	2.0
A01-585	08/10/2001	365.26	-7.792	12/28/2003	83.0	2.1
A01-598	09/06/2001	363.99	-7.739	12/28/2003	82.7	2.1
A01-599	09/06/2001	363.46	-7.739	12/28/2003	82.2	2.1
A01-612	10/31/2001	369.90	-8.011	12/28/2003	77.5	2.1
A01-613	10/31/2001	369.76	-8.011	12/28/2003	74.8	2.0
A02-092	12/09/2001	372.75	-8.185	12/28/2003	72.5	2.1
A02-093	12/09/2001	372.77	-8.185	12/28/2003	74.6	2.1
A02-165	01/09/2002	374.27	-8.216	10/26/2006	76.9	1.7
A02-169	01/09/2002	374.06	-8.216	12/28/2003	78.9	2.4
A02-170	01/09/2002	374.48	-8.216	02/12/2004	74.7	2.1
A02-185	02/17/2002	374.85	-8.274	12/28/2003	74.0	2.7
A02-186	02/17/2002	374.83	-8.274	02/12/2004	74.2	2.0
A02-221	03/22/2002	376.78	-8.365	05/08/2006a	77.1	1.7
A02-224	03/22/2002	376.78	-8.365	12/28/2003	72.5	2.4
A02-225	03/22/2002	376.73	-8.365	02/12/2004	71.1	2.1
A02-254	04/25/2002	376.55	-8.334	12/28/2003	70.4	2.5

Continued on next page

Table B.1 – continued from previous page

Sample ID	Sample Date	CO ₂ (ppm)	$\delta^{13}\text{C}$ (‰)	AMS Date	$\Delta^{14}\text{C}$ (‰)	σ_{Tot} (‰)
A02-255	04/25/2002	376.75	-8.334	02/12/2004	77.5	2.0
A02-352	05/13/2002	376.97	-8.332	12/28/2003	67.4	2.2
A02-353	05/13/2002	376.94	-8.332	02/12/2004	68.3	2.0
A02-368	06/10/2002	375.84	-8.265	05/08/2006a	75.0	1.7
A02-419	06/21/2002	372.97	-8.123	12/28/2003	67.3	2.3
A02-420	06/21/2002	372.81	-8.123	02/12/2004	69.4	2.1
A02-465	07/12/2002	371.03	-7.998	08/19/2005	72.8	1.7
A02-469	07/24/2002	368.68	-7.892	05/08/2006b	74.3	1.7
A02-470	07/24/2002	368.68	-7.892	07/22/2006	79.2	1.7
A02-572	08/06/2002	364.82	-7.713	08/19/2005	74.3	1.7
A02-584	09/09/2002	367.34	-7.858	08/19/2005	70.6	1.7
A02-765	10/11/2002	370.73	-8.021	08/21/2005	72.9	2.2
A02-766	10/11/2002	370.98	-8.021	07/22/2006	72.7	1.7
A03-058	11/09/2002	372.51	-8.063	08/21/2005	70.4	1.9
A03-149	12/17/2002	375.66	-8.284	08/21/2005	70.9	2.0
A03-155	12/29/2002	376.55	-8.303	10/30/2006	69.5	1.7
A03-161	02/07/2003	378.00	-8.377	08/19/2005	75.5	1.7
A03-162	02/07/2003	377.99	-8.377	09/10/2006	66.6	1.7
A03-259	03/04/2003	376.85	-8.279	10/28/2006	71.1	1.7
A03-274	04/10/2003	379.14	-8.405	08/21/2005	66.3	1.8
A03-275	04/10/2003	379.28	-8.405	07/22/2006	65.3	1.7
A03-425	04/24/2003	380.80	-8.508	05/23/2006b	76.2	1.7
A03-426	04/24/2003	380.68	-8.508	07/22/2006	71.8	1.7
A03-460	06/04/2003	379.74	-8.409	10/29/2006	69.1	1.7
A03-601	08/29/2003	367.32	-7.787	08/19/2005	68.6	1.7
A03-607	09/09/2003	367.61	-7.772	07/23/2006	73.1	1.7
A03-608	09/09/2003	367.64	-7.772	07/24/2006	71.1	1.7
A04-013	10/31/2003	375.23	-8.156	09/08/2006	69.7	1.7
A04-019	11/16/2003	377.21	-8.285	09/10/2006	67.4	1.7
A04-020	11/16/2003	377.29	-8.285	10/29/2006	65.8	1.7
A04-117	12/26/2003	378.79	-8.347	09/08/2006	67.9	1.7
A04-247	01/31/2004	380.06	-8.406	05/23/2006b	69.6	1.7
A04-263	02/26/2004	380.30	-8.408	09/09/2006	63.3	1.7
A04-269	03/24/2004	381.32	-8.426	05/23/2006a	61.8	1.7
A04-275	03/26/2004	380.65	-8.403	07/23/2006	66.1	1.7

Continued on next page

Table B.1 – continued from previous page

Sample ID	Sample Date	CO ₂ (ppm)	$\delta^{13}\text{C}$ (‰)	AMS Date	$\Delta^{14}\text{C}$ (‰)	σ_{Tot} (‰)
A04-276	03/26/2004	380.78	-8.403	07/23/2006	65.1	1.7
A04-424	04/20/2004	381.84	-8.476	07/23/2006	62.5	1.7
A04-447	05/26/2004	379.64	-8.353	07/23/2006	63.8	1.7
A04-529	06/09/2004	380.36	-8.369	06/03/2005	63.8	1.8
A04-530	06/09/2004	380.26	-8.369	06/03/2005	62.0	1.7
A04-532	06/09/2004	380.02	-8.369	05/21/2006b	66.7	1.7
A04-690	07/27/2004	374.71	-8.039	08/19/2005	66.8	1.7
A04-691	07/27/2004	374.83	-8.039	08/21/2005	64.4	1.8
A04-734	07/28/2004	373.09	-7.994	08/21/2005	62.2	2.7
A04-735	07/28/2004	372.98	-7.994	08/23/2005	61.0	1.7
A04-740	08/26/2004	369.64	-7.782	09/09/2006	66.4	1.7
A04-786	09/14/2004	370.16	-7.819	09/11/2006	66.2	1.7
A04-792	10/10/2004	375.12	-8.066	07/21/2006	60.1	1.7
A04-793	10/10/2004	375.06	-8.066	07/22/2006	62.9	1.7
A05-047	12/21/2004	380.16	-8.272	10/30/2006	65.7	1.7
AORG126	01/26/2005	379.83	-8.237	02/04/2005	62.0	1.7
AORG338	01/26/2005	379.83	-8.237	02/04/2005	61.5	1.7
AORG416	01/26/2005	379.83	-8.237	02/04/2005	58.2	1.7
AORG420	01/26/2005	379.83	-8.237	02/04/2005	60.8	1.7
CDRG247	01/26/2005	379.83	-8.237	02/04/2005	63.4	1.7
CDRG248	01/26/2005	379.83	-8.237	02/04/2005	60.3	1.7
CDRG249	01/26/2005	379.83	-8.237	02/04/2005	59.5	1.7
CDRG250	01/26/2005	379.83	-8.237	02/04/2005	60.7	1.7
A05-236	02/07/2005	381.96	-8.376	07/24/2006	60.3	1.7
AORG262	03/23/2005	383.24	-8.450	06/03/2005	58.7	2.1
CDRG219	03/23/2005	383.40	-8.450	06/03/2005	60.6	2.2
CDRG222	03/23/2005	383.37	-8.450	06/03/2005	59.0	1.7
A05-288	04/07/2005	383.94	-8.510	06/03/2005	55.7	2.2
AORG366	04/07/2005	383.77	-8.510	06/03/2005	55.0	1.7
A05-308	04/19/2005	384.00	-8.506	07/22/2006	51.4	1.7
A05-309	04/19/2005	384.18	-8.506	07/21/2006	51.8	1.7
A05-349	05/03/2005	383.86	-8.465	05/23/2006b	57.2	1.7
A05-351	05/03/2005	383.93	-8.465	07/21/2006	50.5	1.7
A05-470	06/18/2005	382.27	-8.375	07/21/2006	53.0	1.7
A05-472	06/18/2005	381.92	-8.375	07/23/2006	52.4	1.7

Continued on next page

Table B.1 – continued from previous page

Sample ID	Sample Date	CO ₂ (ppm)	$\delta^{13}\text{C}$ (‰)	AMS Date	$\Delta^{14}\text{C}$ (‰)	σ_{Tot} (‰)
A05-560	07/28/2005	374.56	-8.004	05/21/2006b	59.2	1.7
A05-561	07/28/2005	374.84	-8.004	05/23/2006a	54.9	1.7
A05-680	09/07/2005	373.05	-7.917	07/21/2006	56.2	1.7
A05-681	09/07/2005	372.97	-7.917	07/21/2006	59.7	1.7
A05-721	10/27/2005	378.82	-8.216	07/22/2006	59.7	1.7
A05-722	10/27/2005	378.84	-8.216	07/23/2006	61.4	1.7
A05-777	11/03/2005	378.16	-8.143	05/23/2006a	57.6	1.7
A05-778	11/03/2005	378.28	-8.143	05/23/2006b	59.5	1.7
A06-177	01/25/2006	384.34	-8.388	03/31/2007	53.5	1.7
A06-230	02/15/2006	385.22	-8.445	03/15/2007	53.1	1.7
A06-244	03/17/2006	385.71	-8.503	03/30/2007	50.4	1.7
A06-248	03/17/2006	385.98	-8.503	03/18/2007	51.2	1.7
A06-315	04/21/2006	386.19	-8.491	03/19/2007	50.7	1.7
A06-381	05/22/2006	386.85	-8.535	03/17/2007	58.6	1.7
A06-412	06/12/2006	383.54	-8.357	03/31/2007	56.0	1.7
A06-543	07/17/2006	381.25	-8.194	03/30/2007	56.3	1.7
A06-592	08/03/2006	376.79	-7.996	03/17/2007	57.3	1.7
A06-593	09/13/2006	376.22	-7.987	03/16/2007	54.9	1.7
A06-632	10/06/2006	378.12	-8.061	03/19/2007	56.3	1.7
A06-641	11/09/2006	382.97	-8.274	03/30/2007	56.0	1.7

B.1.2 Measurements from Point Barrow

Table B.2: Measurements from Point Barrow

Sample ID	Sample Date	CO ₂ (ppm)	$\delta^{13}\text{C}$ (‰)	AMS Date	$\Delta^{14}\text{C}$ (‰)	σ_{Tot} (‰)
M99-002	06/12/1999	372.90	-8.453	09/08/2006	91.8	1.7
M99-004	07/03/1999	362.38	-7.962*	08/23/2005	99.0	1.7
M99-006	08/15/1999	353.60	-7.672*	09/09/2006	91.6	1.7
M99-008	09/25/1999	363.75	-7.812*	03/18/2007	93.3	1.7
M99-024	10/22/1999	364.93	-7.960	08/23/2005	97.6	1.8
M99-025	11/19/1999	373.15	-8.152*	03/15/2007	89.0	1.7
M99-027	12/25/1999	374.95	-8.420	08/23/2005	87.9	1.7
M99-028	01/29/2000	374.59	-8.350	03/19/2007	90.7	1.7
M99-029	02/12/2000	375.72	-8.427	09/08/2006	85.7	1.7
M99-031	03/09/2000	374.10	-8.354	08/23/2005	88.8	1.7
M01-030	07/27/2001	362.65	-7.638	03/30/2007	79.8	1.7
M01-032	09/01/2001	363.16	-7.720	08/23/2005	82.6	1.9
M01-046	10/18/2001	369.05	-8.122*	03/17/2007	86.8	1.7
M01-102	12/08/2001	375.23	-8.351	04/01/2007	80.0	1.7
M01-104	02/16/2002	376.79	-8.414	03/16/2007	75.7	1.7
M01-130	03/16/2002	380.42	-8.512*	08/23/2005	71.5	1.8
M01-163	04/20/2002	378.94	-8.452	03/19/2007	72.8	1.7
M01-165	05/28/2002	378.30	-8.430	03/31/2007	71.7	1.7
M01-193	07/26/2002	368.23	-7.842*	05/08/2006b	75.3	1.7
M01-221	10/18/2002	370.00	-8.072*	08/19/2005	77.3	1.7
M01-267	11/18/2002	374.31	-8.225	08/18/2005	80.6	2.0
M01-269	12/25/2002	380.23	-8.372*	08/18/2005	72.8	1.8
M01-298	01/17/2003	377.40	-8.354	08/21/2005	68.4	1.8
M01-300	02/24/2003	383.53	-8.674	08/19/2005	67.1	2.0
M01-322	03/17/2003	382.03	-8.532*	08/21/2005	63.9	1.8
M01-340	05/02/2003	382.71	-8.572*	08/19/2005	61.8	1.7
M01-343	06/13/2003	380.67	-8.523	08/21/2005	69.2	1.8
M01-352	07/12/2003	369.92	-8.004	08/21/2005	70.2	1.8
M01-353	08/16/2003	365.74	-7.682*	08/21/2005	69.9	1.9
M01-385	09/13/2003	367.24	-7.806	08/19/2005	71.7	1.7
M01-387	10/10/2003	371.58	-8.050	09/11/2006	74.1	1.7
M01-453	01/10/2004	383.25	-8.601	09/10/2006	70.0	1.7

Continued on next page

Table B.2 – continued from previous page

Sample ID	Sample Date	CO ₂ (ppm)	$\delta^{13}\text{C}$ (‰)	AMS Date	$\Delta^{14}\text{C}$ (‰)	σ_{Tot} (‰)
M01-476	03/13/2004	381.51	-8.511	05/08/2006b	62.7	1.7
M01-478	04/09/2004	383.93	-8.551	10/26/2006	64.1	1.7
M01-493	05/07/2004	382.94	-8.630	05/08/2006a	63.7	1.7
M01-511	06/10/2004	382.60	-8.481	10/29/2006	62.6	1.7
M01-513	07/01/2004	374.34	-8.126	10/28/2006	60.9	1.7
M01-530	08/13/2004	363.54	-7.549*	05/08/2006a	67.1	1.7
M01-556	09/13/2004	367.12	-7.738	09/09/2006	63.5	1.7
M01-558	10/07/2004	371.24	-7.946*	05/08/2006a	67.2	1.7
M01-568	11/12/2004	380.67	-8.388	09/11/2006	67.4	1.7
M01-641	02/18/2005	384.49	-8.539	10/30/2006	62.7	1.7
M01-642	03/25/2005	385.84	-8.606	10/30/2006	60.3	1.7
M01-659	04/22/2005	385.53	-8.614	10/30/2006	59.7	1.7
M01-661	05/20/2005	385.27	-8.602	10/28/2006	56.5	1.7
M01-682	06/17/2005	383.05	-8.463	10/29/2006	57.9	1.7
M01-684	07/22/2005	373.54	-7.954	09/10/2006	64.9	1.7
M01-727	09/30/2005	373.41	-7.904	10/26/2006	61.4	1.7
M01-729	10/24/2005	377.56	-8.133	11/03/2006	58.8	1.7
M01-757	12/14/2005	384.38	-8.444	11/03/2006	56.1	1.7
M01-777	01/20/2006	386.12	-8.588	03/31/2007	55.9	1.7
M01-792	02/17/2006	386.35	-8.555	03/31/2007	52.9	1.7
M01-800	03/17/2006	387.12	-8.582	03/16/2007	54.8	1.7
M01-814	04/21/2006	387.26	-8.591	04/01/2007	49.1	1.7
M01-840	05/26/2006	389.23	-8.722	03/18/2007	52.5	1.7
M01-841	06/16/2006	386.88	-8.559	03/18/2007	55.4	1.7
M01-852	07/28/2006	368.95	-7.707	03/19/2007	57.0	1.7
M01-882	08/31/2006	370.81	-7.793	03/15/2007	53.3	1.7
M01-883	09/22/2006	374.38	-7.979	03/30/2007	57.1	1.7
M01-894	11/03/2006	383.69	-8.368	03/17/2007	61.1	1.7
M01-925	12/15/2006	387.75	-8.546	04/01/2007	53.0	1.7

B.1.3 Measurements from Kumukahi

Table B.3: Measurements from Kumukahi

Sample ID	Sample Date	CO ₂ (ppm)	$\delta^{13}\text{C}$ (‰)	AMS Date	$\Delta^{14}\text{C}$ (‰)	σ_{Tot} (‰)
M01-028	08/13/2001	366.68	-7.830	10/29/2006	81.3	1.7
M01-029	09/04/2001	368.12	-7.904	05/07/2006a	80.7	1.7
M01-056	10/29/2001	369.35	-8.022	10/29/2006	77.6	1.7
M01-092	11/19/2001	372.45	-8.121	03/19/2007	80.5	1.7
M01-095	01/14/2002	372.98	-8.153	09/08/2006	81.9	1.7
M01-124	02/19/2002	373.74	-8.199	09/11/2006	79.3	1.7
M01-128	03/18/2002	375.83	-8.311	09/09/2006	72.4	1.7
M01-140	04/15/2002	375.17	-8.233	09/10/2006	80.7	1.7
M01-142	04/29/2002	375.49	-8.246	03/15/2007	74.8	1.7
M01-159	05/13/2002	376.38	-8.264	05/07/2006a	71.4	1.7
M01-177	06/17/2002	374.15	-8.147	10/28/2006	74.3	1.7
M01-181	07/15/2002	372.14	-8.029	10/30/2006	79.0	1.7
M01-176	08/12/2002	368.78	-7.833	05/07/2006a	72.5	1.7
M01-210	09/03/2002	366.75	-7.800	08/18/2005	81.0	1.8
M01-212	09/16/2002	366.49	-7.778	03/30/2007	76.8	1.7
M01-214	10/07/2002	369.89	-7.943	08/18/2005	79.7	2.0
M01-256	12/02/2002	373.91	-8.157	08/18/2005	68.1	1.9
M01-258	12/16/2002	376.66	-8.230	05/05/2006b	69.3	1.7
M01-284	01/07/2003	377.00	-8.269	08/21/2005	66.5	2.3
M01-288	02/03/2003	377.66	-8.236	08/18/2005	71.2	1.9
M01-307	03/03/2003	377.81	-8.286	08/18/2005	70.6	1.8
M01-308	03/17/2003	377.31	-8.277	05/05/2006b	66.5	1.7
M01-324	04/14/2003	379.18	-8.333	05/05/2006b	67.0	1.7
M01-329	06/03/2003	379.98	-8.415	08/19/2005	69.9	1.7
M01-364	09/08/2003	370.94	-7.924	11/03/2006	69.4	1.7
M01-398	10/14/2003	372.76	-8.014*	05/05/2006b	71.4	1.7
M01-400	11/10/2003	374.62	-8.108	04/03/2007	69.7	1.7
M01-441	12/15/2003	376.09	-8.174	04/03/2007	68.7	1.7
M01-444	01/12/2004	377.31	-8.180	05/05/2006b	64.3	1.7
M01-445	02/02/2004	378.06	-8.256	11/03/2006	64.0	1.7
M01-459	03/01/2004	377.98	-8.256	09/11/2006	71.4	1.7
M01-485	05/04/2004	380.23	-8.303	03/15/2007	67.4	1.7

Continued on next page

Table B.3 – continued from previous page

Sample ID	Sample Date	CO ₂ (ppm)	$\delta^{13}\text{C}$ (‰)	AMS Date	$\Delta^{14}\text{C}$ (‰)	σ_{Tot} (‰)
M01-497	06/01/2004	381.01	-8.325	05/05/2006b	64.9	1.7
M01-514	07/06/2004	378.33	-8.214	11/03/2006	68.5	1.7
M01-545	08/16/2004	373.77	-7.974	10/26/2006	67.3	1.7
M01-547	09/13/2004	374.76	-8.018	04/03/2007	66.3	1.7
M01-559	10/04/2004	374.87	-8.048	10/29/2006	63.7	1.7
M01-596	11/15/2004	377.84	-8.189	10/26/2006	60.3	1.7
M01-599	12/21/2004	377.89	-8.153	11/03/2006	60.9	1.7
M01-614	01/18/2005	378.35	-8.130	04/03/2007	68.0	1.7
M01-624	02/22/2005	382.30	-8.351	04/03/2007	63.1	1.7
M01-636	03/28/2005	382.12	-8.402	11/03/2006	57.5	1.7
M01-639	04/25/2005	383.50	-8.445	10/30/2006	60.8	1.7
M01-665	05/23/2005	384.14	-8.384	09/09/2006	55.3	1.7
M01-688	06/20/2005	382.17	-8.346	10/26/2006	56.0	1.7
M01-692	07/19/2005	377.63	-8.141	04/03/2007	60.2	1.7
M01-717	09/06/2005	376.04	-7.978	09/08/2006	62.4	1.7
M01-724	10/11/2005	376.54	-8.043	09/08/2006	63.6	1.7
M01-749	11/07/2005	378.56	-8.126	11/03/2006	57.9	1.7
M01-769	01/09/2006	381.78	-8.255	09/10/2006	56.8	1.7
M01-781	01/17/2006	382.23	-8.280	10/28/2006	56.1	1.7
M01-793	02/21/2006	383.19	-8.344	03/18/2007	54.6	1.7
M01-809	03/20/2006	383.23	-8.293	03/19/2007	55.7	1.7
M01-812	04/17/2006	384.61	-8.374	03/16/2007	59.8	1.7
M01-829	05/15/2006	386.98	-8.552	03/18/2007	53.4	1.7
M01-832	06/12/2006	384.80	-8.355	03/17/2007	61.8	1.7
M01-854	07/10/2006	382.23	-8.262	04/01/2007	56.9	1.7
M01-858	08/07/2006	376.34	-7.971	03/30/2007	56.2	1.7
M01-879	09/11/2006	377.45	-7.984	04/01/2007	58.7	1.7
M01-890	10/09/2006	378.02	-8.029	03/17/2007	59.7	1.7
M01-920	11/13/2006	379.38	-8.138	03/31/2007	56.9	1.7
M01-922	12/11/2006	382.41	-8.253	03/31/2007	52.9	1.7

B.1.4 Measurements from Mauna Loa

Table B.4: Measurements from Mauna Loa

Sample ID	Sample Date	CO ₂ (ppm)	$\delta^{13}\text{C}$ (‰)	AMS Date	$\Delta^{14}\text{C}$ (‰)	σ_{Tot} (‰)
M01-024	08/22/2001	369.10	-7.937	05/08/2006a	85.9	1.7
M01-027	09/12/2001	368.87	-7.935	02/15/2004	82.1	2.1
M01-040	09/26/2001	367.50	-7.887	03/30/2007	85.2	1.7
M01-043	10/17/2001	367.99	-7.893	02/15/2004	79.7	2.0
M01-058	11/07/2001	368.83	-7.959	05/21/2006b	86.0	1.7
M01-059	11/14/2001	369.63	-7.990	02/15/2004	79.1	2.1
M01-083	01/16/2002	372.29	-8.090	02/15/2004	79.3	2.1
M01-108	02/13/2002	372.61	-8.094	02/15/2004	79.1	2.1
M01-110	03/01/2002	372.70	-8.132	05/21/2006a	80.0	1.7
M01-118	03/13/2002	373.81	-8.174	02/15/2004	77.5	2.0
M01-122	04/10/2002	373.87	-8.137	02/15/2004	77.2	2.1
M01-144	04/24/2002	375.33	-8.231	05/21/2006a	78.7	1.7
M01-146	05/08/2002	374.05	-8.103	02/15/2004	73.2	2.0
M01-154	05/29/2002	375.83	-8.252	05/21/2006a	78.0	1.7
M01-183	08/07/2002	371.07	-7.985	05/21/2006a	74.0	1.7
M01-185	08/21/2002	371.52	-8.023	02/15/2004	77.9	2.0
M01-200	09/04/2002	369.12	-7.904	05/21/2006b	78.6	1.7
M01-202	09/18/2002	369.60	-7.926	08/19/2005	76.2	1.7
M01-206	10/16/2002	371.49	-7.982	08/18/2005	73.8	1.8
M01-231	11/13/2002	371.67	-8.000	08/18/2005	75.7	1.8
M01-251	12/18/2002	373.37	-8.071	08/19/2005	75.8	1.7
M01-265	01/15/2003	373.62	-8.085	08/19/2005	77.0	1.7
M01-304	03/19/2003	376.15	-8.236	08/19/2005	72.5	1.7
M01-317	04/16/2003	378.42	-8.344	08/18/2005	71.8	1.9
M01-321	05/14/2003	377.26	-8.242	08/18/2005	72.4	1.7
M01-337	05/28/2003	378.97	-8.316	05/21/2006b	72.1	1.7
M01-338	06/04/2003	378.24	-8.264	04/01/2007	73.3	1.7
M01-348	07/16/2003	375.74	-8.221	08/18/2005	71.9	1.8
M01-351	08/13/2003	374.56	-8.062	08/18/2005	73.8	2.2
M01-371	09/10/2003	372.32	-8.042	09/08/2006	73.7	1.7
M01-390	10/01/2003	372.97	-8.033	05/21/2006b	72.5	1.7
M01-394	10/29/2003	373.17	-8.017	05/21/2006a	70.5	1.7

Continued on next page

Table B.4 – continued from previous page

Sample ID	Sample Date	CO ₂ (ppm)	$\delta^{13}\text{C}$ (‰)	AMS Date	$\Delta^{14}\text{C}$ (‰)	σ_{Tot} (‰)
M01-410	01/07/2004	375.80	-8.107	09/08/2006	70.9	1.7
M01-448	02/04/2004	377.46	-8.197	05/08/2006b	69.6	1.7
M01-451	03/01/2004	377.57	-8.214	09/10/2006	72.8	1.7
M01-471	03/24/2004	378.24	-8.241	05/21/2006a	68.0	1.7
M01-486	04/28/2004	380.04	-8.355	05/08/2006a	67.9	1.7
M01-488	05/12/2004	379.77	-8.457	05/08/2006a	67.2	1.7
M01-505	06/16/2004	379.24	-8.304	05/08/2006a	66.2	1.7
M01-522	07/14/2004	375.79	-8.140	09/09/2006	64.7	1.7
M01-527	08/18/2004	375.03	-8.079	05/21/2006a	68.3	1.7
M01-535	09/15/2004	374.05	-7.985	10/28/2006	68.0	1.7
M01-552	10/13/2004	373.94	-8.034	09/08/2006	62.9	1.7
M01-571	11/17/2004	376.44	-8.090	05/21/2006a	66.7	1.7
M01-572	11/24/2004	376.23	-8.131	05/21/2006a	65.8	1.7
M01-590	12/08/2004	377.24	-8.138	05/21/2006a	64.8	1.7
M01-595	01/12/2005	378.66	-8.247	10/28/2006	61.6	1.7
M01-618	02/16/2005	379.95	-8.288	10/28/2006	62.3	1.7
M01-630	03/16/2005	381.75	-8.318	10/30/2006	64.0	1.7
M01-634	04/13/2005	381.44	-8.696	10/28/2006	61.2	1.7
M01-654	05/11/2005	381.99	-8.282	10/26/2006	62.2	1.7
M01-674	07/13/2005	381.36	-8.263	10/30/2006	62.3	1.7
M01-702	08/10/2005	377.92	-8.168	10/29/2006	62.0	1.7
M01-709	09/14/2005	376.04	-8.039	09/11/2006	65.2	1.7
M01-732	10/26/2005	377.05	-8.095	03/31/2007	62.4	1.7
M01-756	12/14/2005	379.21	-8.209	09/10/2006	63.1	1.7
M01-773	01/11/2006	380.91	-8.259	10/26/2006	56.8	1.7
M01-784	02/08/2006	381.78	-8.217	03/19/2007	62.2	1.7
M01-796	03/08/2006	382.63	-8.313	03/18/2007	56.8	1.7
M01-802	04/05/2006	384.03	-8.397	03/19/2007	57.2	1.7
M01-816	05/10/2006	385.13	-8.458	03/16/2007	60.5	1.7
M01-836	06/14/2006	383.73	-8.344	03/30/2007	58.8	1.7
M01-846	07/12/2006	381.61	-8.277	03/18/2007	56.0	1.7
M01-864	08/16/2006	379.77	-8.143	03/15/2007	60.1	1.7
M01-869	09/20/2006	377.98	-8.107	03/16/2007	59.2	1.7
M01-887	10/18/2006	379.03	-8.126	03/18/2007	57.0	1.7
M01-910	11/15/2006	379.64	-8.112	03/15/2007	57.2	1.7

Continued on next page

Table B.4 – continued from previous page

Sample ID	Sample Date	CO ₂ (ppm)	$\delta^{13}\text{C}$ (‰)	AMS Date	$\Delta^{14}\text{C}$ (‰)	σ_{Tot} (‰)
M01-914	12/13/2006	380.67	-8.184	03/31/2007	55.3	1.7

B.1.5 Measurements from Samoa

Table B.5: Measurements from Samoa

Sample ID	Sample Date	CO ₂ (ppm)	$\delta^{13}\text{C}$ (‰)	AMS Date	$\Delta^{14}\text{C}$ (‰)	σ_{Tot} (‰)
M01-049	09/25/2001	369.86	-7.988	08/23/2005	85.5	1.7
M01-084	10/29/2001	369.92	-7.940	08/23/2005	83.7	1.7
M01-085	11/07/2001	369.86	-8.014	02/15/2004	85.4	2.1
M01-112	01/29/2002	370.26	-7.967	08/23/2005	83.1	1.7
M01-132	03/12/2002	371.97	-8.029	02/15/2004	83.9	2.0
M01-136	04/09/2002	370.48	-7.999	02/15/2004	83.1	2.1
M01-137	04/19/2002	370.05	-7.999	08/23/2005	80.0	2.0
M01-150	05/14/2002	370.51	-7.966	02/15/2004	82.0	2.1
M01-171	06/18/2002	371.60	-8.023	02/15/2004	78.5	2.1
M01-188	07/19/2002	371.45	-8.013	02/15/2004	78.9	2.0
M01-189	07/23/2002	371.45	-8.032	08/23/2005	79.8	1.7
M01-196	08/14/2002	371.89	-8.037	02/15/2004	77.5	2.1
M01-197	08/26/2002	371.94	-8.023	08/23/2005	78.2	1.8
M01-225	10/29/2002	372.54	-8.041	03/19/2007	77.5	1.7
M01-228	11/19/2002	373.06	-8.061	08/19/2005	79.5	1.7
M01-271	12/03/2002	373.49	-8.095	03/16/2007	79.7	1.7
M01-275	12/31/2002	372.54	-8.072	03/30/2007	79.9	1.7
M01-293	02/18/2003	372.88	-8.043	08/18/2005	78.5	1.8
M01-311	03/11/2003	374.74	-8.082	08/18/2005	77.8	2.0
M01-313	04/11/2003	374.67	-8.121	09/11/2006	79.5	1.7
M01-315	04/22/2003	373.06	-8.020	03/16/2007	79.3	1.7
M01-331	05/23/2003	373.19	-8.077	08/21/2005	79.3	1.8
M01-359	07/16/2003	373.26	-8.096*	08/18/2005	73.7	1.8
M01-365	07/30/2003	374.30	-8.086	08/23/2005	79.2	1.7
M01-377	09/16/2003	374.20	-8.057	09/09/2006	73.0	1.7
M01-434	11/17/2003	374.30	-8.106	09/09/2006	69.4	1.7
M01-438	12/16/2003	375.41	-8.059	09/08/2006	75.7	1.7
M01-465	02/11/2004	375.95	-8.076	09/11/2006	74.5	1.7
M01-468	03/09/2004	376.22	-8.096	08/23/2005	72.9	2.3
M01-480	04/13/2004	375.88	-8.104	08/23/2005	71.2	1.8
M01-482	04/27/2004	374.94	-8.072	08/23/2005	71.9	1.7
M01-501	05/18/2004	375.24	-8.074	08/23/2005	71.4	2.0

Continued on next page

Table B.5 – continued from previous page

Sample ID	Sample Date	CO ₂ (ppm)	$\delta^{13}\text{C}$ (‰)	AMS Date	$\Delta^{14}\text{C}$ (‰)	σ_{Tot} (‰)
M01-509	06/16/2004	376.11	-8.088	11/03/2006	71.2	1.7
M01-518	07/14/2004	375.38	-8.064	10/29/2006	68.8	1.7
M01-540	08/09/2004	376.01	-8.108	08/23/2005	68.9	1.8
M01-544	09/07/2004	375.76	-8.085	09/09/2006	65.1	1.7
M01-564	11/09/2004	375.67	-8.010	08/23/2005	68.1	1.7
M01-566	11/24/2004	375.94	-8.123	08/23/2005	68.2	1.7
M01-603	01/05/2005	377.57	-8.132	10/26/2006	68.3	1.7
M01-617	02/10/2005	377.32	-8.128	09/10/2006	67.9	1.7
M01-646	04/11/2005	377.71	-8.078	09/10/2006	64.1	1.7
M01-650	05/12/2005	379.36	-8.155	10/30/2006	68.7	1.7
M01-680	06/17/2005	377.61	-8.140	10/26/2006	65.0	1.7
M01-695	07/18/2005	378.14	-8.159	10/30/2006	68.5	1.7
M01-699	08/17/2005	378.05	-8.096	10/28/2006	63.5	1.7
M01-720	09/13/2005	378.40	-8.108	10/28/2006	62.9	1.7
M01-734	10/12/2005	378.05	-8.103	10/29/2006	63.6	1.7
M01-760	11/17/2005	378.79	-8.127	10/30/2006	65.9	1.7
M01-763	12/13/2005	377.67	-8.145	09/11/2006	66.0	1.7
M01-775	01/04/2006	379.67	-8.119	10/26/2006	62.5	1.7
M01-788	02/18/2006	380.58	-8.161	03/17/2007	67.4	1.7
M01-808	03/27/2006	378.55	-8.143	03/15/2007	63.8	1.7
M01-823	04/25/2006	378.61	-8.138	03/18/2007	62.0	1.7
M01-843	06/28/2006	379.73	-8.159	03/30/2007	62.7	1.7
M01-860	07/28/2006	379.69	-8.170	03/16/2007	59.8	1.7
M01-871	08/28/2006	379.69	-8.142	03/19/2007	57.6	1.7
M01-875	09/25/2006	379.26	-8.121	03/18/2007	60.9	1.7
M01-898	10/23/2006	379.45	-8.150	04/01/2007	59.3	1.7
M01-929	12/29/2006	381.43	-8.134	03/16/2007	58.7	1.7

B.1.6 Measurements from Palmer Station

Table B.6: Measurements from Palmer Station

Sample ID	Sample Date	CO ₂ (ppm)	$\delta^{13}\text{C}$ (‰)	AMS Date	$\Delta^{14}\text{C}$ (‰)	σ_{Tot} (‰)
PSA-01A	03/10/2005	375.18	-8.098	03/30/2007	64.6	1.7
PSA-03A	05/19/2005	376.23	-8.107	03/19/2007	59.5	1.7
PSA-04A	07/03/2005	377.00	-8.119	03/31/2007	60.5	1.7
PSA-05A	09/23/2005	378.06	-8.147	04/01/2007	58.1	1.7
PSA-06A	10/20/2005	377.90	-8.128	03/17/2007	65.3	1.7
PSA-07A	11/30/2005	377.26	-8.148	04/01/2007	57.3	1.7
PSA-08A	12/12/2005	377.55	-8.153	03/15/2007	58.2	1.7
PSA-09A	12/30/2005	377.36	-8.099	03/30/2007	58.6	1.7
PSA-10A	01/16/2006	377.47	-8.139	03/15/2007	61.7	1.7
PSA-11A	02/06/2006	377.14	-8.099	03/19/2007	62.0	1.7
PSA-12A	03/02/2006	377.57	-8.087	04/01/2007	62.4	1.7
PSA-13A	03/20/2006	384.73	-8.098	03/19/2007	61.9	1.7
PSA-14A	04/17/2006	378.08	-8.072	03/17/2007	66.2	1.7
PSA-15A	04/29/2006	378.04	-8.093	03/30/2007	59.0	1.7
PSA-16A	06/28/2006	378.97	-8.116	03/18/2007	60.7	1.7
PSA-17A	07/10/2006	378.69	-8.130	03/15/2007	57.6	1.7
PSA-18A	07/24/2006	378.94	-8.158	03/31/2007	57.6	1.7
PSA-19A	08/07/2006	379.14	-8.185	03/17/2007	60.6	1.7
PSA-20A	11/07/2006	379.73	-8.163	04/01/2007	55.7	1.7
PSA-21A	12/02/2006	379.76	-8.174	04/01/2007	54.5	1.7

B.1.7 Measurements from the South Pole

Table B.7: Measurements from the South Pole

Sample ID	Sample Date	CO ₂ (ppm)	$\delta^{13}\text{C}$ (‰)	AMS Date	$\Delta^{14}\text{C}$ (‰)	σ_{Tot} (‰)
M99-010	02/16/1999	364.75	-8.034	04/01/2007	96.0	1.7
M99-011	03/01/1999	364.77	-7.982	04/01/2007	97.9	1.7
M99-012	05/01/1999	365.01	-7.973	08/21/2005	92.7	1.9
M99-013	07/15/1999	365.69	-7.999	09/10/2006	97.1	1.7
M99-014	08/17/1999	365.93	-7.980	10/30/2006	93.0	1.7
M99-016	09/16/1999	366.21	-7.983	10/28/2006	89.4	1.7
M99-018	10/17/1999	366.60	-8.024	09/09/2006	86.3	1.7
M99-020	11/19/1999	369.46	-8.012*	09/08/2006	92.4	1.7
M99-022	01/23/2000	366.35	-8.007	03/19/2007	93.2	1.7
M01-001	02/18/2000	366.35	-8.011	11/03/2006	93.0	1.7
M01-004	04/15/2000	366.51	-8.010	11/03/2006	89.8	1.7
M01-008	06/16/2000	366.58	-7.988	08/21/2005	86.7	1.8
M01-010	07/15/2000	366.87	-7.990	10/26/2006	84.4	1.7
M01-013	09/02/2000	367.46	-8.005	09/11/2006	88.6	1.7
M01-015	10/01/2000	367.57	-7.998	08/23/2005	87.8	1.7
M01-017	11/01/2000	367.81	-7.998	11/03/2006	86.2	1.7
M01-019	12/02/2000	367.66	-7.982	08/21/2005	86.4	2.0
M01-021	01/15/2001	367.75	-7.980	03/15/2007	92.2	1.7
M01-065	02/15/2001	366.87	-7.983	10/26/2006	88.7	1.7
M01-067	03/15/2001	366.98	-7.966	11/03/2006	81.4	1.7
M01-069	04/16/2001	367.13	-7.958	08/21/2005	85.8	1.8
M01-071	05/15/2001	367.46	-7.969	09/11/2006	88.3	1.7
M01-074	07/01/2001	367.84	-7.976	03/30/2007	87.9	1.7
M01-078	09/15/2001	369.20	-7.997	08/21/2005	78.9	2.4
M01-233	02/13/2002	369.01	-8.010	08/21/2005	75.9	1.9
M01-240	07/01/2002	370.29	-7.985	08/21/2005	78.7	1.9
M01-242	08/01/2002	370.65	-8.031	08/18/2005	76.8	1.7
M01-244	09/02/2002	371.13	-8.025	08/18/2005	73.7	1.7
M01-259	11/02/2002	371.34	-8.057	08/18/2005	79.5	1.7
M01-261	12/03/2002	371.29	-8.045	08/19/2005	76.5	1.7
M01-412	02/01/2003	371.57	-8.009	08/18/2005	73.3	1.8
M01-416	04/01/2003	371.76	-8.108	08/21/2005	75.4	1.8

Continued on next page

Table B.7 – continued from previous page

Sample ID	Sample Date	CO ₂ (ppm)	$\delta^{13}\text{C}$ (‰)	AMS Date	$\Delta^{14}\text{C}$ (‰)	σ_{Tot} (‰)
M01-418	05/01/2003	372.00	-8.034	08/18/2005	69.1	1.9
M01-420	06/01/2003	372.10	-8.034	08/21/2005	74.1	1.8
M01-422	07/02/2003	372.45	-8.062	08/19/2005	72.1	1.7
M01-424	08/01/2003	372.91	-8.054	08/19/2005	73.1	1.7
M01-426	09/01/2003	373.66	-8.090	10/29/2006	66.8	1.7
M01-428	10/01/2003	373.70	-8.073	03/31/2007	70.9	1.7
M01-430	11/16/2003	373.54	-8.085	08/21/2005	69.0	1.8
M01-456	01/03/2004	373.52	-8.066	10/30/2006	72.9	1.7
M01-458	02/01/2004	373.27	-8.094	03/18/2007	72.0	1.7
M01-574	03/03/2004	373.70	-8.059	08/21/2005	71.3	1.9
M01-575	04/02/2004	373.62	-8.136	03/17/2007	76.8	1.7
M01-580	06/18/2004	374.40	-8.109	09/09/2006	64.4	1.7
M01-581	07/15/2004	374.70	-8.144	10/28/2006	65.9	1.7
M01-583	08/16/2004	375.15	-8.159	08/23/2005	65.4	1.7
M01-585	09/18/2004	375.30	-8.112	09/11/2006	67.9	1.7
M01-587	10/17/2004	375.26	-8.142	08/23/2005	70.7	2.1
M01-588	11/02/2004	375.49	-8.126	08/23/2005	69.6	2.6
M01-611	01/01/2005	375.27	-8.117	11/03/2006	67.4	1.7
M01-736	02/02/2005	374.83	-8.121	11/03/2006	65.8	1.7
M01-738	03/15/2005	375.52	-8.090	09/08/2006	66.6	1.7
M01-740	05/02/2005	376.06	-8.162	09/10/2006	67.3	1.7
M01-741	06/01/2005	376.05	-8.156	09/09/2006	59.0	1.7
M01-743	06/30/2005	376.55	-8.166	10/29/2006	58.7	1.7
M01-744	09/15/2005	377.45	-8.159	10/26/2006	60.9	1.7
M01-746	10/19/2005	377.98	-8.165	03/15/2007	66.2	1.7
M01-765	11/15/2005	377.56	-8.205	10/30/2006	64.6	1.7
M01-766	12/16/2005	377.53	-8.181	11/03/2006	64.6	1.7
M01-778	01/15/2006	377.60	-8.197	03/19/2007	65.8	1.7
M01-915	02/15/2006	377.17	-8.136	03/17/2007	64.9	1.7
M01-899	04/15/2006	378.83	-8.142	03/16/2007	62.6	1.7
M01-901	05/15/2006	377.57	-8.157	03/31/2007	54.3	1.7
M01-903	07/01/2006	378.19	-8.158	03/30/2007	65.6	1.7
M01-905	08/01/2006	380.33	-8.173	04/01/2007	59.6	1.7
M01-907	09/19/2006	378.93	-8.163	03/18/2007	58.0	1.7
M01-908	10/18/2006	378.94	-8.194	03/17/2007	61.3	1.7

Continued on next page

Table B.7 – continued from previous page

Sample ID	Sample Date	CO ₂ (ppm)	$\delta^{13}\text{C}$ (‰)	AMS Date	$\Delta^{14}\text{C}$ (‰)	σ_{Tot} (‰)
M01-909	11/15/2006	379.10	-8.182	03/30/2007	62.9	1.7

B.2 Monthly values of $\Delta^{14}\text{C}$

Monthly values of $\Delta^{14}\text{C}$ were determined by fitting the observations listed in the previous section to a function incorporating a linear trend, single harmonic and a cubic smoothing spline:

$$y = a + bt + c \cos(2\pi t) + d \sin(2\pi t) + s(t) \quad (\text{B.1})$$

The fitted function was evaluated at the middle of each month over the span of the record to produce the monthly values listed in the following tables. Annual values were computed as a simple average of the monthly values.

B.2.1 Monthly values of $\Delta^{14}\text{C}$ at La Jolla

Table B.8: Monthly values of $\Delta^{14}\text{C}$ at La Jolla

Year	Jan	Feb	Mar	Apr	May	Jun	Jul	Aug	Sep	Oct	Nov	Dec	Annual
1992	130.7	130.1	128.1	126.6	126.8	125.2	133.6	134.8	136.2	134.4	131.8	130.6	
1993	117.8	117.1	116.2	114.0	114.4	115.1	123.3	124.0	125.2	125.4	123.5	120.0	125.7
1994	117.5	113.7	111.8	111.3	112.8	112.4	115.7	116.6	117.5	118.4	119.2	119.4	116.8
1995	109.4	107.8	105.3	104.1	104.3	104.4	104.3	104.8	106.3	108.6	109.1	109.4	111.3
1996	100.7	99.5	99.4	99.9	100.3	100.4	100.0	101.2	101.8	107.2	105.5	102.8	105.5
1997	99.7	98.3	97.2	96.0	94.5	95.3	97.1	98.1	98.3	101.7	101.4	100.8	100.6
1998	93.0	91.3	91.3	91.9	92.1	92.2	92.4	93.2	94.5	94.9	95.0	94.3	93.0
1999	93.3	90.7	87.3	84.8	83.5	83.1	84.2	84.5	84.8	84.8	84.5	84.3	85.8
2000	82.5	78.8	76.2	74.4	75.0	78.8	82.7	83.1	81.1	77.9	75.3	74.8	78.4
2001	75.5	74.7	73.7	72.5	70.8	71.7	73.7	73.7	72.0	71.6	70.8	70.4	72.6
2002	70.5	70.7	69.9	69.9	70.3	69.4	69.2	69.7	70.5	69.7	68.0	67.9	69.6
2003	68.2	66.0	63.8	63.0	63.4	63.8	63.9	65.0	64.9	63.3	64.0	64.6	64.5
2004	62.5	60.1	58.1	54.3	52.5	53.1	55.4	57.5	58.8	59.6	58.7	56.8	57.3
2005	54.4	52.4	51.1	51.9	55.4	56.9	56.8	56.3	55.7	56.0	55.9	55.1	54.8
2006													

B.2.2 Monthly values of $\Delta^{14}\text{C}$ at Point Barrow

Table B.9: Monthly values of $\Delta^{14}\text{C}$ at Point Barrow

Year	Jan	Feb	Mar	Apr	May	Jun	Jul	Aug	Sep	Oct	Nov	Dec	Annual
1999						94.2	95.5	93.5	93.8	94.6	91.4	88.7	
2000	88.3	87.9											
2001								81.7	84.6	85.8	83.4	79.9	
2002	77.2	74.8	72.6	72.0	71.9	72.8	74.5	76.2	77.5	78.5	78.7	74.8	75.1
2003	69.7	66.6	64.2	62.6	64.4	68.3	70.0	70.6	72.2	73.9	73.8	72.1	69.0
2004	69.0	65.5	63.6	63.5	63.0	62.2	63.2	65.3	65.6	66.8	67.3	66.6	65.1
2005	65.0	62.9	61.0	59.1	57.5	58.9	62.8	64.3	62.7	59.9	57.6	56.3	60.7
2006	55.4	54.1	53.0	50.9	51.8	54.6	55.9	55.4	56.5	59.2	58.5	53.5	54.9

B.2.3 Monthly values of $\Delta^{14}\text{C}$ at Kumukahi

Table B.10: Monthly values of $\Delta^{14}\text{C}$ at Kumukahi

Year	Jan	Feb	Mar	Apr	May	Jun	Jul	Aug	Sep	Oct	Nov	Dec	Annual
2001	81.2	78.7	76.1	76.0	73.9	74.6	76.3	81.2	79.8	78.7	79.7	81.2	
2002	68.6	69.6	68.2	67.5	68.6	69.7	70.0	76.7	78.4	77.0	71.9	68.5	75.8
2003	65.3	67.5	69.6	68.6	66.7	66.6	67.8	69.8	70.2	70.7	69.6	67.4	69.2
2004	65.2	63.9	60.6	58.7	56.9	56.5	59.1	67.5	65.6	62.7	60.9	62.1	65.9
2005	56.0	55.3	56.0	57.3	57.1	58.6	57.5	61.7	62.9	61.7	58.6	57.0	60.2
2006								57.4	58.8	58.9	56.4	52.5	56.8

B.2.4 Monthly values of $\Delta^{14}\text{C}$ at Mauna Loa

Table B.11: Monthly values of $\Delta^{14}\text{C}$ at Mauna Loa

Year	Jan	Feb	Mar	Apr	May	Jun	Jul	Aug	Sep	Oct	Nov	Dec	Annual
2001									83.6	82.2	81.5	80.4	
2002	79.6	79.2	78.3	77.1	76.2	76.2	75.8	76.5	76.6	75.1	75.4	76.1	76.8
2003	76.3	74.8	73.0	72.1	72.3	72.5	72.7	73.4	73.1	71.6	70.5	70.4	72.7
2004	70.6	70.8	69.9	68.2	67.0	65.9	65.9	67.3	66.8	65.2	65.5	64.2	67.3
2005	62.4	62.5	62.8	62.0	61.9	61.9	62.2	63.1	64.2	63.5	62.7	61.4	62.5
2006	59.5	59.1	57.8	58.3	59.3	58.4	57.7	59.1	59.1	57.8	56.7	55.2	58.2

B.2.5 Monthly values of $\Delta^{14}\text{C}$ at Samoa

Table B.12: Monthly values of $\Delta^{14}\text{C}$ at Samoa

Year	Jan	Feb	Mar	Apr	May	Jun	Jul	Aug	Sep	Oct	Nov	Dec	Annual
2001										84.8	84.5	84.0	
2002	83.6	83.6	83.3	81.9	80.8	79.5	79.0	78.1	77.6	77.8	78.9	79.7	80.3
2003	79.4	78.6	78.5	79.2	79.0	77.6	76.5	75.8	73.1	70.9	71.1	74.1	76.2
2004	75.2	74.2	72.8	71.7	71.5	70.8	69.2	67.4	66.0	66.7	68.0	68.5	70.2
2005	68.3	67.2	65.9	65.7	67.0	66.7	66.6	64.5	63.2	64.0	65.2	65.0	65.8
2006	64.8	66.0	64.9	63.0	62.3	62.2	60.8	59.1	59.4	59.7	59.4	59.0	61.7

B.2.6 Monthly values of $\Delta^{14}\text{C}$ at Palmer Station

Table B.13: Monthly values of $\Delta^{14}\text{C}$ at Palmer Station

Year	Jan	Feb	Mar	Apr	May	Jun	Jul	Aug	Sep	Oct	Nov	Dec	Annual
2005			64.0	61.8	60.2	59.9	59.7	59.2	59.8	61.8	60.1	58.6	
2006	60.5	62.2	62.8	62.8	60.9	59.7	58.8	59.0	58.2	56.8	55.3	54.2	59.3

B.2.7 Monthly values of $\Delta^{14}\text{C}$ at the South Pole

Table B.14: Monthly values of $\Delta^{14}\text{C}$ at the South Pole

Year	Jan	Feb	Mar	Apr	May	Jun	Jul	Aug	Sep	Oct	Nov	Dec	Annual
1999			95.9	94.1	94.0	95.6	95.9	93.1	89.4	88.1	90.8	92.9	
2000	93.5	93.0	91.7	89.8	87.9	86.2	85.5	86.9	87.8	87.1	86.8	88.8	88.7
2001	90.4	87.6	84.2	85.3	87.7	88.3							
2002							77.5	75.4	75.4	77.5	77.9	76.2	
2003	74.5	74.0	74.0	72.5	72.0	72.8	72.3	70.2	69.1	69.6	69.9	71.2	71.8
2004	72.2	72.4	73.9	74.0	70.1	66.0	65.1	65.8	67.9	69.7	69.6	68.3	69.6
2005	66.8	66.3	66.8	66.6	63.3	59.3	58.1	59.1	61.6	64.6	65.2	65.2	63.6
2006	65.5	65.0	63.5	60.6	58.1	61.0	62.0	59.7	58.8	60.6	63.0	65.1	61.9

Appendix C:

Airborne $\Delta^{14}\text{CO}_2$ Data

The following tables contain data about whole air flask samples collected for $\Delta^{14}\text{C}$ analysis of CO_2 during the Airborne Carbon in the Mountains Experiment (ACME) in Colorado, 2004. Listed within the tables are sampling data: the number and date of the research flight and the start and end time (in Mountain Daylight Time), latitude, longitude and elevation that the air in the flask was sampled. The tables list results of laboratory analysis: CO_2 concentration, $\Delta^{14}\text{C}$, uncertainty in $\Delta^{14}\text{C}$ (σ_{meas}) and $\delta^{13}\text{C}$ (if available). Fossil fuel-derived CO_2 (C_{ff}) and biogenic CO_2 (C_{veg}) were calculated by Equations 5.1 and 5.2. σ_C indicates the total uncertainty in C_{ff} and C_{veg} for each flask sample. Samples designated as “background” are italicized. Mean CO concentration measured *in situ* during the period of flask collection is also shown (if available). Starred samples from research flight 13 were not collected during vertical profiling.

C.1 Airborne measurements, May 2004

Table C.1: Airborne measurements, May 2004

Flight	Date	start (MDT)	end (MDT)	Lon (°W)	Lat (°N)	ASL (km)	AGL (km)	P (mb)	CO ₂ (ppm)	$\Delta^{14}\text{C}$ (‰)	σ_{meas} (‰)	C _{ff} (ppm)	C _{veg} (ppm)	σ_C (ppm)	$\delta^{13}\text{C}$ (‰)	mean CO (ppb)
2	5/14/2004	14:07:53	14:09:35	105.10	40.24	5.140	3.575	537	379.9						-8.20	
2	5/14/2004	14:10:06	14:11:39	105.00	40.09	5.142	3.601	538	379.8	66.4	1.8					
2	5/14/2004	14:15:21	14:17:00	105.12	40.05	3.751	2.159	644	379.9	67.1	2.0					
2	5/14/2004	14:18:54	14:20:23	105.31	40.08	2.961	1.026	711	380.8	57.9	1.7	3.1	-2.1	0.8		
2	5/14/2004	14:24:11	14:25:51	105.26	39.81	2.562	0.534	747	384.7	50.2	2.1	5.8	-1.0	0.9		
2	5/14/2004	14:27:21	14:29:15	105.19	39.94	2.094	0.348	793	394.5	30.5	1.9	13.3	1.3	0.8	-9.05	
3	5/20/2004	7:07:35	7:09:23	106.49	40.28	5.529	2.915	518	380.4	76.8	2.4				-8.38	107.9
3	5/20/2004	7:12:06	7:13:54	106.25	40.11	3.732	1.304	651	380.7	69.4	1.8					111.4
3	5/20/2004	7:17:44	7:19:51	106.34	40.05	2.511	0.228	755	396.0	66.1	1.9	1.2	14.1	1.1	-8.97	137.6
3	5/20/2004	7:21:30	7:23:16	106.39	40.14	3.513	1.101	668	381.3	65.6	1.7	1.4	-0.8	0.8		116.3
3	5/20/2004	10:04:12	10:04:54	105.43	39.60	5.525	2.861	519	380.3	68.7	2.0					110.4
3	5/20/2004	10:10:03	10:10:35	105.24	39.95	2.572	0.860	752	387.8	57.6	2.2	4.0	3.5	1.0	-8.57	181.9
4	5/20/2004	14:22:59	14:23:41	106.07	40.31	5.570	2.775	516	380.9	65.7	1.9					103.6
4	5/20/2004	14:24:18	14:24:56	106.00	40.24	5.579	2.370	516	380.4	68.8	1.8					104.2
4	5/20/2004	14:31:55	14:32:45	105.56	39.83	3.696	0.804	653	381.2							196.5
4	5/20/2004	14:34:14	14:35:00	105.39	39.77	3.078	0.536	704	380.9	56.0	1.9	4.0	-3.7	0.9	-8.18	193.2
4	5/20/2004	14:36:27	14:37:02	105.26	39.82	2.657	0.655	741	381.2	55.5	1.9	4.2	-3.7	0.9		179.2
4	5/20/2004	14:40:32	14:41:09	105.15	39.93	1.894	0.199	812	379.5	60.3	2.1	2.5	-3.6	0.9	-8.23	
6	5/28/2004	15:44:04	15:45:05	105.26	40.18	5.648	3.974	508	379.4	68.7	1.7				-8.30	105.8
6	5/28/2004	15:50:04	15:51:00	105.27	39.91	4.186	2.286	611	379.5	66.3	1.7	0.9	-0.7	0.8	-8.21	127.6
6	5/28/2004	16:01:01	16:01:52	104.85	39.61	1.968	0.232	795	379.6	61.9	1.7	2.4	-2.2	0.8	-8.21	143.4
6	5/28/2004	16:04:04	16:05:24	104.97	39.57	2.390	0.653	757	379.4	67.3	1.7	0.5	-0.4	0.8	-8.25	117.6
6	5/28/2004	16:07:46	16:08:38	105.09	39.72	2.343	0.653	761	380.6	62.2	1.7	2.3	-1.1	0.8	-8.29	181.5

C.2 Airborne measurements, July 2004

Table C.2: Airborne measurements, July 2004

Flight	Date	start (MDT)	end (MDT)	Lon (°W)	Lat (°N)	ASL (km)	AGL (km)	P (mb)	CO ₂ (ppm)	$\Delta^{14}\text{C}$ (‰)	σ_{meas} (‰)	C _{ff} (ppm)	C _{neg} (ppm)	σ_C (ppm)	$\delta^{13}\text{C}$ (‰)	mean CO (ppb)
9	7/20/2004	9:25:43	9:26:22	105.32	39.53	5.574	2.976	523	378.4	68.6	1.8				-8.02	83.7
9	7/20/2004	9:26:34	9:27:04	105.26	39.54	5.322	2.795	541	378.3	70.8	2.0				-8.15	84.8
9	7/20/2004	9:29:21	9:29:56	105.29	39.50	3.480	0.909	676	378.1	68.9	1.9				-8.44	167.0
9	7/20/2004	9:40:40	9:41:12	104.86	39.62	1.963	0.245	807	384.8	55.8	1.7	5.0	1.5	2.4	-8.46	187.3
9	7/20/2004	9:41:41	9:42:13	104.85	39.56	1.883	0.085	815	385.2	55.9	1.7	5.0	1.9	2.4	-8.94	224.4
9	7/20/2004	9:54:38	9:55:05	105.08	39.89	1.835	0.187	820	394.3	41.1	1.7	10.5	5.4	2.4	-8.28	86.1
10	7/20/2004	13:34:17	13:34:41	105.14	39.92	1.843	0.121	819	381.6	53.3	1.7	4.4	-0.8	2.4	-8.19	86.4
10	7/20/2004	13:35:17	13:35:41	105.16	39.96	2.047	0.353	799	380.0	56.7	1.7	3.2	-1.1	2.4	-8.06	85.0
10	7/20/2004	13:37:28	13:37:54	105.12	40.06	3.090	1.523	708	376.3	67.2	1.7				-8.04	83.5
10	7/20/2004	13:40:33	13:41:02	105.24	39.97	4.333	2.637	611	376.3	65.7	1.7				-8.20	77.5
10	7/20/2004	13:43:44	13:44:08	105.46	39.90	5.614	2.924	521	377.9	65.0	1.7				-8.17	93.9
10	7/20/2004	13:50:23	13:50:50	105.95	39.74	7.180	3.565	426	378.0	66.4	1.7				-10.32	96.1
11	7/22/2004	6:48:52	6:49:25	106.00	40.02	5.576	2.764	521	376.1	69.6	2.0				-9.03	97.5
11	7/22/2004	6:52:58	6:53:26	106.14	39.99	3.369	0.843	686	376.6						-8.00	119.1
11	7/22/2004	6:56:33	6:56:59	106.36	40.05	2.330	0.064	775	431.1	65.6	1.7	1.6	53.3	3.6	-8.49	156.6
11	7/22/2004	6:57:36	6:58:07	106.43	40.07	2.706	0.417	741	397.1	66.6	2.0	1.1	19.8	2.6	-7.96	118.2
12	7/26/2004	7:10:22	7:10:59	106.48	40.32	5.570	2.850	522	373.0	66.1	1.7				-9.05	314.1
12	7/26/2004	7:19:20	7:19:56	106.36	40.05	2.349	0.082	775	410.1						-8.64	369.2
12	7/26/2004	7:20:26	7:21:05	106.42	40.08	2.741	0.439	740	386.1	64.2	1.7	0.7	12.3	2.5	-9.03	388.9
12	7/26/2004	9:44:32	9:45:08	105.65	40.04	5.554	1.808	523	373.0	66.5	1.7				-7.96	118.2
12	7/26/2004	9:54:05	9:54:38	105.08	39.89	1.792	0.129	826	396.3						-9.05	314.1
13	7/26/2004	13:29:54	13:30:26	105.14	39.92	1.866	0.149	818	387.7	24.8	2.0	16.1	-3.2	2.4	-8.64	369.2
13	7/26/2004	13:30:43	13:31:16	105.17	39.95	2.104	0.383	795	396.5	6.7	1.8	23.1	-1.5	2.4	-9.03	388.9
13	7/26/2004	13:31:57	13:32:29	105.17	40.01	2.657	1.025	745	372.8	61.9	2.0	2.5	-4.6	2.4	-7.96	103.9
13	7/26/2004	13:44:23	13:44:58	106.08	40.02	6.994	4.281	434	374.9	69.1	1.7	7.6	-1.6	2.4	-8.23	189.3
13*	7/26/2004	14:27:34	14:28:14	105.37	39.97	3.043	0.633	712	378.2	46.6	1.7				-7.96	125.1
13*	7/26/2004	14:34:09	14:34:45	105.55	40.02	3.697	0.683	658	372.2	68.0	1.8				-7.96	125.1

References

- Andres, R., Marland, G., Fung, I., and Matthews, E., 1996: A 1 degrees \times 1 degrees distribution of carbon dioxide emissions from fossil fuel consumption and cement manufacture, 1950-1990. *Global Biogeochemical Cycles*, **54**, 419–429.
- Andrews, A., Boering, K., Wofsy, S., Daube, B., Jones, D., Alex, S., Loewenstein, M., Podolske, J., and Strahan, S., 2001: Empirical age spectra for the midlatitude lower stratosphere from *in situ* observations of CO₂: Quantitative evidence for a subtropical “barrier” to horizontal transport. *Journal of Geophysical Research*, **106**(D10), 10257–10274.
- Appenzeller, C., Holton, J. R., and Rosenlof, K. H., 1996: Seasonal variation of mass transport across the tropopause. *Journal of Geophysical Research*, **101**(D10), 15071–15078.
- Bacastow, R., Adams, J., Keeling, C., Moss, D., Whorf, T., and Wong, C., 1980: Atmospheric carbon dioxide, the Southern Oscillation, and the weak 1975 El Niño. *Science*, **210**(4465), 66–68.
- Bakwin, P. S., Tans, P. P., Hurst, D. F., and Zhao, C., 1998: Measurements of carbon dioxide on very tall towers: results of the NOAA/CMDL program. *Tellus*, **50B**, 401–415.
- Baldwin, M. P., Gray, L. J., Dunkerton, T. J., Hamilton, K., Haynes, P. H., Randel, W. J., Holton, J. R., Alexander, M. J., Hirota, I., Horinouchi, T., et al., 2001: The quasi-biennial oscillation. *Reviews of Geophysics*, **39**(2), 179–230.
- Battle, M., Bender, M., Tans, P., White, J., Ellis, J., Conway, T., and Francey, R., 2000: Global carbon sinks and their variability inferred from atmospheric O₂ and ¹³C. *Science*, **287**(5462), 2467.
- Baxter, M. S., and Walton, A., 1971: Fluctuations of atmospheric carbon-14 concentrations during the past century. *Proceedings of the Royal Society of London. Series A, Mathematical and Physical Sciences*, **321**(1544), 105–127.

- Bender, M., 1971: Variations in the $^{13}\text{C}/^{12}\text{C}$ ratios of plants in relation to the pathway of photosynthetic carbon dioxide fixation. *Phytochemistry*, **10**, 1239–1244.
- Blasing, T., Broniak, C., and Marland, G., 2004a: Estimates of annual fossil-fuel CO_2 emitted for each state in the U.S.A. and the District of Columbia for each year from 1960 through 2001. In *Trends: A Compendium of Data on Global Change*. Carbon Dioxide Information Analysis Center, Oak Ridge National Laboratory, U.S. Department of Energy, Oak Ridge, TN.
- Blasing, T., Broniak, C., and Marland, G., 2004b: Estimates of monthly carbon dioxide emissions and associated $\delta^{13}\text{C}$ values from fossil-fuel consumption in the USA. In *Trends: A Compendium of Data on Global Change*. Carbon Dioxide Information Analysis Center, Oak Ridge National Laboratory, U.S. Department of Energy, Oak Ridge, TN.
- Bolin, B., and Keeling, C., 1963: Large-scale atmospheric mixing as deduced from the seasonal and meridional variations of carbon dioxide. *Journal of Geophysical Research*, **68**, 3899.
- Bousquet, P., Peylin, P., Ciais, P., Le Quere, C., Friedlingstein, P., and Tans, P., 2000: Regional changes in carbon dioxide fluxes of land and oceans since 1980. *Science*, **290**(5495), 1342.
- Braud, H., Bousquet, P., and Ramonet, M., 2004: CO/CO_2 ratio in urban atmosphere: Example of the agglomeration of Paris, France. Notes des Activités Instrumentales (N.A.I) 42, Institut Pierre Simon Laplace (IPSL), Paris.
- Braziunas, T., Fung, I., and Stuiver, M., 1995: The preindustrial atmospheric $^{14}\text{CO}_2$ latitudinal gradient as related to exchanges among atmospheric, oceanic, and terrestrial reservoirs. *Global Biogeochemical Cycles*, **9**(4), 565–584.
- Brenninkmeijer, C. A. M., Lowe, D. C., Manning, M. R., Sparks, R. J., and van Velthoven, P. F. J., 1995: The ^{13}C , ^{14}C , and ^{18}O isotopic composition of CO , CH_4 , and CO_2 in the higher southern latitudes lower stratosphere. *Journal of Geophysical Research*, **100**(D12), 26163–26172.
- Broecker, W., Peng, T., Ostlund, G., and Stuiver, M., 1985: The distribution of bomb radiocarbon in the ocean. *Journal of Geophysical Research*, **90**(c4), 6953–6970.
- Brown, T., and Southon, J., 1997: Corrections for contamination background in AMS ^{14}C measurements. *Nuclear Instruments and Methods in Physics Research Section B: Beam Interactions with Materials and Atoms*, **123**, 208–213(6).
- Burchuladze, A. A., Pagava, S. V., Povinec, P., Togonidze, G. I., and Usacev, S., 1980: Radiocarbon variations with the 11-year solar cycle during the last century. *Nature*, **287**(5780), 320–322.

- Burchuladze, A. A., Pagava, S. V., Togonidze, G. I., and Avtandilashvili, M. V., 1993: Radiocarbon and 11-year variations of cosmic rays. *Radiocarbon*, **35**(3), 347–350.
- Caldeira, K., Rau, G. H., and Duffy, P. B., 1998: Predicted net efflux of radiocarbon from the ocean and increase in atmospheric radiocarbon content. *Geophysical Research Letters*, **25**(20), 3811–3814.
- Campbell, J. E., Carmichael, G. R., Tang, Y., Chai, T., Vay, S. A., Choi, Y.-H., Sachse, G. W., Singh, H. B., Schnoor, J. L., Woo, J., Vukovich, J. M., Streets, D. G., Huey, L. G., and Stanier, C. O., 2007: Analysis of anthropogenic CO₂ signal in ICARTT using a regional chemical transport model and observed tracers. *Tellus*, **B59**, 199–210. doi:10.1111/j.1600-0889.2006.00239.x.
- Canadell, J., Le Quere, C., Raupach, M., Field, C., Buitenhuis, E., Ciais, P., Conway, T., Gillett, N., Houghton, R., and Marland, G., 2007: Contributions to accelerating atmospheric CO₂ growth from economic activity, carbon intensity, and efficiency of natural sinks. *Proceedings of the National Academy of Sciences*. doi:10.1073/pnas.0702737104.
- Chavez, F., Ryan, J., Lluch-Cota, S., and Ñiquen C, M., 2003: From Anchovies to Sardines and Back: Multidecadal Change in the Pacific Ocean. *Science*, **299**(5604), 217–221.
- Ciais, P., Tans, P., Trolier, M., White, J., and Francey, R., 1995: A large northern hemisphere terrestrial CO₂ sink indicated by the ¹³C/¹²C ratio of atmospheric CO₂. *Science*, **269**(5227), 1098–1102.
- Conway, T., and Tans, P., 2004: Atmospheric carbon dioxide mixing ratios from the NOAA CMDL Carbon Cycle Cooperative Global Air Sampling Network (2004). In *Trends: A Compendium of Data on Global Change*. Carbon Dioxide Information Analysis Center, Oak Ridge National Laboratory, U.S. Department of Energy, Oak Ridge, TN.
- Craig, H., 1957: Isotopic standards for carbon and oxygen and correction factors for mass-spectrometric analysis of carbon dioxide. *Geochimica Cosmochimica Acta*, **12**, 133–149.
- Davis, J. C., 1989: The LLNL multi-user tandem laboratory. *Nuclear Instruments and Methods in Physics Research B*, **4041**, 7058.
- Davis, J. C., Proctor, I. D., Southon, J. R., Caffee, M. W., Heikkinen, D. W., Roberts, M. L., Moore, T. L., Turteltaub, K. W., Nelson, D. E., Loyd, D. H., and Vogel, J. S., 1990: LLNL/UC AMS facility and research program. *Nuclear Instruments and Methods in Physics Research B*, **52**(34), 26972.

- Denman, K., Brasseur, G., Chidthaisong, A., Ciais, P., Cox, P., Dickinson, R., Hauglustaine, D., Heinze, C., Holland, E., Jacob, D., et al., 2007: Couplings between changes in the climate system and biogeochemistry, chapter 7. In *Climate Change 2007: The Physical Science Basis, The IPCC Fourth Assessment Report*. Intergovernmental Panel on Climate Change.
- Denning, A., Fung, I., and Randall, D., 1995: Latitudinal gradient of atmospheric CO₂ due to seasonal exchange with land biota. *Nature*, **376**(6537), 240–243.
- Donahue, D., Linick, T., and Jull, A., 1990: Isotope-ratio and background corrections for accelerator mass spectrometry radiocarbon measurements. *Radiocarbon*, **32**(2), 135–142.
- Dutta, K., 2002: Coherence of tropospheric ¹⁴CO₂ with El Niño/Southern Oscillation. *Geophysical Research Letters*, **29**, 1987. doi:10.1029/2002GL014753.
- Ebisuzaki, W., 1997: A method to estimate the statistical significance of a correlation when the data are serially correlated. *Journal of Climate*, **10**(9), 2147–2153.
- Ellison, S. L. R., Rosslein, M., and Williams, A., editors, 2000: *EURACHEM/CITAC Guide: Quantifying Uncertainty in Analytical Measurement*. London, second edition.
- Energy Information Administration (EIA), 2007: *Renewable Energy Trends in Consumption and Electricity, 2005*. US Department of Energy, Washington, DC. Available at: <http://www.eia.doe.gov/cneaf/solar.renewables/page/trends/trends.pdf>.
- Environmental Protection Agency (EPA), 2006: *Inventory of U.S. Greenhouse Gas Emissions and Sinks: 1990-2004*.
- Fallon, S. J., Guilderson, T. P., and Brown, T. A., 2007: CAMS/LLNL ion source efficiency revisited. *Nuclear Instruments and Methods in Physics Research B*, **259**(1), 106110.
- Fan, S., Gloor, M., Mahlman, J., Pacala, S., Sarmiento, J., Takahashi, T., and Tans, P., 1998: A large terrestrial carbon sink in north america implied by atmospheric and oceanic carbon dioxide data and models. *Science*, **282**(5388), 442.
- Feely, R., Wanninkhof, R., Takahashi, T., and Tans, P., 1999: Influence of El Niño on the equatorial Pacific contribution to atmospheric CO₂ accumulation. *Nature*, **398**(6728), 597.
- Friedlingstein, P., J.-L., D., M., C. P., and P., R., 2003: How positive is the feedback between climate change and the carbon cycle? *Tellus*, **B55**, 692–700. Doi:10.1034/j.1600-0560.2003.01461.x.

- Gamnitzer, U., Karstens, U., Kromer, B., Neubert, R. E. M., Meijer, H. A. J., Schroeder, H., and Levin, I., 2006: Carbon monoxide: A quantitative tracer for fossil fuel CO₂? *Journal of Geophysical Research*, **111**:D22302. doi:10.1029/2005JD006966.
- Gerbig, C., Lin, J. C., Wofsy, S. C., Daube, B. C., Andrews, A. E., Stephens, B. B., Bakwin, P. S., and Grainger, C. A., 2003: Toward constraining regional-scale fluxes of CO₂ with atmospheric observations over a continent: 2. Analysis of COBRA data using a receptor-oriented framework. *Journal of Geophysical Research*, **108**(D24):4757. doi:10.1029/2003JD003770.
- Gerbig, C., Schmitgen, S., Kley, D., Volz-Thomas, A., Dewey, K., and D., H., 1999: An improved fast-response vacuum-UV resonance fluorescence CO instrument. *Journal of Geophysical Research*, **104**, 1699–1704.
- Gettelman, A., and Sobel, A. H., 2000: Direct diagnoses of stratosphere-troposphere exchange. *Journal of the Atmospheric Sciences*, **57**(1), 3–16.
- Gibbons, J., and Chakraborti, S., 2003: *Nonparametric Statistical Inference*. CRC Press, fourth edition.
- Gibert, F., Schmidt, M., Cuesta, J., Ciais, P., Ramonet, M., Xueref, I., Larmanou, E., and Flamant, P. H., 2007: Retrieval of average CO₂ fluxes by combining in situ CO₂ measurements and backscatter lidar information. *Journal of Geophysical Research*, **112**:D10301. doi:10.1029/2006JD008190.
- Godwin, H., 1962: Half-life of radiocarbon. *Nature*, **195**(4845), 984.
- Goudriaan, J., 1992: Biosphere Structure, Carbon Sequestering Potential and the Atmospheric ¹⁴C Carbon Record. *Journal of Experimental Botany*, **43**(8), 1111–1119.
- Graven, H. D., Guilderson, T. P., and Keeling, R. F., 2007: Methods for high-precision ¹⁴C AMS measurement of atmospheric CO₂ at LLNL. *Radiocarbon*, **49**, 349–356.
- Gruber, N., Keeling, C., Bacastow, R., Guenther, P., Lueker, T., Whalen, M., Meijer, H., Mook, W., and Stocker, T., 1999: Spatiotemporal patterns of carbon-13 in the global surface oceans and the oceanic Suess effect. *Global Biogeochemical Cycles*, **13**, 307–335.
- Guenther, P. R., Bollenbacher, A., Keeling, C., Stewart, E. F., and Wahlen, M., 2001: *Calibration methodology for the Scripps ¹³C/¹²C and ¹⁸O/¹⁶O stable isotope program, 1996-2000*. 118 p.
- Guilderson, T., Caldeira, K., and Duffy, P., 2000: Radiocarbon as a diagnostic tracer in ocean and carbon cycle modeling. *Global Biogeochemical Cycles*, **14**(3), 887–902.

- Guilderson, T. P., Roark, E. B., Quay, P. D., Flood Page, S. R., and Moy, C., 2006: Seawater radiocarbon evolution in the Gulf of Alaska: 2002 observations. *Radiocarbon*, **48**, 1–15.
- Guilderson, T. P., and Schrag, D. P., 1998: Abrupt shift in subsurface temperatures in the tropical Pacific associated with changes in El Niño. *Science*, **281**(5374), 240–3.
- Guilderson, T. P., Schrag, D. P., and Cane, M. A., 2004: Surface water mixing in the Solomon Sea as documented by a high-resolution coral ^{14}C record. *Journal of Climate*, **17**(5), 1147–1156.
- Gurney, K., Law, R., Denning, A., Rayner, P., Baker, D., Bousquet, P., Bruhwiler, L., Chen, Y. H., Ciais, P., Fan, S., et al., 2002: Robust regional estimate of annual CO_2 sources and sinks. *Nature*, **415**, 626–30.
- Hamilton, K., and Fan, S., 2000: Effects of the stratospheric quasi-biennial oscillation on long-lived greenhouse gases in the troposphere. *Journal of Geophysical Research*, **105**(D16), 20581–20588.
- Harder, S., Warren, S., and Charlson, R., 2000: Sulfate in air and snow at the South Pole: Implications for transport and deposition at sites with low snow accumulation. *Journal of Geophysical Research*, **105**(D18), 22825–22832.
- Henne, S., Furger, M., Nyeki, S., Steinbacher, M., Neining, B., deWecker, S. F. J., Dommen, J., Spichtinger, N., Stohl, A., and Prévôt, A. S. H., 2004: Quantification of topographic venting of boundary layer air to the free troposphere. *Atmospheric Chemistry and Physics*, **4**, 497–509.
- Hesshaimer, V., Heimann, M., and Levin, I., 1994: Radiocarbon evidence for a smaller oceanic carbon dioxide sink than previously believed. *Nature*, **370**(6486), 201–203.
- Holton, J. R., Haynes, P. H., McIntyre, M. E., Douglass, A. R., Rood, R. B., and Pfister, L., 1995: Stratosphere-troposphere exchange. *Reviews of Geophysics*, **33**(4), 403–439.
- James, P., Stohl, A., Forster, C., Eckhardt, S., Seibert, P., and Frank, A., 2003: A 15-year climatology of stratosphere-troposphere exchange with a Lagrangian particle dispersion model: 2. Mean climate and seasonal variability. *Journal of Geophysical Research*, **108**(D12), 8522. doi:10.1029/2002JD002639.
- Joos, F., Orr, J. C., and Siegenthaler, U., 1997: Ocean carbon transport in a box-diffusion versus a general circulation model. *Journal of Geophysical Research*, **102**, 12.
- Keeling, C., 1960: The concentration and isotopic abundances of carbon dioxide in the atmosphere. *Tellus*, **12**(2), 200–203.

- Keeling, C., Adams Jr, J., Ekdahl Jr, C., and Guenther, P., 1976: Atmospheric carbon dioxide variations at the South Pole. *Tellus*, **28**(6), 552–564.
- Keeling, C., Bacastow, R., Carter, A., Piper, S., Whorf, T., Heimann, M., Mook, W., and Roeloffzen, H., 1989: A three-dimensional model of atmospheric CO₂ transport based on observed winds: 1. Analysis of observational data. In *Aspects of Climate Variability in the Pacific and the Western Americas*, *Geophysical Monograph 55:165-235*, editor D. Peterson.
- Keeling, C., Bollenbacher, A., and Whorf, T., 2005a: Monthly atmospheric ¹³C/¹²C isotopic ratios for 10 SIO stations. In *Trends: A Compendium of Data on Global Change*. Carbon Dioxide Information Analysis Center, Oak Ridge National Laboratory, U.S. Department of Energy, Oak Ridge, TN.
- Keeling, C., Guenther, P., Emanuele, G., Bollenbacher, A., and Moss, D., 2002: *Scripps Reference Gas Calibration System for Carbon Dioxide-in-Nitrogen and Carbon Dioxide-in-Air Standards: Revision of 1999, A Report Prepared for the Global Environmental Monitoring Program of the World Meteorological Organization*. 83 p.
- Keeling, C., and Whorf, T., 2005: Atmospheric CO₂ records from sites in the SIO air sampling network. In *Trends: A Compendium of Data on Global Change*. Carbon Dioxide Information Analysis Center, Oak Ridge National Laboratory, U.S. Department of Energy, Oak Ridge, TN.
- Keeling, C. D., 1958: The concentration and isotopic abundances of atmospheric carbon dioxide in rural areas. *Geochimica Cosmochimica Acta*, **13**, 322–334.
- Keeling, C. D., Piper, S. C., Bacastow, R. B., Wahlen, M., Whorf, T. P., Heimann, M., and Meijer, H. A., 2005b: Atmospheric CO₂ and ¹³CO₂ exchange with the terrestrial biosphere and oceans from 1978 to 2000: observations and carbon cycle implications. In *A History of Atmospheric CO₂ and its effects on Plants, Animals and Ecosystems*, editors J. Ehleringer, T. E. Cerling, and M. D. Dearing, 83–113. Springer Verlag, New York.
- Keeling, C. D., Whorf, T. P., Wahlen, M., and van der Plicht, J., 1995: Interannual extremes in the rate of rise of atmospheric carbon dioxide since 1980. *Nature*, **375**(6533), 666–670.
- Keeling, R., Piper, S., and Heimann, M., 1996: Global and hemispheric CO₂ sinks deduced from changes in atmospheric O₂ concentration. *Nature*, **381**(6579), 218–221.
- Keeling, R., Stephens, B., Najjar, R., Doney, S., Archer, D., and Heimann, M., 1998: Seasonal variations in the atmospheric O₂/N₂ ratio in relation to the kinetics of air-sea gas exchange. *Global Biogeochem. Cycles*, **12**(1), 141–163.

- Keeling, R. F., Blaine, T., Paplawsky, B., Katz, L., Atwood, C., and Brockwell, T., 2004: Measurement of changes in atmospheric Ar/N₂ ratio using a rapid-switching, single capillary mass spectrometer system. *Tellus*, **B56**, 332–338.
- Key, R. M., Quay, P., Schlosser, P., McNichol, A., von Reden, K., Schneider, R., Elder, K., Stuiver, M., and Östlund, H., 2002: WOCE Radiocarbon IV: Pacific Ocean Results; P10, P13N, P14C, P18, P19 & S4P. *Radiocarbon*, **44**(1), 239–392.
- Kitagawa, H., Mukai, H., Nojiri, Y., Shibata, Y., Kobayashi, T., and Nojiri, T., 2004: Seasonal and secular variations of atmospheric ¹⁴CO₂ over the Western Pacific since 1994. *Radiocarbon*, **46**(2), 901–910.
- Krakauer, N., Randerson, J. T., Primeau, F. W., Gruber, N., and Menemenlis, D., 2006: Carbon isotope evidence for the latitudinal distribution and wind speed dependence of the air-sea gas transfer velocity. *Tellus*, **B58**(5), 390–417.
- Lal, D., and Rama, 1966: Characteristics of global tropospheric mixing based on man-made ¹⁴C, ³H, and ⁹⁰Sr. *Journal of Geophysical Research*, **71**, 2865.
- Langford, A. O., 1999: Stratosphere-troposphere exchange at the subtropical jet: Contribution to the tropospheric ozone budget at midlatitudes. *Geophysical Research Letters*, **26**(16), 2449–2452.
- Lassey, K. R., Enting, I. G., and Trudinger, C. M., 1996: The earth's radiocarbon budget: A consistent model of the global carbon and radiocarbon cycles. *Tellus*, **B48**(4), 487–501.
- Le Quéré, C., Aumont, O., Bopp, L., Bousquet, P., Ciais, P., Francey, R., Heimann, M., Keeling, C., Keeling, R., Khesghi, H., et al., 2003: Two decades of ocean CO₂ sink and variability. *Tellus B*, **55**(2), 649.
- Levin, I., Böisinger, R., Bonani, G., Francey, R., Kromer, B., Münnich, K., Suter, M., Trivett, N., and Wölfl, W., 1992: Radiocarbon in atmospheric carbon dioxide and methane: global distribution and trends. In *Radiocarbon after four decades*, 503–518. Springer-Verlag, New York, New York.
- Levin, I., Hammer, S., Kromer, B., and Meinhardt, F., 2008: Radiocarbon observations in atmospheric CO₂: Determining fossil fuel CO₂ over Europe using Jungfraujoch observations as background. *The Science of the Total Environment*, **391**(2-3), 211–216.
- Levin, I., and Hesshaimer, V., 2000: Radiocarbon a unique tracer of global carbon cycle dynamics. *Radiocarbon*, **42**(1), 6980.
- Levin, I., and Karstens, U., 2007: Inferring high-resolution fossil fuel CO₂ records at continental sites from combined ¹⁴CO₂ and CO observations. *Tellus*, **B59**, 245–250. doi:10.1111/j.1600-0889.2006.00244.x.

- Levin, I., and Kromer, B., 1997: Twenty years of atmospheric $^{14}\text{CO}_2$ observations at Schauinsland station, Germany. *Radiocarbon*, **39**(2), 205–218.
- Levin, I., and Kromer, B., 2004: The tropospheric $^{14}\text{CO}_2$ level in mid-latitudes of the Northern Hemisphere (1959-2003). *Radiocarbon*, **46**(3), 126172.
- Levin, I., Kromer, B., Schmidt, M., and Sartorius, H., 2003: A novel approach for independent budgeting of fossil fuel CO_2 over Europe by $^{14}\text{CO}_2$ observations. *Geophysical Research Letters*, **30**(23):2194. doi:10.1029/2003GL018477.
- Levin, I., Kromer, B., Schoch-Fischer, H., Bruns, M., Mnnich, M., Berdau, B., Vogel, J. C., and Mnnich, K. O., 1985: 25 years of tropospheric ^{14}C observations in Central Europe. *Radiocarbon*, **27**(1), 119.
- Levin, I., Kromer, B., Wagenbach, D., and Münnich, K. O., 1987: Carbon isotope measurements of atmospheric CO_2 at a coastal station in Antarctica. *Tellus*, **39B**(1-2), 89–95.
- Libby, W., 1946: Atmospheric helium three and radiocarbon from cosmic radiation. *Physical Review*, **69**(11-12), 671–672.
- Libby, W., Anderson, E., and Arnold, J., 1949: Age determination by radiocarbon content: World-wide assay of natural radiocarbon. *Science*, **109**(2827), 227–228.
- Lingenfelter, R. E., 1963: Production of carbon 14 by cosmic-ray neutrons. *Reviews of Geophysics*, **1**(1), 35–55.
- Lloyd, D., Vogel, J., and Trumbore, S., 1991: Lithium contamination in AMS measurements of ^{14}C . *Radiocarbon*, **33**(3), 297–301.
- Lowe, D. C., and Allan, W., 2002: A simple procedure for evaluating global cosmogenic ^{14}C production in the atmosphere using neutron monitor data. *Radiocarbon*, **44**(1), 149–157.
- MacKay, C., Pandow, M., and Wolfgang, R., 1963: On the chemistry of natural radiocarbon. *Journal of Geophysical Research*, **68**(13), 3929–3931.
- Manning, A. C., and Keeling, R. F., 2006: Global oceanic and land biotic carbon sinks from the Scripps atmospheric oxygen flask sampling network. *Tellus B*, **58**(2), 95–116.
- Manning, M. R., Lowe, D. C., Melhuish, W. H., Sparks, R. J., Wallace, G., Breninkmeijer, C. A. M., and McGill, R. C., 1990: The use of radiocarbon measurements in atmospheric studies. *Radiocarbon*, **32**(1), 3758.
- Mantua, N., and Hare, S., 2002: The Pacific Decadal Oscillation. *Journal of Oceanography*, **58**(1), 35–44.

- Marland, G., Boden, T., and Andres, R., 2007: Global, regional, and national fossil fuel CO₂ emissions. In *Trends: A Compendium of Data on Global Change*. Carbon Dioxide Information Analysis Center, Oak Ridge National Laboratory, U.S. Department of Energy, Oak Ridge, TN.
- McCormac, F., Hogg, A., Higham, T., Lynch-Stieglitz, J., Broecker, W., Baillie, M., Palmer, J., Xiong, L., Pilcher, J., Brown, D., et al., 1998: Temporal variation in the interhemispheric ¹⁴C offset. *Geophysical Research Letters*, **25**(9), 1321–1324.
- McKinley, G., Takahashi, T., Buitenhuis, E., Chai, F., Christian, J., Doney, S., Jiang, M., Lindsay, K., Moore, J., Le Quere, C., et al., 2006: North Pacific carbon cycle response to climate variability on seasonal to decadal timescales. *Journal of Geophysical Research*, **111**.
- Meijer, H. A. J., Pertuisot, M. H., and van der Plicht, J., 2006: High accuracy ¹⁴C measurements for atmospheric CO₂ samples by AMS. *Radiocarbon*, **48**(3), 35572.
- Meijer, H. A. J., Smid, H. M., Perez, E., and Keizer, M. G., 1996: Isotopic characterization of anthropogenic CO₂ emissions using isotopic and radiocarbon analysis. *Physics and Chemistry of the Earth*, **21**(5-6), 483–487.
- Miller, A., Cayan, D., Barnett, T., Graham, N., and Oberhuber, J., 1994: The 1976-77 climate shift of the Pacific Ocean. *Oceanography*, **7**(1), 21–26.
- Miller, J. B., editor, 2006: *13th WMO/IAEA Meeting of Experts on Carbon Dioxide Concentration and Related Tracers Measurement Techniques*.
- Naegler, T., 2005: *Simulating Bomb Radiocarbon: Consequences for the Global Carbon Cycle*. Ph.D. thesis, Insitutut fur Umweltphysik, University of Heidelberg, Heidelberg, Germany.
- Naegler, T., Ciais, P., Rodgers, K., and Levin, I., 2006: Excess radiocarbon constraints on air-sea gas exchange and the uptake of CO₂ by the oceans. *Geophysical Research Letters*, **33**(L11802). doi:10.1029/2005GL025408.
- Nakamura, T., Nakazawa, T., Nakai, N., Kitagawa, H., Honda, H., Itoh, T., Machida, T., and Matsumoto, E., 1992: Measurement of ¹⁴C concentrations of stratospheric CO₂ by accelerator mass spectrometry. *Radiocarbon*, **34**(3), 745–752.
- Nakazawa, T., Miyashita, K., Aoki, S., and Tanaka, M., 1991: Temporal and spatial variations of upper tropospheric and lower stratospheric carbon dioxide. *Tellus*, **B43**, 106–117.

- Nevison, C. D., Kinnison, D. E., and Weiss, R. F., 2004: Stratospheric influences on the tropospheric seasonal cycles of nitrous oxide and chlorofluorocarbons. *Geophysical Research Letters*, **31**(L20103), 20. doi:10.1029/2004GL020398.
- Nisbet, E., 2005: Emissions control needs atmospheric verification. *Nature*, **433**(7027), 683.
- Nydal, R., 1968: Further investigation on the transfer of radiocarbon in nature. *Journal of Geophysical Research*, **73**(12), 361735.
- Nydal, R., and Lövseth, K., 1965: Distribution of radiocarbon from nuclear tests. *Nature*, **206**(4988), 1029–1031.
- Nydal, R., and Lovseth, K., 1983: Tracing bomb ^{14}C in the atmosphere 1962-1980. *Journal of Geophysical Research - Oceans and Atmospheres*, **88**(C6), 362142.
- Nydal, R., and Lövseth, K., 1996: Carbon-14 measurements in atmospheric CO_2 from Northern and Southern Hemisphere sites, 1962-1993. Technical report, ORNL/CDIAC-93, Oak Ridge National Lab., TN (United States); Oak Ridge Inst. for Science and Education, TN (United States).
- Oeschger, H., Siegenthaler, U., Schotterer, U., and Gugelmann, A., 1975: A box diffusion model to study carbon dioxide exchange in nature. *Tellus*, **27**, 168.
- Pataki, D. E., Alig, R. J., Fung, A. S., Golubiewski, N. E., Kennedy, C. A., McPherson, E. G., Nowak, D. J., Pouyat, R. V., and Romero Lankao, P., 2006: Urban ecosystems and the North American carbon cycle. *Global Change Biology*, **12**, 2092–2102. doi: 10.1111/j.1365-2486.2006.01242.x.
- Pataki, D. E., Bowling, D. R., and Ehleringer, J. R., 2003a: Seasonal cycle of carbon dioxide and its isotopic composition in an urban atmosphere: Anthropogenic and biogenic effects. *Journal of Geophysical Research*, **108**(D23):4735. doi:10.1029/2003JD003865.
- Pataki, D. E., Ehleringer, J. R., Flanagan, L. B., Yakir, D., Bowling, D. R., Still, C. J., Buchmann, N., Kaplan, J. O., and Berry, J. A., 2003b: The application and interpretation of Keeling plots in terrestrial carbon cycle research. *Global Biogeochemical Cycles*, **17**(1):1022. doi:10.1029/2001GB001850.
- Patra, P., Ishizawa, M., Maksyutov, S., Nakazawa, T., and Inoue, G., 2005a: Role of biomass burning and climate anomalies for land-atmosphere carbon fluxes based on inverse modeling of atmospheric CO_2 . *Global Biogeochemical Cycles*, **19**.
- Patra, P., Maksyutov, S., Ishizawa, M., Nakazawa, T., Takahashi, T., and Ukita, J., 2005b: Interannual and decadal changes in the sea-air CO_2 flux from atmospheric CO_2 inverse modeling. *Global Biogeochemical Cycles*, **19**.

- Philander, S. G. H., 1983: El Niño Southern Oscillation phenomena. *Nature*, **302**(5906), 295–301.
- Potosnak, M. J., Wofsy, S. C., Denning, A. S., Conway, T. J., Munger, J. W., and Barnes, D. H., 1999: Influence of biotic exchange and combustion sources on atmospheric CO₂ concentrations in New England from observations at a forest flux tower. *Journal of Geophysical Research*, **104**(D8), 9561–9569.
- Pypker, T., Unsworth, M., Mix, A., Rugh, W., Ocheltree, T., Alstad, K., and Bond, B., 2007: Using nocturnal cold air drainage flow to monitor ecosystem processes in complex terrain. *Ecological Applications*, **17**(3).
- Rafter, T., and Fergusson, G., 1957: “atom bomb effect” - Recent increase of Carbon-14 content of the atmosphere and biosphere. *Science*, **126**(3273), 557–558.
- Rafter, T. A., 1955: ¹⁴c variations in nature and the effect on radiocarbon dating. *New Zealand Journal of Science and Technology*, **B37**(1), 20–38.
- Ramsey, C. B., Higham, T., and Leach, P., 2004: Towards high-precision AMS: Progress and limitations. *Radiocarbon*, **46**, 17–24(8).
- Randerson, J. T., Enting, I. G., Schuur, E. A. G., Caldeira, K., and Fung, I. Y., 2002: Seasonal and latitudinal variability of troposphere δ¹⁴CO₂: Post bomb contributions from fossil fuels, oceans, the stratosphere, and the terrestrial biosphere. *Global Biogeochemical Cycles*, **16**(4). doi:10.1029/2002GB001876.
- Rayner, P. J., Law, R. M., and Dargaville, R., 1999: The relationship between tropical CO₂ fluxes and the El Niño-Southern Oscillation. *Geophysical Research Letters*, **26**, 493496.
- Rivier, L., Ciais, P., Hauglustaine, D., Bakwin, P., Bousquet, P., Peylin, P., and Klonecki, A., 2006: Evaluation of SF₆, C₂Cl₄, and CO to approximate fossil fuel CO₂ in the Northern Hemisphere using a chemistry transport model. *Journal of Geophysical Research*, **111**.
- Rotty, R. M., 1987: Estimates of seasonal variation in fossil fuel CO₂ emissions. *Tellus*, **39B**, 184202.
- Rozanski, K., Levin, I., Stock, J., Guevara Falcon, R. E., and Rubio, F., 1995: Atmospheric ¹⁴CO₂ variations in the equatorial region. *Radiocarbon*, **37**(2), 509–515.
- Sarmiento, J., and Gruber, N., 2002: Sinks for anthropogenic carbon. *Physics Today*, **55**(8), 30–36.

- Southon, J., and Roberts, M., 2000: Ten years of sourcery at CAMS/LLNL—evolution of a Cs ion source. *Nuclear Instruments and Methods in Physics Research B*, **172(14)**, 25761.
- Southon, J. R., 1989: The calculation of ^{14}C ages from AMS $^{14}\text{C}/^{13}\text{C}$ ratio measurements. 7 p.
- Staebler, R. M., and Fitzjarrald, D. R., 2004: Observing subcanopy CO_2 advection. *Agricultural and Forest Meteorology*, **122**, 139–156.
- Stephens, B., Gurney, K., Tans, P., Sweeney, C., Peters, W., Bruhwiler, L., Ciais, P., Ramonet, M., Bousquet, P., Nakazawa, T., et al., 2007: Weak northern and strong tropical land carbon uptake from vertical profiles of atmospheric CO_2 . *Science*, **316(5832)**, 1732.
- Stohl, A., Wernli, H., James, P., Bourqui, M., Forster, C., Liniger, M. A., Seibert, P., and Sprenger, M., 2003: A new perspective of stratosphere-troposphere exchange. *Bulletin of the American Meteorological Society*, **84(11)**, 1565–1573.
- Stuiver, M., and Polach, H. A., 1977: Discussion: reporting of ^{14}C data. *Radiocarbon*, **19(3)**, 35563.
- Stuiver, M., Quay, P., and Östlund, H., 1983: Abyssal water Carbon-14 distribution and the age of the world oceans. *Science*, **219(4586)**, 849–851.
- Stuiver, M., and Quay, P. D., 1981: Atmospheric ^{14}C changes resulting from fossil fuel CO_2 release and cosmic ray flux variability. *Earth and Planetary Science Letters*, **53(3)**, 349–362.
- Sweeney, C., Gloor, E., Jacobson, A., Key, R., McKinley, G., Sarmiento, J., and Wanninkhof, R., 2007: Constraining global air-sea gas exchange for CO_2 with recent bomb ^{14}C measurements. *Global Biogeochemical Cycles*, **21(2)**.
- Takahashi, H. A., Konohira, E., Hiyama, T., Minami, M., Nakamura, T., and Yoshida, N., 2002: Diurnal variation of CO_2 concentration, $\delta^{14}\text{C}$ and $\delta^{13}\text{C}$ in an urban forest: estimate of the anthropogenic and biogenic CO_2 contributions. *Tellus*, **B54**, 97–109.
- Trumbore, S., 2000: Age of soil organic matter and soil respiration: radiocarbon constraints on belowground C dynamics. *Ecological Applications*, **10(2)**, 399–411.
- Turnbull, J. C., Lehman, S. J., Miller, J. B., Sparks, R. J., Southon, J., and Tans, P. P., 2007: A new high precision $^{14}\text{CO}_2$ time series for North American continental air. *Journal of Geophysical Research*, **112:D11310**. doi:10.1029/2006JD008184.

- Turnbull, J. C., Miller, J. B., Lehman, S. J., Tans, P. P., Sparks, R. J., and Southon, J., 2006: Comparison of $^{14}\text{CO}_2$, CO, and SF_6 as tracers for recently added fossil fuel CO_2 in the atmosphere and implications for biological CO_2 exchange. *Geophysical Research Letters*, **33**:L01817. doi:10.1029/2005GL024213.
- Van der Werf, G., Randerson, J., Collatz, G., Giglio, L., Kasibhatla, P., Arellano Jr, A., Olsen, S., and Kasischke, E., 2004: Continental-Scale Partitioning of Fire Emissions During the 1997 to 2001 El Niño/La Niña Period. *Science*, **303**(5654), 73–76.
- Winer, B. J., 1971: *Statistical Principles of Experimental Design*. McGraw-Hill, New York, NY.
- Wofsy, S., Kaplan, W., and Harriss, R., 1988: Carbon dioxide in the atmosphere over the Amazon Basin. *Journal of Geophysical Research*, **93**, 1377–1387.
- Wofsy, S. C., and Harriss, R. C., 2002: *The North American Carbon Program (NACP)*. U.S. Global Change Research Program, Washington, DC.
- Zahn, A., Neubert, R., and Platt, U., 2000: Fate of long-lived trace species near the Northern Hemispheric tropopause, 2. Isotopic composition of carbon dioxide ($^{13}\text{CO}_2$, $^{14}\text{CO}_2$, and $\text{C}^{18}\text{O}^{16}\text{O}$). *Journal of Geophysical Research*, **105**(D5), 6719–6736.
- Zeng, G., and Pyle, J. A., 2005: Influence of El Niño Southern Oscillation on stratosphere/troposphere exchange and the global tropospheric ozone budget. *Geophysical Research Letters*, **32**(L01814). doi:10.1029/2004GL021353.